aRJ

[redacted]

CENTRAL RESEARCH LIBRARY
DOCUMENT COLLECTION

MARTIN MARIETTA ENERGY SYSTEMS LIBRARIES
3 4456 0360666 7

ORNL-1587
Progress
4a

LABORATORY RECORDS
1954

CHEMISTRY DIVISION

SEMIANNUAL PROGRESS REPORT

FOR PERIOD ENDING JUNE 20, 1953

CENTRAL RESEARCH LIBRARY
DOCUMENT COLLECTION

LIBRARY LOAN COPY

DO NOT TRANSFER TO ANOTHER PERSON

If you wish someone else to see this document, send in name with document and the library will arrange a loan.

OAK RIDGE NATIONAL LABORATORY
OPERATED BY
CARBIDE AND CARBON CHEMICALS COMPANY
A DIVISION OF UNION CARBIDE AND CARBON CORPORATION
UCC
POST OFFICE BOX P
OAK RIDGE, TENNESSEE

[redacted]

[redacted]

[redacted]

DECLASSIFIED

CLASSIFICATION CHANGED TO
BY AUTHORITY TID-1148
BY D. Mosnier 2/26/57

ORNL 1587

This document consists of 124 pages
Copy 4 of 136 copies Series A

Contract No W 7405-eng 26

CHEMISTRY DIVISION

SEMIANNUAL PROGRESS REPORT

for Period Ending June 20, 1953

S C Lind Acting Director
G E Boyd M A Bredig Associate Directors

DATE ISSUED

OCT 6 1953

OAK RIDGE NATIONAL LABORATORY
Operated by
CARBIDE AND CARBON CHEMICALS COMPANY
A Division of Union Carbide and Carbon Corporation
Post Office Box P
Oak Ridge Tennessee

[redacted]

[redacted]

3 4456 0360666 7

[redacted]

ORNL-1587

This document consists of 124 pages.
Copy 13 of 136 copies. Series A.

Contract No. W-7405-eng-26

CHEMISTRY DIVISION

SEMIANNUAL PROGRESS REPORT

for Period Ending June 20, 1953

S. C. Lind, Acting Director
G. E. Boyd, M. A. Bredig, Associate Directors

DATE ISSUED

OCT 6 1953

OAK RIDGE NATIONAL LABORATORY
Operated by
CARBIDE AND CARBON CHEMICALS COMPANY
A Division of Union Carbide and Carbon Corporation
Post Office Box P
Oak Ridge, Tennessee

[redacted]

[redacted]

ORNL-1587
Progress

INTERNAL DISTRIBUTION

1. C. E. Center
2. Biology Library
3. Health Physics Library
4-5. Central Research Library
6-12. Laboratory Records Department
13. Laboratory Records, ORNL RC
14. Reactor Experimental Engineering Library
15. C. E. Larson
16. W. B. Humes (K-25)
17. L. B. Emlet (Y-12)
18. A. M. Weinberg
19. E. H. Taylor
20. E. J. Murphy
21. E. D. Shipley
22. S. C. Lind
23. F. C. VonderLage
24. R. C. Briant
25. J. A. Swartout
26. R. L. Culler
27. A. H. Snell
28. A. Hollaender
29. M. T. Kelley
30. G. H. Clewett
31. K. Z. Morgan
32. T. A. Lincoln
33. A. S. Householder
34. C. S. Harrill
35. C. E. Winters
36. D. W. Cardwell
37. E. M. King
38. J. A. Lane
39. G. E. Boyd
40. M. A. Bredig
41. R. W. Stoughton
42. R. B. Briggs
43. G. W. Parker
44. C. J. Borkowski
45. G. H. Jenks
46. K. A. Kraus
47. H. A. Levy
48. R. S. Livingston
49. T. E. Willmarth
50. G. H. Secoy
51. C. J. Hochanadel
52. W. H. Baldwin
53. A. P. Brosi
54. R. [illegible] Lyon
55. S. A. Reynolds
56. P. F. Thomason
57. E. G. Bohlmann
58. C. P. Keim
59. C. D. Susano
60. D. D. Cowen
61. P. M. Reyling
62. R. Livingston
63. G. H. Cartledge
64. E. R. VanArtsdalen
65. G. C. Williams
66. R. W. Johnson
67. S. D. Schiffman (K-25)
68. E. P. Wigner (consultant)

EXTERNAL DISTRIBUTION

[redacted]

69-76. Argonne National Laboratory
77-84. Atomic Energy Commission, Washington
85-88. Brookhaven National Laboratory
89-92. Carbide and Carbon Chemicals Company (Y-12 Plant)
93-96. E. I. du Pont de Nemours and Company

[redacted]

[redacted]

97-98. Knolls Atomic Power Laboratory
99-104. General Electric Company, Richland
105. Idaho Operations Office (Phillips Petroleum Co.)
106-109. Los Alamos Scientific Laboratory
110. Nevada Laboratory
111-113. New York Operations Office
114. Patent Branch, Washington
115. Savannah River Operations Office, Augusta
116-130. Technical Information Service, Oak Ridge
131-134. University of California Radiation Laboratory
135-136. Westinghouse Electric Corporation

[redacted]

[redacted]

Chemistry Division quarterly progress reports previously issued in this series are as follows:

ORNL-65	March, April, May, 1948
ORNL-176	June, July, August, 1948
ORNL-229	September, October, November, 1948
ORNL-336	December, 1948, January and February, 1949
ORNL-286	Period Ending June 30, 1949
ORNL-499	Period Ending September 30, 1949
ORNL-607	Period Ending December 31, 1949
ORNL-685	Period Ending March 31, 1950
ORNL-795	Period Ending June 30, 1950
ORNL-870	Period Ending September 30, 1950
ORNL-1036	Period Ending December 31, 1950
ORNL-1053	Period Ending March 31, 1951
ORNL-1116	Period Ending June 30, 1951
ORNL-1153	Period Ending September 30, 1951
ORNL-1260	Period Ending December 31, 1951
ORNL-1285	Period Ending March 31, 1952
ORNL-1344	Period Ending June 30, 1952
ORNL-1432	Period Ending September 30, 1952
ORNL-1482	Period Ending December 31, 1952

[redacted]

[redacted]

CONTENTS

	Page
SUMMARY	1
INORGANIC AND PHYSICAL CHEMISTRY	7
Thorium Chemistry	7
Studies on solid thorium salts	7
Thorium perchlorate	7
Thorium nitrate	7
Solubility of aqueous thorium fluoride–sulfate systems at 24 and 70°C	8
Activity Coefficients with the Ultracentrifuge	8
Study of Hydrolytic Polymers with an Ultracentrifuge	9
Anion Exchange Studies	9
1. Titanium	10
2. Vanadium	10
3. Chromium	11
4. Separation of titanium, vanadium, and iron	11
5. Palladium, iridium, and platinum	11
6. Separation of 0.82 sec Pb^{207} from Bi^{207}	13
Chemistry of Corrosion	13
Studies on electrode potentials	13
Action of corrosion inhibitors	17
Hydrogen overvoltage on amalgams	19
Thermodynamics of Boron Nitride	19
Low-temperature heat capacity	20
Heat and free energy of formation	23
Chemistry of Fused Salts	25
Electrical conductivity	25
Transport numbers	26
Cryoscopy	26
Calorimetry	27
NUCLEAR CHEMISTRY	28
Heavy-Isotope Buildup in Core of U^{233} Breeder	28
Cerium-144 Decay	29
Half-Life Measurements	31
Recovery of Fission Iodine-129 from Hanford Silver-Bed Reactors	35
Dissolution of silver iodide	36
Analysis of I^{129} by neutron activation	38
Separation of silver and iodine by sulfide precipitation	39

[redacted]

[redacted]

RADIO-ORGANIC CHEMISTRY 40

Organic Reaction Mechanism Studies 40
Molecular rearrangements – the 1,2,2-triphenylethyl system 40
Molecular rearrangements – the 1,1,2-triphenylethyl system 41
The rates and migration ratios observed in the S_N1 and S_N2 type solvolyses of 2-phenyl-2-(*p*-tolyl)ethanol-1-C^{14} tosylate 41
Isotope-Effect Studies 45
Isotope effects during catalytic hydrogenations 45
Hydrogenation of C^{14}-labeled cinnamic acids 46
The iodoform reaction of acetone-1-C^{14} 47
Reactions of benzoic-α-C^{14} anhydride 48
Bromination of C^{14}-labeled methyl cinnamate 50
Reactions of carbonyl-C^{14} ethyl benzoates and acetophenones 50
Study of Scintillation Counting of Carbon-14 in Solution 50

CHEMISTRY OF SEPARATION PROCESSES 53

Ion Exchange 53
Application of the osmotic coefficient concept to mixed-resin systems 53
Effect of capacity on resin moisture 58
Organic Chemistry of Solvents 61
Hydrotropic solutions 61
Dealkylation of esters 61

CHEMICAL PHYSICS 63

Radio-Frequency Spectroscopy 63
Quadrupole spectroscopy 63
The iodine problem 64
Infrared Spectroscopy of Methyl Halides at Liquid Nitrogen Temperature 64
Neutron Diffraction Studies 66
Crystal structures of potassium dihydrogen phosphate and arsenate 66
Crystal structure of ice 66
Crystal structure of oxalic acid dihydrate 66
Crystal structure of iodic acid, HIO_3 67
Experiments in Chemical Kinetics with Molecular Beams 67

RADIATION CHEMISTRY 68

Gas-Phase Radiation 68
Effects of Gamma Rays on Ice and Frozen Solutions 68
Decomposition of Sulfuric Acid by Cobalt Gamma Radiation 71
Effect of Light-Particle Radiation on Corrosion of Type 347 Stainless Steel by Uranyl Sulfate Solutions 72

[redacted]

[redacted]

Addition of Bromotrichloromethane to Cyclohexene Initiated by Ultraviolet Light and by Gamma Rays 72
Some Effects of Hydrogen and Oxygen on the Photolysis of Hydrogen Peroxide Solutions 73
Hydrogen Peroxide Formation by Cobalt Gamma Radiation 74
Oxygen effect 74
pH effect 74
Reduction reactions in acid solutions 74
Some Effects of Cobalt Gamma Radiation on Aqueous Benzene Solutions 75

CHEMISTRY OF SOLID STATE 77

Thermal Expansion in Layer Lattice Structures 77
Molten Metal-Metal Halide Systems 79
Sodium-sodium chloride 79
Sodium-sodium bromide 80
Potassium-potassium fluoride 81
Calcium-calcium chloride 83

INSTRUMENTATION 84

Multichannel Pulse Analyzers 84
Oscillograph galvanometer pulse height analyzer 84
Channel-selector matrix 85

REACTOR CHEMISTRY 87

Behavior of the Silver, Silver Sulfate and the Mercury, Mercurous Sulfate Electrodes at High Temperatures 87
Cathodic Protection of Type 347 Stainless Steel Exposed to Uranyl Sulfate Solutions 89
Results at 100°C 89
Results at 250°C 90
Conclusions 90
Thermal-Phase Stability Studies of the ThO_2-H_3PO_4-H_2O System 90
Corrosion 93
Light scattering 93
In-Pile Corrosion by Homogeneous Solutions 94
Radiation Studies of Pertechnetate Solutions 95
Solubility of Hydrogen at High Temperatures and Pressures in Solutions of Uranyl Sulfate 96
Kinetic method for the determination of the solubility of hydrogen 97
Homogeneous Catalysis: The Mechanism of the Reaction Between Dissolved Hydrogen and Oxygen in Aqueous Solutions of Cupric Salts 98
Catalysis by cupric perchlorate–perchloric acid mixtures 99
Effect of sulfuric acid 99
Effect of uranyl sulfate 101
Effect of uranyl sulfate plus sulfuric acid 101
Decomposition of Peroxide in Aqueous Uranium Systems 106
Mechanism of peroxide decomposition 106

[redacted]

[redacted]

Apparatus for Phase-Stability Studies and Corrosion Tests on 2-ml Solution Volumes 109
Description of apparatus 109
Proposed use of apparatus 110
Comment on the System Uranyl Dichromate–Water 110
Exploratory Phase Investigations of Systems Involving $CuSO_4$, UO_2SO_4, and H_2O at Uranium Concentrations below 30 g per Liter 111
Further Investigation on the Use of a Cation-Exchange Resin for the Anion Analysis of Uranyl Salts in Water 114
The System UO_3–SO_3–H_2O 114
Oxidation of Sulfur Dioxide in Uranyl Sulfate Solution 115
Vapor Pressures of Aqueous Uranyl Sulfate Solutions 116

[redacted]

CHEMISTRY DIVISION SEMIANNUAL PROGRESS REPORT

SUMMARY

INORGANIC AND PHYSICAL CHEMISTRY

Some evidence was obtained for the existence of anhydrous thoryl perchlorate, $ThO(ClO_4)_2$, and of a hydrated thorium nitrate, $Th(NO_3)_4 \cdot 2.55H_2O$. The presence of fluoride in aqueous thorium sulfate in the range of 0.5 to 2.0 moles of fluoride per mole of thorium does not increase the thorium solubility but decreases it markedly.

Calculations of activity coefficients of uranyl fluoride in water at 30°C on the basis of ultracentrifuge, refractive index, and density measurements were refined. The data indicate that ΔH of dimerization is close to zero between 0 and 30°C.

A critical mathematical review of factors that may influence sedimentation equilibria for low-molecular-weight polymers in the ultracentrifuge indicates the disturbing effect of particle charge.

The systematic survey of the anion-exchange behavior of metals in hydrochloric acid solutions was continued, and the results obtained with the elements titanium, vanadium, chromium, palladium, iridium, and platinum are summarized. An interesting application of these anion-exchange studies to the separation of short-lived radioactive daughters has been made in the case of the Pb^{207} daughter of Bi^{207}.

Apparatus permitting measurements of electrical conductivity, density, transport numbers, and freezing-point depressions in fused salts under very carefully controlled conditions has been assembled. Preliminary data indicate that Ag^+ and Na^+ in fused silver nitrate–sodium nitrate mixtures carry essentially all the current in very roughly equivalent quantities and that freezing-point depressions in molten sodium nitrate by NaCl, KCl, K_2SO_4, and $K_3Fe(CN)_6$ indicate complete dissociation into the respective ions.

Measurements concerned with the thermodynamics of boron nitride gave a T^2 dependence of the low-temperature specific heat below 66°K, well in agreement with its known layer structure. The functions S^0, $-(F^0 - H_0^0)/T$, and $(H^0 - H_0^0)/T$ were tabulated between 20 and 300°K. From the heat of combustion, also measured during this period, a heat of formation $\Delta H = -62.8 \pm 0.6$ kcal/mole is obtained, and a free energy of formation $\Delta F = -56.6$ kcal/mole and an entropy of formation $\Delta S = -20.77$ e.u. are computed.

Experiments on the electrode potential of stainless steel at 85°C were extended to solutions of 0.1 *N* sulfuric acid to which various salts were added. Three types of ennobling behavior were observed. Quite generally, the potentials rise linearly with the logarithm of the salt concentration.

The study of the inhibition, by the pertechnetate ion, TcO_4^-, of the corrosion of steel was continued and extended to include elements in the periodic system that are adjacent to a line through chromium, technetium, and osmium and which form XO_4^{n-} ions. The corrosion of carbon steel in water is inhibited by pertechnetate ion, even at 250°C. In deaerated fused silica tubes, type 347 stainless steel is also protected at 250°C in uranyl sulfate solution containing 300 g of uranium per liter. In one test, the presence of oxygen seems to have prevented technetium from producing significant inhibition under these conditions. Attempts to elucidate the mechanism of corrosion inhibition by the XO_4^{n-} type of ion are reported in detail.

NUCLEAR CHEMISTRY

In the conversion-electron and the beta spectra of Ce^{144}-Pr^{144} measured up to 140 kev with the beta spectrometer readjusted for high resolution, and by the use of a specially purified source, two new lines were observed at low energies.

Tentative conclusions from a series of measurements made to determine, within a period of a few months, radioisotope half lives of the order of years are reported for the isotopes Ce^{144}, Co^{60}, and Kr^{85}.

Among the principal results of detailed computations of heavy-isotope buildup in the core of a U^{233} breeder reactor are the following: The total uranium content of the reactor at equilibrium will have increased substantially, that is, by approximately a factor of 3; problems of chemical processing, corrosion, etc. will therefore be increased; and in no case do neutron losses become large, despite the increased total uranium content.

A process worked out for the recovery of 100-g quantities of fission-product I^{129} from the Hanford silver-bed reactors involves the steps of dissolution and reprecipitation of silver iodide with potassium cyanide and concentrated silver nitrate solutions. This is followed by removal of the silver as sulfide, after which the iodine is oxidized, extracted with organic solvent, and finally recovered as sodium iodide.

RADIO-ORGANIC CHEMISTRY

1,2,2-Triphenylethanol-1-C^{14} (I) has been acetylated and the resulting acetate (II) deacetylated with no radiochemical rearrangement. Dehydration of carbinol I with phosphoric anhydride in xylene, however, yielded 1,1,2-triphenylethylene-1,2-C_1^{14} (IIIab) having an equal distribution of radioactivity over the ethylene skeleton. The carbinol I was converted into its *p*-toluenesulfonate ester (IV). Acetolysis of tosylate IV proceeded with pheny migration, the latter reaching 50% when glacial acetic acid was used as the solvolyzing medium. Similar results were obtained during formolysis of tosylate IV. The addition of sodium acetate to acetolysis mixtures of tosylate IV resulted in a diminished extent of phenyl migration. These results are most simply interpreted in terms of the formation of a symmetrical phenonium-ion intermediate during acetolysis, with a possible, competing, direct second-order displacement of tosylate by acetate ion. Hydrolysis of tosylate IV in aqueous acetone proceeded with 22% phenyl migration, while lithium aluminum hydride reduction led to only 9% phenyl migration.

1,1,2-Triphenylethanol-1-C^{14} (VI) has been dehydrated by means of aqueous sulfuric or glacial acetic acid to yield the unrearranged olefin, 1,1,2-triphenylethylene-1-C^{14} (IIIa). When this olefin was heated under reflux with dry xylene containing an equal weight of phosphoric anhydride, a complete isotopic position isomerization occurred, which yielded a 50:50 mixture of IIIa and 1,1,2-triphenylethylene-2-C^{14} (IIIb). This observation can best be rationalized in terms of Cram's symmetrical phenonium ion.

A kinetic analysis has now been accomplished for the system 2-phenyl-2-(*p*-tolyl)ethanol tosylate and 2-phenyl-2-(*p*-tolyl)ethanol-1-C^{14} tosylate.

Isotope effects during the heterogeneous catalytic reductions of labeled olefin and carbonyl groups are reported. Stilbene-α-C^{14} is reduced to dibenzyl-α-C^{14} with a 2% isotope effect by the use of Raney nickel in benzene, or of platinum in ethanol. Acetophenone-α-C^{14} is reduced to 1-phenylethanol-1-C^{14} with an 11.5% isotope effect by the use of platinum in ethanol and with an 8% isotope effect by the use of lithium aluminum hydride in ether.

Cinnamic acids labeled with C^{14} in three positions have been hydrogenated over a platinum catalyst in ethanol solution at 25°C. No carbon isotope fractionation has been found.

Preliminary results in an attempt to check earlier work on a reverse intramolecular isotope effect reported from another laboratory for the iodoform reaction of acetone-1-C^{14} indicate no isotope effect at all in this reaction.

Two intramolecular isotope-effect studies in reactions of benzoic-α-C^{14} anhydride are reported. The fractionation factors measured, although temperature independent as predicted by the Bigeleisen theory, are not in quantitative agreement with this theory.

No isotope fractionation has been found in the bromination of methyl cinnamate-β-C^{14}.

The two studies of the effect of ring substituents on the degree of carbon isotope fractionation in the reactions of ethyl benzoates (α-C^{14}) and acetophenones (α-C^{14}) have been completed. In both studies, it was found that those substituents which supply electrons to the side chain increase the isotope fractionation ratio, k_{14}/k_{12}.

The solution scintillation counter for C^{14} has been modified to accommodate a third cell which permits corrections for background. For a case in which the two solutions compared were identical (ratio = 1.000), the ratio indicated by this instrument was 1.007 ± 0.007. This is about the same precision as that obtained with the vibrating-reed electrometer.

CHEMISTRY OF SEPARATION PROCESSES

The composition and practical application, for uranium extraction, of hydrotropic solutions, that is, the formation of third phases between an aqueous and an ether phase in systems containing sodium hydroxide, water, sodium dibutyl phosphate (or di (2 ethyl hexyl) phosphinate), and dibutyl ether, are discussed. Advantages of the use of ethanolamine for the dealkylation of phosphoric and phosphonic acid esters are indicated.

It is demonstrated that the cation-exchange systems Na-Li and Na-Cs with Dowex-50 resin behave as concentrated aqueous solutions and obey Harned's rule for the interaction of salts in such solutions. In a continued study of the effect of resin capacity upon moisture uptake, it was found that at low water activities this uptake increases with capacity, whereas at high activities it decreases with increasing capacity for the highly cross-linked resin but not for the low-cross-linked one. These observations are explained on the basis of free-energy changes of absorption involving contributions from near neighbors in high-capacity resins and of free-energy changes associated with volume changes, that is, of volume density of dipoles, for low and high activities, respectively.

CHEMICAL PHYSICS

The first of the experiments in the field of chemical kinetics with molecular beams led to the surprising result that a potassium atom beam at 500°K did not react with the hydrogen bromide molecules of an effusive spray at 150°K.

Differentiation between potassium atoms and KBr molecules was possible by means of a double-filament detector, tungsten and platinum, of which only the tungsten filament was found to ionize both the potassium atoms and the KBr molecules; the efficiency of the platinum filament was 50% for potassium atoms but only 0.1% for KBr molecules.

The quadrupole spectra for bromine and iodine in a number of additional alkyl halides were measured. An extensive study of the Zeeman effect in iodine quadrupole resonance spectra of a single crystal of iodic acid, HIO_3, gave results of unusual interest because of the uncommonly large asymmetry parameter, η, of the substance. Correlation with the known crystal structure and consideration of the interaction with the magnetic field of the proton led to explanations of various apparently anomalous observations on line splitting and of intensity effects as a function of the orientation of the external magnetic field and of the polarization of the radio-frequency energy.

Methyl iodide was prepared from I^{131} carrier-free starting material purified in a process described previously. Difficulties experienced on evaporation for measurement of the microwave spectrum and determination of the nuclear moment of I^{131} are now being overcome by an improved technique.

A study of the infrared spectra of solid methyl halides was undertaken in order to correlate frequency shifts of vibrational bands with shifts in nuclear quadrupole constants when the gaseous substances are solidified. The infrared shifts indicate slightly perturbed electronic states in the crystal, which may lead to a change in the nuclear quadrupole coupling constant. Also the lowering of the carbon-halogen stretching frequencies suggests that this bond may be stretched in the solid state.

Neutron-diffraction studies of compounds of the type KD_2AsO_4 led to a determination of the positions of the deuterium nuclei which form hydrogen bonds with an oxygen-deuterium distance of 1.05 Å and connect a three-dimensional network of arsenate ions. The coherent neutron-scattering amplitude of arsenic was found to be 0.7×10^{-12} cm. Data for the $h0l$ zone of a single crystal of deuterium ice at −52°C yielded a confirmation of the Pauling model with random distribution of hydrogen atoms along lines connecting adjacent oxygen atoms, and distances of O-D = 1.00 Å, O-O = 2.76 Å, and an angle D-O-D = 109 degrees. The structural data for oxalic acid dihydrate, though still in the state of being refined, show that the acid molecule has an at least approximately planar configuration. Bond distances are: O-H, both in carboxyl and water, about 1.0 Å; C-O, 1.2 and 1.3 (hydroxyl) Å. Preliminary data on iodic acid, HIO_3, confirm that hydrogen is linked to the oxygen atom having the longest I-O distance, as was previously deduced from x-ray data.

RADIATION CHEMISTRY

A radon collecting station has been completed which incorporates the novel feature of recombining hydrogen and oxygen gases continuously on a hot platinum filament. As a basis for comparison in subsequent studies, the rate of the recombination reaction of hydrogen and oxygen in the presence of radon was measured, and the result was found to agree well with earlier values.

In experiments on the effect of gamma radiation on ice and frozen solutions, some unknown species that forms during irradiation and is stable at −196°C, such as a free radical or trapped charge, was found to react with hydrogen peroxide at

temperatures above −180°C. A broad ultraviolet absorption band with a peak at 2800 Å appears in ice irradiated at −196°C and disappears when the ice is warmed in the same temperature range, namely, −180 to −140°C.

The results of a study are reported on the gamma irradiation of sulfuric acid as a function of concentration and the presence of helium, hydrogen, oxygen, and hydrogen peroxide; the last two substances inhibit and suppress, respectively, the production of SO_2.

A small stainless steel thermal circulation loop for the study of Van de Graaff radiation effects on corrosion in uranyl sulfate solutions has been constructed.

A long-chain reaction is indicated in cobalt gamma radiolytic (G = 280 molecules/100 ev) but not in photolytic (quantum yield = 1.8) production of 1-bromo-2(trichloromethyl)cyclohexane from air-saturated mixtures of bromotrichloromethane and cyclohexene.

The effects of dissolved hydrogen and oxygen, singly and in combination, upon the photolytic decomposition of hydrogen peroxide can be explained by the production, through the reaction $H_2 + OH \longrightarrow H_2O + H$, of hydrogen atoms and their reaction with H_2O_2 and O_2. Results also indicate an effect of pH less than 2 upon either the formation of hydrogen atoms or upon their reaction with H_2O_2.

With cobalt gamma radiation, the rate of formation of hydrogen peroxide in water containing oxygen and the steady-state concentration in pure water are dependent upon, that is, increase with, the oxygen, because oxygen removes hydrogen atoms which decompose H_2O_2. The effects of pH and oxygen are closely related; the rate of reaction of hydrogen atoms with H_2O decreases with increased acidity. From the stoichiometric equivalence of the reduction of $K_2Cr_2O_7$ in 0.8 N H_2SO_4 (0.42 molecule/100 ev) with the formation of H_2O_2 (1.26 molecules/100 ev), it is again concluded that hydrogen peroxide is the intermediate in this reduction reaction with cobalt gamma rays.

An ultraviolet absorption peak at 345 mμ which occurs during gamma irradiation of aqueous benzene solutions is tentatively attributed to a peroxide of benzene, and it is proposed that the formation of phenol occurs through the intermediate formation and hydrolysis of phenylperoxy radicals.

CHEMISTRY OF THE SOLID STATE

The data for the solubility of sodium metal in molten sodium chloride were revised on the basis of new tests in which an improved technique was employed.

An unexpectedly high solubility of potassium fluoride in liquid potassium metal was found, with every indication of miscibility in all proportions at temperatures above 950°C. This rather significant discovery, apparently the first case of extensive solubility of a typical salt in a typical electropositive metal, is interpreted to be a forecast of high solubility of salt in metal in other systems, especially those in which the anion of the salt is smaller than the atom of the metal, for example, in the combination cesium fluoride–cesium metal. Differences observed in absolute magnitude and temperature dependence of solubility of sodium metal in molten sodium chloride and bromide are also interpreted in terms of similar size relationships. The rapid increase of solubility with temperature in the chloride system is considered to be indicative of considerable solubility of the salt in the metal.

A new type of anisotropy in the thermal expansion of layer lattice structures is indicated in measurements with the orthorhombic yellow modification of PbO. If its crystal structure, as known from x-ray diffraction studies, is assumed to be correct, the strongest expansion appears to be not in the direction perpendicular to the atomic layers but within these layers. The explanation is based upon the polarization of highly polarizable cations such as Pb^{++} by highly polarizing anions such as O^{--}.

INSTRUMENTATION

A satisfactory method for making the grids for the new type of multichannel pulse analyzer was devised. In one grid having 127 channels in a 4-in. length, sufficiently well-resolved pulses were obtained to make it usable in a 120-channel analyzer cathode-ray tube.

Various benefits are derived from the new features in the design of the 32-channel galvanometer type of pulse-height analyzer which may be modified for 64 channels.

REACTOR CHEMISTRY

A study of the silver, silver sulfate and mercury, mercurous sulfate electrodes for use in potential measurements at elevated temperatures up to 250°C

showed that the potential as measured in 0.5 *N* H_2SO_4 up to 150°C is the theoretically expected one. Above this temperature, the silver electrode is attacked by the acid, and deviations from the theoretical curve occur as a result of hydrolysis at temperatures above 100°C in weaker acids.

Cathodic protection was found essentially ineffective in decreasing the corrosion rate of type 347 stainless steel in uranyl sulfate solutions containing 300 g of uranium per liter at 100°C, whereas at 250°C, the rate was found to decrease by a factor of about 2.3.

The solubility and the stability against hydrolytic solid-phase separation of thorium phosphate in phosphoric acid solutions at elevated temperatures were studied. Concentrations satisfactory for breeding purposes were observed, but rapid corrosion, even of zirconium and titanium metals, will require a search for a more stable, probably unconventional, container material.

The corrosion of type 347 stainless steel was studied in the homogeneous reactor type of solution containing uranyl sulfate in various concentrations and degrees of U^{235} enrichment, as well as 0.01 *M* cupric sulfate. The solution was under an oxygen gas pressure of 100 to 500 psi in a reactor radiation field of 3.5×10^{12} slow neutrons/cm^2·sec, which corresponds to a power density of 4.5 to 6.0 kw/liter. The corrosion was found to proceed at a slow rate proportional to the square root of time, which indicates diffusion to be the rate-controlling process for a period of one or two weeks. After this time interval, a sudden increase in the corrosion rate was initiated. However, in the case of one test with a power density of only 0.5 kw/liter, the sudden increase did not occur.

Pertechnetate ion, TcO_4^-, considered as a possible corrosion inhibitor, appears to be stable under reactor irradiation and also in cobalt gamma radiation when air is present. With hydrogen gas, reduction to colloidal TcO_2 takes place.

Preliminary test results of the study of the solubility of hydrogen at high temperatures and pressures in aqueous and uranyl solutions are reported.

The mechanisms of the homogeneous catalytic reaction between dissolved hydrogen and oxygen in aqueous solutions of cupric salts was studied further. The invariance of the rate constant with increasing perchloric acid concentration in 0.0010 *M* copper perchlorate solutions suggests that the value for the uncomplexed cupric ion is represented by this constant. No direct participation of hydrogen ions in the reaction is indicated. Hydrolytic phase instability leads to lack of reproducibility in solutions of low acidity. This instability has thus far prevented a more detailed study of the increased rate in low concentrations of sulfate or bisulfate ions, which is indicative of the presence of a complex ionic species of much higher catalytic activity than uncomplexed cupric ion. Thus, heterogeneous catalysis with cupric hydroxide or related compounds is suggested.

Equilibrium constants in aqueous sulfate and perchlorate systems ($K_{SO_4} = 4.7$ and $K_{ClO_4} = 1.1$) for the reaction of uranyl ion with hydrogen peroxide, $UO_2^{++} + H_2O_2 \rightleftharpoons UO_4(aq) + 2H^+$, were derived from measurements of peroxide decomposition rates considered proportional to the concentrations of UO_4 or H_2O_2, depending on the conditions.

An apparatus is described which was used for phase-stability and corrosion tests on 2-ml solution volumes at elevated temperatures and which utilizes a magnetic rotor for stirring.

Use of the semimicro phase apparatus gave indications that uranyl dichromate, similarly to uranyl phosphate, is soluble in supercritical water.

In connection with the use of cupric ion for the catalytic combination of hydrogen and oxygen in a homogeneous system, an exploratory study was made of temperatures and compositions for water solutions of cupric sulfate, uranyl sulfate, and their combinations with each other and with sulfuric acid, corresponding to the limits of hydrolytic phase stability. Cupric sulfate hydrolyzes between 90 and 140°C in concentrations at least from 1.0 to 1.0×10^{-3} *M*. At 250°C, the minimum concentration of uranyl sulfate is 0.017 *M*, but it is subject to influence by other solutes. Minimum concentrations of acid for phase stability in solutions of various ratios of uranyl sulfate to cupric sulfate were determined.

A method is described for the anion analysis of uranyl salts by use of the cation-exchange resin Dowex-50 for removal of the uranium. The method permits an accuracy of ±0.15%.

An attempt at refinement and extension of previous data on the phase equilibria of the system UO_3–SO_3–H_2O has produced indications

of the existence of two heretofore unknown solid phases, one with the approximate composition of $8UO_3 \cdot 3SO_3 \cdot 14\text{-}20H_2O$, and the other possibly a new form of anhydrous UO_3.

Small-scale laboratory tests in quartz tubing indicate that the proposed method for oxidation of sulfur dioxide in uranyl sulfate solution to offset acidity decrease caused by corrosion is a satisfactory one with respect to the chemistry involved.

Evaluation is in progress of relative partial molal free energies of water and uranyl sulfate in solutions 0.6 to 4.2 *m*; the data were obtained from vapor-pressure measurements at temperatures ranging from 25 to 90°C.

INORGANIC AND PHYSICAL CHEMISTRY

THORIUM CHEMISTRY

W. C. Waggener R. W. Stoughton

Studies on Solid Thorium Salts

Stoichiometric studies of solid thorium salts prepared from aqueous solutions have progressed slowly this period, pending development of more satisfactory methods of preparation and manipulation of samples. The strong hygroscopicity of thorium perchlorates and thiocyanates which are under study has necessitated a redesign of the gas-solid equilibration apparatus described previously.[1]

Ten-milliliter, calibrated, pyrex centrifuge cones with standard-taper glass stoppers, used for sample containers and reactor vessels and previously attached to a gas manifold in an open drying oven, are now being equilibrated individually in pyrex vacuum ovens (approximately 30 mm ID by 150 mm long). All stoppering and transfer operations for the weighing of samples are conducted in an efficient dry-box.

With the revised apparatus, a sample of thorium salt (0.15 to 0.20 mmole) may be deposited from an aqueous solution in a thin film by slowly rotating the centrifuge cone (horizontally placed) in the cylindrical pyrex oven at a controlled pressure and temperature. A 20-mm platinum-clad bar magnet mounted to the tail of the cone by means of a Teflon fitting is coupled magnetically with an external U-shaped permanent magnet which is rotated outside the oven by a 2-rpm Bodine motor. Under the influence of the moving magnetic field, the sample container turns about its conical axis and constantly presents a fresh surface of solution during the evaporation

Thorium Perchlorate

The preparation of solid thorium perchlorate of the composition $Th(OH)_2(ClO_4)_2$ or $ThO(ClO_4)_2 \cdot H_2O$ has been reported.[1] Thermogravimetric experiments during this period have given some evidence for the existence of anhydrous thoryl perchlorate, $ThO(ClO_4)_2$. A series of seven samples of thorium perchlorate was prepared by fuming down 0.10-mmole samples of thorium nitrate several times with concentrated perchloric acid at 160 to 190°C. The samples then were equilibrated at 200°C with a stream of air which was dried previously by passing it over $Mg(ClO_4)_2$, and the weights of the samples were checked at various time intervals. Table 1 gives the resulting sample weights expressed as "formal molecular weight" of thorium salt. The calculated molecular weight of thoryl perchlorate is 447.0. The powder x-ray pattern of this product will be compared with that already obtained for $Th(OH)_2(ClO_4)_2$, and a complete stoichiometric analysis will be made.

TABLE 1. RESULTS OF HEATING THORIUM PERCHLORATE IN DRY AIR AT 200°C AND ATMOSPHERIC PRESSURE

HEATING TIME (hr)	FORMAL MOLECULAR WEIGHT OF SEVEN SAMPLES	
	Average	Deviation
12	454	±2
24	452	1
48	449	2
96	447	2
144	447	2
192	446	3

The preparation of thorium perchlorates by fuming the nitrate or chloride with concentrated perchloric acid will detect the presence of traces of sulfate owing to the insolubility of thorium sulfate in 70% $HClO_4$. A sample of solid thorium nitrate or chloride containing as little as 0.05 to 0.10 mg of sulfate will develop a turbidity in 1 ml of concentrated perchloric acid upon heating to fumes. The sulfate may be removed from the perchlorate-perchloric acid mixture by centrifugation.

Thorium Nitrate

A study of the species present in the dehydration and hydrolysis of solid, hydrated thorium nitrate is being continued. Previous experiments in air at 114°C have indicated that the decomposition of the nitrate under these conditions involves a loss of water to $Th(NO_3)_4 \cdot 2.3H_2O$ or $Th(OH)_{0.5}(NO_3)_{3.5} \cdot 2.05H_2O$, followed by internal hydrolysis with loss

[1] W. C. Waggener and R. W. Stoughton, *Chem. Quar. Prog. Rep. Dec. 31, 1952*, ORNL-1482, p. 4.

of nitric acid.[1] Present experiments are being conducted on samples of $Th(NO_3)_4 \cdot 4.8H_2O$ at 25°C over $CaSO_4$ at 1 to 3 mm pressure. In five months, these samples have lost weight and approximate the composition, $Th(NO_3)_4 \cdot 2.55H_2O$, if simple dehydration only is involved. As soon as constant weight is established under the above set of conditions, the samples will be analyzed for measurable hydrolysis.

Solubility of Aqueous Thorium Fluoride–Sulfate Systems at 24 and 70°C

Interest in a thorium solution system for a breeder reactor led to an exploration of the possibility of a solubilizing effect of fluoride in the aqueous thorium sulfate system. The relatively stable aqueous ions, ThF^{+++} and ThF_2^{++}, are known to be appreciably soluble even though thorium fluoride itself has a low aqueous solubility. For example, in the titration of thorium with fluoride, precipitation occurs, in general, only after the addition of two equivalents of fluoride ion.

A series of 15 solutions was made up, and the thorium solubilities were measured as follows: Solutions were prepared in 100-ml Lusteroid test tubes by dissolving approximately 5 mmoles of freshly precipitated thorium hydroxide with stoichiometric mixtures of HF and H_2SO_4 (HF:Th mole ratios from 0.0 to 2.0) and by adding 0.1 milliequivalent of H_2SO_4 in excess of the stoichiometric requirement for dissolution. The initial volumes of solution were approximately 40 to 45 ml.

Each solution was stirred magnetically at room temperature for one month, and during this time, more or less precipitation occurred in all the sample solutions. At the end of this period, each solution was centrifuged, and an aliquot was sent to the Analytical Chemistry Division for the analysis of thorium. Each of the open circles of Fig. 1 represents the average of three solutions of identically prepared stoichiometric composition.

The slurries resulting after one month of equilibration at room temperature were transferred to a thermostated water bath and were shaken for 15 days at 70°C. Additional precipitation was noted in all tubes during this period at higher temperature. At the end of the test, each tube was centrifuged and sent to the Analytical Chemistry Division for thorium analysis; results are represented by the closed circles of Fig. 1.

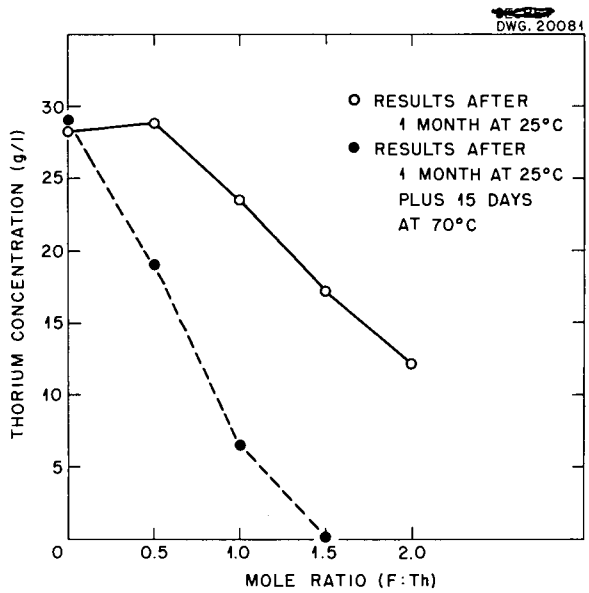

Fig. 1. Solubility of Thorium in Aqueous Fluoride-Sulfate Mixtures.

An undetermined amount of hydrolysis occurred during equilibration at 70°C, as evidenced by a drop in the pH of the solutions – from an average of 1.55 to 1.24 – as measured with a glass electrode. Hydrolysis increased with increasing ratio of fluoride in the samples.

These experiments indicate that increasing the fluoride in stoichiometric aqueous thorium-fluoride-sulfate media in the range of 0.5 to 2.0 moles F:Th decreases the thorium solubility markedly, rather than effecting an increase of any consequence.

ACTIVITY COEFFICIENTS WITH THE ULTRACENTRIFUGE

K. A. Kraus J. S. Johnson

A recalculation of ultracentrifuge data on activity coefficients of UO_2F_2 in water at 30°C was completed, using newer refractive index and density data[2] and other refinements. Because of the interest in extending this method to higher temperatures and the paucity of reproducibility studies at room temperature, check centrifugations were made with UO_2F_2 at 30°C for a number of concentrations. The precision was satisfactory.

[2] J. S. Johnson and K. A. Kraus, *J. Am. Chem. Soc.* (in print); J. S. Johnson and K. A. Kraus, *Chem. Quar. Prog. Rep. Sept. 30, 1952*, ORNL-1432, p. 4; J. S. Johnson and K. A. Kraus, *Chem. Quar. Prog. Rep. Dec. 31, 1952*, ORNL-1482, p. 7.

These results are to be published separately. It will only be mentioned here that they do not radically differ from those previously reported.[3] However, the heat of dimerization of uranyl fluoride given earlier is now believed to be too high. The newer data indicate that ΔH of dimerization is close to zero between 0 and 30°C.

STUDY OF HYDROLYTIC POLYMERS WITH AN ULTRACENTRIFUGE

K. A. Kraus R. W. Holmberg
J. S. Johnson

Study has been resumed[4] on the problem of interpretation of equilibrium centrifugation data dealing with low-molecular-weight polymers carrying an unknown, and possibly high, charge. Two approaches are being used:

1. An experimental study is being made of the aqueous $BaCl_2$-HCl system for which the necessary activity coefficients are known.[5] Centrifugations have been carried out and the pertinent partial specific volumes have been determined. Calculations are now in progress to check the results against theory.

2. In cooperation with the Mathematics Panel, calculations are being carried out to determine what observations would be expected at sedimentation equilibrium for certain typical polymers under different conditions. The conditions of particular interest are effect of ionic strength, charge of the polymer, concentration of the polymer, and the molecular weight of the supporting electrolyte.

The calculations indicate that charge effects can indeed be very serious if molecular weights are calculated by the traditional methods, which essentially involve the slope of a plot of log $(dn/dx)/x$ vs. x^2, where dn/dx is the refractive index gradient and x is the radius of rotation.[6] For example, a molecular weight of 300 would be obtained if a polymer of molecular weight ca. 1000 carrying a charge of 8 were centrifuged under typical experimental conditions. At the same weight concentration, a polymer of twice this weight and with a charge of 16 would give a molecular weight of about 400. Since the number of charges per particle is usually unknown, one is obviously faced with very serious problems in trying to determine molecular weights. Discrepancies result (1) from the fact that assumptions made in the equations usually used for interpretation are inapplicable, (2) from disturbance of supporting electrolyte distribution by the polymer, and (3) from uncertainties connected with converting (observed) refractive index gradients to concentration gradients.

A few calculations are being carried out to determine the experimental conditions under which protein molecular weight determinations would be seriously affected.

The implications of the results on this method of studying low-molecular-weight inorganic polymers have not been completely evaluated. In the cases where the polymers are not highly charged, it seems possible to establish this fact by means of experiments under different conditions of ionic strength, concentration, and media, supplemented with data on concentration distribution with the use of partition cells. These can then be handled fairly well by the standard methods. The same type of data should, in principle, allow elucidation of the more highly charged species, especially if there is some knowledge of the number of charges per "monomeric" unit. However, this is more difficult, especially with the refractive index technique in use at present.

ANION EXCHANGE STUDIES

F. Nelson K. A. Kraus

The systematic survey of the anion exchange behavior of metals in hydrochloric acid solutions was continued, and the results with the elements, titanium, vanadium, chromium, palladium, iridium, and platinum, are summarized below. In addition, an interesting application of these anion exchange studies to the separation of short-lived radioactive daughters has been made in collaboration with E. C. Campbell of the Physics Division. A summary of this work is given below in Section 6.

All work was carried out at room temperature with the same batch of strong-base anion exchange resin, Dowex-1, which was used in the earlier work.

---

[3] J. S. Johnson and K. A. Kraus, *Chem. Quar. Prog. Rep. March 31, 1952*, ORNL-1285 p. 8.

[4] J. S. Johnson and K. A. Kraus, *Chem. Quar. Prog. Rep. Dec. 31, 1951*, ORNL-1260, p. 1.

[5] H. S. Harned, private communication.

[6] O. Lamm, *Arkiv Kemi, Mineral. Geol.* 17A, Paper 25 (1944).

1. Titanium

a. **Ti(IV).** The adsorbability of Ti(IV) from strong HCl solutions was studied by the equilibrium method with (initially) 1.3×10^{-3} *M* Ti(IV) solutions. The Ti(IV) solutions were prepared from analytical grade Ti(III) chloride solutions by oxidation with peroxide and back-titration with Ti(III). Titanium concentrations were determined colorimetrically before and after equilibration (*ca.* 62 hr) with the peroxide method.[7] A Beckman Model DU spectrophotometer was used and optical densities measured near 410 mμ.

The observed distribution coefficients are given in Table 2. No distribution experiments were carried out for *M* HCl < 8.9 since at low hydrochloric acid concentrations, Ti(IV) tends to precipitate, probably due to hydrolysis. No slow precipitation was found for *M* HCl > 9 after the solutions had been standing for several days. At these high hydrochloric acid concentrations, the titanium solutions are yellow, and the intensity of the color increases with *M* HCl, probably due to the increased concentration of chloride complexes. In column experiments Ti(IV) was found to adsorb as a yellow band, indicating that the adsorbed negatively charged complex (or complexes) is also yellow.

b. **Ti(III).** The adsorbability of Ti(III) was studied by the column method in 9 and 12 *M* HCl. Titanium concentrations were determined in the effluent by the peroxide method. Ti(III) was found to be very slightly adsorbed. Thus, $E = 1.1$[8] was found in 12 *M* HCl by using a 17.2 cm × 0.21 cm^2 column. Although Ti(III) is slowly oxidized to Ti(IV), such reaction has negligible influence on the determination of E of Ti(III), since Ti(IV) is strongly adsorbed under these conditions and remains as a yellow band at the top of the column.

TABLE 2. ADSORBABILITY OF Ti(IV)

HCl (*M*)	*D**
8.9	0.6
9.9	2.6
10.8	14.3
11.7	66

*The experiments were carried out at less than 3% loading (L), where L is defined by the equation $L = n\ m_r/C$, where n is the charge of the adsorbed ion (assumed $n = 1$), m_r is the concentration of the ion in the resin phase, and C is the capacity of the resin in the same units as m_r.

[7] See, e.g., N. L. Allport, *Colorimetric Analysis*, Chapman and Hall, London, 1945.

[8] E is the elution constant which was earlier defined [K. A. Kraus and G. E. Moore, *J. Am. Chem. Soc.* 73, 9 (1951)] by the equation $E = dA/V$, where d is the distance (cm) the band maximum travels after V cc of eluent have passed through a column of cross-sectional area A cm^2.

2. Vanadium

a. **V(V).** Vanadium(V) solutions were prepared by dissolving ammonium vanadate in HCl or by dissolving vanadium metal in aqua regia and fuming repeatedly with HCl. In the latter case large amounts of V(IV) are formed. In strong hydrochloric acid solutions V(V) forms an intensely brown solution. When vanadium is in the form of this brown complex, it can be strongly adsorbed by the anion exchange resin and will yield a dark-brown band. Estimates of the elution constant of V(V) in 9 and 12 *M* HCl were obtained by first adsorbing a large amount of V(V) on a 4.0 cm × 0.25 cm^2 column, eluting with 9 or 12 *M* HCl, and averaging the distance that the upper and lower adsorption edges traveled. The approximate values $E = 0.02$ and 0.005 were found for 9 and 12 *M* HCl solutions, respectively. These correspond to distribution coefficients on a weight basis of 100 and 400, respectively.

b. **V(IV).** The adsorbability of V(IV) was studied in the range 1 to 12 *M* HCl, and no region was found where considerable adsorption occurred. Best adsorption was found in 12 *M* HCl where E of V(IV) is approximately 1.15. This adsorption is sufficient to permit separation from nonadsorbable elements if relatively long columns (e.g., 50 cm long) are used.

The V(IV) solutions were prepared by permitting V(V) solutions to reduce partially with concentrated HCl and then separating the oxidation states by passing the mixture through a small Dowex-1 column. Unreduced V(V) remained on the column, while the effluent was a pure V(IV) (blue) solution. The reduction of V(V) by HCl appears to be increased when adsorption by the resin takes place. Passing concentrated HCl solutions over the V(V) bands causes relatively rapid and complete reduction. This effect is probably connected with the fact that chlorine (as well as other halogens) is strongly adsorbed by the resin, while V(IV) is not appreciably adsorbed.

c. V(III). Solutions of V(III) were prepared by reduction of V(IV) solutions with stannous chloride. The adsorbability of V(III) was studied by the column method and only slight adsorption occurred. In 12 *M* HCl, E = 1.3 was found.

3. Chromium

Cr(III) was earlier reported[9] not to be appreciably adsorbed from strong hydrochloric acid solutions. A reinvestigation essentially confirmed these results, although it was found that under some conditions sufficiently strong adsorption of Cr(III) takes place to permit its removal from nonadsorbable elements. Thus, in general, elution in 12 *M* HCl yields with Cr(III) two separate bands, one of which moves with an elution constant E = 2.4 and one which moves with E = 1.3. If Cr(III) solutions are heated for several minutes at 100°C in 12 *M* HCl in a small glass bomb, essentially all chromium is converted to a species moving with E = 1.3 at this acidity. This slightly adsorbed band moves somewhat more rapidly at lower hydrochloric acid concentrations (E = 1.4 in 9 *M* HCl), which indicates that the adsorbable species is in equilibrium with some nonadsorbable species. This behavior is somewhat surprising, since these species, in turn, are apparently not in equilibrium with lower chloride complexes.

[9] G. E. Moore and K. A. Kraus, *J. Am. Chem. Soc.* 72, 5792 (1950).

4. Separation of Titanium, Vanadium, and Iron

As described in Section 1, titanium is sufficiently strongly adsorbed to permit its ready separation from other elements. To demonstrate the procedure, the separation of titanium, vanadium, and iron was carried out with an 18.6 cm × 0.49 cm^2 column of Dowex-1 using a 1 ml sample containing 0.05 *M* V(IV), 0.018 *M* Ti(IV), and 0.025 *M* Fe(III) in 12 *M* HCl. As shown in Fig. 2, the separation of these three elements is satisfactory, V(IV) appearing rapidly in the effluent in 12.1 *M* HCl, Ti(IV) being eluted in a reasonably narrow band near 9 *M* HCl, under which condition Fe(III) is still held strongly on the column.[3] Fe(III) was removed with 1.0 *M* HCl.

5. Palladium, Iridium, and Platinum

Some of the earliest experiments on anion exchange of negatively charged complexes were carried out with the platinum elements by Nachod and Sussman,[10,11] who suggested this method for

[10] F. C. Nachod, U. S. Patent 2,371,119 (March 6, 1945) to Permutit Co.

[11] S. Sussman, F. C. Nachod, and W. Wood, *Ind. Eng. Chem.* 37, 618 (1945).

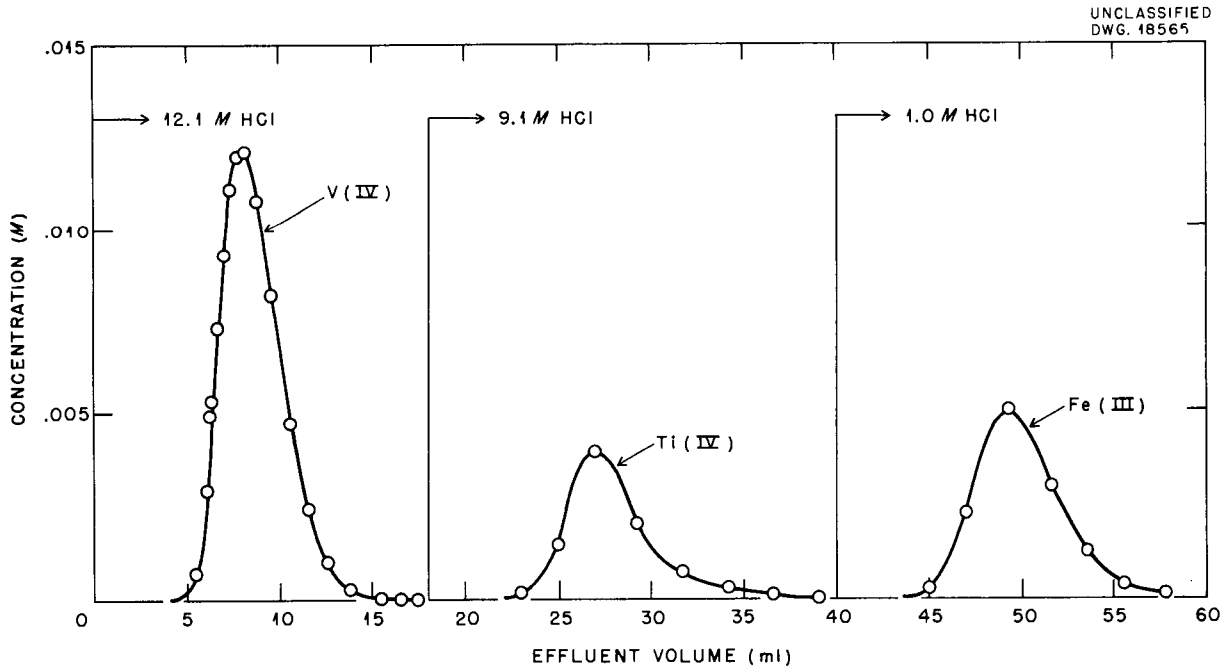

Fig. 2. Separation of V(IV), Ti(IV), and Fe(III) by Anion Exchange. 18.6 cm × 0.49 cm^2 Dowex-1 column, 1 ml: 0.05 *M* V(IV), 0.018 *M* Ti(IV), 0.025 *M* Fe(III) in 12 *M* HCl.

the isolation of certain elements. They found that platinum, gold, and other elements which form very stable negatively charged complexes are adsorbed by various anion exchange materials, including certain weak-base synthetic exchangers. Most of the complexes which have been discussed in the present and earlier papers were relatively weak and could be decomposed by decreasing (or changing) the concentration of the ligand. Thus, a simple method for controlling the degree of adsorption became available, since a minor change in the composition of the solution can cause a change from strong adsorption to rapid elution. The complexes studied by Nachod and Sussman were very stable and usually were not in rapid equilibrium with neutral or positively charged species. Hence, for those elements, the removal of the complexes from the resin by decreasing the ligand concentration is essentially precluded. Instead, a decrease in the concentration of the ligand generally will cause an increase in adsorbability.

a. **Pd(II).** The adsorbability of Pd(II) was studied by the equilibrium method in the range 0.1 to 12 *M* HCl by using a spectrophotometric method of analysis. Pd(II) has an absorption band in the visible region with maximum located near 475 mμ for HCl concentrations from 1 to 12 *M*. In this HCl range, the spectrum is essentially constant, showing only minor changes in the extinction coefficients of this band with change in *M* HCl. For *M* HCl < 1 the spectrum is different, indicating a change in species. The absorption maximum is located near 450 mμ in 0.1 *M* HCl and near 420 mμ in 0.002 *M* HCl. In addition, at low acidities the spectrum changes slowly with time.

Pd(II) was found to be strongly adsorbed throughout the experimental range, as shown in Table 3, with distribution coefficients D decreasing with increasing hydrochloric acid concentration. Unfortunately, even in concentrated hydrochloric acid, the adsorbability of this element is still sufficiently large to preclude its easy removal from the resin. The continued rapid decrease of D_{Pd} suggests that reasonably rapid elution might be achieved with more concentrated hydrochloric acid solutions, e.g., solutions where the partial pressure of HCl is greater than 1 atmosphere.

The removal of palladium in a relatively narrow band without excessive tailing was achieved by displacement with other strongly adsorbed complexes, e.g., cadmium chloride[12] in HCl or zinc chloride in HCl. Thus, by using 1 *M* $CdCl_2$ in 6 *M* HCl, palladium was essentially completely removed from a 4 cm × 0.25 cm^2 column in about seven column volumes at 88°C.

b. **Pt(IV).** The adsorbability of Pt(IV) was studied by the equilibrium method in the range 0.1 to 12 *M* HCl by using a spectrophotometric method of analysis and utilizing the absorption region between 350 and 450 mμ. The position of the absorption maximum, which lies below 350 mμ, was not investigated.

Pt(IV) was strongly adsorbed throughout the whole experimental range and, as in the case of Pd(II), the distribution coefficients decreased with increasing hydrochloric acid concentration

[12] Cadmium chloride has been found to be strongly adsorbed from dilute and concentrated HCl solutions in a manner similar to Zn(II), although its adsorption starts at a lower *M* HCl than that of Zn(II).

TABLE 3. ADSORPTION OF Pd(II) AND Pt(IV) FROM HCl SOLUTION

HCl (*M*)	Pd(II)		Pt(IV)	
	D	Loading* (%)	D	Loading* (%)
0.10	1600	85	> 10,000	55
1.0	870	50	5,560	26
4.0	300	20	2,480	28
7.9	79	5	914	16
11.6	40	3	440	10

*For definition of L, see footnote Table 2. D is expected to increase considerably with decreasing L when L is larger than a few per cent. For calculation of L assumed charge $n = 2$.

(see Table 3). The adsorbability of Pt(IV) was considerably larger than that of Pd(II).

c. Iridium – Separation of Iridium from Palladium and Platinum. The adsorbabilities of Ir(III) and Ir(IV) were studied in the range 0.1 to 11.5 *M* HCl by the equilibrium and column methods using spectrophotometric and radiometric (Ir^{192}) methods of analysis.

Ir(IV) was found to be strongly adsorbed throughout this hydrochloric acid concentration range. Ir(III), on the other hand, showed negligible adsorption in this range but showed some adsorption at lower hydrochloric acid concentrations.

The low adsorbability of Ir(III) intrinsically permits the separation of this element from other "platinum elements." For example, a 0.03 *M* platinum solution was heated with iridium tracer (using Ir^{192}) in aqua regia, then fumed with hydrochloric acid to remove the nitric acid. During the fuming, Ir(III) is apparently formed. After making the solution 10 *M* in HCl, a 0.5 ml sample was placed on an 8.0 cm × 0.25 cm^2 column. Approximately 99% of the iridium tracer appeared in the first few column volumes of effluent, while Pt(IV) was held tightly as an orange band at the top of the column. Similar results were found with a 10 *M* HCl solution which was 0.03 *M* in Pd(II) and contained Ir^{192} tracer. Only about 1% of the iridium remained on the column after three column volumes of 10 *M* HCl had been passed through it, as determined by counting the small column directly in a "re-entrant hole" sodium iodide scintillation counter.

By combining these observations on iridium with the technique of eluting with strongly adsorbed complex ions, as discussed in the section on Pd(II), the separation of iridium and palladium, described in Fig. 3, was carried out. A solution, 0.1 ml of Pd(II), 0.04 *M* and containing Ir^{192} tracer was placed on a 4.0 cm × 0.25 cm^2 column. Iridium rapidly appeared in the effluent with 6 *M* HCl. Pd(II) was eluted in a reasonably sharp band with 6 *M* HCl–1 *M* $ZnCl_2$.

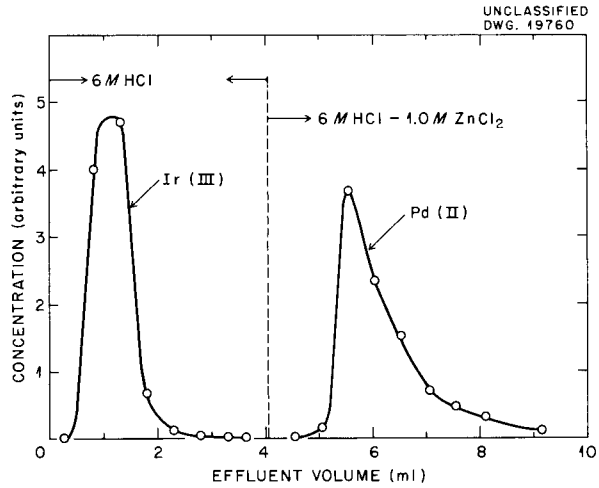

Fig. 3. Separation of Iridium and Palladium. 4.0 cm × 0.25 cm^2 Dowex-1 column, 0.1 ml 0.04 *M* Pd(II), tracer Ir^{192}, 90°C, flowrate ca. 0.8 cm/min.

6. Separation of 0.82 sec Pb^{207} from Bi^{207}

Experiments have recently been performed[13] in which the short-lived Pb^{207} daughter of Bi^{207} was shown to exist and to be rapidly separable from the Bi^{207} parent by anion exchange. The separation makes use of the fact that Bi(III) in hydrochloric acid solution is strongly adsorbed, i.e., D = ca. 5 × 10^4 in 0.5 *M* HCl, decreasing to D = 60 in 12 *M* HCl, while Pb(II) is weakly adsorbed, i.e., the adsorbability of Pb(II) increases with HCl concentration to a slight maximum near 1 *M* HCl (D = ca. 20) and then decreases. Thus, when Bi^{207} was adsorbed from hydrochloric acid solution on a small column (ca. 0.2 ml) and 0.5 *M* HCl was rapidly passed through it, the short-lived Pb^{207} daughter could be detected in the effluent in satisfactory yield and with very little "background" contamination of the long-lived Bi^{207} parent.

CHEMISTRY OF CORROSION

G. H. Cartledge

Studies on Electrode Potentials

R. P. Yaffe

The experiments on the electrode potential of stainless steel under varying conditions previously reported[14] were extended to solutions of 0.1 *N* sulfuric acid to which foreign salts were added. The potential of a composite electrode of low chemical activity, such as stainless steel, is doubtlessly determined by a number of anodic and cathodic local-action processes occurring with

[13] E. C. Campbell and F. Nelson, *Phys. Quar. Prog. Rep. Dec. 20, 1952*, ORNL-1496, p. 8.

[14] R. P. Yaffe, *Chem. Quar. Prog. Rep. Dec. 31, 1952*, ORNL-1482, p. 53.

rates that are subject to the conditions prevailing at the interface between the metal and its immediate environment. It is therefore possible that a survey of the influence of added ions of a wide range of types may shed light on the details of the processes responsible for the electrode potential.

Potential measurements were made with a vibrating-reed electrometer and a Brown recorder by using a Ag,Ag_2SO_4 reference electrode and bridges containing 0.1 N H_2SO_4. All measurements were referred to the saturated calomel electrode.

The electrodes were made from type 347 stainless steel 10-mil sheet. The exposed surface was a square, 1 cm on an edge; the connecting lead was painted with Glyptal to prevent effects caused by an air-liquid surface. The experiments were conducted at 85 ± 1°C, and the solution was continuously and vigorously stirred, with free access of air. Since the work previously reported showed that the ennobling effect of conventional passivating treatments is quickly lost under the conditions of these experiments, the electrodes were prepared exclusively either by hand-polishing with 600 grit abrasive paper or by electropolishing.

Preliminary experiments showed that electrodes so prepared attained relatively stable potentials after being held in the acid bath at 85°C for approximately 6 hours. Thereafter, the potentials became more noble by only about 2 mv/hr, whereas the experiments usually required only 1 to 3 hr and involved potential changes of 200 mv or more. The stabilized potentials required were approximately 150 to 250 mv for electropolished electrodes and about 50 to 150 mv for hand-polished electrodes.

Standardized solutions of the various salts were prepared in 0.1 N H_2SO_4. The cations were all introduced as sulfates, with the exception of $PtCl_6^{--}$. In each experiment, a pair of new electrodes was used, one being hand-polished and the other being electropolished. In later experiments, a platinum electrode was also included for reference. After stabilization of the electrodes, the salt solution was added in increments to produce concentrations up to 10^{-3} f, and after each addition, sufficient time was allowed for the potentials to become stabilized again. A number of experiments have been performed with each salt. The majority of the salts investigated produced no detectable effect; the reducing salt, stannous sulfate, debased the potential; and several ions had ennobling effects. Figures 4, 5, and 6 illustrate three types of ennobling behavior observed; Tables 4 and 5 summarize the experiments completed so far.

It was quite generally found that, for the salts which ennoble the electrodes, the potentials rise linearly with the logarithm of the concentration of the added salt. The slopes of these curves may be expressed as RT/nF, in which n is usually close to either 1 or 0.5. The n value, however, is not always related in any obvious manner to the valence changes characterizing the redox system of the added salt alone. When the added salt was progressively removed and replaced by fresh acid, the potentials usually fell along curves showing hysteresis types of effect.

Studies with radioactive silver indicated that, at the conclusion of an experiment, the electrodes retained an amount of silver sufficient to form a monomolecular layer if the silver were uniformly distributed, which is doubtlessly not the case. From Fig. 6, it appears that even the minute amount of

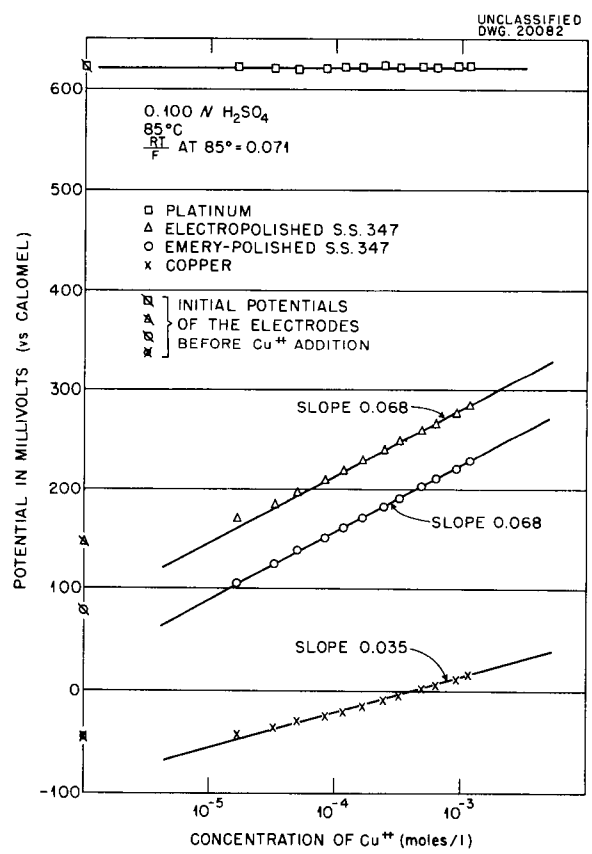

Fig. 4. Electrode Potentials at 85°C vs. Saturated Calomel Electrode at 25°C in Presence of Added Cupric Sulfate.

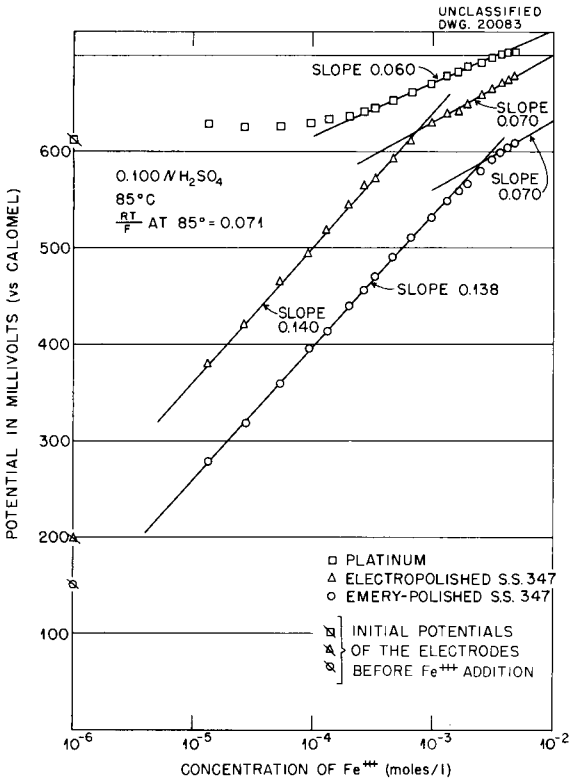

Fig. 5. Electrode Potentials at 85°C vs. Saturated Calomel Electrode at 25°C in Presence of Added Ferric Sulfate.

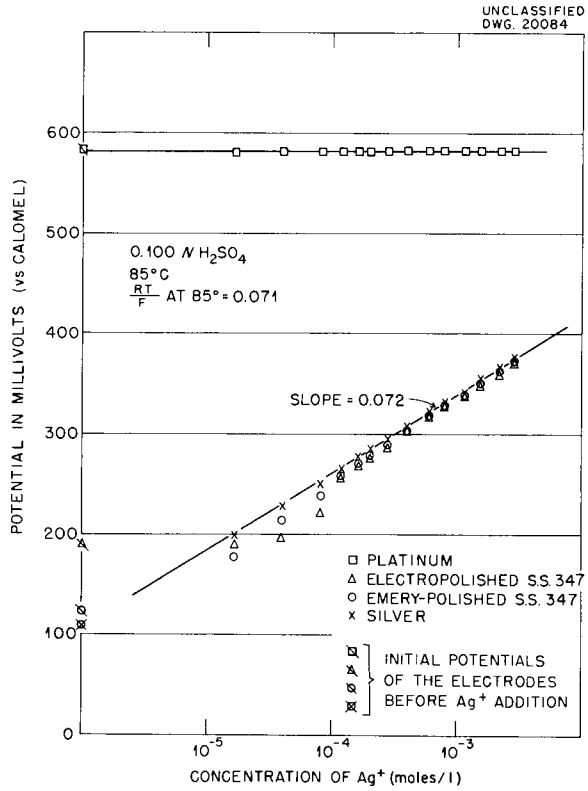

Fig. 6. Electrode Potentials at 85°C vs. Saturated Calomel Electrode at 25°C in Presence of Added Silver Sulfate.

TABLE 4. SUMMARY OF OBSERVATIONS ON ELECTRODE POTENTIALS – IONS WITHOUT SIGNIFICANT EFFECT

IONS	CONCENTRATION RANGE (f)	COMMENTS
Cl^-, Na^+, Tl^+, Ca^{++}, Cd^{++}, Mn^{++}, Ni^{++}, Cr^{+++}, Ce^{+++}	3×10^{-5} to 2×10^{-3}	
Pb^{++}	1×10^{-8} to 9×10^{-7}	Limited by solubility
Bi^{+++}	1×10^{-7} to 5×10^{-4}	Limited by solubility
Zn^{++}, UO_2^{++}, La^{+++}	3×10^{-5} to 2×10^{-3}	Gave slight effects, possibly because of impurities

TABLE 5. SUMMARY OF OBSERVATIONS ON ELECTRODE POTENTIALS – IONS WITH ENNOBLING EFFECT AND WITH DEBASING EFFECT

IONS	CONCENTRATION (moles/liter)	POTENTIAL (mv)									COMMENTS
		Hand-polished Electrodes			Electropolished Electrodes			Platinum Electrodes			
		Initial	Final	RT/nF*	Initial	Final	RT/nF	Initial	Final	RT/nF	
Ions with Ennobling Effect											
Ag^{+}	5×10^{-6} to 4×10^{-3}	150	350	0.07	250	350	0.07	580	580	0.00	Slope of hand-polished and electropolished electrodes was occasionally 0.08 to 0.09 at high-concentration end of graph; temperature studies indicated that slope has theoretical temperature dependence; a pure silver electrode in the same solution had an RT/F slope and a potential identical with that of the steel electrodes
Cu^{++}	3×10^{-6} to 1×10^{-3}	50	200	0.07	100	300	0.07	620	620	0.00	A pure copper electrode in same solution had an $RT/2F$ slope and a potential 200 mv lower than that of the steel
Fe^{+++}	1×10^{-5} to 5×10^{-3}	100	600	0.13 to 0.15 and 0.065 to 0.075	200	700	0.13 to 0.14 and 0.065 to 0.075	600	700	0.055 to 0.06	For hand-polished and electropolished electrodes, the $RT/\frac{1}{2}F$ slope was observed first, with a definite break to RT/F at higher concentration; reversal (removal of Fe^{+++}) gave both slopes with hysteresis effects
Hg_2^{++}	2×10^{-7} to 8×10^{-5}	100	400	0.12 to 0.13 and 0.06 to 0.07	200	400	0.12 to 0.14 and 0.07	Not studied			For hand-polished and electropolished electrodes, the $RT/\frac{1}{2}F$ slope was observed first, with a break to RT/F at higher concentration; reversal gave only the RT/F slope
Hg^{++}	6×10^{-7} to 2×10^{-4}	200	400	0.065 to 0.075	250	400	0.07	550	650	0.05 to 0.07	RT/F slope, but hand-polished electrode was erratic
Zr^{4+}	3×10^{-5} to 3×10^{-3}	100	150	0.07	200	300	0.07	500	500	0.00	RT/F slope for steel; zero for platinum
Pt^{4+}	2×10^{-6} to 7×10^{-4}	100	550		250	400	0.07 to 0.075	550	600	0.065 to 0.075	RT/F slope was stable for electropolished and platinum electrodes; hand-polished electrode was ennobled several hundred millivolts, but response was erratic and unreproducible; removal of Pt^{4+} gave RT/F slope for both steel electrodes
CrO_4^{--}	3×10^{-3} to 1×10^{-3}	200	500	0.13 to 0.14	250	500	0.13 to 0.14	Not studied			$RT/\frac{1}{2}F$ slope; removal of CrO_4^{--} gave hysteresis effects
Ion with Debasing Effect											
Sn^{++}	3×10^{-5} to 2×10^{-3} f	125	75	−0.03	200	100	−0.03	450	200	−0.075	The two steel electrodes had slopes of approximately $-RT/2F$, while the platinum electrode had a slope of $-RT/F$

*RT/F at 85°C = 0.071.

silver deposited is sufficient to make the steel electrodes function essentially like the silver electrode. It may be noted that cupric sulfate produced an ennobling of the steel with a slope of RT/F (one electron), whereas the pure copper electrode in the same solution had the conventional two-electron slope. Furthermore, the potentials of the steel electrodes were approximately 200 mv more noble than the potential of the copper electrode. In none of the experiments were the surfaces of the electrodes visibly altered. The experiments will be extended to include a few more cations and several anions.

Action of Corrosion Inhibitors

G. H. Cartledge R. P. Yaffe

It was previously reported[15] that the pertechnetate ion, TcO_4^-, is an effective inhibitor of corrosion under a variety of conditions. A summary of the earlier experiments was issued in February 1953.[16] These tests were continued and the work was broadened to include a number of the elements adjacent to a line through chromium, technetium, and osmium in the periodic system.

Tests on SAE 1010 carbon steel in water alternately at 100°C and at room temperature ran for a total of 23 weeks. At a concentration of 5×10^{-4} f $KTcO_4$ (50 ppm of technetium), there was no detectable corrosion, even with 10 ppm of chloride ion present. A control specimen (no technetium) was discarded at the end of 12 weeks, at which time the loss in weight of the 0.5-g specimen had reached 48.5 mg.

The corrosion of carbon steel by water is inhibited even at 250°C. Specimens weighing about 0.25 g were mounted in a Teflon block contained in platinum-lined bombs. To one bomb, 100 ppm of technetium, as $KTcO_4$, was added and the bombs were held at 250°C in a salt bath for 93 hours. At the end of this time, the control specimen had lost 9.0 mg; the solution remained water-clear in the bomb containing the pertechnetate, and there was no change in weight of the specimen (± 0.1 mg).

Tests on type 347 stainless steel in uranyl sulfate (300 g of uranium per liter) were made in fused silica tubes held at 250°C. In the first tests, the tubes were largely deaerated before being sealed. In this case, the technetium gave definite inhibition for 74 hr, whereas a precipitate quickly formed in the uninhibited solution. In a second test, hydrogen peroxide was added to the uranium solution in sufficient quantity to produce an oxygen pressure of about 50 psi. In this one test, technetium did not produce significant inhibition. Dynamic loop tests will be required to determine the possible benefit of technetium in areas on which oxide films are prevented from forming by gas bubbles or turbulence.

Most of the recent work was devoted to studies relating to a more detailed understanding of the action of corrosion inhibitors of the XO_4^{n-} type. According to the theoretical considerations that led to the discovery of the inhibition by the pertechnetate ion, it is the unreduced XO_4^{n-} particle adsorbed at the metal surface that has the effect in question. If the ion is reduced, for example, to a film of solid TcO_2 or Cr_2O_3, this film may or may not affect the corrosion rate, depending upon its properties. Means were therefore sought to differentiate experimentally between reduced and permanently deposited technetium, on the one hand, and dynamically adsorbed ions, on the other hand.

With both carbon steel and stainless steel, the amount of technetium that remains on the uncorroded metal after it is washed and dried is highly dependent upon the condition of the surface of the metal. Thus, on carbon steel (SAE 1010), beta activities from less than 100 counts/min/cm^2 to 2×10^6 counts/min were observed, with complete inhibition in both cases. The specimen corroded in either case, however, when it was subsequently exposed either to a moist atmosphere or to water containing no technetium. It may be calculated that, on the counter used, approximately 2×10^7 counts/min correspond to 1 mg of technetium in a very thin film. This indicates that activities of less than 3400 measured counts/min/cm^2 correspond to less than a monomolecular film of deposited technetium. Hence, it is evident that the permanent film may be far from a complete covering in an inhibited condition, whereas inhibition does not persist in the absence of unreduced ions, even when a visible film of considerable thickness is present.

Autoradiograms of the technetium deposited under a variety of conditions were made; an example is

[15] G. H. Cartledge, *Chem. Quar. Prog. Rep. Dec. 31, 1952*, ORNL-1482, p. 54.

[16] G. H. Cartledge, *Summary of Experiments on the Inhibition of Corrosion by the Pertechnetate Ion*, ORNL CF-53-2-234 (Feb. 24, 1953).

shown in Fig. 7. The figure represents a specimen of stainless steel which was partly polished and then scratched with a file before digestion in an acidic solution containing the pertechnetate ion. The autoradiogram shows that the technetium was selectively deposited in the scratches on the chemically more active metal.

Other experiments of a different type have been initiated to elucidate the inhibitory action more thoroughly. By following a technique devised by Chyzewski and Evans,[17] an electrolytic cell was set up which had three compartments made of Lucite and separated by cellophane diaphragms. A carbon-steel electrode was inserted in one compartment; the other electrode was either zinc or copper. The electrolyte was potassium sulfate 0.05 to 0.10 *f*. The electrodes were connected through an ammeter having the ranges of 0 to 20 μa, 0 to 200 μa, and 0 to 2 ma. The details of the experiment will be more fully reported after the experiment has been further refined, but the following observations have already been made. When the iron was combined with the zinc electrode, the iron became the cathode, and a steady current was read on the meter. When the solution in the cathode compartment was replaced by potassium sulfate containing 0.001 *f* $KTcO_4$, the current dropped by 30 to 45%, depending upon the conditions. When the pertechnetate solution was next withdrawn and replaced by potassium sulfate alone, the current returned to its original value after several flushings. During the electrolysis, appreciable amounts of technetium were reduced to a blue or bronze film. This film remained after the removal of the technetium solution but did not prevent the current from returning to its initial value. It is therefore evident that the diminution of the cathodic current was due to the dissolved and adsorbed technetium, rather than to the oxide film. Similar experiments were performed in which the iron was anodic to copper. The results demonstrated inhibition of both the anodic and cathodic processes in the presence of the pertechnetate ions.

According to the theory being developed, inhibition is expected to result only (1) if the adsorbed particle is structurally suitable to the metal lattice, (2) if it has a high activation energy for reduction and not too high a redox potential, and (3) if there is a considerable separation of charge within the particle itself. The investigation was therefore extended to the highest oxidation states of the other elements adjacent to a line in the periodic table through chromium, technetium,

[17] E. Chyzewski and U. R. Evans, *Trans. Electrochem. Soc.* 76, 215 (1939).

Unclassified
Plate P-150

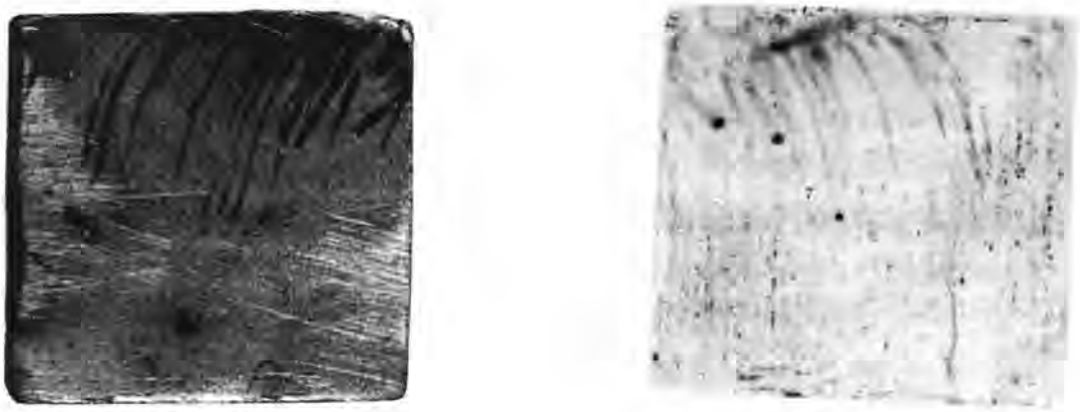

Fig. 7. Autoradiogram (right) of Stainless Steel Specimen (left) after Exposure to Potassium Pertechnetate in Sulfuric Acid at 85°C. Note that the beta activity concentrated in the scratches; also note the flaws in the metal in the rolling direction.

and osmium. This phase of the work is not complete, but more or less thorough studies were made on osmium, vanadium, molybdenum, tungsten, rhenium, and ruthenium.[18]

The tests were made by exposing test pieces of SAE 1010 steel to the solutions alternately at 100°C and at room temperature in static systems with access of air. Osmium was studied rather extensively, and it was found that a solution containing 1 g of OsO_4 per 100 ml "passivates" steel at room temperature without the formation of a visible film; that is, a piece of steel cleaned and dipped in the osmium solution for a few seconds failed to liberate copper from a cupric sulfate solution. At 100°C, the results depended upon the concentration of the solution. Solutions containing 0.5 to 1.0% OsO_4 produced a thin bronze-colored film which prevented corrosion for several days. The film was very sensitive to rupture, however, and after failure, caused a severe pitting type of corrosion.

At concentrations in the range of 0.1 to 0.2% OsO_4, the steel reduced the osmium to a black deposit, presumably OsO_2, and corrosion followed. The reduction proceeded rapidly at localized areas on the metal, again leading to pitting. Experiments showed that the black film, or deposit, becomes cathodic and has a sufficiently high conductivity to become plated with copper when the partially corroded specimen was immersed in a suitable solution of cupric sulfate. Complete inhibition resulted when a specimen that had failed in the osmium solution was transferred to a solution containing 50 ppm of technetium.

The provisional results on the remaining elements studied may be summarized as follows. A saturated solution of vanadium pentoxide was prepared by long agitation at room temperature. Chloride ion at a concentration of 10 ppm was added, and portions of the solution were adjusted to pH's of 3 and 8. In both cases, reduction to a green oxide occurred locally, followed soon by corrosion.

Similarly, a saturated solution of molybdic oxide, MoO_3, was prepared, 10 ppm of chloride ion was added, and the pH was adjusted to 8.5. There was temporary inhibition (10 hr at 100°C and overnight at 23°C) followed by formation of a heavy film and progressive corrosion. More dilute solutions failed sooner.

Sodium tungstate was prepared at concentrations of 0.1, 0.01, and 0.001 *f*, with 20 ppm of chloride. The two more concentrated solutions (pH's 9 and 7) gave complete protection for the three weeks the test was in progress; no visible film was formed. The specimen in 0.001 *f* solution is corroding in two small areas.

Rhenium was used as a 0.003 *f* solution of potassium perrhenate, $KReO_4$. At 100°C, the solution was rapidly reduced to a black oxide, and corrosion proceeded rapidly.

Ruthenium was used as a solution of RuO_4 containing approximately 0.8 g of RuO_4 per 100 ml and as dilutions thereof. All solutions were rapidly reduced to a black oxide, and corrosion was greatly accelerated.

In one experiment, a specimen was exposed in a solution containing both OsO_4 (0.4%) and technetium (50 ppm). In this case, there was apparently a synergistic action, in that a visible but unweighable amount of osmium was reduced to a bronze film and no technetium count was obtained until the sixth day, when about 75 counts/min/cm^2 was observed.

Future work will include a more exact study of the separate processes involved in the action of technetium at iron anodes and cathodes separately. It is also planned to devote more study to the other elements, especially to rhenium, in order to clarify more explicitly the role of the specific properties of the ions responsible for their inhibitory properties.

Hydrogen Overvoltage on Amalgams

W. E. Clark

An investigation of the hydrogen overvoltage characteristics of amalgams was recently undertaken, and equipment for making the necessary measurements is being assembled. Attempts will be made to correlate the Tafel overvoltage equation with the rate constant in the equation expressing the kinetics of the spontaneous decomposition of alkali-metal amalgams in aqueous systems.

THERMODYNAMICS OF BORON NITRIDE

A. S. Dworkin D. J. Sasmor
E. R. VanArtsdalen

Considerable interest is attached to boron nitride because it is not only isoelectronic with graphite but its crystal lattice parameters are very similar

[18] W. D. Robertson, *J. Electrochem. Soc.* **98**, 94 (1951), and others have shown that the ions MoO_4^{--} and WO_4^{--} are inhibitors in tests made at room temperature.

to those of graphite, and it resembles graphite in being very refractory and having lubricating properties. Although these substances possess remarkable similarity, there are two very noteworthy differences; namely, boron nitride is white and is an electrical insulator, while graphite is black and is a conductor, which indicates considerable differences in the mobility of at least certain of the electrons in boron nitride and graphite. In recent years, much interest has developed in the chemistry of boron-nitrogen six-membered ring compounds, borazole and its derivatives. Recently, the heat of formation of B-trichloroborazole was determined[19] and some rough estimates were made of bond strengths in this compound. Boron nitride represents the ultimate in giant boron-nitrogen fused rings. Therefore, it seemed to be particularly desirable to determine the low-temperature heat capacity and the heat of formation of boron nitride in the hope that these properties would have not only practical significance but also theoretical implications.

Low-Temperature Heat Capacity

Experimental. The heat capacity of microcrystalline boron nitride was measured in the temperature range of 15 to 300°K by using an adiabatic calorimeter at the K-25 laboratories; the calorimeter has been described by Oliver and Grisard.[20] The actual calorimeter can was fabricated of copper, was heavily silver plated, and had a reentrant well for the heater and platinum resistance thermometer. The cover was made the full size of the top of the can to facilitate easy filling. A fine copper tube was silver-soldered to the cover for purposes of evacuation and admission of helium. The temperature scale was established by using a platinum resistance thermometer which had been calibrated from 10°K to 500°C by the National Bureau of Standards. Heat capacities were obtained by measuring the temperature rise produced by supplying a carefully measured quantity of electrical energy to the calorimeter heater. The relation 1 cal = 4.1840 abs. joules was used to convert electrical to thermal energy. The calorimeter can weighed 56.3980 g, including thermometer and heater, and it was calibrated by making adiabatic runs from 12°K to room temperature. Liquid hydrogen was the refrigerant below 50°K, and liquid nitrogen was used above this temperature. After calibration, the can was charged with 20.1034 g of finely powdered and carefully dried boron nitride. About 3 to 5 mm of helium at room temperature was admitted to the can in order to ensure sufficiently rapid heat transfer.

The sample of boron nitride used in these studies was supplied by C. T. Henson of the Norton Company. Both spectroscopic and wet chemical analyses at ORNL showed that this boron nitride contained 1.5% of iron as Fe_3O_4; and, indeed, the sample was very slightly magnetic. X-ray investigation indicated that the boron nitride was satisfactorily microcrystalline, for good agreement was obtained with the data given by Pease,[21] and this indicated that the sample was only very slightly less well crystallized than the one reported by him. For the purposes of these studies, recrystallization did not seem to be warranted since such small imperfections as did exist could not have caused observable effects in heat capacity or heat of formation data.

Results and Discussion. Nine separate series of determinations of heat capacity were made – two in the liquid-hydrogen range and the others in the liquid-nitrogen range. The temperature rise of each individual heat-capacity measurement was approximately 6 to 8 degrees. The raw data were corrected for the presence of the impurity, Fe_3O_4, by making use of Millar's[22] determination of the heat capacity of Fe_3O_4. By taking the analytical result of 1.50% Fe, a presumed mole of BN (24.828 g) was calculated to contain 0.9793 mole of BN and 0.002222 mole of Fe_3O_4. Thus, to compute the true molar heat capacity, 0.002222 times the heat capacity of Fe_3O_4 was subtracted from the raw data and the result was multiplied by 1/0.9793. A small-scale graph showing C_p for BN is given in Fig. 8. The high-temperature measurements are by Magnus and Danz,[23] and, as shown by the dotted line, the two sets of data extrapolate into each other smoothly.

---

[19] E. R. Van Artsdalen and A. S. Dworkin, *J. Am. Chem. Soc.* 74, 3401 (1952).

[20] G. Oliver and J. Grisard, *J. Am. Chem. Soc.* 73, 1688 (1951); G. D. Oliver, J. W. Grisard, and V. E. Anderson, *A Low Temperature Cryostat*, K-550 (Jan. 20, 1950).

[21] R. S. Pease, *Acta Cryst.* 5, 356 (1952).

[22] R. W. Millar, *J. Am. Chem. Soc.* 51, 215 (1929).

[23] A. Magnus and H. Danz, *Ann. Physik* 81, 407 (1926).

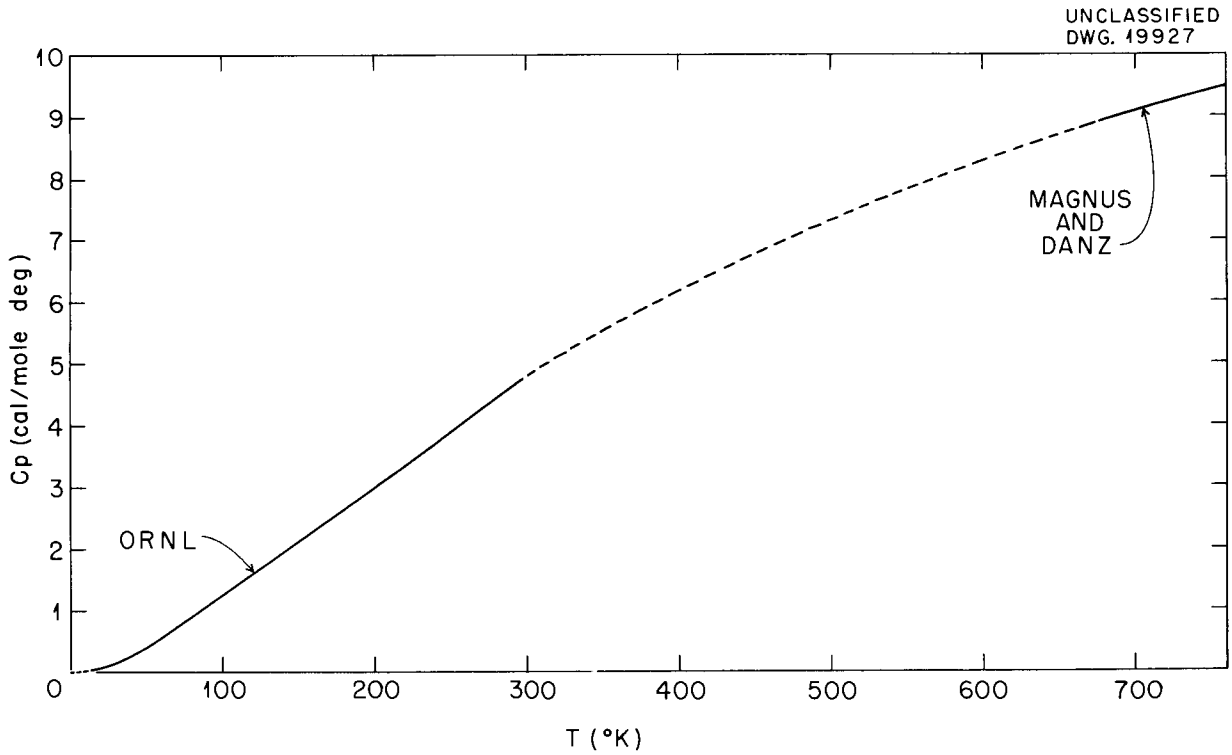

Fig. 8. Heat Capacity of Boron Nitride.

Values of the thermodynamic functions S^0, $-(F_0^0 - H_0^0)/T$, and $(H^0 - H_0^0)/T$ have been derived from the measured C_p determinations, and smoothed values of these functions, as well as C_p, are recorded in Table 6 at 10-deg intervals from 20 to 300°K. S^0 was obtained by integrating the area under a large-scale plot of C_p/T vs. T for each experimental C_p value corrected for impurity, as described above. Another large-scale plot of S^0 vs. T was made and used to evaluate $-(F^0 - H_0^0)/T$ at 10-deg intervals. $(H^0 - H_0^0)/T$ was computed from S^0 and $-(F^0 - H_0^0)/T$.

The extremely interesting discovery was made that, in the range from 20 to 65°K, the heat capacity of boron nitride follows a T^2 dependence rather than the usual Debye T^3 relationship.[24] This is shown clearly in Fig. 9, where C_v has been plotted against T^2. It is also seen from this plot that C_v extrapolates to zero at 0°K, according to the T^2 relation. C_v was calculated for each experimental C_p value by means of the equation

$$C_p - C_v = \frac{a^2VT}{\beta} \qquad (1)$$

where the coefficient of expansion, a, and the molar volume, V, were obtained from the x-ray crystallographic data of Pease.[21] Unfortunately, the compressibility coefficient, β, has not been reported for boron nitride; so it has been, admittedly, approximated to be the same as that of graphite.[25] Although this introduces some uncertainty in the values of C_v, it is not serious, for even a 20% error in β introduces a completely negligible error in the calculated value of C_v in the low-temperature range where C_p and C_v differ very slightly in absolute magnitude.

A T^2 dependence of the heat capacity of graphite[26] has also been observed, and several other

[24] A. S. Dworkin, D. J. Sasmor, and E. R. VanArtsdalen, *J. Chem. Phys.* 21, 954 (1953).

[25] T. W. Richards, *J. Am. Chem. Soc.* 37, 1643 (1915) gives for graphite $\beta = 3 \times 10^{-6}$ cm^2/kg.

[26] W. W. Tyler and W. DeSorbo, *Phys. Rev.* 83, 878 (1951).

TABLE 6. SMOOTHED THERMODYNAMIC FUNCTIONS OF BN*

T (°K)	C_p (cal/mole deg)	S^0 (e.u.)	$\frac{-(F^0 - H_0^0)}{T}$	$\frac{H^0 - H_0^0}{T}$
20	0.065	0.034	0.012_0	0.022_0
30	0.144	0.074	0.025_7	0.048_3
40	0.257	0.131	0.047_3	0.083_7
50	0.396	0.203	0.070_8	0.132_2
60	0.563	0.290	0.100_0	0.190_0
70	0.743	0.390	0.134_4	0.255_6
80	0.928	0.501	0.173_1	0.327_4
90	1.108	0.621	0.217	0.404
100	1.280	0.747	0.264	0.483
110	1.444	0.876	0.314	0.562
120	1.596	1.009	0.366	0.643
130	1.754	1.143	0.421	0.722
140	1.926	1.280	0.477	0.803
150	2.096	1.418	0.535	0.883
160	2.270	1.559	0.595	0.964
170	2.451	1.702	0.656	1.046
180	2.631	1.847	0.718	1.129
190	2.812	1.994	0.782	1.212
200	2.994	2.143	0.846	1.297
210	3.176	2.294	0.912	1.382
220	3.357	2.446	0.978	1.468
230	3.539	2.599	1.045	1.554
240	3.721	2.754	1.113	1.641
250	3.904	2.910	1.182	1.728
260	4.087	3.066	1.251	1.815
270	4.268	3.224	1.322	1.902
280	4.450	3.382	1.392	1.990
290	4.633	3.542	1.464	2.078
298.16	4.783	3.673	1.523	2.150
300	4.815	3.702	1.535	2.167

*Corrected for impurity of 1.5% Fe as Fe_3O_4.

substances with layered lattices, such as gallium,[27] show the same behavior. The authors believe that the T^2 dependence of heat capacity at low temperature can be attributed directly to the pronounced layered structure of boron nitride which makes it a quasi two-dimensional crystal. This view has been expressed previously by Tarassov[28] in the case of a number of other substances, but there are numerous flaws in his arguments, including choice of data which do not extend below 50°K. Gurney[29] has presented a theory of the T^2 law for graphite by using the concept of a two-dimensional lattice in an otherwise conventional Debye treatment, and he has derived the expression

$$C_v = \frac{9.6RT^2}{\theta^2} \qquad (2)$$

[27] W. DeSorbo, *J. Chem. Phys.* 21, 168 (1953).

[28] V. V. Tarassov, *Compt. rend. acad. sci. U. R. S. S.* 46, 20 (1945); *ibid.*, p. 110; V. V. Tarassov, *Compt. rend. acad. sci. U. R. S. S.* 54, 795 (1946); V. V. Tarasov, *Doklady Akad. Nauk S. S. S. R.* 58, 577 (1947); V. V. Tarasov, *Zhur. Fiz. Khim.* 24, 111 (1950).

[29] R. W. Gurney, *Phys. Rev.* 88, 465 (1952); R. Gurney, *Report for January, February, and March 1947; Experimental Nuclear Physics Division and Theoretical Nuclear Physics Division*, CP-3801, p. 37.

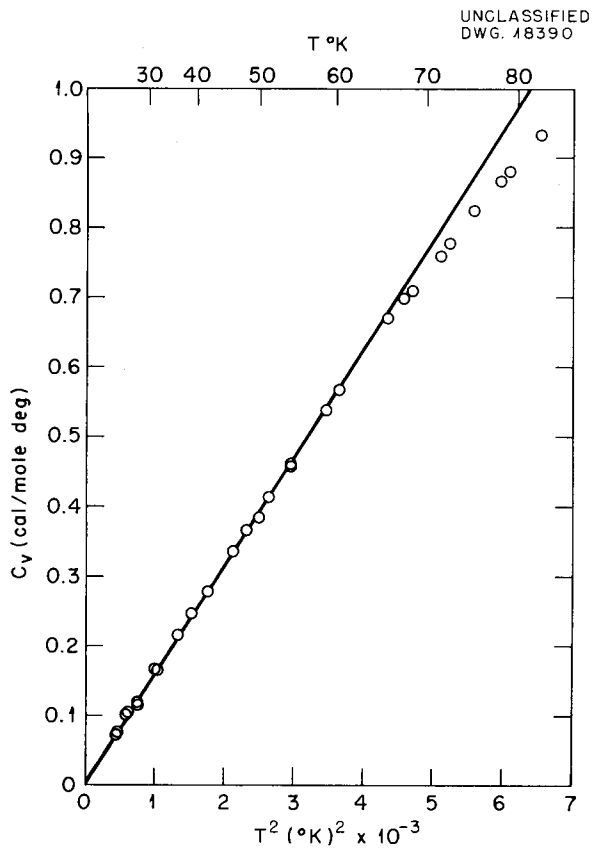

Fig. 9. Low-Temperature Heat Capacity of Boron Nitride.

However, it appears that his assumptions are in error regarding the method of summing the degrees of freedom per atom, and the relationship should be

$$C_v = \frac{14.4RT^2}{\theta^2} \tag{3}$$

A very thorough investigation of the lattice vibrations of graphite has been made by Krumhansl and Brooks,[30] and they have been able to present a coherent theory for the T^2 heat capacity dependence in the case of graphite. By making certain simplifying assumptions, their theory reduces to Eq. 3.

This theory was considered in the case of boron nitride, where it is reasonably applicable, because the average atomic weight of boron and nitrogen closely approximates the atomic weight of carbon; the approximation for boron nitride becomes

$$C_v = \frac{28.8RT^2}{\theta^2} \tag{4}$$

where θ is a Debye-type characteristic temperature. The factor 28.8 is used in place of the 14.4 of Eq. 3 to account for the fact that the simplest formula of boron nitride, BN, is diatomic, whereas that of graphite, C, is monatomic. Constancy of θ^2 is obtained within 2% up to 66°K, but above that temperature, deviation becomes progressively greater, as illustrated by Fig. 9. The characteristic Debye temperature for the quasi two-dimensional BN lattice is θ = 604°K, which is to be compared with θ = 950°K found by Krumhansl and Brooks[30] for graphite.

Heat and Free Energy of Formation

Experimental. The heat of combustion of boron nitride when amorphous boric oxide and nitrogen are formed was measured in a Parr oxygen bomb calorimeter which had been modified to operate isothermally rather than adiabatically. Temperature of the isothermal water jacket in the calorimeter was maintained constant at about 27°C by means of a thermistor used as the temperature-sensitive element in a bridge circuit employing a variable zero suppression Speedomax recorder-controller operating a low-lag knife-blade heater at about 25 volts. A small stream of cooling water was also used continuously to give more rapid control. It was observed that temperature fluctuations of the order of somewhat less than 0.001°C in both directions around the control temperature took place but that no drift was found during a combustion. Temperature in the calorimeter was measured with a precision Mueller bridge and a calibrated copper resistance thermometer designed to have an extremely rapid time constant. This particular thermometer has the designation CUV-7 and has been described by Van Artsdalen and Dworkin.[19] The calorimeter was operated so that the final temperature after combustion was always somewhat lower than the jacket temperature, and in this way vaporization from the calorimeter was minimized.

The calorimeter was calibrated according to Bureau of Standards recommendations by combustion of NBS benzoic acid when 1 g of water was present in the bomb and the initial oxygen pressure was 30 atm at room temperature. A series of nine

[30] J. Krumhansl and H. Brooks, private communication (manuscript in press).

calibrations made during the course of measuring the heat of combustion of boron nitride gave, for the thermal equivalent of the calorimeter, 2519.7 ±4.3 cal (±0.17%). Corrections were made for the presence of the small amount of water in the bomb, for slightly varying weights of water in the calorimeter from run to run, for the amount of ignition wire burned, and for the heat introduced by the current through the ignition wire prior to its rupture.

In the runs with boron nitride, 30 atm of oxygen was used, but no water was added to the bomb. Combustion was effected without promoters, the BN being ignited directly by the fuse wire. The process is complicated by the fact that complete combustion was not achieved, and hence the actual amount of boron nitride burned had to be determined by analysis of the products for boric oxide after hydration to boric acid. No oxides of nitrogen were detected among the products, and hence it is assumed that the reaction goes to amorphous boric oxide and nitrogen. As a further check on this point, some of the sublimed product was subjected to x-ray analysis and found to correspond to the product of combustion of elemental boron in the bomb, where boric oxide is known to be formed. Some of the product was also dissolved in water in a small calorimeter, and the heat of solution was found to correspond closely with that for amorphous boric oxide given by Van Artsdalen and Anderson.[31] Perhaps the best proof of the identity of the products lies in the fact that the amount of boric oxide found by analysis plus the weight of the residue (unburned BN) gave a stoichiometric balance within 0.3 to 0.4% of the initial boron nitride. Corrections were applied as in the calibrations and, in addition, for the difference in specific heats of materials in the bomb during combustion of boron nitride. No correction was made for conversion to a constant pressure process nor for correction to 25°C, since these amounted to less than 0.01%. Likewise, no correction was made for any traces of oxides of nitrogen, since it was demonstrated that amounts which would have eluded detection would cause an error no greater than 0.05%.

[31] E. R. Van Artsdalen and K. P. Anderson, *J. Am. Chem. Soc.* 73, 579 (1951).

Results and Discussion. The results of six combustions of boron nitride are given in Table 7. The percentage of boron nitride burned was determined by analysis of all material remaining in the bomb after combustion. The value for the heat of combustion given in Table 7 must be corrected for the change in number of moles according to the reaction

$$BN(cryst) + \tfrac{3}{4}O_2 = \tfrac{1}{2}B_2O_3(amorph) + \tfrac{1}{2}N_2 \quad (5)$$

from which

$$\Delta H_c = -90.08 + \Delta nRT = -90.08 + (-\tfrac{1}{4})(0.5923)$$

$$\Delta H_c = -90.23 \text{ kcal/mole}$$

The heat of formation of amorphous boric oxide has been given most recently as $\Delta Hf = -306.11 \pm 0.75$ kcal/mole by Prosen, Johnson, and

TABLE 7. HEAT OF COMBUSTION OF BN

WEIGHT OF BN (g)	BN BURNED (%)	TEMPERATURE RISE (°C)	MEDIAN TEMPERATURE	$-\Delta H$ (kcal/mole)
0.5422	78.84	0.630	24.3	91.17
0.6146	83.91	0.741	24.6	88.97
0.4475	86.21	0.563	24.1	90.41
0.6287	88.39	0.804	24.4	89.77
0.4624	87.31	0.588	24.6	90.08
0.6552	87.58	0.833	24.3	90.09
				Average 90.08 ± 0.47 (±0.52%)

Pergiel;[32] therefore it is now possible to write

$$\begin{array}{lcl} BN(cryst) + \frac{3}{4}O_2 = \frac{1}{2}B_2O_3(amorph) + \frac{1}{2}N_2 & \Delta H = & -90.2_3 \\ B(cryst) + \frac{3}{4}O_2 = \frac{1}{2}B_2O_3(amorph) & = & -153.0_6 \\ \hline B(cryst) + \frac{1}{2}N_2 = BN(cryst) & \Delta H = & -62.8_3 \end{array} \quad (6)$$

The best value for the heat of formation of BN in its standard crystalline state at 25°C is, thus, exothermic 62.8 ± 0.6 kcal/mole.

Previously, Lorenz and Woolcock[33] obtained 28.1 kcal/mole as the heat of formation of BN, and Satoh[34] had recalculated the results by using different heat-capacity values and obtained 28.5 kcal/mole. The method used by Lorenz and Woolcock is open to some question, since it involves a presumed determination of the dissociation equilibrium

$$BN(cryst) = B(cryst) + \frac{1}{2}N_2 \quad (7)$$

the experiments being performed in the range 1695 to 2045°C by measuring pressures of permanent gas produced. They did not prove that this was the only reaction to occur, and it is now known that BN sublimes somewhat at these elevated temperatures; therefore it is conceivable that they may have measured a combination of heat of sublimation and heat of dissociation of gaseous BN. Furthermore, it has been only recently that reasonably pure boron nitride has been available, and it is clear that a volatile or unstable impurity could have caused spurious results.

Cartledge[35] has shown that it is possible to correlate heats of formation with the ionic potential and, by certain well-established trends, to draw important conclusions concerning bonding type. The high value of the heat of formation of BN reported here would appear to indicate considerable double-bond character in this substance. However, in order to make quantitative use of Cartledge's relationship, it will be necessary to have more data on heats of formation of other nitrides with ionic potentials similar to the ionic potential of boron; consequently, further work with such nitrides is contemplated.

The free energy of formation of boron nitride has been calculated from the heat of formation and entropy of BN by using Bureau of Standards[36] values of the entropy of elemental boron and nitrogen. It was computed that for Eq. 6, $\Delta S = -20.77$ e.u. and that $\Delta F = -56.6_4$ kcal/mole. This large negative value for the free energy of formation is consistent with the great stability of boron nitride.

CHEMISTRY OF FUSED SALTS

A. S. Dworkin I. S. Yaffe
D. J. Sasmor E. R. Van Artsdalen

Electrical Conductivity

Considerable progress has been made in the measurement of electrical conductivity of fused alkali halides. Problems of adequate temperature control of furnaces at high temperatures seem to have been overcome by using the special Speedomax recorder-controller and DAT unit mentioned in the last report[37] for operating a 3½-in. bore Marshall precision furnace containing an Inconel tube and a heavy nickel lining to increase the heat capacity. Because of its location, the control thermocouple slightly anticipates temperature changes in the fused salt and indicates that, in the range from 650 to 900°C, temperature fluctuations are not over 0.2°C, the limit of detection. A thermocouple in the molten salt itself shows that the temperature is constant to better than 0.1°C. The types of cells and electrodes for measuring conductivity have been reasonably well standardized. It has

(32) E. J. Prosen, W. H. Johnson, and F. Y. Pergiel, *Heat of Reaction of Diborane with Water*, NBS-1552 (March 26, 1952).

(33) R. Lorenz and J. Woolcock, *Z. anorg. u. allgem. Chem.* 176, 289 (1928).

(34) S. Satoh, *Sci. Papers Inst. Phys. Chem. Research (Tokyo)* 29, 53 (1936).

(35) G. H. Cartledge, *J. Phys. Chem.* 55, 248 (1951) and earlier papers.

(36) F. D. Rossini *et al.*, *Selected Values of Chemical Thermodynamic Properties* (Circular 500, National Bureau of Standards) U. S. Government Printing Office, Washington, 1952.

(37) A. S. Dworkin, D. J. Sasmor, I. S. Yaffe, and E. R. Van Artsdalen, *Chem. Quar. Prog. Rep. Dec. 31, 1952*, ORNL-1482, p. 8.

been possible to use a cell for several days with molten potassium chloride and then to remove the cell and redetermine its cell constant with standard potassium chloride solution. The cell constant had changed by less than 0.15%.

Determinations of conductivity of molten lithium chloride, potassium chloride, and certain mixtures of the two have been carried out; however, the data are still incomplete. Density measurements, which are required for calculation of equivalent conductance, have been made on these systems. A noticeable frequency effect on conductivity was observed as the frequency increased above about 4000 cps. It remains to be determined whether this is a true property of the materials or some extraneous effect, and this point is under study at present.

Transport Numbers

A type of transport experiment was mentioned in an earlier report,[38] but work since then has indicated that certain modifications are desirable. While the use of inert electrodes (platinum) proved to be unsatisfactory, it has been found that reactive electrodes can be used with success. Exploratory experiments show that a measure of the transport numbers of Ag^+, Na^+, and NO_3^- can be obtained by using silver electrodes in a mixture of fused $AgNO_3$ and $NaNO_3$. Analyses of both anode and cathode compartments, as well as of the bulk of material in the intermediate compartment, are required for maximum confidence in the results. The first data seem to indicate that Ag^+ and Na^+ carry essentially all the current in very roughly equivalent quantities, whereas NO_3^- carries none of the current. This would seem to be in agreement with existing qualitative theory. However, for detailed analysis of such transport data, the partial molal volumes of all components of mixtures are required with high precision in order to correct for volume changes in both anode and cathode compartments. A recent experiment indicates that these volume changes may be more important than had been anticipated, and work on transport phenomena is continuing.

[38] A. S. Dworkin, D. J. Sasmor, I. S. Yaffe, and E. R. Van Artsdalen, *Chem. Quar. Prog. Rep. Sept. 30, 1952*, ORNL-1432, p. 14.

Cryoscopy

The stability of complex ions in molten salts presents a most intriguing question. General experience indicates that some ions, such as NO_3^-, SO_4^{--}, $Cr_2O_4^{--}$, etc., are reasonably stable in the absence of reducing agents, but few quantitative data are available. Consequently, several experimental methods have been considered for investigating the stability and chemical reactivity of complex ions. One very promising method is to determine the number of ions formed per mole of solute dissolved in some fused salt solvent. A reasonably direct approach is to determine the lowering of the freezing point of appropriate fused solvents caused by the addition of small amounts of substances which contain or can produce complex ions. Only one or two references to this sort of measurement are to be found in the literature.

Several series of measurements of freezing-point lowering have been made. In the case of molten sodium nitrate as the solvent (freezing point ca. 307°C), it was found that a low concentration (up to ca. 0.1 *m*) of potassium chloride depresses the freezing point twice as much as sodium chloride, while potassium sulfate gives a threefold depression. Thus, only ions (or molecules) which are not common with those of the solvent cause lowering of the freezing point. The data obtained so far indicate that salts such as $NaNO_3$, NaCl, KCl, K_2SO_4, etc. are essentially completely dissociated into Na^+, K^+, NO_3^-, Cl^-, and SO_4^{--} ions. It should be possible to choose a variety of solvents with widely differing melting points so that the effect of temperature on the stability of particular complexes may be investigated, as well as the effects of varying ionic environment. It is planned to continue these studies and to widen the range of substances investigated.

Sometimes in the course of this work it has been observed that more or less vigorous chemical reactions take place when certain substances are added to particular molten salts. For example, interesting acid-base type reactions may be observed in fused salts, and a host of these is known, with many others no doubt remaining to be found. Oxidation-reduction reactions have been observed. As a specific example, it was found that the addition of $K_3Fe(CN)_6$ to molten $NaNO_3$ gave rise to a freezing-point depression corresponding to dissociation into ten ions. However, a slight odor of cyanogen had been noticed when

the $K_3Fe(CN)_6$ was added, and at the end of the measurements, a precipitate of ferric oxide was found. On repeating the experiment visually in a test tube, it was observed that a Prussian-blue color was formed at the moment of addition of the ferricyanide, which means that at least some of the iron must have been reduced to the ferrous state, and presumably this was accomplished by simultaneous oxidation of some CN^- to cyanogen. As the blue color gradually disappeared, gas was evolved and brown ferric oxide precipitated. It is hoped that it will be possible to study further this rather complicated sequence of oxidation-reduction reactions. It seems likely that many new and interesting reactions in fused salts will be found as this work progresses.

It is desirable to measure freezing-point depression to the order of 0.01°C, and this poses serious problems of temperature measurement and control. It was found that multijunction thermocouples gave fair sensitivity, but, for recording with zero suppression on a Speedomax recorder, they required too frequent standardization of bucking battery voltage in the potentiometer circuit to be practical. Therefore a type of recording Mueller bridge circuit was adapted. A calorimetric type platinum resistance thermometer is used with a G-1 Mueller bridge, and in place of the usual galvanometer, there is a very constant, low-gain d-c microvolt amplifier feeding a 10-mv Speedomax recorder. In practice, a small unbalance is left in the Mueller bridge and this is then recorded on the Speedomax, which gives a time-temperature record. Sensitivity better than 0.005°C has been obtained at 325°C, and stability appears to be very good as no reset is required over several hours of operation. This apparatus has very recently been put into use for cryoscopic measurements.

Calorimetry

The low-temperature adiabatic calorimeter used in studies of the heat capacity of boron nitride (cf. "Thermodynamics of Boron Nitride," this report) has been transferred from the K-25 laboratories to X-10 and is now being set up and put into operation with some minor alterations, notably the use of a G-2 Mueller bridge rather than a White potentiometer for temperature measurement. The calorimeter can has recently been recalibrated and loaded with cadmium iodide, and it is anticipated that low-temperature heat capacity of CdI_2 will be measured as soon as the assembly of all the cryostat and measuring apparatus is complete.

During the past six months, detailed plans have been completed and construction was begun on an adiabatic calorimeter to be used for precision heat-capacity measurements up to about 1000°C. The present status of this project follows. Most of the shop fabrication of the calorimeter can, adiabatic shield, and furnace assembly has been completed. Recording and controlling equipment for the furnace and adiabatic shield is on order from the vendor, as well as component parts for for the energizing circuit for calorimeter heaters. Special, matched, precious-alloy thermocouple wire has been received. Components for the high-vacuum pumping system are being assembled. It is anticipated that full-scale testing of the performance of certain parts of this calorimeter will be made within the next several months.

NUCLEAR CHEMISTRY

HEAVY-ISOTOPE BUILDUP IN CORE OF U^{233} BREEDER[1]

J. Halperin R. W. Stoughton

The isotopic composition of the uranium in the core of a U^{233} breeder will change markedly (e.g., from 100% U^{233} to ~30% U^{233}) from the startup time until equilibrium is attained at the flux-time product of about 10^{24}. This latter figure of 10^{24} corresponds to a reactor operating at an average flux of 3×10^{14} for about 100 years. Since no reactor will be operating at or near the equilibrium values in any reasonable time, the major concern lies in the evaluation of the losses in the time-dependent region where changes in the concentration of the various isotopes are taking place. The growth of the several pertinent uranium isotopes and the losses to the reactor system are computed here as a function of the flux-time product. This problem has previously been considered by Halperin and Stoughton;[2] however, the availability of newer nuclear data permits a more detailed investigation to be made.

The principal heavy isotopes and their modes of formation may be depicted by the following diagram:

$$\begin{array}{ccccccc} & & \uparrow (n,\ \text{fission}) & & & & \\ U^{232} & \xleftarrow{(n,2n)} & U^{233} & \xrightarrow{(n,\gamma)} & U^{234} & \xrightarrow{(n,\gamma)} & \end{array}$$

Neither U^{237} nor U^{232} will be considered here since these isotopes may be expected to attain only low concentrations and will thus affect neutron losses negligibly, provided, of course, that some unusually high cross sections are not present. Furthermore, their exact contribution is difficult to estimate because the pertinent cross-section data are not yet well known.

Five cases will be considered here:

1. pure U^{233} in core at start; pure U^{233} added to core as fuel is consumed;
2. pure U^{233} in core at start; U^{233} containing 5% U^{234} added to core as fuel is consumed;
3. U^{233} containing 5% U^{234} at start; fuel replenished with this same fuel mixture;
4. pure U^{235} in core at start; pure U^{233} added to core as fuel is consumed;
5. pure U^{235} in core at start; U^{233} containing 5% U^{234} added to core as fuel is consumed.

In any practical case, the core will probably start with U^{235}. As this material is consumed, U^{233} produced in the blanket will replace the spent fuel. Some U^{234} will be produced in the blanket by neutron capture of the members of the 233 chain (Th^{233}, Pa^{233}, and U^{233}). It appears that an upper limit on the U^{234}/U^{233} ratio for the blanket product will be about 5% if the over-all losses are to be kept within reasonable bounds. Hence, any practical case is expected to lie somewhere between cases 4 and 5. Cases 1, 2, and 3 are included for comparison and because some future reactor may actually start with U^{233} in the core. The values of the various cross sections used here are listed in Table 8.

The methods used for case 1 have been described[2] and have been modified only slightly for cases 2 and 3 to allow for the enhancement of U^{234} in the production terms of the differential equations. In these cases, the concentration of U^{233} is kept constant.

$$\begin{array}{ccccccc} \uparrow (n,\ \text{fission}) & & & & \uparrow (\beta^-,\ \text{6.7-day}) & & \\ U^{235} & \xrightarrow{(n,\gamma)} & U^{236} & \xrightarrow{(n,\gamma)} & U^{237} & & \end{array}$$

TABLE 8. THERMAL CROSS SECTIONS AND ETA VALUES

NUCLIDE	σ_a	σ_c	η
U^{233}	50	564	2.30
U^{234}	90	90	
U^{235}	106	682	2.12
U^{236}	8	8	

In cases (4 and 5) in which the reactor starts up with pure U^{235} and the spent fuel is replenished with U^{233}, none of the four isotopes have a constant concentration, and it becomes necessary to assume a relation between the U^{235} and the

[1] The material presented here is described in greater detail in ORNL-1567 (to be published).

[2] J. Halperin and R. W. Stoughton, *Some Effects of Transmutation Products on U^{233} Breeder Pile Operation*, ORNL-1368 (Oct. 13, 1952).

U^{233}. The assumption made here is that U^{233} is added at such a rate that the net neutrons reproduced in the core fuel is kept constant; that is,

$$(\eta_{25} - 1)\, N^0_{25}\sigma_a(25) = (\eta_{25} - 1)\, N'''_{25}\sigma_a(25) + (\eta_{23} - 1)\, N'_{23}\sigma_a(23) \qquad (1)$$

where N^0 refers to the original concentration, N''' refers to the isotope resulting from the original U^{235}, and N' refers to the isotope resulting from the added U^{233}. The restriction between N^0_{25}, N'''_{25}, and N'_{23} could just as well have been made on a neutron reproduction basis [i.e., keeping $\eta_{25}N'''_{25}\sigma_a(25) + \eta_{23}N'_{23}\sigma_a(23)$ constant] or on the basis of keeping the fuel absorption cross section constant. The use of one of these different bases would not have significantly altered the net losses caused by the heavy-isotope buildup as calculated here, except for the different factor in the denominator of the loss expression depending on the different basis.

The loss term is here described as

$$\frac{L(23)}{\eta_{23} - 1} = \frac{N_{24}\sigma_a(24)}{N_{23}\sigma_a(23)\,(\eta_{23} - 1)} - \frac{N_{25}\sigma_a(25)\,(\eta_{25} - 1)}{N_{23}\sigma_a(23)\,(\eta_{23} - 1)} + \frac{N_{25}\sigma_a(26)}{N_{23}\sigma_a(23)\,(\eta_{23} - 1)} \qquad (2)$$

and

$$\frac{L(25)}{\eta_{25} - 1} = \frac{N_{24}\sigma_a(24)}{N^0_{25}\sigma_a(25)\,(\eta_{25} - 1)} - \frac{N'_{25}}{N^0_{25}} + \frac{N_{26}\sigma_a(26)}{N^0_{25}\sigma_a(25)\,(\eta_{25} - 1)} \qquad (3)$$

where $L/(\eta - 1)$ refers to neutron loss per net neutron reproduced in the reactor core, and N'_{25} refers to N_{25} which originated from N_{23} and N_{24} only. $L(23)$ and $L(25)$ respectively refer to the systems starting with U^{233} and with U^{235}; each isotopic loss is then expressed in terms of the net neutrons reproduced from the constant U^{233} or from the original U^{235}, respectively. It should be noted that in cases (4 and 5) in which the reactor is started up with U^{235}, the loss in Eq. 3 can be expressed equally well in terms of N^∞_{23} (i.e., N_{23} at infinite time). By making use of the equality expressed in Eq. 1, Eq. 4 follows:

$$(\eta_{25} - 1)\, \sigma_a(25)\, N^0_{25} = (\eta_{23} - 1)\, \sigma_a(23)\, N^\infty_{23} \qquad (4)$$

$$1.0418 N^0_{25} = N^\infty_{23}$$

Table 9 lists the equilibrium concentrations of the various isotopes and the equilibrium losses for the five cases.

It should be noted that the total uranium content of the reactor will have increased substantially at equilibrium. In fact, except for case 1, there will be more U^{236} than U^{233} present at equilibrium. It follows that the problems associated with total uranium concentrations will become more severe (e.g., chemical processing, corrosion, etc.).

Figures 10, 11, 12, and 13 show the total relative concentrations of each isotope and the total losses in each of the five cases considered. The losses go through a maximum, varying from about 0.5 to 0.9% at $ft \sim 3 \times 10^{21}$ and through a minimum, varying from about –0.5 to –0.9% at $ft \sim 5 \times 10^{22}$, depending upon the particular case. At an average flux of 3×10^{14}, the maximum and minimum losses correspond to about 4 months and 5 years, respectively. The negative loss represents a net neutron gain to the reactor system (due to the U^{235} growing in from the U^{234}).

It is apparent that in no case do the neutron losses become large, despite the rise in the total uranium content by a factor of about 3. In fact, if the losses were averaged over the entire period of the reactor's operation, rather than the instantaneous losses which are plotted here, the resulting loss curve plotted against flux-time would be flatter and the maximum losses appreciably less.

CERIUM-144 DECAY

B. H. Kettelle A. R. Brosi

The decay schemes of Ce^{144} and Pr^{144} are of interest because the ground state to ground state

TABLE 9. ISOTOPIC CONTENT OF URANIUM AND NEUTRON LOSSES AT EQUILIBRIUM

EQUILIBRIUM ISOTOPIC RATIOS AND NEUTRON LOSSES	CASE			
	1	2 or 3	4	5
$\frac{N_4}{N_3}$ or $\frac{N_4}{N_5^0}$	0.556	0.869	0.579	0.905
$\frac{N_5}{N_3}$ or $\frac{N_5}{N_5^0}$	0.073	0.115	0.076	0.119
$\frac{N_6}{N_3}$ or $\frac{N_6}{N_5^0}$	0.971	1.519	1.012	1.583
$\frac{N\ (\text{total})}{N_3}$	2.600	3.503	2.60	3.503
$\frac{L}{\eta - 1}$ (%)	0.242	0.378	0.242	0.378

beta transitions of each isotope appear to be zero-zero transitions. Since only a few cases of this type are known, it is desirable to study the spectra.

It is possible to write a decay scheme for Pr^{144} which includes the observed radiations and which is consistent with the observed gamma-gamma angular correlation and the unique shaped beta spectrum coincident with one of the gamma rays. However, it appears difficult to write a decay scheme for Ce^{144} consistent with the published conversion-line spectra.

Since the conversion electron spectrum of Ce^{144}-Pr^{144} contains many lines at low energies, an effort was made to improve the resolution of the thin-lens beta-ray spectrometer before attempting to study this spectrum. A series of photographs of the electron patterns of the Cs^{137} conversion lines was taken by placing films at various points along the axis of the spectrometer and was of aid in placing the defining baffles at the ring focus position. Critical alignment of the instrument was then made by using a Cs^{137} source and by studying the conversion line shapes and widths. In addition, a study was made of the effectiveness of the earth's magnetic field compensation coils, in which the conversion lines of Te^{125} at 30, 78, and 105 kev were used. The resolution at low energy was determined by use of the *K*-conversion line of the 92-kev gamma in Ga^{67}. The full width at half height of this line at 82 kev shown in Fig. 14 is 0.88%. Finally, in order to demonstrate the reliability of the shape of a beta distribution taken with the instrument adjusted to this high resolution, the spectrum of Pm^{147} was observed. The Kurie plot as shown in Fig. 15 is linear down to 50 kev, with the window cutoff becoming serious between 30 and 20 kev.

Some of the transitions in the Ce^{144}-Pr^{144} decay scheme occur in low abundance; so it was considered desirable to prepare extremely pure source material. This was done by starting with old fission-product Ce^{144} obtained from the Operations Division. Further purification was obtained by using a high-temperature, Dowex-50, ion-exchange column. In addition to the activity peak for Ce^{144}, low intensity peaks were observed that were due to Cs^{137}, Y^{91}, Eu^{155}, and Pm^{147}. It is desirable to reduce such impurities to much less than 1%, since the Cs^{137} gamma ray is approximately the same energy as a gamma ray

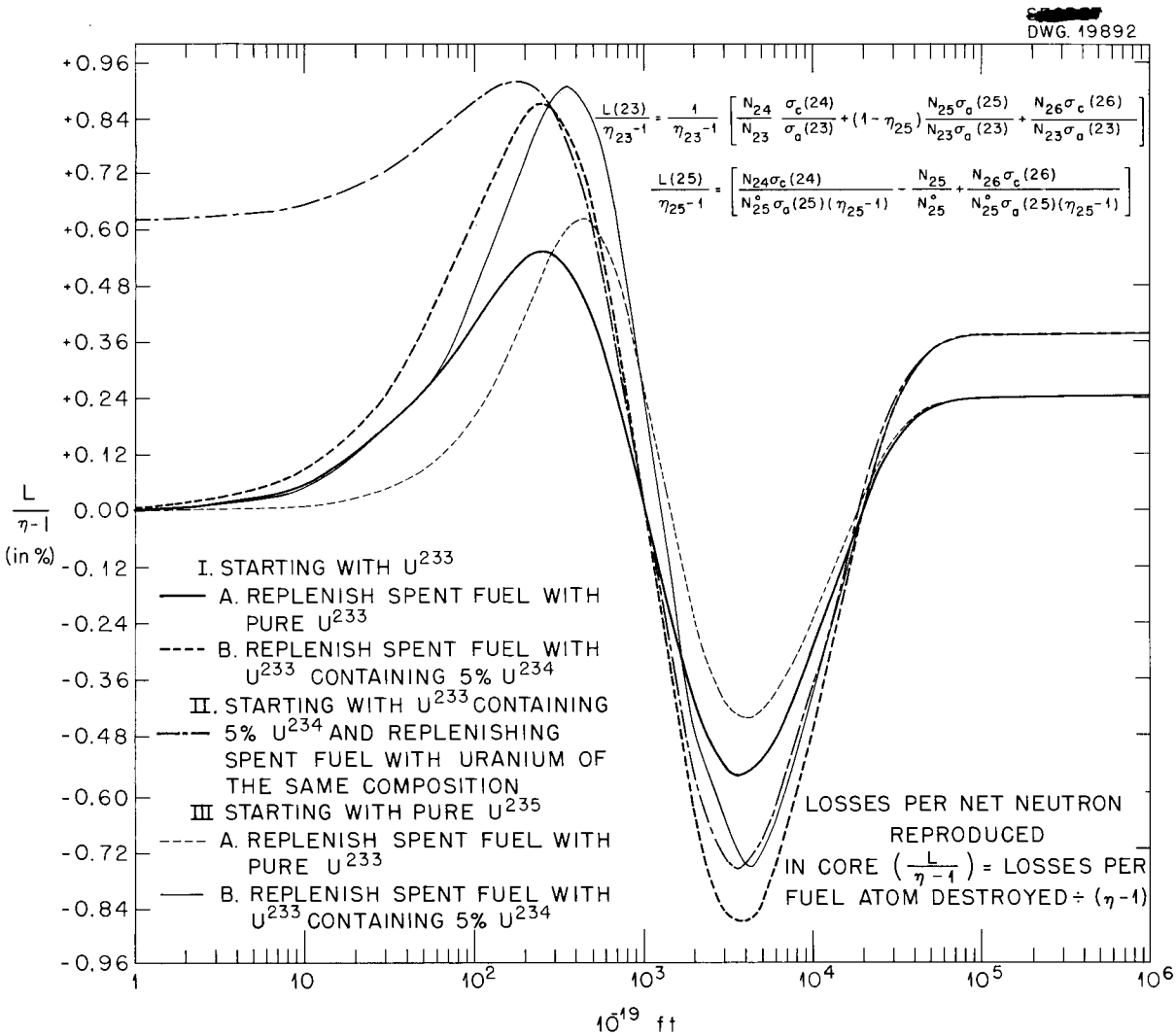

Fig. 10. Losses (per Net Neutron Reproduced) in the Core as a Result of the Growth of Uranium Isotopes.

in Pr^{144} occurring in about 1% of the disintegrations and since the several low-energy conversion lines of Eu^{155} lie in the same region as those of Ce^{144}. The spectrometer source contained no added cerium carrier and was prepared by evaporating a small volume of HCl containing the tracer on a thin Formvar film coated with gold to make it a conductor.

The conversion electron and the beta spectra of Ce^{144}-Pr^{144} up to 140 kev are shown in Fig. 16. Most of the lines reported by Cork were observed, and, in addition, two lines at energies below his counter window cutoff were seen. Before a final assignment is given to these lines, it is desirable to study the Auger electron spectra of other isotopes in the rare-earth region.

HALF-LIFE MEASUREMENTS

A. R. Brosi B. H. Ketelle

A series of measurements to determine, within a period of a few months, radioisotope half lives of the order of years was mentioned in the last progress report.[3] These measurements have now

[3] A. R. Brosi and B. H. Ketelle, *Chem. Quar. Prog. Rep. Dec. 31, 1952*, ORNL-1482, p. 11.

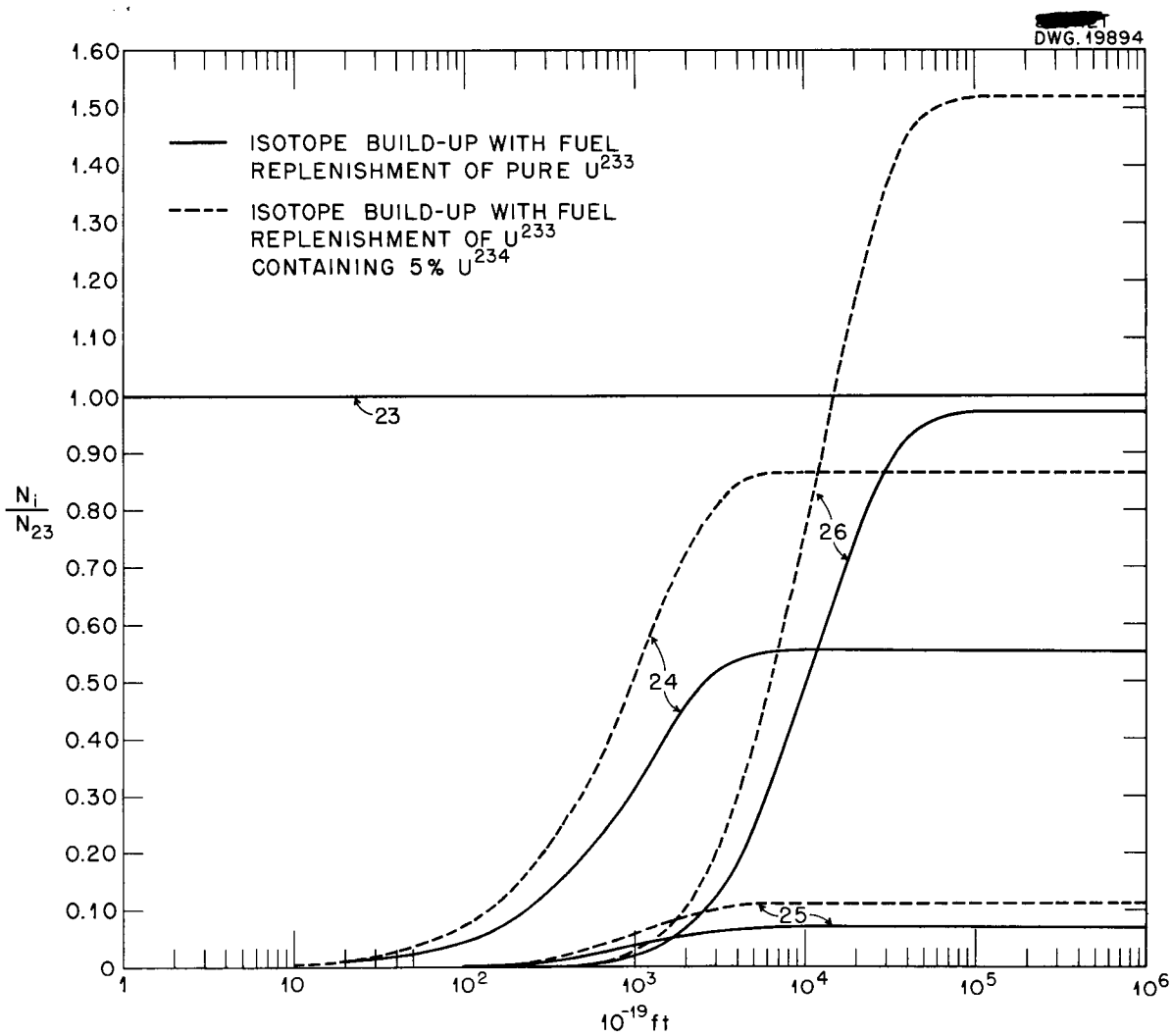

Fig. 11. Uranium Isotope Buildup in Core of Reactor Starting with Pure U^{233} (i.e., $N_{24}/N_{23} = 0$) and Replenishing Spent Fuel with (1) Pure U^{233} and (2) with U^{233} Containing 5% U^{234}.

been continued long enough for some tentative conclusions to be drawn.

A vibrating-reed electrometer was used to determine the rate at which a condenser was charged by the ionization current produced in a re-entrant-tube ion chamber by the radioactive sample. Rates were determined daily with a precision of 0.1%. Ce^{144} purified on a cation-exchange column, Co^{60} purified on an anion-exchange column, Kr^{85} and A^{39} purified on gas-adsorption columns, and Ra^{226} were included in the measurements. The ionization currents produced by the samples were approximately equal and were low enough to avoid any appreciable nonlinearity resulting from ion recombination. All measurements were made relative to Ra^{226} in order to correct for changes in the instrument.

Least-squares analyses of the data gave the half lives shown in Table 10. In addition to the rate-of-drift measurements, the ionization currents produced by the Kr^{85} samples were also determined about once each week by measuring the potential drop across a resistor. Least-squares analyses of these data are also included in Table 10.

It can be seen that the Kr^{85} and Co^{60} half lives reported here are considerably longer than previously published values. A least-squares analysis

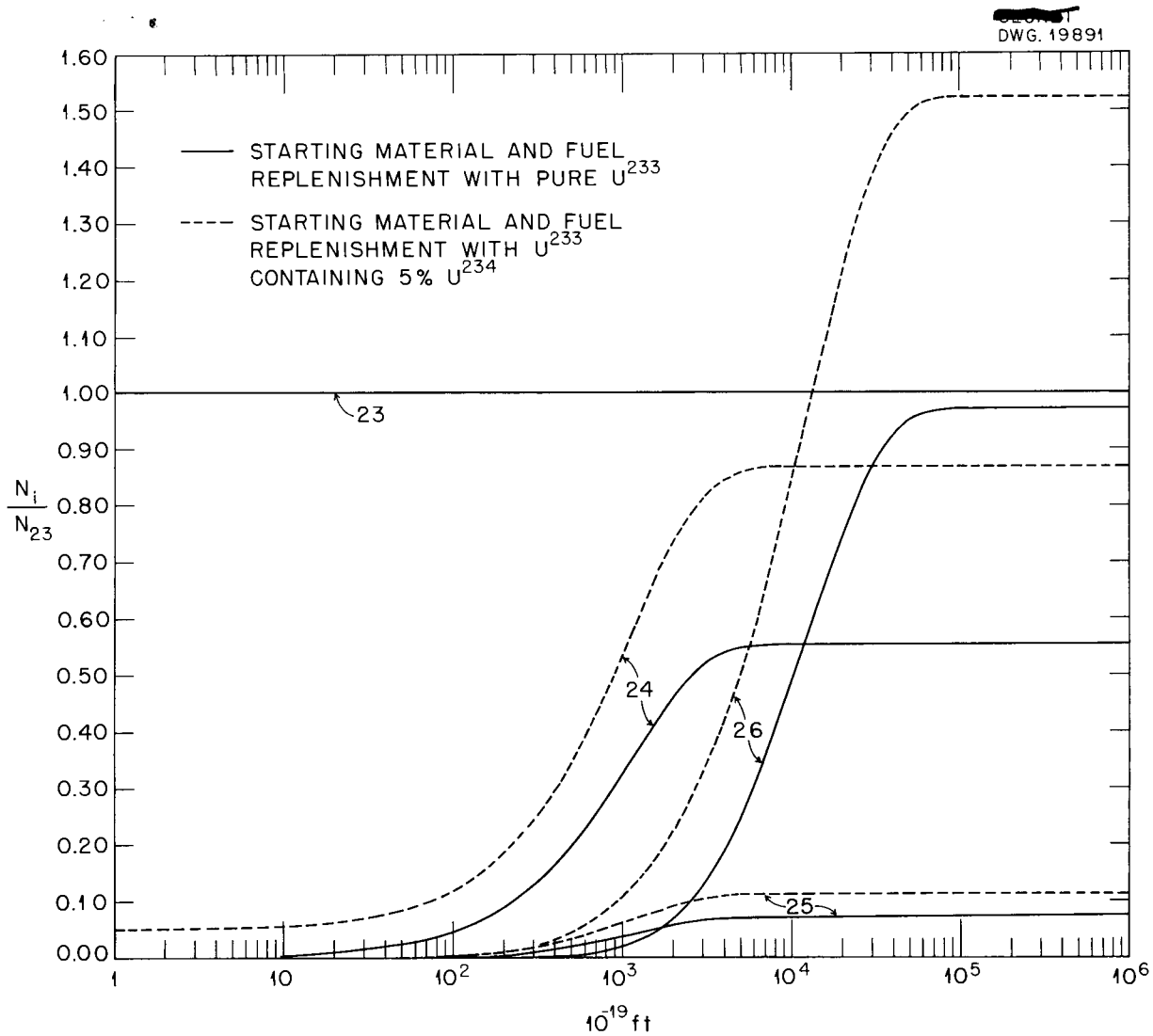

Fig. 12. Uranium Isotope Buildup in Core of Reactor (1) Starting with Pure U^{233} (i.e., $N_{24}/N_{23} = 0$) and Replenishing Spent Fuel with Pure U^{233}, and (2) Starting with U^{233} Containing 5% U^{234} and Replenishing the Spent Fuel with Uranium of the Same Composition.

of coincidence-counter data taken for the last three years on a Co^{60} sample prepared by W. C. Peacock in 1946 by a cyclotron bombardment gave an even longer half life, which is also included in Table 10.

In further measurements, it is planned to include an additional Ra^{226} standard and several Co^{60} samples with different bombardment and cooling histories.

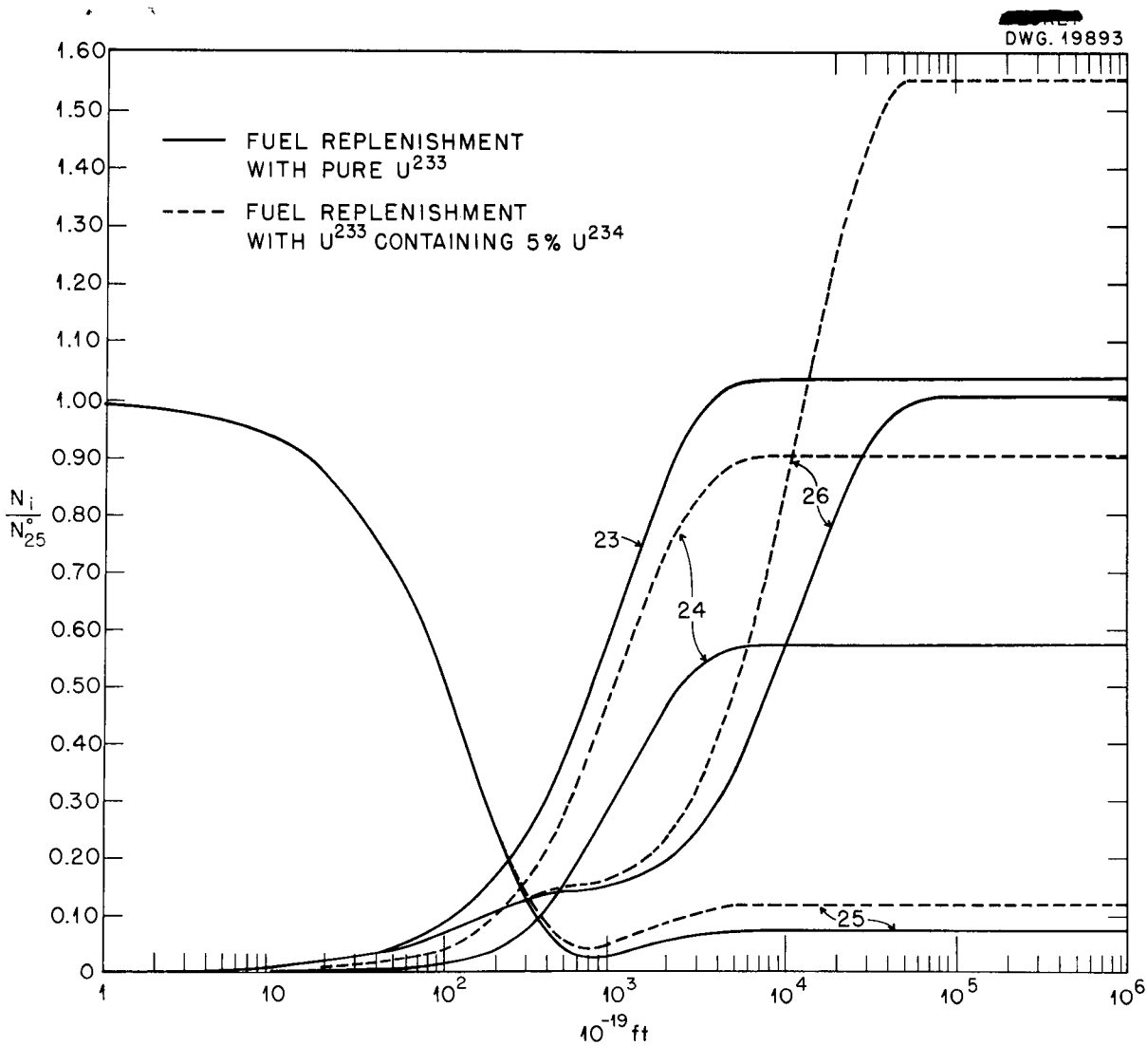

Fig. 13. Uranium Isotope Buildup in Core of Reactor Starting with U^{235} and Replenishing Fuel with (1) Pure U^{233} (i.e., $N_{24}/N_{23} = 0$) and (2) with U^{233} Containing 5% U^{234}.

TABLE 10. HALF LIVES OF Ce^{144}, Co^{60}, AND Kr^{85}

ISOTOPE	HALF LIVES			
	Rate-of-Drift Measurement	Constant-Deflection Measurement	Coincidence Measurement	Previously Published Value
Ce^{144}	285.7 ± 0.5 d			282 ± 3 d
Co^{60}	5.63 ± 0.06 y		5.96 ± 0.06 y	5.27 ± 0.07 y
Kr^{85}, sample 1	10.8 ± 0.2 y	10.2 ± 0.3 y		9.4 ± 0.4 y
Kr^{85}, sample 2	10.3 ± 0.2 y	10.4 ± 0.3 y		

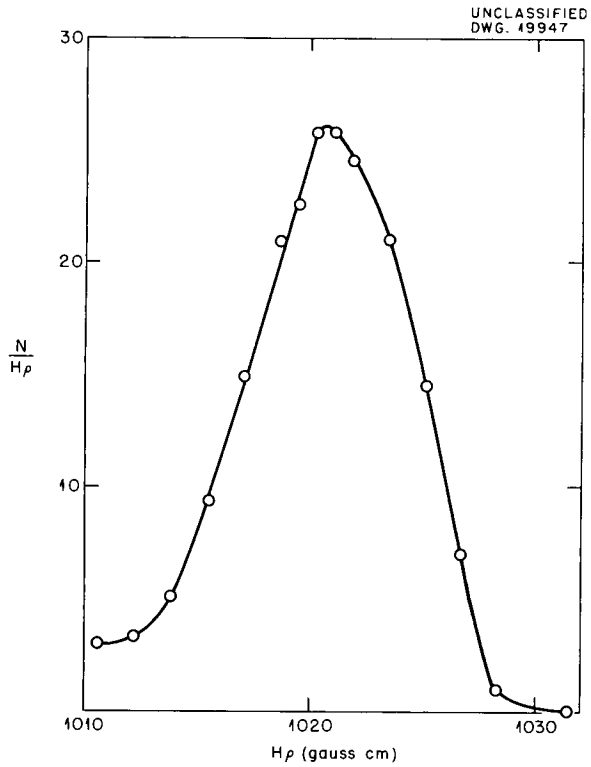

Fig. 14. Conversion Electron Line of 92-kev Gamma Rays in Ga^{67}.

RECOVERY OF FISSION IODINE-129 FROM HANFORD SILVER-BED REACTORS

G. W. Parker G. M. Hebert

Expanding interests[4,5] requiring a large-scale isolation of fission product I^{129} have led to the investigation of the possible recovery of 100-g quantities of high specific activity I^{129} occurring as a product of the decontamination of dissolver vent gases at Hanford.

Previously,[6] milligram amounts of 85% I^{129} have been obtained principally from dissolver vent condensates of strong nitric acid recovered by inserting a cold trap in the stack vent pipes. Because of the low probability of passage through the dissolver reflux column, very small percentages of the total iodine were found in the large quantity of nitric acid collected. However, this source has been continuously exploited for the past three years and yielded limited amounts of apparently chemically undiluted fission iodine.

The source at ORNL recently was first modified[7] and then terminated after a total recovery of about 50 mg of iodine had been accomplished. The modification of the ORNL Pilot Plant dissolver vent-gas treatment incorporated a special iodine removal unit and a heated silver-bed reactor patterned after the original units already in use at Hanford.[8]

As a result of an earlier inquiry relating to the possible procurement of the packing or of an iodine-bearing extract from the reactor, a recent communication has been received relating to the removal of two such units from service. Further information reveals a possible content of iodine to the extent of 279 g in each unit. This figure is based only upon the total plutonium content of the dissolved metal and apparently is not corrected for less than quantitative yields of iodine. General experience would suggest a yield of nearer 35% of the maximum, or about 100 grams.

The Hanford silver reactors are, essentially, packed-column units 2 ft in diameter by 8 ft in bed volume that contain 25 ft^3 of unglazed saddles coated with silver nitrate. The packing is prepared by dipping the saddles in hot 20 *m* silver nitrate solution, after which they are dried and charged into the reactor. The reactor unit is continuously maintained at a temperature of about 425°F. The amount of silver nitrate in a large reactor is 50 lb, which gives it a theoretical capacity of 16,900 g of iodine. However, apparently no such capacity is obtained, since the units taken out of service were reported to have been operated to break-through of iodine after two years of use.

---

(4) R. Livingston, O. R. Gilliam, and W. Gordy, *Phys. Rev.* **76**, 149 (1949); H. Walchli, R. Livingston, and G. Hebert, *Phys. Rev.* 82, 97 (1951); W. Gordy, O. R. Gilliam, and R. Livingston, *Phys. Rev.* **76**, 443 (1949).

(5) B. T. Feld, "Proposal to Use I^{129} in Molecular Beam Experiments," private communication to A. M. Weinberg.

(6) G. W. Parker, G. E. Creek, G. M. Hebert, P. M. Lantz, and W. J. Martin, *Chem. Quar. Prog. Rep. June 30, 1949*, ORNL-286, p. 53.

(7) W. B. Watkins *et al.*, *Summary of the ORNL Pilot Plant Development of the Radioactive Gas Separation Process*, ORNL-1410, p. 9 (March 17, 1953).

(8) A. G. Blasewitz, R. V. Carlisle, B. F. Judson, M. F. Katzer, E. F. Kurtz, W. C. Schmidt, and B. Weidenbaum, *Decontamination of Dissolver Vent Gases at Hanford*, HW-20332 (Feb. 16, 1951).

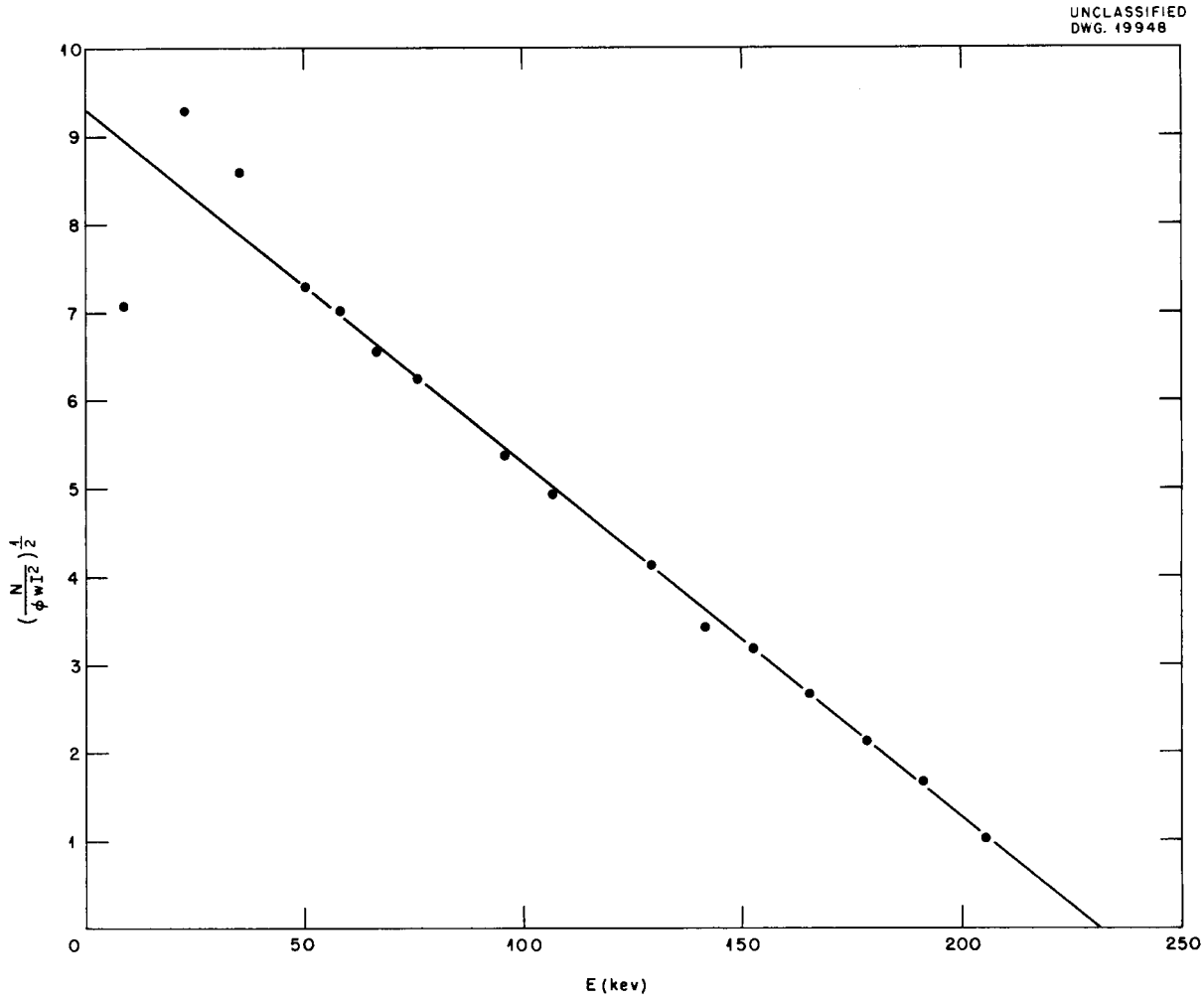

Fig. 15. Kurie Plot of Pm^{147} Beta Spectrum.

By coincidence, the ORNL Pilot Plant silver reactor, a much smaller unit, had also been removed from service after a short period of operation. Thereby, an actual scale model of the Hanford equipment was on hand for a trial of any extraction method conceived. This particular unit has a square cross section of 8 in. and a packed depth of 6 feet. It was found that the saddles were easily removed in increments, which were preserved to permit a comparison of the iodine content over the height of the packing (see Table 11).

Dissolution of Silver Iodide

In order that a practical method can be proposed for the extraction of silver and silver iodide, the value of the few known complexing agents, $Na_2S_2O_3$, KCN, and $AgNO_3$, has been roughly surveyed, together with a silver sulfide process already successfully used on tracer iodine by Livingston and Benjamin.[9]

The most efficient solvents for silver compounds are apparently the alkali cyanides which form the simple complex

$$AgI(s) + 2CN^- \longrightarrow Ag(CN)_2^- + I^-$$

Studies by Randall and Helford (Seidell) show the solubility of AgI in KCN to be roughly half molar in silver with respect to the concentration

[9] R. Livingston and B. Benjamin, *Chem. Quar. Prog. Rep. Dec. 31, 1952*, ORNL-1482, p. 27.

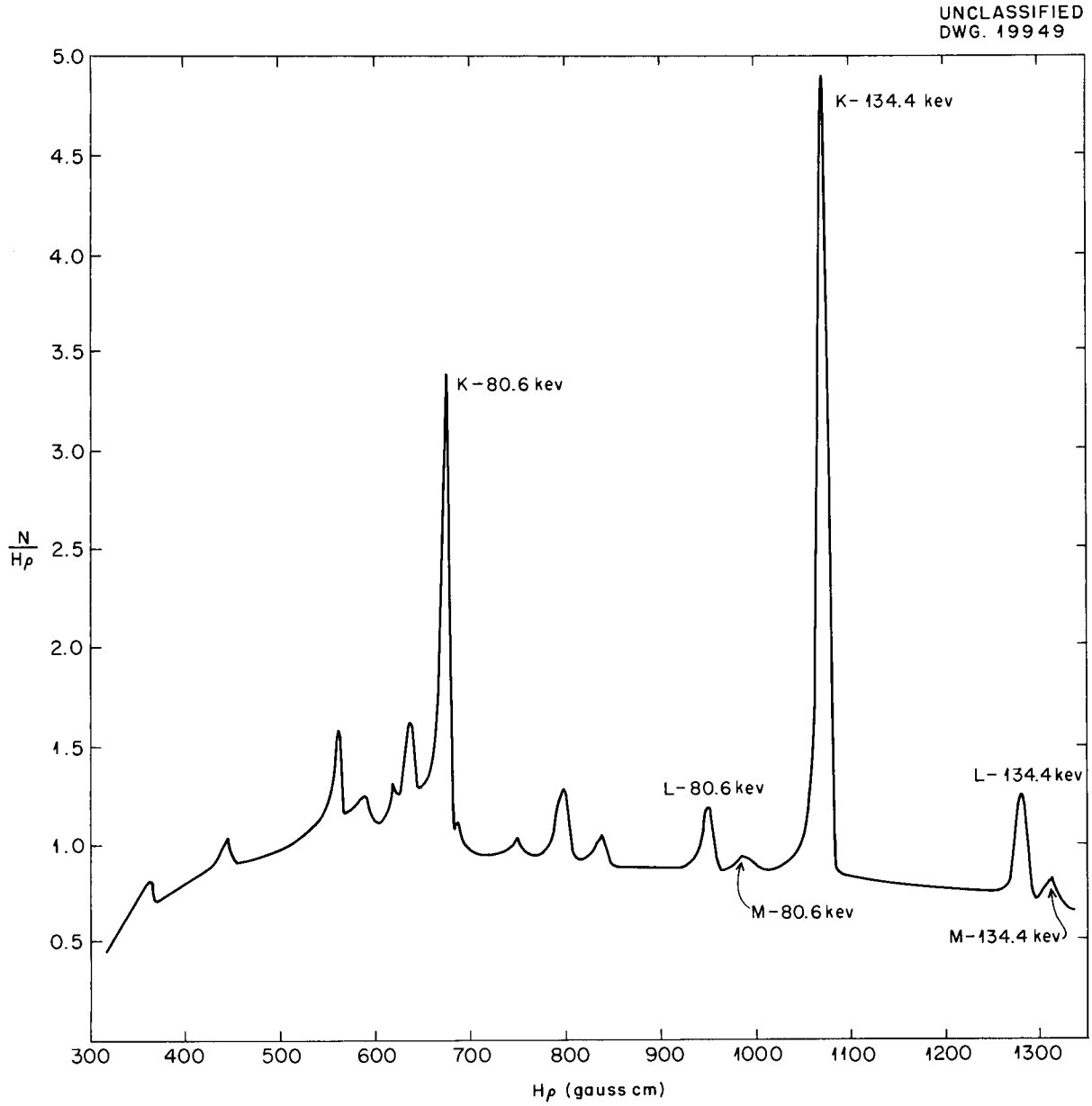

Fig. 16. Ce^{144}–Pr^{144} Conversion Electron and Beta Spectra.

of cyanide. For example, a solution 0.318 *M* in KCN will become saturated when it is 0.147 *M* in AgI. A solution 0.398 *M* in KCN was 0.184 *M* in AgI. On this basis, a method involving extraction into 1 *M* KCN was explored to the extent of determining both the amount of iodine extracted and the amount which could be further recovered from the cyanide solution. The recovery of AgI is simplified by the presence of the large excess of silver which is readily precipitated as AgCN on acidification with HNO_3 and which quantitatively carries AgI even when present only in tracer amounts. Yields of tracer iodine were compared after acidification and found to range from 99 to

TABLE 11. RESULTS OF ACTIVATION ANALYSIS OF ORNL SILVER REACTOR BERL SADDLES FOR I^{129}

PACKED-COLUMN LAYER NUMBER	I^{129} FOUND (mg per sample of 8 saddles)	TOTAL I^{129} (mg)
1	0.475	63
2	0.340	46
3	0.194	112
4	0.124	65
5	0.040	20
6	0.008	4
7	0.003	1
8	Not analyzed	

99.5% at 0.5, 1.0, and 1.5 *N* HNO_3. The quantity of silver carrier in solution was between 1 and 2 mg/ml.

The value of $Na_2S_2O_3$ as a complexing agent for AgI is subject to contradiction. Seidell (Valenta) reports a solubility of 0.15 g of AgI in 100 g of 0.3 *M* $Na_2S_2O_3$ solution and a calculated value (Cohn) of 2.996 g in 100 g of solvent. At any rate, the solubility of AgI in $Na_2S_2O_3$ observed in this experiment was more nearly in agreement with the smaller figure and was therefore ruled unsatisfactory.

A rather impressive solubility of AgI in strong silver nitrate solution (Hellwig) was found to be quite useful in the activation analysis of AgI^{129}. By dissolving 40 mg of AgI in 2 ml of 4 *N* $AgNO_3$ and by diluting to 50 ml with hot water, a doubly effective decontamination was obtained in the reprecipitated AgI by providing a specific precipitation of iodine and an isotopic dilution of the activated silver. The yield in this step is determined by the amount of iodine carrier used, since a definite solubility of AgI in 0.15 *N* $AgNO_3$ ($\sim$0.05 mg/ml) exists.

Analysis of I^{129} by Neutron Activation

The completeness of extraction of AgI^{129} from the ORNL silver-reactor packing was estimated by comparing yields of iodine activity in successive 1 *M* KCN extractions. Since the normal activity of I^{129} is only 2 μc/mg, the presence of large quantities of spray-carried activities (mainly ruthenium) led to the development of a much more convenient method based on irradiating six or eight saddles from each increment of the packing and relying on the greater activity of the 12.5-hr I^{130}, which was then also compared with the amount of 12.5-hr portion in a known amount of irradiated I^{129} (see Table 11).

The purification of the I^{129}-I^{130} was easily accomplished in two steps. First, all the silver and a small amount of carrier iodine were precipitated from 1 *M* KCN by acidifying with HNO_3. The precipitate was centrifuged, washed, and redissolved in 4 *M* $AgNO_3$ solution. If necessary, any residue (likely to be AgCN) was extracted again and then removed by centrifugation. The clear supernatant was diluted at least twentyfold with hot water which reprecipitated the AgI and some of the AgCN. Since some activation also occurs in the silver, it was necessary to repeat this step once to obtain a decontamination factor of about 10^5. Iodine-130 purified in this manner was observed to decay with a 12.5-hr half life through a factor of 30 or more. A correction for the chemical yield of iodine was finally determined by weighing the AgI.

The chemical steps used may be symbolized as follows:

$$AgI + KCN \longrightarrow Ag(CN)_2^- + I^-$$

$$Ag(CN)_2^- + H^+ + I^- \longrightarrow AgI(s) + AgCN(s) + HCN \text{ (unionized)}$$

$$AgI(s) + AgCN(s) + AgNO_3 \xrightarrow{\text{conc. } AgNO_3 \text{ soln.}} Ag_3(NO_3)_2^+ + I^- + CN^-$$

$$Ag_3(NO_3)_2^+ + I^- + CN^- \xrightarrow{H_2O \text{ dilution}} AgI(s) + AgCN(s) + AgNO_3$$

In the ORNL silver reactor, a 2-hr extraction at room temperature by contacting the irradiated saddles with 1 *M* KCN was sufficient to dissolve at least 95% of the iodine, although active silver continued to be extracted after 24 hr in a steam bath. The distribution of iodine on the saddles was found to be concentrated in the lower half of the reactor; the total amount was estimated at about 300 mg.

Separation of Silver and Iodine by Sulfide Precipitation

At present, the most attractive method for the separation of silver from iodine involves the precipitation of silver sulfide from a dilute alkali-cyanide solution. This behavior is based on the relatively high dissociation of the silver cyanide complex and the extremely low solubility product constant of Ag_2S. In alkaline solution, silver is completely removed from the cyanide complex by treatment with H_2S. This step, followed by acidification with H_2SO_4 and careful heating to remove the remaining gases, HCN and H_2S (for convenience in handling), leaves the iodine in a form readily oxidizable and extractable into $CHCl_3$ or CCl_4. The iodine then is easily recovered in a stoichiometric amount of $NaHSO_3$.

It is planned to recover the limited amount of I^{129} available in the ORNL silver reactor and to obtain one of the Hanford reactors as soon as radiation levels permit. The recovered I^{129} will be made available for general use.

RADIO-ORGANIC CHEMISTRY

ORGANIC REACTION MECHANISM STUDIES

Molecular Rearrangements – the 1,2,2-Triphenylethyl System

W. A. Bonner C. J. Collins

1,2,2-Triphenylethanol-1-C^{14} (I) has been acetylated and the resulting acetate (II) has been deacetylated, with no radiochemical rearrangement. Dehydration of carbinol I with phosphoric anhydride in xylene, however, yielded 1,1,2-triphenylethylene-1,2-C_1^{14} (IIIab) having an equal distribution of radioactivity over the ethylene skeleton. The carbinol I was converted into its *p*-toluenesulfonate ester (IV); the acetolysis of tosylate IV proceeded with phenyl migration, the latter reaching 50% when glacial acetic acid was used as the solvolyzing medium. Similar results were obtained during formolysis of tosylate IV. The addition of sodium acetate to acetolysis mixtures of tosylate IV resulted in a diminished extent of phenyl migration. These results are most simply interpreted in terms of the formation of a symmetrical phenonium ion intermediate[1] during acetolysis, with a possible, competing, direct, second-order displacement of tosylate by acetate ion. Hydrolysis of tosylate IV in aqueous acetone proceeded with 22% phenyl migration, while lithium aluminum hydride reduction led to only 9% phenyl migration.

Shown in Chart 1 is the synthetic method used to prepare carbinol I, as well as the degradative method employed to demonstrate the radiochemical structures. As seen in Chart 1, where the relative radioactivity assays of the pertinent products are indicated as fractions of the base radioactivity of carbinol I, only 0.97% of the radioactivity was found in the supposedly nonradioactive benzophenone fraction. This small amount is in all probability the consequence of slight phenyl migration during the oxidative degradation of carbinol I. The benzoic acid fraction in this oxidation shows a radioactivity assay, however, only 92% that of the base level. The low assay here and also in the benzoic acid fraction shown in the bottom line of Chart 1 was found by the application of carrier technique to be

(1) D. J. Cram, *J. Am. Chem. Soc.* 71, 3863 (1949); *ibid.*, p. 3875.

CHART 1

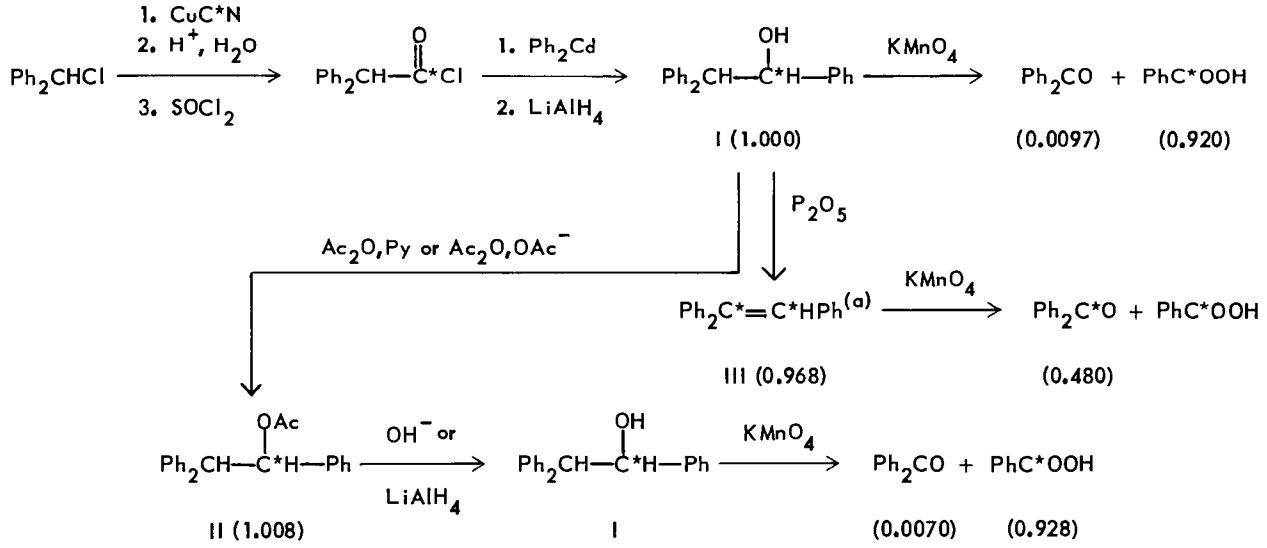

(a) Double asterisks here and in Chart 2 indicate a mixture of the two singly labeled radiochemical isomers $Ph_2C^*{=}CHPh$ (IIIa) and $Ph_2C{=}C^*HPh$ (IIIb) and *not* a doubly labeled structure.

the consequence of partial oxidation of the benzophenone fraction under the oxidative conditions employed. Thus, when benzophenone-α-C^{14} was subjected to the oxidizing conditions and the unprocessed oxidation mixture was treated with nonradioactive benzoic acid, the benzoic acid that was reisolated was found to be radioactive to an extent permitting calculation that 8% of the benzophenone-α-C^{14} had been oxidized. In view of this result, greater reliability can be placed on the radioactivity assay of the benzophenone fractions from such oxidations as being an indication of the extent of phenyl migration during the reactions outlined in Chart 2. This chart summarizes the results of the solvolyses reactions on the *p*-toluenesulfonate ester (IV) of carbinol I, as well as the result of the lithium aluminum hydride reduction of IV. The radiochemical consequences of these reactions, as indicated by the oxidative degradations shown, are summarized in the right-hand column as the percentage of phenyl migration occurring during each reaction.

Table 12 is a summary of the experimental data concerning the acetolyses of compound IV under varying conditions; Table 13 is a summary of the radiochemical data upon which the results cited in Charts 1 and 2 are based. These data constitute excellent radiochemical confirmation of the symmetrical phenonium ion postulated by Cram[1] on stereochemical grounds.

Molecular Rearrangements – the 1,1,2-Triphenylethyl System

C. J. Collins W. A. Bonner

1,1,2-Triphenylethanol-1-C^{14} (VI) has been dehydrated by means of aqueous sulfuric or glacial acetic acids to yield the unrearranged olefin, 1,1,2-triphenylethylene-1-C^{14} (IIIa). When this olefin was heated under reflux with dry xylene containing an equal weight of phosphoric anhydride, a complete isotopic position isomerization occurred which yielded a 50:50 mixture of IIIa and 1,1,2-triphenylethylene-2-C^{14} (IIIb). This observation can best be rationalized in terms of Cram's symmetrical phenonium ion.[1]

The semipinacolic dehydrobromination of 2-bromo-1,1,2-triphenylethanol-1-C^{14} (VII) to phenyl benzhydryl ketone-C^{14} (VIII) has been shown to take place with exclusive phenyl migration.

The reactions carried out are summarized in Chart 3. Molar radioactivities are reported as fractions of the molar radioactivity of labeled desoxybenzoin (V). The latter compound was prepared by the method of Collins and Neville.[2] Summarized in Table 14 are the radiochemical data upon which the molar radioactivities in Chart 3 are based.

The Rates and Migration Ratios Observed in the S_N1 and S_N2 Type Solvolyses of 2-Phenyl-2-(*p*-tolyl)ethanol-1-C^{14} Tosylate

J. G. Burr, Jr.

The migration ratios observed in the Wagner-Meerwein rearrangement of several substituted

[2] C. J. Collins and O. K. Neville, *J. Am. Chem. Soc.* 73, 2471 (1951).

TABLE 12. ACETOLYSES OF TOSYLATE IV UNDER VARYING CONDITIONS

	SAMPLE NUMBERS		
	1	2	3
Tosylate			
Grams	0.90	1.10	1.24
Millimole	2.10	2.58	2.90
Sodium acetate			
Grams	0.00	0.20	4.00
Millimoles	0.00	2.44	48.8
Sodium acetate/tosylate	0.00	0.95	16.9
Acetic acid[a] (ml)	8	10	20
Time (min)	60	45	60
Acetate			
Grams	0.43	0.64	0.83
Per cent	59	79	91
Melting point (°C)	142-145[b]	154-155	154-155
Carbinol			
Grams	0.34	0.53[c]	0.66[c]
Per cent	100	95[c]	93[c]
Melting point (°C)	(d)	86-87	87-88.5

[a] Containing 0.1 ml of acetic anhydride.

[b] Recrystallized from dilute acetic acid to give 0.39 g; m.p. 154-155°C.

[c] Refers to purified, crystalline product.

[d] Oxidized without recrystallization.

CHART 2

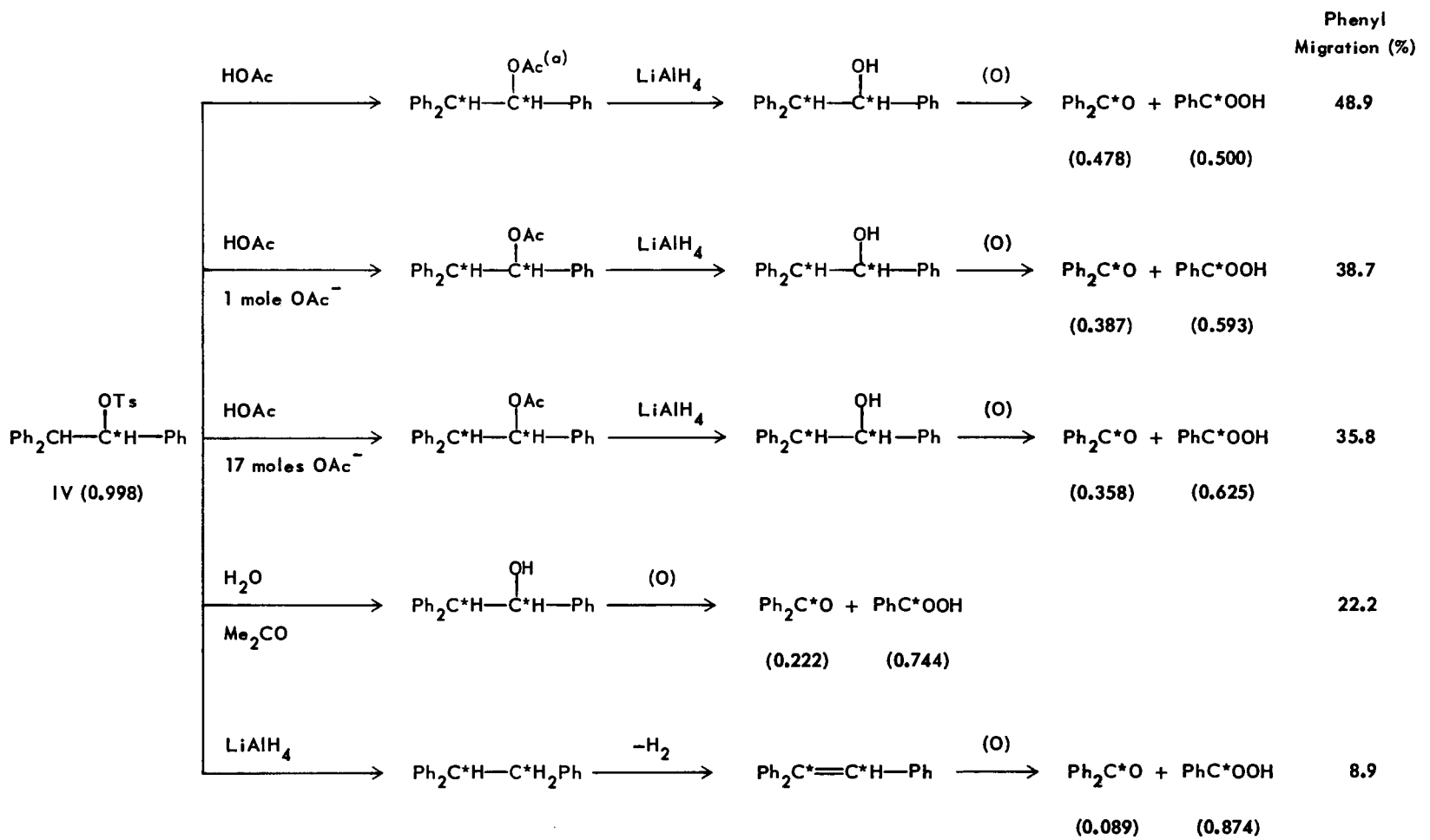

(a) See footnote, Chart 1.

TABLE 13. RADIOCHEMICAL DATA FOR OXIDATION PRODUCTS FROM VARIOUS 1,2,2-TRIPHENYLETHANOL-C^{14} AND 1,1,2-TRIPHENYLETHYLENE-C^{14} SAMPLES

	RADIOACTIVITY ASSAY[a] (mc/mole)	
	Benzoic Acid	Benzophenone 2,4-DNPH
Carbinol from:		
NaOH hydrolysis of acetate II	2.499 ± 0.020	0.0190
$LiAlH_4$ deacetylation of acetate II	2.482	0.0184
Tosylate acetolysis, run No. 1	1.281 ± 0.004	1.341
Tosylate acetolysis, run No. 2	1.591 ± 0.009	1.038 ± 0.002
Tosylate acetolysis, run No. 3	1.675	0.964
Tosylate hydrolysis	1.995	0.595 ± 0.004
Olefin from:		
Dehydration of carbinol I		1.287 ± 0.001
Tosylate formolysis		1.342
Tosylate reduction with $LiAlH_4$ then dehydrogenation	2.343	0.240 ± 0.002

[a]All radioactivity assays reported in this paper were conducted on a vibrating-reed electrometer after the usual wet combustion procedure [O. K. Neville, *J. Am. Chem. Soc.* **70**, 3499 (1948)] modified to handle compounds of high nitrogen content (W. A. Bonner and C. J. Collins, *J. Am. Chem. Soc.*, in press).

TABLE 14. SUMMARY OF DATA FOR PERMANGANATE OXIDATIONS OF IIIa, IIIab, AND VIII

COMPOUND OXIDIZED	RADIOACTIVITY ASSAY OF FRACTION ISOLATED (mc/mole)	
	Benzophenone 2,4-DNPH	Benzoic Acid
IIIa[a]		0.0322
IIIa[b]	2.432	0.0564
IIIab[c]	1.238; 1.238	1.203
IIIab[d]		0.645; 0.628
VIII[e]	0.026	2.392
VIII[f]	0.022	2.485[g]

[a]Prepared by the method of Adkins and Zartman (ref. 3).
[b]Prepared by the method of Lane and Walters (ref. 4).
[c]From the phosphorous pentoxide isomerization of IIIa, experiment No. 1.
[d]From the phosphorous pentoxide isomerization of IIIa, experiment No. 2.
[e]From rearrangement of the bromohydrin VII.
[f]From direct synthesis.
[g]This molar radioactivity is not consistent with the molar radioactivities of the other compounds described in this paper because of the different origin of the sample of VIII oxidized.

CHART 3

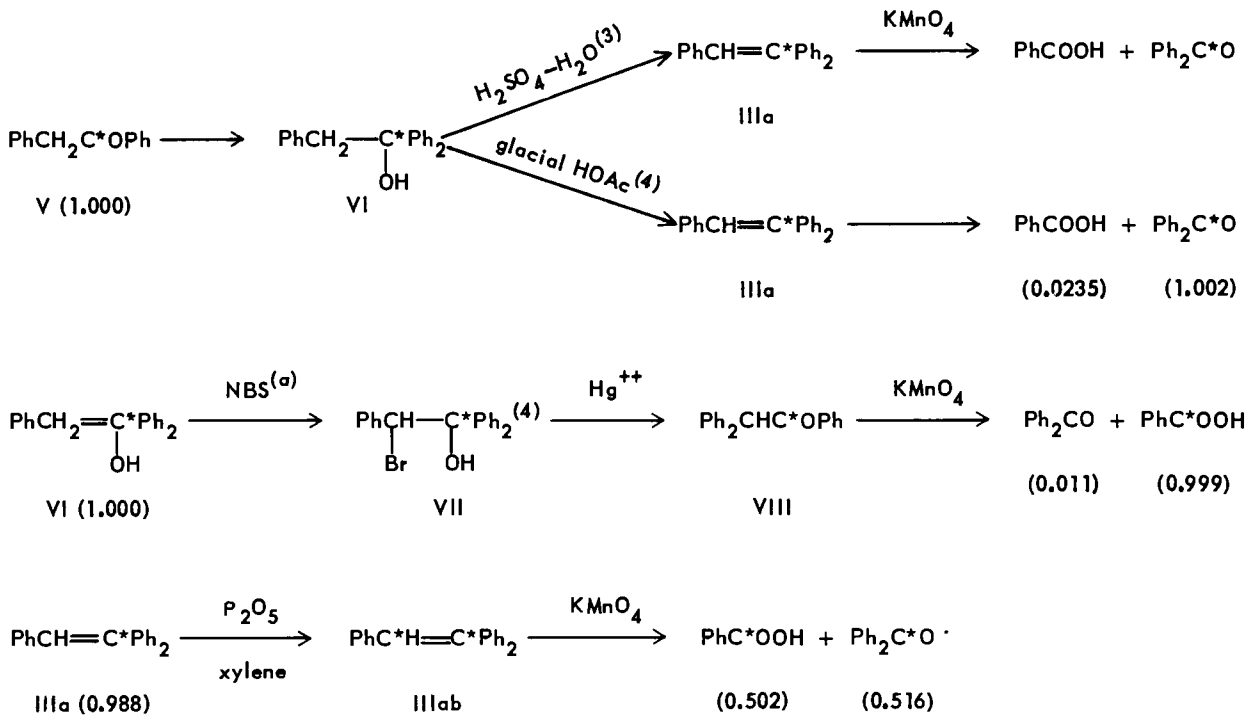

(a)NBS = N-bromosuccinimide.

2,2-diphenylethanols-1-C^{14} were reported recently.[5] The results obtained were discussed in terms of neighboring group participation of the aryl groups in the presumable rate-determining removal of hydroxyl for this acid-catalyzed dehydration-rearrangement.

A kinetic analysis has now been accomplished for the 2-phenyl-2-(*p*-tolyl)ethanol tosylate (I) and 2-phenyl-2-(*p*-tolyl)ethanol-1-C^{14} (Ia) tosylate system.

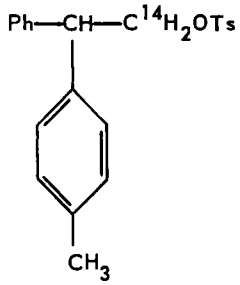

Ia

$(C_6H_5)_2{=}CHCH_2OTs$

II

$(p\text{-}CH_3C_6H_4)_2{=}CHCH_2OTs$

III

These compounds have been prepared and solvolyzed in glacial acetic acid. The rate of solvolysis for I and the migration ratio observed in the solvolysis of Ia are recorded in Table 15. Since the evidence for the extent of aryl group participation in this

(3)A. H. Blatt (ed.), *Organic Syntheses*, collective vol. II, p. 606, John Wiley and Sons, New York, 1943.

(4)J. F. Lane and D. R. Walters, *J. Am. Chem. Soc.* 73, 4234 (1951).

(5)J. G. Burr, Jr. and L. S. Ciereszko, *J. Am. Chem. Soc.* 74, 5426 (1952).

TABLE 15. SUMMARY OF RATE CONSTANTS

COMPOUND AND CONCENTRATION	SOLVENT	REAGENT AND CONCENTRATION	TEMPERATURE (°C)	k_1 (liters/mole·sec)	k_2 (liters/mole·sec)
$(C_6H_5)CHCH_2OTs$					
0.0513 *M*	HOAc		99.40	$3.51 \pm 0.04 \times 10^{-5}$	
0.0460 *M*	MC[a]	NaOMe, 0.0460 *M*	78.30		0.0187 ± 0.0016
C_6H_5 \ $CHCH_2OTs$ / $p\text{-}C_7H_7$					
0.0478 *M*	HOAc		99.50	$5.68 \pm 0.16 \times 10^{-5}$	
0.0460 *M*	MC	NaOMe, 0.0460 *M*	77.80		0.0117 ± 0.0005
$(p\text{-}C_7H_7)_2CHCH_2OTs$					
0.0526 *M*	HOAc		99.22	$29.2 \pm 0.05 \times 10^{-5}$	
0.0460 *M*	MC	NaOMe, 0.0460 *M*	78.00		0.00718 ± 0.00029

[a]Methyl cellosolve.

reaction can be gained only by comparison of the rate of this solvolysis with the rate of solvolysis of two reference compounds: 2,2-diphenylethanol tosylate (II) and 2,2-di(*p*-tolyl)ethanol tosylate (III), these rates are also recorded in Table 15. At least two independent determinations of each rate were made. Four independent determinations were made of the rate for the solvolysis of 2-phenyl-2-(*p*-tolyl)ethanol tosylate, since the rate constant for this compound tended to rise a little during each run. The data for a typical rate run on each compound are reported in Table 16.

The solvolysis rate of these same three esters was measured in a reaction which would be a bimolecular displacement process. Some difficulty was encountered in accomplishing this; however, it was found that the reaction of these esters with 0.05 *M* sodium methoxide in dry methyl cellosolve was cleanly second order. The bimolecular rate constants observed for these three compounds are shown in Table 17.

TABLE 16. SOLVOLYSES IN ACETIC ACID

(5.00-ml sample titrated for each time period)

TIME (sec)	NET AMOUNT OF 0.0510 *M* KOAc IN HOAc (ml)	k (sec^{-1})
Solvolysis of 0.0513 *M* 2-Phenyl-2-(*p*-tolyl)ethanol Tosylate at 99.50°C		
1,800	0.0894	5.67×10^{-5}
3,600	1.555	5.46×10^{-5}
5,400	2.117	5.40×10^{-5}
7,200	2.565	5.54×10^{-5}
10,920	3.255	5.71×10^{-5}
15,250	3.715	5.84×10^{-5}
Infinite	4.270	
	Average	$5.94 \pm 0.17 \times 10^{-5}$
Solvolysis of 0.0526 *M* 2,2-Di(*p*-tolyl)ethyl Tosylate at 99.22°C		
960	0.869	30.7×10^{-5}
1,920	1.509	30.5×10^{-5}
2,940	1.979	29.5×10^{-5}
5,460	2.759	30.4×10^{-5}
	Average	$30.2 \pm 0.04 \times 10^{-5}$

ISOTOPE-EFFECT STUDIES

Isotope Effects During Catalytic Hydrogenations

W. A. Bonner C. J. Collins

Isotope effects during the heterogeneous catalytic reductions of labeled olefin and carbonyl groups

are reported. Stilbene-α-C^{14} is reduced to dibenzyl-α-C^{14} with a 2% isotope effect by the use of Raney nickel in benzene or platinum in ethanol. Acetophenone-α-C^{14} is reduced to 1-phenylethanol-1-C^{14} with an 11.5% isotope effect by using platinum in ethanol, and with an 8% isotope effect by using lithium aluminum hydride in ether. No equilibration of hydrogen between stilbene-α-C^{14} and dibenzyl or between acetophenone-α-C^{14} and 1-phenylethanol or ethanol was observed under the conditions of catalytic reduction employed. The reductions were studied from both ends of the scale for completeness of reaction. That is, the reactions were conducted to 10% completion, and the product of 10% reduction was examined; then the reactions were conducted to 90% completion, and the 10% unreduced product was examined. Quantitative physical and/or chemical methods previously worked out on known mixtures were employed for separation of unreacted material and reaction product, and all radiochemical comparisons were made on the basis of solid crystalline derivatives of known physical properties. The results of these reduction experiments are shown in Tables 18 and 19.

TABLE 17. SOLVOLYSES WITH SODIUM METHOXIDE IN METHYL CELLOSOLVE

TIME (sec)	NaOH BACK TITRE (ml)[a]	k_2 (liter mole^{-1}sec^{-1})
0.0460 M 2,2-Diphenylethyl Tosylate at 78.30°C		
0	0.930	
600	1.679	0.0126
1200	2.132	0.0125
1800	2.420	0.0120
3000	2.852	0.0123
4200	3.050	0.0116
6000	3.260	0.0111
		Average 0.0120
0.0460 M 2-Phenyl-2-(*p*-tolyl)ethyl Tosylate at 77.80°C		
0	1.272	
360	1.840	0.0185
780	2.358	0.0217
1200	2.650	0.0187
1800	2.840	0.0187
2700	3.027	0.0163
3600	3.245	0.0175
		Average 0.0189
0.0460 M 2,2-Di(*p*-tolyl)ethyl Tosylate at 78.00°C		
0	0.800	
1200	1.753	0.00782
1800	1.990	0.00728
2700	2.320	0.00733
4200	2.622	0.00682
6000	2.920	0.00690
7740	3.115	0.00704
		Average 0.00720

[a]Each sample was 5.00 ml and was added to 5.00 ml of 0.0529 M HCl and back-titrated with 0.0514 M NaOH.

Hydrogenation of C^{14}-labeled Cinnamic Acids

A. J. Weinberger V. F. Raaen
G. A. Ropp

Since catalytic hydrogenation of acetophenone-α-C^{14} was shown to be accompanied by carbon isotope fractionation,[6] it was of interest to test for similar isotope effects in the hydrogenation of a carbon-to-carbon double bond labeled with C^{14}. The three cinnamic acids, I, II, and III, containing carbon labels in three positions have been prepared:

$$C_6H_5—C^{14}H{=}CH—COOH$$

I

$$C_6H_5—CH{=}C^{14}H—COOH$$

II

$$C_6H_5—CH{=}CH—C^{14}OOH$$

III

Acids I and II were hydrogenated in ethanol solution over platinum at 25°C with sufficient hydrogen to give saturation of half the molecules present in each case; the remaining unreacted cinnamic acid

[6]G. A. Ropp and V. F. Raaen, *Chem. Quar. Prog. Rep. Dec. 31, 1952*, ORNL-1482, p. 14.

TABLE 18. ISOTOPE EFFECT DURING CATALYTIC REDUCTION OF STILBENE-α-C^{14}

STILBENE-α-C^{14} ASSAY (mc/mole)	CATALYST	SOLVENT	COMPLETION OF REACTION (%)	PRODUCT ASSAYED	ASSAY OF PRODUCT (mc/mole)
1.076	Raney nickel	Benzene	10	Dibenzyl-α-C^{14}	1.054
1.076	Raney nickel	Benzene	90	Benzaldehyde-α-C^{14}-2,4-DNPH	1.097
2.654	Platinum	Ethanol	11	Dibenzyl-α-C^{14}	2.596

TABLE 19. ISOTOPE EFFECT DURING REDUCTION OF ACETOPHENONE-α-C^{14}

ACETOPHENONE-α-C^{14} ASSAY (mc/mole)	CATALYST	SOLVENT	COMPLETION OF REACTION (%)	PRODUCT ASSAYED	ASSAY OF PRODUCT (mc/mole)
2.626	Platinum	Ethanol	10	α-Phenylethyl-α-C^{14} 3,5-dinitrobenzoate	2.311
2.626	Platinum	Ethanol	90	Acetophenone-α-C^{14}-2,4-DNPH	3.237
2.974	$LiAlH_4$	Ether	15	α-Phenylethyl-α-C^{14} 3,5-dinitrobenzoate	2.720

then was separated – by recrystallization from ligroin and sublimation – from the product, hydrocinnamic acid. In the hydrogenation of acids I and II, no carbon isotope effects were found, and the unreacted cinnamic acid in each case had the same specific activity as the original cinnamic acid used. Study of the hydrogenation of acid III has been started, since it seems possible that the rate-controlling process in the hydrogenation might involve some process, such as the following, in which an isotope effect would be observed only if the carboxyl carbon were labeled:

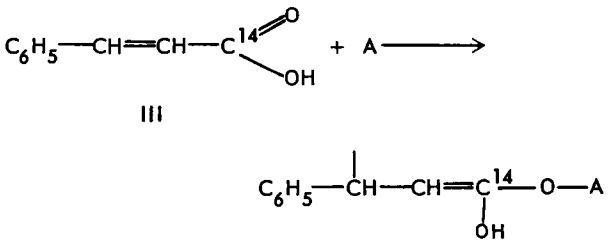

According to this scheme, the entity A, whether neutral or charged, could attach itself to the oxygen of the carboxyl group to give an ion or radical of the type shown.

The Iodoform Reaction of Acetone-1-C^{14}

M. T. Clark[7] G. A. Ropp

The iodoform reaction of acetone-1-C^{14}

$$CH_3-\overset{O}{\overset{\|}{C}}-C^{14}H_3 + 3I_2 + 4NaOH \longrightarrow$$

$$C^{14}H_3-COONa + C^{14}HI_3 + 3NaI + 3H_2O$$

has been reported[8] to go with a reverse intramolecular isotope effect. That is, the C^{14}-C^{12} bond is reported to cleave faster than the C^{12}-C^{12} bond. Since such a result is contrary to that usually found in carbon isotope fractionation, this study is being repeated. Preliminary results indicate no isotope effect at all; however, the results reported here are from a single run. As shown in the following summary, the iodoform produced had approximately one-half the specific activity of the

[7] ORINS.

[8] A. Roe and E. L. Albenesius, *J. Am. Chem. Soc.* 74, 2402 (1952).

acetone; the latter was radioassayed as the solid 2,4-dinitrophenylhydrazone.

	Acetone (mc/mole)	Iodoform (mc/mole)
Sample 1	1.491	0.743
Sample 2	1.475	0.732
Mean	1.483	0.738

Reactions of Benzoic-α-C^{14} Anhydride

V. F. Raaen G. A. Ropp

Comparisons of experimentally measured values of intramolecular carbon isotope effects with theoretically calculated values are of particular interest since the theory[9] appears to predict very definite and easily calculated ratios of rate constants. It can also be developed from the theory that the rate-constant ratio for a given intramolecular isotope effect should have the same value at all temperatures, in contrast to intermolecular isotope effects which vary decidedly with temperature.

The intramolecular isotope-effect study described here is concerned with the reactions of the symmetrical compound, benzoic-α-C^{14} anhydride (I). The reactions involved are:

The ethanolysis reaction, A, was carried out in ethanol solution at two temperatures, and each isotope-effect value was calculated as the ratio of specific activities of III and II. The specific activity of III was measured after the ester was isolated and completely hydrolyzed to benzoic-α-C^{14} acid. The ethanolysis, A, was very slow, particularly at the lower temperature, 30°C, and required 33 days to effect 93% reaction, as measured by titration of the acid, II. The reaction, B, was carried out in dry hydrocarbon solvents and went to completion rapidly. However, the intramolecular isotope-effect ratios for A or B can be calculated at any stage during the reaction as the specific activity ratios, II/III and IV/V.

It is believed that for reactions A and B, the symmetry-destroying steps (and hence the steps which decide the distribution of isotopes between the two products of each reaction) are, respectively, A′ and B′ which involve attacks at the labeled

[9] J. Bigeleisen, *J. Chem. Phys.* 17, 425 (1949); J. Bigeleisen, *A Theoretical Evaluation of the Nitrogen Isotope Effect in the Thermal Deammonation of Phthalamide*, BNL-1068.

Reaction A

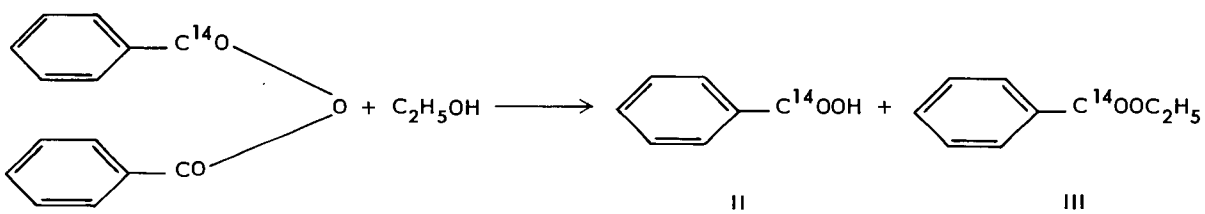

I II III

Reaction B

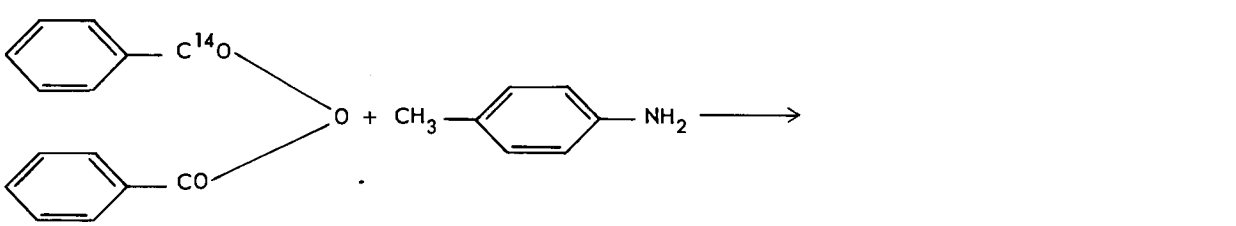

IV V

carbon of the carbonyl group:

Reaction A′

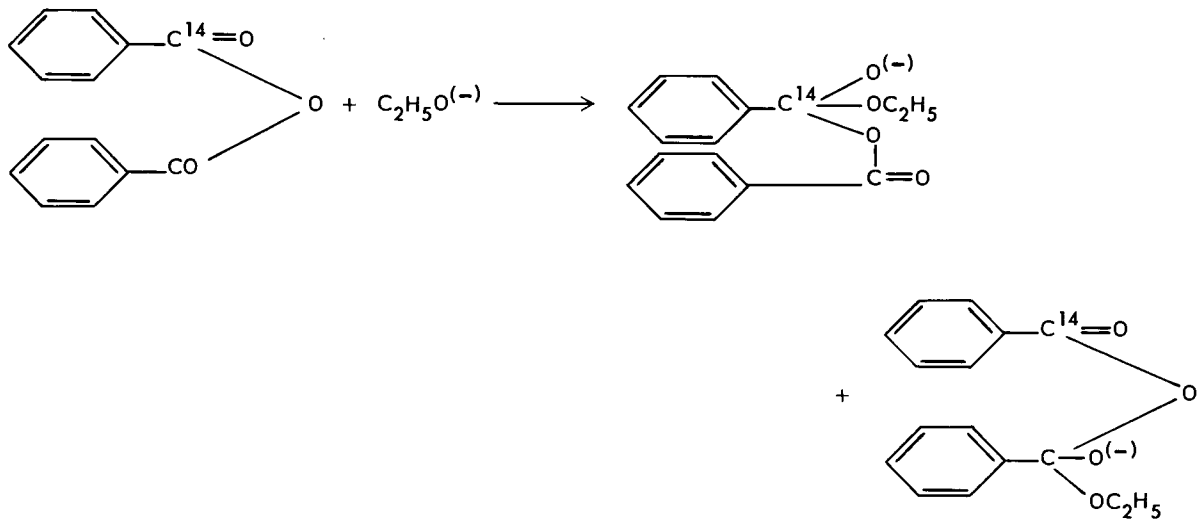

Reaction B′

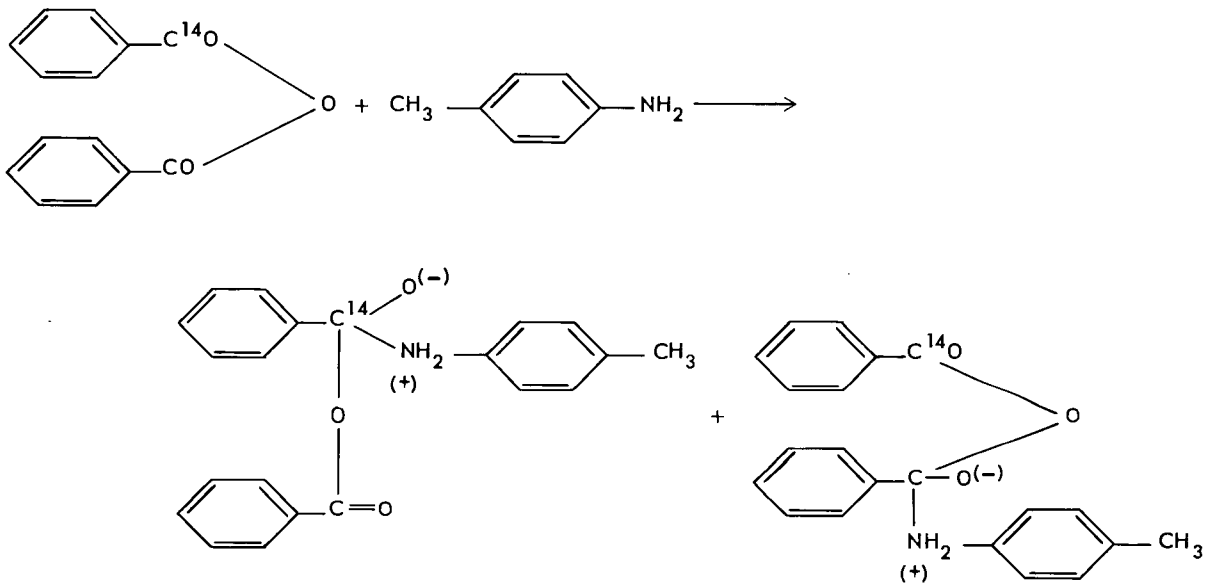

The results are presented in Table 20.

From the results in Table 20, it appears that there is no appreciable variation of these isotope-effect ratios with temperature, in agreement with the theory. However, the lack of agreement between experimental and calculated isotope fractionation factors, which is apparent in Table 20, has also been noted in other intramolecular isotope-effect studies.[10]

[10] The extent of agreement between theory and experiment for C^{14} intramolecular isotope effects has been tabulated in the review, G. A. Ropp, *Nucleonics* 10, No. 10, 22 (1952).

TABLE 20. SUMMARY OF ETHANOLYSIS REACTIONS

REACTION	TEMPERATURE (°C)	SPECIFIC ACTIVITIES (mc/mole)	k_{12}/k_{14}	THEORETICAL VALUE*
A	30	II = 3.99, III = 3.54	1.127	For making a C-O bond: 1.043
	78	II = 4.03, III = 3.57	1.129	
B	30	IV = 3.92, V = 3.65	1.073	For making a C-N bond: 1.040
	138	IV = 3.86, V = 3.60	1.071	

*See ref. 9.

Bromination of C^{14}-labeled Methyl Cinnamate

G. A. Ropp V. F. Raaen

In earlier reports,[11] the brominations of methyl cinnamate-α-C^{14}, styrene-α-C^{14}, and styrene-β-C^{14} were stated as not being accompanied by carbon isotope fractionation. This study has been extended to the addition of bromine to methyl cinnamate-β-C^{14}, which has also been shown not to involve isotope fractionation:

$$C_6H_5—C^{14}H{=}CH—COOCH_3 + Br_2 \longrightarrow C_6H_5—C^{14}HBr—CHBr—COOCH_3$$

Reactions of Carbonyl-C^{14} Ethyl Benzoates and Acetophenones

V. F. Raaen G. A. Ropp

The isotope fractionation study for the saponification of ring-substituted ethyl benzoates[12] (α-C^{14}) and the parallel study of the formation of 2,4-dinitrophenylhydrazones of acetophenones[13] (α-C^{14}) have now been completed. Final isotope-effect ratios in these studies are presented in Tables 21 and 22. As Table 22 shows, the isotope fractionation ratio, k_{14}/k_{12}, increases and the reaction rate, k_{12}, decreases in both the ketone and ester series,[14] as the electron-releasing ability of the substituent increases.

STUDY OF SCINTILLATION COUNTING OF CARBON-14 IN SOLUTION

J. B. Davidson[15] A. J. Weinberger
G. A. Ropp

The instrument, previously reported,[16] for measuring the relative activity level of two solutions containing C^{14} has been modified. A third glass cell has been added that will contain only a solution of the scintillator (terphenyl or quarterphenyl-terphenyl mixture); this cell will serve for the determination of the background count. The register counts (A) measured for this cell are subtracted from the register counts (B and C) measured for each of the other two cells before the ratio of B to C is calculated. Table 23 indicates the precision experimentally obtained for this ratio. Since B and C were obtained for identical toluene solutions containing the same amount of ethyl benzoate-α-C^{14} (about 1 μc in each cell) and the same amount of terphenyl, the ratio should be 1.000. In the data for Table 23, B and C represent about 2000 register counts on each of the cells;

(11) V. F. Raaen and G. A. Ropp, *Chem. Quar. Prog. Rep. Sept. 30, 1952*, ORNL-1432, p. 22.

(12) G. A. Ropp and V. F. Raaen, *Chem. Quar. Prog. Rep. Sept. 30, 1951*, ORNL-1153, p. 33; see also more recent ORNL chemistry quarterly reports.

(13) V. F. Raaen and G. A. Ropp, *Chem. Quar. Prog. Rep. Dec. 31, 1952*, ORNL-1482, p. 12.

(14) G. A. Ropp and V. F. Raaen, *J. Chem. Phys.* 20, 1823 (1952).

(15) Instrument Department.

(16) G. A. Ropp and J. Davidson, *Chem. Quar. Prog. Rep. Sept. 30, 1952*, ORNL-1432, p. 26.

TABLE 21. EFFECT OF VARYING TEMPERATURE, SOLVENT, ESTER CONCENTRATION, AND THE ALKYL GROUP ON THE ISOTOPE EFFECT IN ETHYL BENZOATE-α-C^{14} SAPONIFICATION AND ETHYL *p*-METHOXY BENZOATE SAPONIFICATION

ESTER	TEMPERATURE (°C)	SOLVENT	ESTER CONCENTRATION IN SOLVENT (M)	$S_3/S_{100} = k_{14}/k_{12}$
Ethyl benzoate-α-C^{14}	0	90% ethanol	0.32	0.918
	25	90% ethanol	0.32	0.929
	78.5	90% ethonol	0.32	0.939
Ethyl benzoate-α-C^{14}	25	56% acetone	0.32	0.928
Ethyl *p*-methoxy benzoate-α-C^{14}	25	90% ethanol	0.32	0.916
	25	56% acetone	0.32	0.917
Ethyl benzoate-α-C^{14}	25	90% ethanol	1.60	0.926
t-Butyl benzoate-α-C^{14}	25	56% acetone	0.32	0.939

TABLE 22. ISOTOPE-EFFECT DATA FOR THE INDIVIDUAL REACTIONS FORMING 2,4-DINITROPHENYLHYDRAZONES OF THREE RING-SUBSTITUTED ACETOPHENONES (α-C^{14})

SUBSTITUENT	TEMPERATURE (°C)	REACTION OF KETONE (%)	SPECIFIC ACTIVITY (μc/mg)	S/S_{100}	k_{14}/k_{12}	MEAN k_{14}/k_{12}
p-OCH_3	25	100	4.209×10^{-3}	0.947	0.936	
		30	3.984×10^{-3}			
	25	100	4.341×10^{-3}	0.935	0.931	
		10	4.060×10^{-3}			
	25	100	4.303×10^{-3}	0.936	0.932	0.933
		10	4.028×10^{-3}			
None	−75	100	9.09×10^{-3}	0.910	0.908	0.908
		5	8.27×10^{-3}			
	25	100	8.97×10^{-3}	0.945	0.943	
		5	8.48×10^{-3}			
	25	100	8.94×10^{-3}	0.951	0.949	0.946
		10	8.50×10^{-3}			
None	78	100	8.97×10^{-3}	0.966	0.959	
		30	8.67×10^{-3}			
	78	100	9.15×10^{-3}	0.965	0.958	0.959
		30	8.83×10^{-3}			
m-NO_2	25	100	6.95×10^{-3}	0.962	0.960	0.960
		10	6.68×10^{-3}			

the counting required 10 to 15 min and included 10 to 15 cycles of the instrument. By averaging the last column of Table 23, the mean experimentally determined ratio was calculated as 1.007 ± 0.007. The precision index refers to the average deviation from the mean. This precision is of the same order as that obtained with the vibrating-reed electrometer in counting[17] C^{14} samples.

[17] V. F. Raaen and G. A. Ropp, *Anal. Chem.* **25**, 174 (1953).

TABLE 23. PRECISION OBTAINED IN THE PRELIMINARY RUNS WITH SOLUTION SCINTILLATION COUNTER FOR C^{14}-LABELED ETHYL BENZOATE

DATE	VOLTAGE	GAIN	A BACKGROUND	$B - A$	$C - A$	$\frac{B - A}{C - A}$
5/27/53	926	30	18	3,424	3,438	0.9960
5/28/53	900	40	20	3,078	3,007	1.024
5/28/53	900	80	15	5,379	5,353	1.005
5/28/53	900.5	80	7	2,132	2,114	1.009
5/28/53	900.5	100	3	2,007	2,009	0.999
5/28/53	931.7	100	11	2,941	2,944	0.999
5/29/53	890.5	70	6	2,636	2,613	1.009
5/29/53	890.5	70	9	2,045	2,025	1.010
5/29/53	1000.2	100	28	5,048	5,024	1.005
6/2/53	1001.2	100	14	3,087	3,035	1.017
6/2/53	900	60	23	5,495	5,313	1.034
6/3/53	950	50	21	5,003	4,963	1.008
6/3/53	950	50	11	2,163	2,121	1.020
6/4/53	950	50	573	5,322	5,320	1.000
6/4/53	950	50	602	5,268	5,268	1.000
6/4/53	950	70	754	18,448	18,472	0.999
6/4/53	950	70	203	5,545	5,545	1.000
6/4/53	950	70	293	3,590	3,584	1.002
6/4/53	950	70	153	2,481	2,471	1.004
					Mean:	1.007 ± 0.007
					Theoretical:	1.000

CHEMISTRY OF SEPARATION PROCESSES

ION EXCHANGE

B. A. Soldano G. E. Myers
Q. V. Larson

Application of the Osmotic Coefficient Concept to Mixed-Resin Systems

Previous investigation of ion-exchange selectivities of trace cations has been extended to include mixed systems consisting of two cation pairs. These measurements have been made in order to subject the so-called "solution" concept of ion-exchange resins to a more stringent test of its general validity.

The solution concept considers the resin phase, in equilibrium with an external aqueous salt solution, to behave as an aqueous solution of the resin ions and their counterions. Because of the resin cross links this inner solution exists under a swelling pressure, P, which is a function of the particular cross-linked resin and its composition. Thus, when a distribution of two ions between an external solution and the resin phase is considered, it can be shown thermodynamically that the following equation should hold:

$$\log K_d - \frac{P(v_1^0 - v_2^0)}{2.3RT} = \log\left(\frac{\gamma_1}{\gamma_2}\right)_r - \log\left(\frac{\gamma_1}{\gamma_2}\right)_0$$

where P is the swelling pressure, v_1^0 and v_2^0 are the partial molal volumes of the two ions at infinite dilution, $(\gamma_1/\gamma_2)_r$ and $(\gamma_1/\gamma_2)_0$ are the ratios of the activity coefficients of the two ions in the resin phase and outside solution, respectively, and K_d is the function $(m_2/m_1)_r/(m_2/m_1)_0$ in which m represents the molality.

K_d and P are independently measurable, the v^0's are available in the literature, and $(\gamma_1/\gamma_2)_0$ may be assumed to be unity at a concentration of 0.1 M. Thus, to test the theory, it remains either to measure $(\gamma_1/\gamma_2)_r$ independently or to determine whether the ratio, as measured by this means, follows a pattern typical of electrolytes in ordinary concentrated aqueous solutions. At present, it is not possible to measure $(\gamma_1/\gamma_2)_r$ independently; therefore recourse must be taken to the application of Harned's rule for concentrated aqueous solutions, which states that

$$\log\left(\frac{\gamma_1}{\gamma_2}\right)_r = \log\left(\frac{\gamma_1^0}{\gamma_2^0}\right)_r - a_{12}(m_2)_r + a_{21}(m_1)_r$$

Here (γ_1^0/γ_2^0) is the ratio of the activity coefficients of the two pure resin forms, and a_{12} and a_{21} are the so-called "interaction coefficients" for the two resin salts. The interaction coefficients are constant at a given total molality, m, and usually are found to approach constancy with increasing molality. Further, Glueckauf has shown that $\log (\gamma_1^0/\gamma_2^0)_r$ may, with some approximation, be set equal to $(2/2.3)(\phi_1^0 - \phi_2^0)$, where ϕ_1^0 and ϕ_2^0 are the osmotic coefficients of the pure resin salts at some particular molality; these are obtainable from isopiestic moisture equilibrations (see Fig. 17). Therefore, by measuring the selectivity, the swelling pressure, the pure osmotic coefficients, and the moisture content (molality) of a series of resins, it is possible to test the application of Harned's rule and thus the validity of the model.

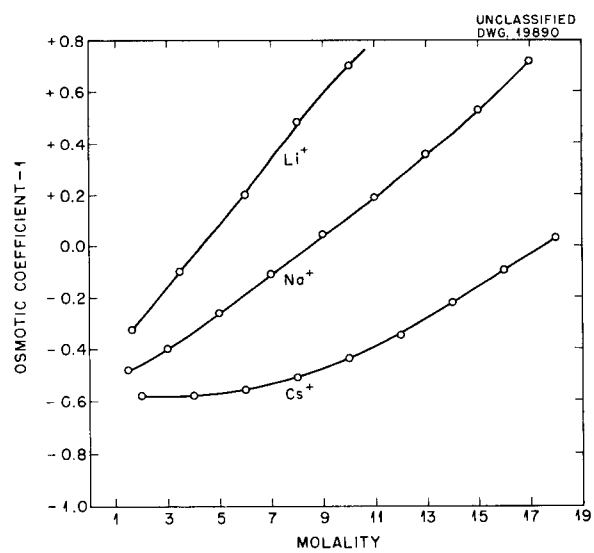

Fig. 17. Osmotic Coefficient vs. Molality of Li^+ Na^+, Cs^+.

Such measurements have now been made as a function of resin cross linking and equivalent loading for the following systems: Dowex-50, Na-Li and Na-Cs at seven cross linkings, and 1 to 24% DVB. The measured selectivities for a series of mixed forms of Na-Li exchangers as a function of cross linking are listed in Table 24 and shown in Fig. 18. As expected, the selectivity of Na/Li increases with cross linking and is a function of the loading of the exchanger for any given cross linking. In Table 25 are listed the molalities of the pure forms of the NaR and LiR in equilibrium with 0.1 *N* chloride solutions. It has been found that, for five complete systems varying from 1 to 24% DVB, the molality of a mixed resin is an exact linear function of the mole fraction of the exchanger. Therefore, if the molality of the pure forms is known, the other values can be easily calculated. The values for a_{12} and $-a_{21}$ in Table 25 are the interaction coefficients calculated from the experimental K_d's at $F = 0.2$ and 0.8. (It should be pointed out that in this particular system the $P\Delta V^0$ correction is negligible.) In the main, it appears that the a_{12} values decrease with increasing molality but tend to level off at high concentrations. The a_{21} values decrease in a somewhat more erratic pattern. It is not surprising that the calculated interaction coefficients should change with cross linking, since they are a function of molality, and molality increases rapidly with cross linking. The tendency toward constant a_{12} values at higher cross linking is a further reflection of the usual behavior of such interaction coefficients. Since molality

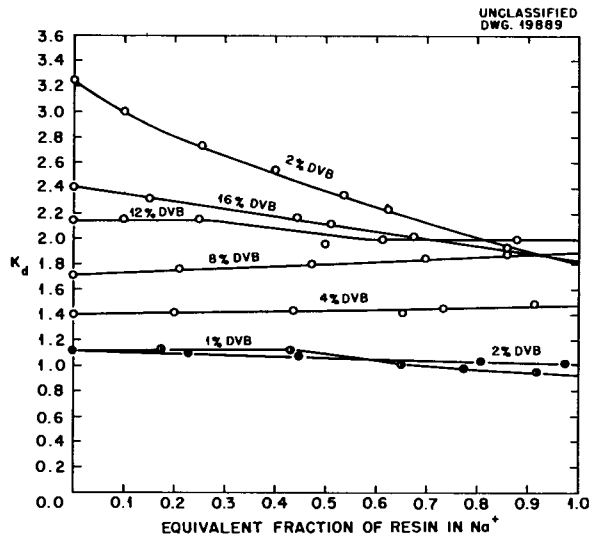

Fig. 18. Variation of Na^+-Li^+ Selectivities with Polymer Cross Linking.

TABLE 24. DEPENDENCE OF F* AND K_d FOR Na-Li ON CROSS LINKING AND MOLE FRACTION**

1% DVB		2% DVB		4% DVB		8% DVB		12% DVB		16% DVB		24% DVB	
F	K_d	F	K_d	F	K_d	F	K_d	F	K_d	F	K_d	F	K_d
0	1.12	0	1.12	0	1.4	0	1.715	0	2.15	0	2.40	0	3.25
0.05	1.12	0.05	1.12	0.20	1.41	0.215	1.76	0.10	2.16	0.15	2.31	0.10	3.00
0.175	1.13	0.16	1.1	0.435	1.43	0.475	1.80	0.25	2.16	0.445	2.17	0.255	2.73
0.43	1.13	0.4	1.09	0.655	1.42	0.70	1.85	0.50	1.96	0.51	2.12	0.40	2.54
0.65	1.02	0.45	1.08	0.735	1.45	0.86	1.88	0.615	2.00	0.675	2.025	0.535	2.34
0.775	0.98	0.625	1.14	0.915	1.49	0.92	1.84	0.88	2.00	0.86	1.925	0.625	2.23
0.92	0.95	0.79	1.06					0.92	1.93			0.875	1.93
		0.87	0.82									0.91	1.90
		0.90	0.86										

*F = equivalent fraction of resin in Na^+ form.

**$K_d = \dfrac{(Na/Li)_r}{(Na/Li)_0}$

TABLE 25. VARIATION OF INTERACTION COEFFICIENTS WITH MOLALITY

DVB (%)	MOLALITY OF NaR IN 0.1 N NaCl SOLUTION	MOLALITY OF CsR IN 0.1 N CsCl SOLUTION	MOLALITY OF LiR IN 0.1 N LiCl SOLUTION	Na-Li		Na-Cs	
				$+a_{12}$	$-a_{21}$	$+a_{12}$	$+a_{21}$
1		1.92				0.016	0.145
2	1.95	2.89	1.59	0.0674	0.0474	0.0121	0.061
4	3.02	4.29	2.81	0.01504	0.02194	0.029	0.044
8	5.98	6.95	5.09	0.00962	0.010287	0.041	0.015
12	8.66	9.25	7.72	0.01842	0.01082	0.038	0.009
16	10.10	10.90	8.43	0.0237	0.00976	0.036	0.012
24	14.00	16.90	12.43	0.0226	0.00386	0.033	0.019

changes with mole fraction are only moderate for any given cross linking, it is not unreasonable to expect relative constancy of the a's within each cross linking; this assumption was, of course, implicity made in calculating these coefficients from the data at two values of F. Thus, for each cross linking it should be possible to calculate the entire selectivity vs. mole-fraction curve by using the particular interaction coefficients obtained above.

In Table 26 is listed a comparison of the measured values of K_d with those calculated. The correlation is extremely close indeed and does not seem to be affected by the degree of cross linking. In most cases, the calculated values agree with the experimental answer within 1%. It would therefore appear that the treatment for the Na-Li system is valid.

This approach was then extended to the Na-Cs system where there is a large $P\Delta V^0$ correction that is due to the great difference in the hydrated partial molar volume of sodium and cesium ions at infinite dilution. The measured selectivities for cesium over sodium are presented in Table 27 and Fig. 19, along with the corresponding $P\Delta V^0$ corrections and the resulting values of log $(\gamma_{Na}/\gamma_{Cs})_r$; it may be seen that the correction here is indeed of significant magnitude. As with the Na-Li system, the interaction coefficients were calculated for each cross linking from the values of log $(\gamma_{Na}/\gamma_{Cs})_r$ at $F = 0.2$ and 0.8, and are tabulated in Table 25. Here also, a_{12} and

TABLE 26. COMPARISON OF THE CALCULATED WITH THE EXPERIMENTAL K_d AS A FUNCTION OF CROSS LINKING IN THE Na-Li SYSTEM

DVB (%)	K_d									
	$F = 0$		$F = 0.2$		$F = 0.5$		$F = 0.8$		$F = 1.0$	
	Calculated	Measured	Calculated	Measured	Calculated	Measured	Calculated	Measured	Calculated	Measured
2	1.11	1.11	1.10	1.10	1.08	1.09	1.05	1.05	1.04	1.05
4	1.38	1.40	1.41	1.41	1.43	1.43	1.46	1.46	1.47	1.47
8	1.78	1.72	1.75	1.76	1.83	1.81	1.86	1.87	1.93	1.91
12	2.19	2.15	2.17	2.17	2.15	2.01	1.97	1.97	2.0	2.0
16	2.34	2.40	2.29	2.29	2.16	2.13	1.96	1.95	1.85	1.85
24	3.19	3.25	2.82	2.82	2.38	2.40	2.0	2.0	1.7	1.82

TABLE 27. SELECTIVITY DATA FOR Na-Cs–DOWEX-50

F^*	K_d^{**}	$\frac{-P\Delta V^0}{2.3RT}$	LOG K_d	LOG $K_d - \frac{P\Delta V^0}{2.3RT}$ = LOG $(\gamma_{Na}/\gamma_{Cs})_r$
			1% Dowex-50	
0	1.25	0.0066	0.0969	0.1035
0.15	1.26	0.0057	0.1004	0.1061
0.43	1.36	0.0049	0.1335	0.1384
0.57	1.45	0.0042	0.1614	0.1658
0.77	1.52	0.0036	0.1818	0.1854
0.87	1.55	0.0033	0.1903	0.1936
1.00	1.59	0.0028	0.2014	0.2042
			2% Dowex-50	
0	1.31	0.0129	0.1173	0.1302
0.13	1.35	0.0125	0.1303	0.1428
0.36	1.43	0.0117	0.1553	0.1670
0.59	1.52	0.0110	0.1818	0.1928
0.87	1.63	0.0100	0.2122	0.2222
0.895	1.64	0.0100	0.2148	0.2248
1.00	1.70	0.0097	0.2305	0.2402
			4% Dowex-50	
0	1.27	0.0225	0.1038	0.1263
0.13	1.33	0.0219	0.1239	0.1458
0.315	1.48	0.0210	0.1703	0.1913
0.545	1.59	0.0198	0.2014	0.2212
0.575	1.64	0.0198	0.2148	0.2346
0.78	1.80	0.0188	0.2553	0.2741
0.875	1.85	0.0184	0.2672	0.2856
1.0	1.96	0.0178	0.2923	0.3101
			8% Dowex-50	
0	1.16	0.0292	0.0645	0.0937
0.13	1.27	0.0316	0.1038	0.1354
0.375	1.54	0.0364	0.1875	0.2239
0.545	1.74	0.0396	0.2406	0.2802
0.565	1.82	0.0400	0.2601	0.3001
0.725	2.00	0.0432	0.3010	0.3442
0.86	2.13	0.0457	0.3284	0.3741
1.00	2.44	0.0485	0.3874	0.4359

TABLE 27 (continued)

F^*	K_d^{**}	$\frac{-P\Delta V^0}{2.3RT}$	LOG K_d	LOG $K_d - \frac{P\Delta V^0}{2.3RT}$ = LOG $(\gamma_{Na}/\gamma_{Cs})_r$
		12% Dowex-50		
0	1.09	0.0615	0.0374	0.0989
0.13	1.25	0.0647	0.0969	0.1616
0.40	1.65	0.0720	0.2175	0.2895
0.565	1.94	0.0765	0.2878	0.3643
0.59	1.98	0.0768	0.2967	0.3735
0.725	2.25	0.0804	0.3522	0.4326
0.86	2.50	0.0840	0.3979	0.4819
1.00	2.94	0.0876	0.4684	0.5560
		16% Dowex-50		
0	1.10	0.0705	0.0419	0.1124
0.125	1.28	0.0750	0.1072	0.1822
0.36	1.56	0.0835	0.1931	0.2766
0.54	1.98	0.0905	0.2967	0.3872
0.58	2.04	0.0920	0.3096	0.4016
0.855	2.67	0.1018	0.4265	0.5283
1.00	3.18	0.1073	0.5024	0.6097
		24% Dowex-50		
0	0.834	0.1571	−0.0788	0.0783
0.135	1.27	0.1621	+0.1038	0.2659
0.30	1.52	0.1693	0.1818	0.3511
0.49	1.82	0.1762	0.2601	0.4363
0.57	2.00	0.1799	0.3010	0.4809
0.80	3.45	0.1890	0.5378	0.7268
1.00	5.89	0.1970	0.7701	0.9671

$^*F$ = equivalent fraction of resin in Na^+ form.

$^{**}K_d = \frac{(Cs/Na)_r}{(Cs/Na)_0}$.

a_{21} vary with cross linking, although that variation becomes considerably lessened at higher cross linking, that is, molality. This increasing constancy is further demonstrated by the better agreement between experimental and calculated values of log $(\gamma_{Na}/\gamma_{Cs})_r$ at the higher cross linkings, and the comparison is shown in Table 28. The correlation here does not appear to be nearly as quantitative as it was in the Na-Li system. However, considerably greater uncertainty is to be expected in the Na-Cs system because of the relatively large $P\Delta V^0$ correction required.

In summary, it may be stated that the Na-Li– and Na-Cs–Dowex-50 systems appear to behave as concentrated aqueous solutions and obey Harned's rule for the interactions of salts in concentrated aqueous solutions. Indeed, it would have been possible, in principle, to calculate selectivities as a complete function of loading merely from the relatively simple measurement

of selectivities of trace components, that is, at $F = 0$ and 1.0.

Effect of Capacity on Resin Moisture

The effect of capacity on the moisture characteristics of an ion exchanger is of fundamental importance in determining the behavior of the exchanger. An early attempt was made by Boyd, Soldano, and Bonner to determine the effects of capacity on the equilibrium and rate properties of ion exchangers. This work had one complicating factor: to achieve resins of varying capacity, the material was subjected to a temperature of 200°C for varying periods in order to hydrolyze off the sulfonate groups. This drastic treatment introduced the possibility of cross-linking breakage and lack of constant structure as the capacity was reduced. The authors found that the amount of water per equivalent at water activity equal to 1 increased as the capacity was reduced. It was not possible, however, to rule out the possibility that some, if not all, this increase could be attributed to breaking cross links.

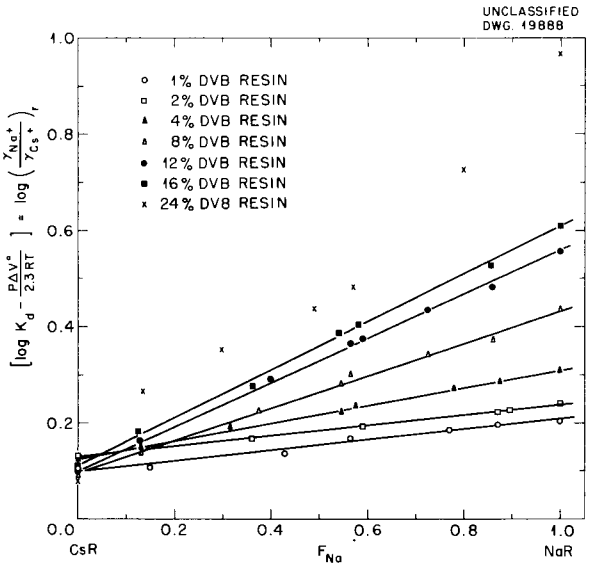

Fig. 19. Sodium-Cesium Selectivity Data.

Previously, Pepper in England had sulfonated polystyrene beads to varying degrees and had found that the amount of water per equivalent was independent of capacity. Unfortunately, the author was unable to sulfonate the beads homogeneously. In essence, a bead became partially sulfonated but retained an inner core of unsulfonated polymer. It is therefore not surprising that the amount of water per equivalent of ion present remained independent of capacity.

In an attempt to circumvent these difficulties, the moisture characteristics of carboxylic resins were investigated. A series of both 0.5% DVB and 8% DVB carboxylic resins was prepared that varied in composition from the pure hydrogen form to the pure sodium form. Because of the weak acid character of the carboxyl group it was expected that the effective capacity of such resins would be equal to the number of Na^+ ions, that is, neutralized carboxyl groups, and further, that

TABLE 28. COMPARISON OF CALCULATED AND OBSERVED LOG $(\gamma_{Na}/\gamma_{Cs})_r$ AS A FUNCTION OF CROSS LINKING

DVB (%)	LOG $(\gamma_{Na}/\gamma_{Cs})_r$									
	$F_{Na} = 0$		$F_{Na} = 0.2$		$F_{Na} = 0.5$		$F_{Na} = 0.8$		$F_{Na} = 1.0$	
	Calculated	Observed	Calculated	Observed	Calculated	Observed	Calculated	Observed	Calculated	Observed
1	0.073	0.100	0.121	0.121	0.167	0.155	0.188	0.188	0.175	0.205
2	0.122	0.130	0.151	0.151	0.197	0.185	0.218	0.218	0.225	0.240
4	0.108	0.125	0.162	0.162	0.231	0.218	0.274	0.274	0.296	0.310
8	0.084	0.093	0.162	0.162	0.265	0.263	0.365	0.365	0.418	0.431
12	0.106	0.100	0.191	0.191	0.322	0.330	0.469	0.469	0.522	0.559
16	0.116	0.112	0.211	0.211	0.372	0.360	0.510	0.510	0.600	0.608
24	0.088	0.078	0.295	0.295	0.509	0.436	0.727	0.727	0.851	0.967

the amount of water associated with the H^+ carboxylic groups would be much smaller than that associated with the Na^+ carboxylic groups. Thus, it would be possible to determine the effect of capacity upon resin moisture characteristics.

In Table 29 are shown the equivalent moisture values found for eight different preparations, as determined by equilibration with water vapor at activities varying from unity to 0.05. The weak acid characteristics of both the 0.5% and 8% DVB H^+ forms are demonstrated in Fig. 20, where curves 1 and 2 are identical up to activities of 0.98. If any significant amount of dissociation had occurred, the 0.5% resin would have contained more water. When only 2.43 equivalents of Na^+ were substituted in the 8% H^+ form, the amount of water per equivalent at $a = 1$ for the mixed resin was over twice that obtained for the pure H^+ form, and the moisture uptake increased drastically as the resins were progressively converted to the Na^+ form. On the basis of this behavior, it can be safely assumed that the amount of water per equivalent of H^+ is far smaller than that associated with one equivalent of Na^+ ions. Therefore little error is introduced by assuming further that, at a given water activity, the amount of water per equivalent of H^+ ions is constant and by attributing the remaining water to the Na^+ ions. By this method, the effects of changing the Na^+ capacity on equivalent moisture characteristics could be determined.

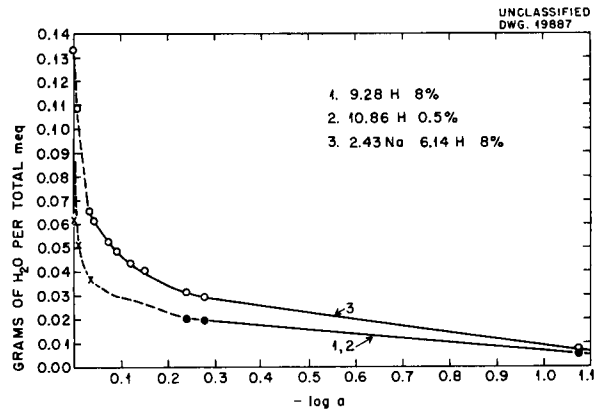

Fig. 20. Isopiestic Moisture Contents of Hydrogen and Sodium Carboxylic Resins.

TABLE 29. MOISTURE CONTENT OF THE MIXED FORMS OF CARBOXYLIC RESINS AT TWO WATER ACTIVITIES

PREPARATION	MILLIEQUIVALENTS OF H^+ PER GRAM OF DRY RESIN	MILLIEQUIVALENTS OF Na^+ PER GRAM OF DRY RESIN	GRAMS OF WATER PER MILLIEQUIVALENT OF H^+		GRAMS OF WATER PER MILLIEQUIVALENT OF Na^+	
0.5% DVB						
			$a = 0.98$	$a = 0.05$	$a = 0.98$	$a = 0.05$
I	10.86	0	0.0536	0.00572	0	0
II	7.33	2.44	0.0536	0.00572	0.384	0.01255
III	4.22	5.45	0.0536	0.00572	0.427	0.0149
IV	0	8.78	0	0	0.373	0.01786
8% DVB						
			$a = 1$	$a = 0.05$	$a = 1$	$a = 0.05$
I	9.28	0	0.062	0.00573	0	0
II	6.14	2.43	0.062	0.00573	0.311	0.01242
III	2.59	5.54	0.062	0.00573	0.247	0.0156
IV	0	7.71	0	0	0.229	0.01786

The results of these calculations are shown in Table 30 and in Fig. 21. It should be noted that in the case of the 0.5% DVB preparations the highest activity measured was 0.98. To go above that activity would result in tremendous errors in the moisture values since these loosely knit preparations contain over 80% moisture at $a = 1$. Curve I definitely shows that in the case of the 8% preparations at high activity the amount of water per equivalent of Na^+ increases as the capacity is reduced. On the other hand, it can be noted in Table 29 that the amount of water per equivalent of Na^+ in the case of the 0.5% preparations is reasonably independent of the capacity.

Curve II in Fig. 21 shows another interesting result. At low activities, the amount of water per equivalent of Na^+ decreases as the capacity of Na^+ is reduced. This linear relationship is independent of the cross linking of the exchanger, with both the 0.5% and 8% DVB results falling on the same straight line. This agreement is not surprising since at low activities moisture properties of ion exchangers usually are independent of their DVB content.

Two phenomena must be explained:

1. At low activities the moisture uptake increases with capacity.
2. At high activities the moisture uptake decreases with increasing capacity for the highly cross-linked resin but not for the low-cross-linked resin.

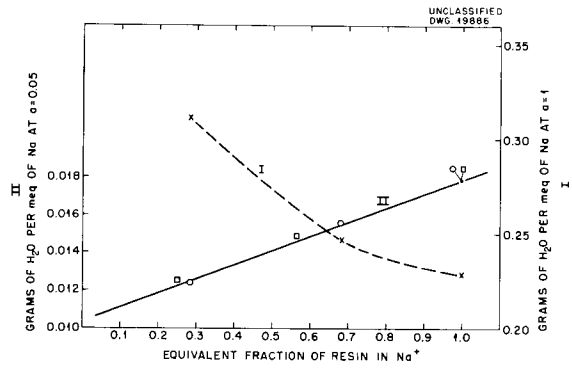

Fig. 21. Effect of Water Activity on the Capacity Effect in a Cation Exchanger.

TABLE 30. CAPACITY OF THE MIXED FORMS OF CARBOXYLIC RESINS

MILLIEQUIVALENTS OF H^+ PER GRAM OF DRY RESIN	MILLIEQUIVALENTS OF Na^+ PER GRAM OF DRY RESIN	TOTAL MILLIEQUIVALENTS PER GRAM OF DRY RESIN	H^+ (%)	THEORETICAL CALCULATED TOTAL CAPACITY IN EQUIVALENTS PER GRAM OF DRY RESIN FOR THE MIXED FORM*
0.5% Carboxylic Resin				
10.86	0	10.86	100	10.86
7.35	2.44	9.79	75	9.5
7.31	2.43			
4.22	5.45	9.67	43.6	9.58
0	8.78	8.78	0	8.78
8% Carboxylic Resin				
9.28	0	9.28	100	9.28
6.14	2.43	8.57	71.6	8.77
2.59	5.54	8.13	31.9	8.13
0	7.71	7.71	0	7.71

*Percentage composition found by experimentation is used.

These apparently divergent features are reconcilable on the following basis: At low activities (or water uptake) the free-energy change of the resin matrix can be neglected, since the total volume change is negligible. The high-capacity resin adsorbs more water because a water molecule adsorbed on a given ion pair has a free-energy change of adsorption which contains contributions from near neighbor ion pairs. These will all act to decrease the free energy of the water in the sorbed state. The effect is, of course, less for lower capacity. At high activities, the free-energy change of the network becomes important since the volume increases. A high, negative, free-energy change is associated with isotropically expanding a lattice of ion pairs (or dipoles). The amount of the free-energy change depends, of course, on the volume-density of the dipoles. The high-capacity high-cross-linked resin then sorbs less water than the low-capacity high-cross-linked resin.

The effect will be negligible for low-cross-linked resins because at high activities they contain so much more water that the dipoles are shielded from one another by the highly dielectric material.

ORGANIC CHEMISTRY OF SOLVENTS

W. H. Baldwin C. E. Higgins

Hydrotropic Solutions

The third phases[1] that are formed during the equilibration of systems containing sodium hydroxide, water, sodium dibutyl phosphate, and dibutyl ether can be classed as hydrotropic solutions.[2] More reliable analyses than those reported previously[1] show the hydrotropic solution to have the following average composition: water, 45.3%; sodium dibutyl phosphate, 39.3%; dibutyl ether, 7.3%; and sodium hydroxide, 5.12%. The above results from five separate preparations were obtained with 0.05 *M* sodium dibutyl phosphate in the aqueous phase before equilibration. When the concentration of the sodium dibutyl phosphate was doubled (0.1 *M*), the volume of the hydrotropic solution increased but the chemical composition of the hydrotropic solution was not detectably different.

Di(2-ethyl hexyl)phosphinic acid was tested as the sodium salt in the hydrotropic solutions. Equilibrating an aqueous phase that contained 1 *M* sodium hydroxide and 0.05 *M* di(2-ethyl hexyl)phosphinate produced a hydrotropic solution (third phase) that was composed of 31.5% water, 34.2% sodium salt of the phosphinate, 30.1% dibutyl ether, and 0.3% sodium hydroxide. The phosphinate in the third phase accounted for 97% of the total.

The hydrotropic solutions described here form between the two phases and thereby lend themselves to practical application. Organo-phosphorus acids extract uranium from aqueous solution into organic liquids. The stripping of uranium back into aqueous solution requires high concentrations of an acid such as 6 *M* sulfuric acid or the formation of water soluble complexes. Alkali carbonates can be employed to strip uranium from organic solutions by forming complex carbonates in the aqueous phase. The alkali metal salts of the phosphorus acids do not accompany the uranium into the aqueous phase but are concentrated in the hydrotropic solution between the phases. The aqueous phase containing the uranium and the solvent can be readied for re-use by contact with aqueous acid.

Dealkylation of Esters

It has been shown previously that tributyl phosphate can be dealkylated with sodium acetate to form dibutyl phosphoric acid.[1] Ethanolamine has proved useful for the same reaction; only one butyl group being removed even in the presence of excess ethanolamine. One advantage of ethanolamine is that the reaction mixture becomes homogeneous above room temperature (anhydrous sodium acetate dissolves during the reaction). It has been found possible to study the reaction quantitatively by titrating the excess amine. The reaction can be summarized as follows:

$$(RO)_3PO + NH_2CH_2CH_2OH \longrightarrow [(RO)_2P(O)]^- [RNH_2CH_2CH_2OH]^+$$

Confirmation of the reaction as postulated lies in the formation of N-butyl ethanolamine and N,N-dibutyl ethanolamine, and qualitative evidence has recently been obtained for both compounds.

(1) W. H. Baldwin and C. E. Higgins, *Chem. Quar. Prog. Rep. Dec. 31, 1952*, ORNL-1482, p. 26.

(2) E. C. Lumb and P. A. Winsor, *Ind. Eng. Chem.* 45, 1086 (1953).

Scouting tests have indicated that at 200°C, ethanolamine dealkylates tributyl phosphate, triphenyl phosphate, tri(2-ethyl hexyl)phosphate, bis(2-ethyl hexyl)-2-ethyl hexyl phosphonate, and tetrakis(2-ethyl hexyl)ethylene diphosphonate.

Compounds of the type represented by tetrakis(2-ethyl hexyl)ethylene diphosphonate (I) are particularly interesting since the removal of one alkyl and establishment of one acid group on each phosphorus atom (II) could lead to chelate-forming compounds.

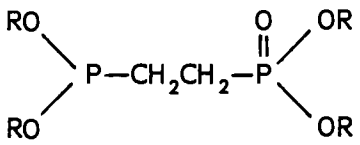

I

tetrakis(2-ethyl hexyl)ethylene diphosphonate

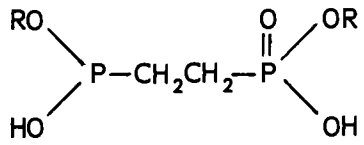

II

P,P′-bis(2-ethyl hexyl)P,P′-dihydrogen ethylene diphosphoric acid

The dealkylation reaction is being studied further to attempt the preparation of compound II from compound I.

CHEMICAL PHYSICS

RADIO-FREQUENCY SPECTROSCOPY

Quadrupole Spectroscopy

R. Livingston H. Zeldes

The quadrupole spectra for bromine and iodine in a number of alkyl halides in addition to those already reported[1] have been measured. It was necessary to purify several of the compounds before resonance lines could be found. The final results are being published elsewhere.[2]

An extensive study on the Zeeman effect of the iodine quadrupole resonance in a single crystal of iodic acid (HIO_3) is well under way. The initial purpose of the study was to locate the principal axes of the field gradient tensor, evaluate the asymmetry parameter,

$$\eta = \frac{\phi_{xx} - \phi_{yy}}{\phi_{zz}}$$

and relate these results to the structure.

Although an x-ray diffraction study[3] has been made on iodic acid, the Neutron Diffraction Group (Levy and Garrett) has undertaken a study to evaluate the unknown hydrogen atom parameters and to check the iodine and oxygen parameters obtained by the x-ray workers.

Iodic acid is orthorhombic, with four molecules in the unit cell. All iodine atoms are crystallographically equivalent, and, in the absence of a magnetic field, there is a single quadrupole line appearing near 203 megacycles/sec for the $\pm\frac{1}{2} \longrightarrow \pm\frac{3}{2}$ transition and another line at a higher frequency for the $\pm\frac{3}{2} \longrightarrow \pm\frac{5}{2}$ transition. In general, a quadrupole line for the $\pm\frac{1}{2} \longrightarrow \pm\frac{3}{2}$ transition splits into four Zeeman components with the application of a homogeneous magnetic field to a single crystal. The nature of the splitting depends, in part, on the orientation of the magnetic field to the directions of the principal axes of the field gradient tensor for the iodine. In iodic acid, each of the four iodine atoms in the unit cell has its own field gradient tensor. Thus there are four sets of field gradient directions, and, in general, 16 Zeeman components will appear. The Zeeman pattern is simplified, however, for special orientations of the magnetic field as a result of symmetry properties of the crystal lattice. If the magnetic field is oriented in a basal plane, as far as quadrupole spectroscopy is concerned, the iodine atoms are equivalent in pairs and, in general, no more than eight lines should appear. Moreover, if the field is oriented along a crystal axis, all atoms are equivalent and only four lines should appear.

The above expectations were confirmed for the *ac* plane of the crystal. However, in mapping the Zeeman components with the magnetic field in the *ab* and *bc* planes, extra lines were seen. The extra lines were found near and along the *b* direction. Thus, instead of finding four lines along the *b* direction (two central strong lines and two outer weak lines), a total of six lines was seen. The outer weak lines were split into doublets. This doublet splitting was due to the magnetic field of the protons in the crystal. The proton magnetic moment, aligned in the externally applied magnetic field, contributes a small field that either adds to or subtracts from the main field. All the Zeeman components should be split into doublets, except for special angles, but because of the line width the doublets were only resolved near the *b* direction. The doublet separation varies as $(3 \cos^2 \theta - 1)$, where θ is the angle between the applied magnetic field and the vector joining the iodine and the nearby proton. Work is nearly complete on locating the position of this vector, or more correctly, the four vectors, one for each iodine in the unit cell. The preliminary result is that the vectors are all parallel to lines lying in the *bc* plane, inclined in pairs at ±5 deg from *b* toward *c*. The distance, *r*, of the proton from the iodine can be measured quite accurately, since the doublet separation depends on μ/r^3, where μ is the proton magnetic moment. This measurement is not complete, but *r* can probably be determined to about 1%.

Other unusual features have appeared in the study of iodic acid. Bersohn's[4] perturbation calculations for the energy levels to first order in

(1) R. Livingston and H. Zeldes, *Chem. Quar. Prog. Rep. Dec. 31, 1952*, ORNL-1482, p. 27

(2) H. Zeldes and R. Livingston, *J. Chem. Phys.* (in press).

(3) M. T. Rogers and L. Helmholz, *J. Am. Chem. Soc.* 63, 278 (1941).

(4) R. Bersohn, *J. Chem. Phys.* 20, 1505 (1952).

field strength and second order in η indicate that η should be fairly simply determined from the mapping of Zeeman components in the basal planes of the crystal. The asymmetry, η, could not be evaluated as expected, however, because of η having such a large value that the second-order treatment was not valid. A separate determination of η was made by measuring the transition frequencies for the $\pm\frac{1}{2} \longrightarrow \pm\frac{3}{2}$ transition (202.8696 megacycles/sec) and the $\pm\frac{3}{2} \longrightarrow \pm\frac{5}{2}$ transition (325.9518 megacycles/sec) in the absence of an applied magnetic field. It was necessary to develop a higher frequency quadrupole spectrometer for this measurement. A calculation of η, by using exact theory, gave 0.4505. This value is over twice that of any other compound measured.

Some Zeeman studies were next made of the higher frequency transition, and twice as many lines as were expected were seen. The "extra" lines were demonstrated to be "forbidden" transitions. It appears that for $\eta \neq 0$ they are not forbidden and only the large value of η in iodic acid made their observation possible. The theory for the transition probability of these lines has not yet been developed.

Another anomaly found in iodic acid has been a line-intensity effect. Equivalent magnetic field orientations to the crystal, related by crystal symmetry, should give identical Zeeman patterns. In such cases, the frequencies of the Zeeman components were equivalent, but the line intensities were not. It was experimentally verified that this effect was related to the manner in which the radio-frequency coil was wrapped around the crystal. The essentially polarized radio-frequency energy coupled differently with the different iodine atoms in the unit cell. Reorienting the magnetic field through crystal symmetry operations has the effect of interchanging iodine atoms in the unit cell. In the above case, an identical experimental configuration is not established because of the preferred direction of winding of the coil. In a sense, the iodine atoms in the unit cell are labeled by the line intensity.

The main unfinished problem with iodic acid is that of determining the location of the directions of the field gradient principal axes. Levy and Garrett of the Neutron Diffraction Group have given valuable assistance in the above work.

The Iodine Problem

R. Livingston B. Benjamin

A method for chemically purifying carrier-free I^{131} in order to reduce the total salt content and to give a product suitable for synthesizing CH_3I has been developed. The method, as indicated before,[1] consists of electroplating the iodine onto a silver anode and then stripping the iodine into a dilute H_2S solution containing a small amount of NaOH. A test experiment with 100 mc of I^{131} and several micrograms of I^{129} yielded an excellent CH_3I product from starting material purified in the above manner.

Two, 750-mc, carrier-free, I^{131} experiments have been carried out in order to study the microwave spectrum of CH_3I and to determine the nuclear moments of I^{131}. The first of these was a failure. Although the initial purification process worked reasonably well, the radiation effects in a subsequent 8-hr evaporation step were sufficient to oxidize the iodine and to cause serious loss of activity from the solution.

By using a heating coil, the long evaporation step was reduced to about ½ hour. In the second run, activity was still lost from the solution, but this time not as oxidation products. The combination of high local heat from the heater and pumping on the solution apparently caused steam distillation of the microquantity of sodium iodide present. Nevertheless, a small amount of CH_3I was synthesized and several very weak but sharp microwave lines were seen. These lines were all due to I^{127} and indicate that the isotope was at least twice as abundant as I^{131} in the sample. With an improved chemical yield, it is hoped that the I^{131} lines will also be seen. The evaporation procedure has now been modified and another experiment will be carried out soon.

INFRARED SPECTROSCOPY OF METHYL HALIDES AT LIQUID NITROGEN TEMPERATURE

H. M. Rosenstock

The study of the infrared spectroscopy of methyl halides at liquid nitrogen temperature was initiated with the aim of gaining some understanding of the physical interactions leading to differences in the nuclear quadrupole coupling values observed for some molecules in the gaseous state (by hyperfine

structure of microwave absorption lines) and in the solid state (by pure quadrupole spectroscopy).[5] Some values for quadrupole coupling are given in Table 31.

A preliminary survey of the literature dealing with infrared spectroscopy indicated that a number of compounds which showed differences in vibrational frequencies, as measured in the gaseous and liquid state, also showed differences in quadrupole coupling values in the gaseous and solid state.

The methyl halides were chosen because all those possessing a nuclear quadrupole moment did show a pronounced change in coupling values, their normal vibrations were all active in the infrared, and they presented a homologous series.

The low-temperature spectra were obtained by freezing the appropriate vapor onto a plate of silver chloride cooled to approximately 77°K with liquid nitrogen and by measuring the transmission on a Perkin-Elmer recording infrared prism spectrometer. This technique produced solid films showing less than 20% scattering at wavelengths longer than 3 microns. The gas-phase spectra were measured in the usual fashion and were in agreement with the values reported in the literature.[6] Table 32 gives the vibration frequencies of the methyl halides. The CH_3I values were taken from the work of Mador and Quinn.[7]

Infrared spectra in condensed phases differ markedly from those in gases, mainly because of the freezing out of rotational fine structure and because of molecular interactions.[8] Thus, solid-state infrared "bands" are actually sharp lines having a width of the order of 10 cm^{-1}.

[5] B. P. Dailey, *J. Phys. Chem.* 57, 490 (1953).

[6] G. Herzberg, *Infrared and Raman Spectra of Polyatomic Molecules*, Van Nostrand, New York, 1945.

[7] I. L. Mador and R. S. Quinn, *J. Chem. Phys.* 20, 1837 (1952).

[8] D. F. Hornig, *J. Chem. Phys.* 16, 1063 (1948).

TABLE 31. QUADRUPOLE COUPLINGS[5]

	eqQ (megacycles)	
	Gas	Solid (77°K)
CH_3Cl	75.13	68.4
CH_3Br	577.0	528.9
CH_3I	1931.5	1753.0

TABLE 32. VIBRATION FREQUENCIES OF THE METHYL HALIDES

SPECIES	FREQUENCY (cm^{-1})								
	CH_3I*			CH_3Br			CH_3Cl		
	Vapor at 298°K	Solid at 77°K	$\Delta\nu$	Vapor at 298°K	Solid at 77°K	$\Delta\nu$	Vapor at 298°K	Solid at 77°K	$\Delta\nu$
$\nu_3(A_1)$	532.8	520	−13	611	591	−20	732	704	−30
$\nu_6(E)$	882	888 895	+10	952	958 963	+ 9	1015	1022	+ 7
$\nu_2(A_1)$	1252	1236 1241	−13	1305	1292	−13	1355	1338 1348	−12
$\nu_5(E)$	1440	1399 1422	−29	1445	1421 1436	−16	1455	1442 1448	−10
$2\nu_5(A_1)$				2861	2831	−30	2879	2846	−33
$\nu_1(A_1)$	2970	2938	−32	2972	2946	−26	2966	2951	−15
$\nu_4(E)$	3061	3037 3052	−16	3056	3042	−14	3042		

*CH_3I values taken from Mador and Quinn (ref. 7) except for the $\nu_3(A_1)$ value which was measured here.

The line splittings observed here are due to two distinct factors. Splitting of degenerate (species E) lines may result from either a lowered symmetry of the molecule in the solid or from the presence of more than one molecule in the unit cell. Splitting of nondegenerate (species A) lines can only result from the presence of more than one molecule in the unit cell. Further, the line width of approximately 10 cm^{-1} may leave some splittings unresolved.

Thus, the observed splittings show the presence of more than one molecule per unit cell but leave the question of molecular symmetry undecided. A recent x-ray study of solid methyl chloride[9] indicated the presence of four molecules per unit cell and a lower molecular symmetry than in the gas phase.

The frequency shifts, shown in Table 32, indicate that the molecules are in perturbed electronic states in the solid, as compared with the gaseous state. The lowering of the carbon-halogen stretching frequencies ($\nu_3 A_1$) upon condensation indicates that the carbon-halogen distances of the methyl halides are somewhat stretched in the solid state. It is interesting to note that gas-phase measurements of quadrupole couplings of, say, chlorine in various compounds show a decrease of coupling with increasing bond length.[10] Thus, the infrared data seem to correlate at least qualitatively with the quadrupole-coupling decrease in going from the gaseous to the solid state. The x-ray data of Burbank[9] also indicated that the C-Cl bond may have been stretched, but the data were not conclusive.

It is proposed to continue the infrared study with CH_3F to obtain a more complete picture of the characteristics of the solid methyl halides and also to elaborate on the rather tentative correlation of quadrupole-coupling shifts given above.

NEUTRON DIFFRACTION STUDIES

H. A. Levy S. W. Peterson

Crystal Structures of Potassium Dihydrogen Phosphate and Arsenate

Neutron diffraction studies have been undertaken on the following three crystals of similar structure: KH_2PO_4, KH_2AsO_4, and KD_2AsO_4. Locations of all atoms except hydrogen have been previously determined by x-ray studies;[11] thus, the primary goal of this study has been the elucidation of the arrangement of hydrogen atoms.

At the present time, complete data have been collected at room temperature from the $hk0$ and $h0l$ zones of KH_2PO_4 and from the $hk0$ zones of KH_2AsO_4 and KD_2AsO_4. Treatment of the data by Fourier syntheses has yielded reliable structural information as yet only for KD_2AsO_4. In this case, the structure clearly consists of a three-dimensional network of arsenate ions joined by hydrogen bonds. The deuterium atoms are situated substantially along the lines joining close-approaching oxygen atoms of neighboring ions and are distributed at random close to one or the other of the oxygen atoms. Refinement of parameters is nearly complete; the usual measure of agreement,

$$R = \frac{\Sigma \left| |F_{obs}| - |F_{calc}| \right|}{\Sigma |F_{obs}|}$$

is 5.9% at the present stage. The oxygen-to-deuterium bond distance is about 1.05 Å. The coherent neutron scattering amplitude of arsenic appears to be about 0.7×10^{-12} cm, appreciably higher than that given by Shull and Wollan.[12]

Crystal Structure of Ice

Complete neutron diffraction data have been collected from the $h0l$ zone of a single crystal of deuterium ice at −50°C. The observed structure factors proved to be in general agreement with the Pauling model of the structure of ice, in which hydrogen atoms are situated along the lines connecting adjacent oxygen atoms, at random about 1 Å from one or the other. Refinement of parameters by Fourier synthesis has led to the following characteristic distances and angle in the structure: O-D = 1.00 Å, O-O = 2.76 Å, ∠D-O-D = 109 degrees. The agreement factor at the present stage, which is not yet final, is 9.7%.

Crystal Structure of Oxalic Acid Dihydrate

B. S. Garrett

Neutron diffraction data were collected at room temperature from the $h0l$ and $0kl$ zones of oxalic acid dihydrate. Consideration of the positions of

[9] R. D. Burbank, *J. Am. Chem. Soc.* 75, 1211 (1953).

[10] E. B. Wilson, Jr., *Ann. N. Y. Acad. Sci.* 55, 943 (1952).

[11] R. W. G. Wyckoff, *Crystal Structures*, vol. II, chap. VIII, Interscience, New York, 1951.

[12] C. G. Shull and E. O. Wollan, *Phys. Rev.* 81, 527 (1951).

carbon and oxygen atoms, known from x-ray studies,[13] and application of the Harker-Kasper inequality relations[14] led to the assignment of phase angles to nearly all the observed $h0l$ structure factors without any trial assumption as to the arrangement of hydrogen atoms. A Fourier synthesis then yielded a projection showing discrete oxalic acid molecules and water molecules. Phase angles were assigned to $0kl$ structure factors by giving the hydrogen atoms trial positions in accord with the $h0l$ projection and expected interatomic distances, and a Fourier projection was computed from these data. Refinement of parameters is not yet complete, but it has progressed sufficiently far to yield some information about the structure. The arrangement of hydrogen bonds is as has been deduced from the x-ray studies.[13] The O-H distance is about 1.0 Å, both in carboxyl and in water. The acid molecule is at least approximately plane. The carbon-to-oxygen bond distances are about 1.3 (hydroxyl) and 1.2 Å, close to single- and double-bond values. The agreement factors for the two zones are 13 and 15%.

Crystal Structure of Iodic Acid, HIO_3

B. S. Garrett

Neutron diffraction data were collected from the $h0l$ and $0kl$ zones of HIO_3 single crystals. Phase angles were assigned from consideration of the iodine and oxygen positions, known from x-ray studies,[15] and from trial hydrogen locations deduced from the neutron data. Preliminary Fourier projections have been computed for both zones and yield the following structural information. The hydrogen atom is linked to the oxygen atom having the longest I-O bond distance, as deduced by Rogers and Helmholz.[15] The arrangement of hydrogen bonds, however, is not of the bifurcated type, but rather as suggested by Wells.[16] Refinement of parameters has not progressed far enough to yield reliable interatomic distances.

[13] J. D. Dunitz and J. M. Robertson, *J. Chem. Soc.*, p. 142 (1947).

[14] *International Tables for X-ray Crystallography*, vol. I, p. 540, Kynoch Press, Birmingham, England, 1952.

[15] M. T. Rogers and L. Helmholz, *J. Am. Chem. Soc.* 63, 278 (1941).

[16] A. F. Wells, *Acta Cryst.* 2, 128 (1949).

EXPERIMENTS IN CHEMICAL KINETICS WITH MOLECULAR BEAMS

S. Datz E. H. Taylor

Three experiments were performed near the end of this period on the scattering of a molecular beam of potassium by an effusive spray of HBr. This is the first of the experiments toward which this program has been directed since its inception.

In this experiment, scattered, unreacted potassium and KBr were detected with about equal efficiency (90%) with a surface ionization gage that used a tungsten filament. It was originally intended to distinguish reacted KBr from scattered potassium by a neutron-activation analysis for bromine, but the use of neutron-activation analysis was obviated in this instance by the discovery that a platinum filament would ionize potassium atoms with roughly 50% efficiency, but that it would ionize and thus detect KBr with only about 0.1% efficiency. A gage with two filaments, one tungsten and one platinum, used separately, was therefore built and used in the present experiments.

The three experiments so far completed were all done with potassium at about 500°K and HBr at about 150°K, the differences between the runs being merely minor improvements in alignment and temperature control. The profiles of the unscattered and of the scattered beam are somewhat uncertain at the shoulders of the beam where the intensity falls most rapidly with distance, apparently because of a slight tilt in the platinum filament on heating. This makes it impossible to make a precise statement about the fate of all the potassium atoms which are thrown out of the beam by collisions with HBr, but measurements of scattered material that is farther than the shoulders from the center show that all the scattered material in this region consists of potassium atoms and not of KBr, indicating that very little, if any, reaction has occurred. This is contrary to what would be predicted from the zero activation energy apparently observed by Hartel.[17]

It is intended next to study the effect of temperature variations, particularly of the HBr, and then to conduct similar experiments with potassium and bromine.

[17] H. v. Hartel, *Z. physik. Chem.* B11, 316 (1931).

RADIATION CHEMISTRY

GAS-PHASE RADIATION

P. S. Rudolph S. C. Lind

A radon collecting station for use in the studies of gas-phase radiation has been completed and appears to be functioning satisfactorily. This system differs from any described in the literature in that the H_2 and O_2 evolved by the decomposition of the water in the radium chloride solution storage flask is continuously recombined on a hot platinum filament and distilled back into the storage flask. To date, three charges of radon have been extracted and the pressure buildup over the $RaCl_2$ solution has not exceeded 1 cm between collections. The pressure increased about 3 cm between the sealing of the $RaCl_2$ solution into the system and the initial radon extraction. This is to be expected, as excess H_2 would be liberated until H_2O_2 equilibrium was established.

If it is assumed that 100% conversion of the $RaSO_4$ to $RaCl_2$ was accomplished and all the $RaCl_2$ is in solution, the minimum yield of radon is about 70% of the theoretical yield. This efficiency is based on extractions employing only one pumping with the Toepler pump. If an additional pumping with the Toepler pump is employed, the yield will be at least 78%, based on the same assumptions and the volumes of the system.

Pumping time for radon extraction dropped from 47 min for the first extraction to 32 and 34 min for the second and third extractions, respectively.

Although the radiation exposure to the operator was somewhat greater than the accepted tolerance levels, it decreased with each extraction as experience was gained. Some slight modifications to the system have suggested themselves and will further reduce the operator's exposure. The modifications have been initiated and will be completed as soon as feasible.

An apparatus to calibrate the radon extracted is completed. This apparatus employs a Lind electroscope[1] and three standards that consist of 140.1, 59.26, and 1.20 mg of radium.

The radon collected will be primarily used for gas-phase radiation studies. The recombination of H_2 and O_2 in the presence of radon has been studied as an introductory experiment. This reaction was chosen because it has been thoroughly studied[2] by means of the present techniques and therefore would give a basis for comparison.

A reaction vessel with a volume of 7.90 cm^3 at 24°C and with an approximate outside diameter of 2.5 cm was used. An initial pressure of 429.0 mm Hg of electrolytic H_2 and O_2 at 23.5°C was introduced into this vessel along with an initial charge of 98.7 mc of radon. The velocity constant for this reaction was determined by using Lind's equation:[3]

$$\left(\frac{k\mu}{\lambda}\right)' = \frac{\log_e \frac{P_1}{P_2}}{E_0(e^{-\lambda t_1} - e^{-\lambda t_2})}$$

where P_1 and P_2 are the pressures at time t_1 and t_2, respectively, $e^{-\lambda t_1}$ and $e^{-\lambda t_2}$ are the per cent of radon remaining at t_1 and t_2, and E_0 is the initial intensity of radon. The average velocity constant was found to be 14.8, which is in good agreement with the values found by Lind.

The next reaction to be studied is that of $H_2 + O_2 + CO_2$ when under the influence of the alpha rays of radon.

EFFECTS OF GAMMA RAYS ON ICE AND FROZEN SOLUTIONS

J. A. Ghormley A. C. Stewart

The formation of hydrogen and hydrogen peroxide in ice subjected to gamma radiation has been reported previously.[4] The formation and disappearance of hydrogen peroxide in ice initially containing hydrogen peroxide has now been studied. The conditions that were varied in the experiments included total dose, temperature, concentration, and dissolved gases present during freezing.

---

(1) S. C. Lind, *Ind. Eng. Chem.* 7, 406 (1915); *Op. cit.* 12, 469 (1920).

(2) S. C. Lind, *J. Am. Chem. Soc.* 41, 531 (1919).

(3) S. C. Lind, *The Chemical Effects of Alpha Particles and Electrons*, 2nd ed., p. 119, Chemical Catalogue Co., New York, 1928.

(4) A. C. Stewart and J. A. Ghormley, *Chem. Quar. Prog. Rep. Sept. 30, 1952*, ORNL-1432, p. 47; *Chem. Quar. Prog. Rep. Dec. 31, 1952*, ORNL-1482, p. 37.

The initial rate of gamma-ray-induced disappearance of hydrogen peroxide in samples prepared by freezing hydrogen peroxide solutions saturated with helium or hydrogen is shown in Fig. 22. This rate, in hydrogen-saturated samples, increased continuously with temperature in the range from −175 to −5°C. The increase was most marked, sevenfold, between −100 and −50°C. In helium-saturated samples, the disappearance represents the radiation-induced decomposition of peroxide. The large difference between the rates of disappearance in hydrogen-saturated, as opposed to helium-saturated, samples at higher temperatures is attributed to the radiation-induced reaction between hydrogen and hydrogen peroxide.

The data in Fig. 23 show that hydrogen peroxide concentrations decreased when samples were subjected to 10-min irradiations at −196°C. After 30 min (upper curve), the peroxide concentration increased. However, when a sample was subjected to two or more 10-min irradiations at −196°C and allowed to warm to −180°C or above between irradiations, the observed final concentration of hydrogen peroxide was less than that for an equivalent continuous irradiation at −196°C. Figure 24 shows the results obtained when samples were given two 10-min irradiations at −196°C and warmed to various temperatures between irradiations. It will be noted that again there is increased disappearance of hydrogen peroxide

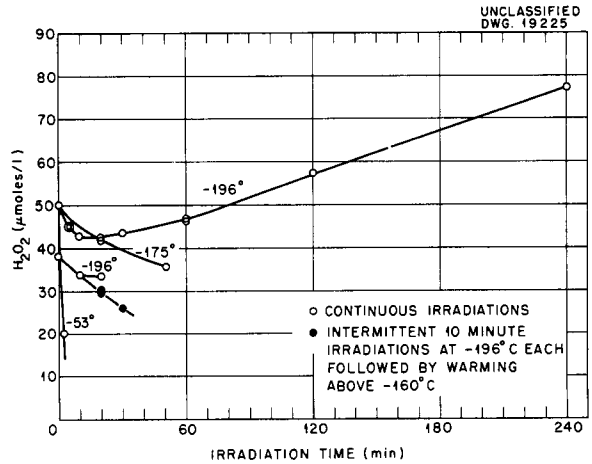

Fig. 23. Effect of Gamma Radiation (1.90×10^{17} ev/ml/min) on Frozen H_2O_2 Solution Saturated with Hydrogen.

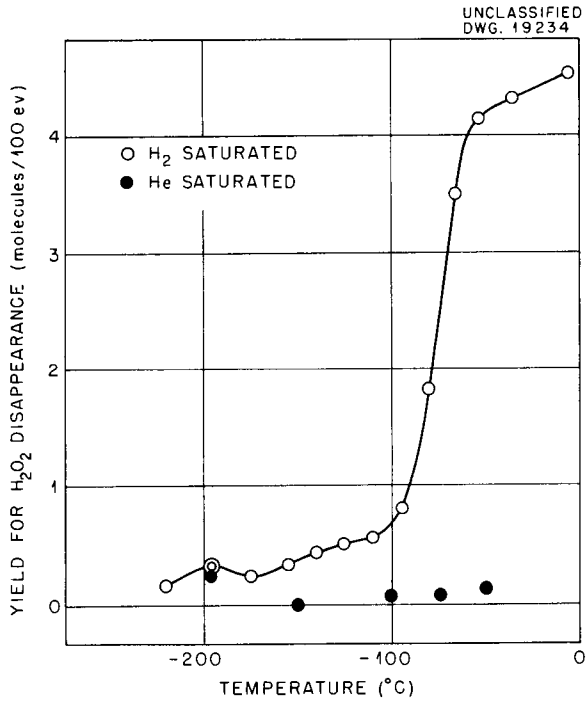

Fig. 22. Initial Yields for Disappearance of H_2O_2 in a Frozen Solution Containing 50 μmoles of H_2O_2 per Liter Saturated with Hydrogen or Helium.

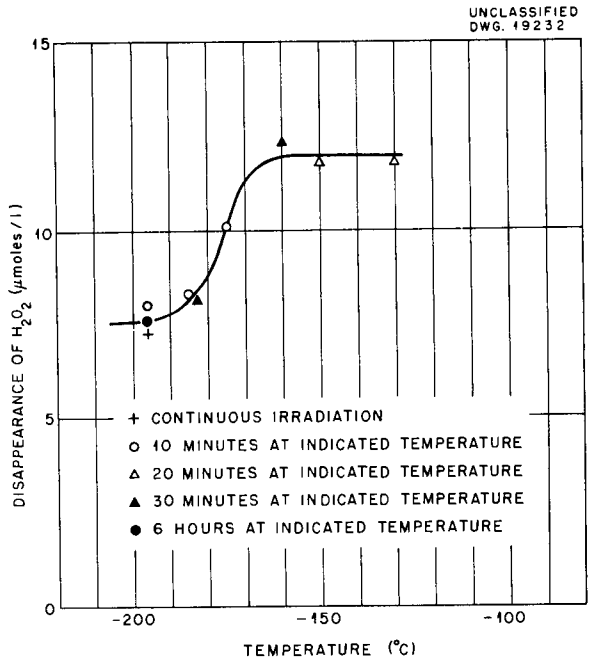

Fig. 24. H_2O_2 Disappearance Observed for Two 10-min Irradiations at −196°C, with Sample Warmed to Indicated Temperature Between Irradiations.

associated with intermittent warming of the sample. This increased reaction above −180°C can be interpreted as reaction induced by some species such as a free radical or trapped charge that is formed during irradiation and is stable at −196°C but able to react with peroxide at temperatures above −180°C.

Effects of other gases and of another solute, potassium bromide, which is known to influence corresponding radiation-induced reactions in liquid water, are shown in Fig. 25. The presence of potassium bromide has a marked effect on the behavior of the ice prepared from oxygen-saturated hydrogen peroxide solutions.

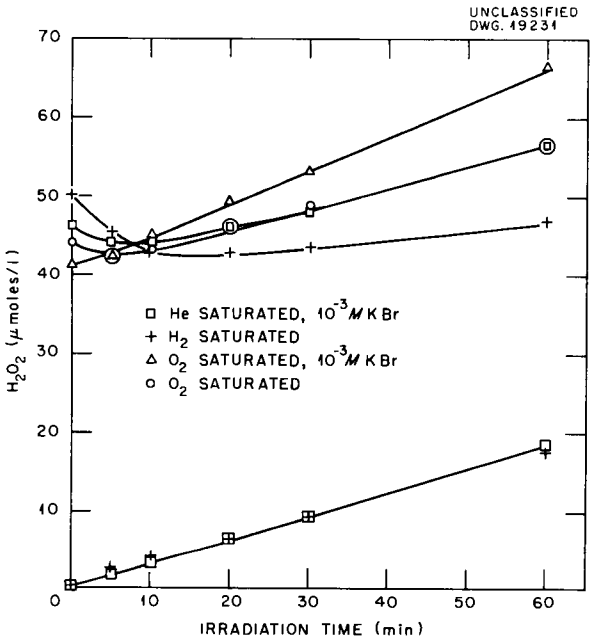

Fig. 25. H_2O_2 Formation and Disappearance in Solutions Saturated with Various Gases, Frozen Rapidly, and Irradiated at −196°C.

Since these chemical experiments indicated a species present in ice irradiated at −196°C which was not stable at higher temperatures, it was thought desirable to study the absorption spectrum of irradiated ice at −196°C by means of a Cary recording spectrophotometer. Clear, unirradiated samples of ice that contained hydrogen peroxide in concentrations up to 10^{-2} M showed no appreciable absorption at −196°C in the range 2100 to 8000 Å. When samples were irradiated at −196°C, a broad absorption band with a peak at 2800 Å, as shown in Fig. 26, was always observed. No visible coloration has been observed in large clear samples of ice irradiated at −196°C. The initial rate of buildup of the 2800-Å absorption peak is lower in pure ice than in ice containing hydrogen peroxide or ice previously irradiated at −196°C and warmed to −140°C or above. The observed absorption anneals out completely on warming to −143°C at a rate of about 10°C/min, as shown in Fig. 27. The point

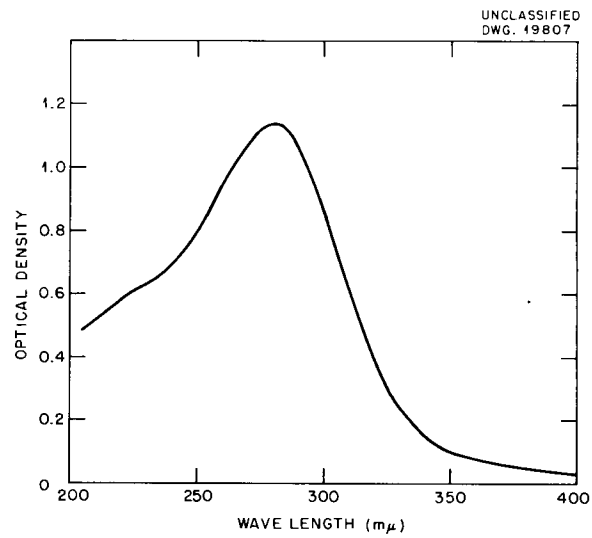

Fig. 26. Absorption Spectrum at −196°C of 1½-cm-thick Ice Sample Irradiated at −196°C with Co^{60} Gammas for 28 hr at ~3000 r/min.

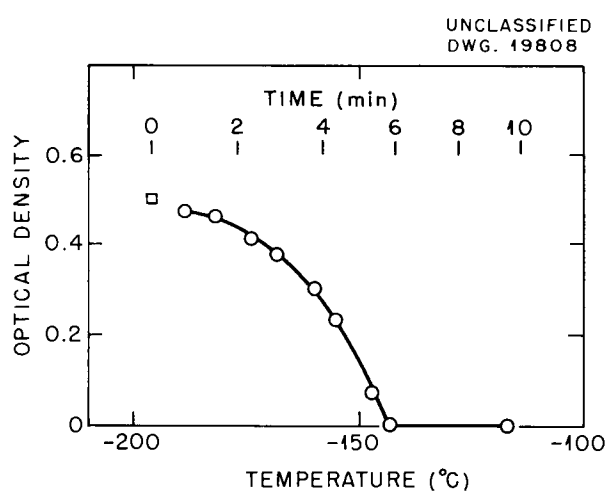

Fig. 27. Disappearance of 2800-Å Absorption Peak when Ice Irradiated at −196°C with Co^{60} Gammas for 2 hr at 1000 r/min Was Warmed.

at −196°C was obtained with the ice immersed in liquid nitrogen, while the other points were taken from spectra recorded after the liquid nitrogen was poured off and were therefore subject to different conditions for scattering of light. The plotted points are the difference between optical density at 2800 and 4000 Å. The shape of the curve, which has been verified by continuous measurements at 2800 Å during warming, suggests the possibility of two different processes occurring; one reaches a maximum rate at about −180°C and the other at about −150°C. The temperature range over which the 2800-Å absorption band disappears corresponds closely with that at which peroxide disappears on intermittent warming following irradiations at −196°C, as shown in Fig. 24.

DECOMPOSITION OF SULFURIC ACID BY COBALT GAMMA RADIATION

J. A. Ghormley C. J. Hochanadel
T. J. Sworski

Some effects observed in radiation chemistry studies of dilute sulfuric acid solutions were attributed to reactions of sulfuric acid with radicals[5,6] and to absorption of energy by the sulfuric acid.[7] It seemed of interest to determine the radiation stability of concentrated sulfuric acid solutions wherein most of the energy would be absorbed by the acid itself.

The decomposition of acid solutions in the concentration range from 0.5 *M* up to slightly fuming acid was determined by measuring the SO_2 that could be swept out of solution during or after irradiation. A stream of purified helium gas was swept through the acid while the acid was in a radiation cell containing a fritted glass disc. The gas was then bubbled through two cells, in series, containing dilute ceric sulfate solution, and the change in optical absorption at 3200 Å was measured by using a Beckman Model DU spectrophotometer. Dissolved SO_2 was also identified by its ultraviolet absorption at 2800 Å. Solutions were prepared from Baker's Analyzed Reagent sulfuric acid, Baker's Analyzed Reagent 20% fuming sulfuric acid, and Baker and Adamson Reagent c.p. sulfuric acid. No difference was observed in the decomposition of the different acids.

In all solutions, a small amount of SO_2 was present before irradiation. Prior to irradiation, helium was swept through the acid and then through the ceric sulfate solution until a constant optical density was obtained for the ceric sulfate solution. Solutions were irradiated with cobalt gamma rays at an intensity of 3500 r/min.

For acid concentrations below about 60 wt %, little or no SO_2 could be detected from the irradiated samples. For concentrations above 60 wt %, SO_2 was produced and the measured initial yield increased with increasing acid concentration, as shown in Fig. 28. In each irradiation, some SO_2 was swept out of solution during irradiation and some was removed over periods up to 30 min after the irradiation. Each point in Fig. 28 represents the total measurable amount of SO_2 determined by sweeping with helium until the optical density of the ceric solution became constant. The yield decreases with increasing dose, thus indicating some back reaction. The sweeping technique was chosen in order to eliminate back reaction insofar as possible and to allow the decomposition to be measured. Each curve in Fig. 28 was obtained by successive irradiations of the same solution, and the curvature probably results from buildup of

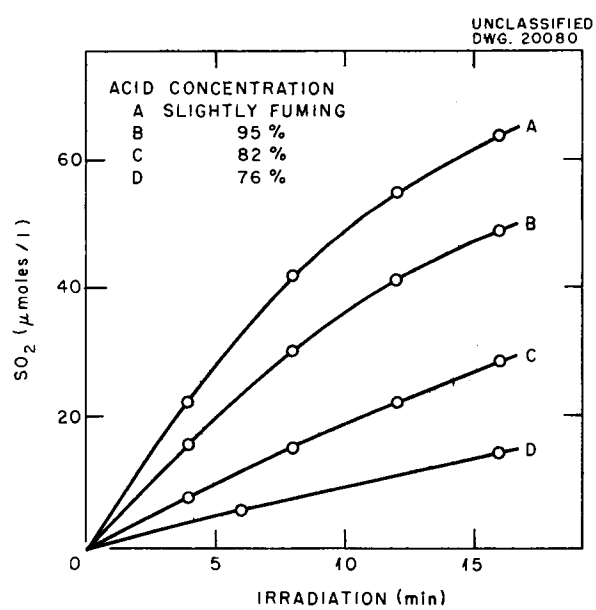

Fig. 28. SO_2 Production from Sulfuric Acid Solutions Irradiated with Gamma Rays.

(5) A. O. Allen, C. J. Hochanadel, J. A. Ghormley, and T. W. Davis, *J. Phys. Chem.* 56, 575 (1952).

(6) T. J. Sworski, *J. Chem. Phys.* 21, 375 (1953).

(7) E. R. Johnson and A. O. Allen, *J. Am. Chem. Soc.* 74, 4147 (1952).

oxidant in solution. Addition of hydrogen peroxide to the solution before irradiation resulted in no measurable SO_2 production. Sweeping 95% acid solutions with oxygen instead of helium resulted in greatly reduced SO_2 production, while sweeping with hydrogen gave the same results as sweeping with helium.

The initial yields in terms of molecules of SO_2 per 100 ev,[8] based on the first 4-min irradiations, are plotted in Fig. 29. The measured yield was very dependent on the helium-sweeping rate at the lower acid concentration, whereas at the higher acid concentrations the yield varied to a much smaller extent with sweeping rate. With the 95% acid, for example, the yield was only 10 to 20% lower with no sweeping than it was with sweeping. The lower measured yields at low acid concentrations may therefore be partly due to more rapid back reaction at the lower concentrations.

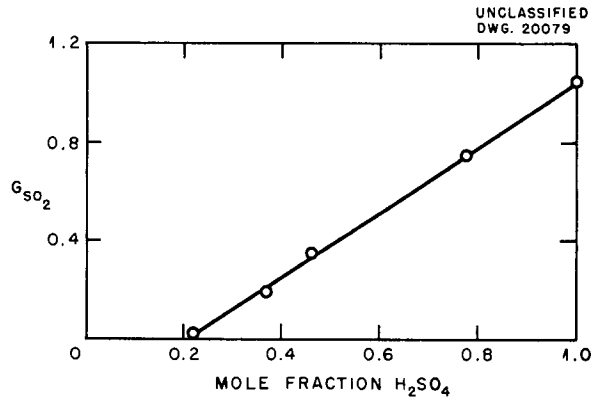

Fig. 29. Measured Initial Yields of SO_2 in the Decomposition of Sulfuric Acid by Co^{60} Gamma Rays.

EFFECT OF LIGHT-PARTICLE RADIATION ON CORROSION OF TYPE 347 STAINLESS STEEL BY URANYL SULFATE SOLUTIONS

J. A. Ghormley W. F. Kieffer
C. Hochanadel

Results obtained by Sweeton *et al.*[9] indicate that reactor irradiation considerably enhances the corrosion of type 347 stainless steel by uranyl sulfate solutions in static, bomb-type systems. The effect of radiation may result from direct action on the metal or protective film by displacement of atoms or electrons, introduction of fission-product atoms, "thermal spikes," and from chemical action of ions and free radicals produced in the solution. Experiments are under way to examine the effects on corrosion by chemical action of the irradiated solution and by displacement and trapping of electrons in the protective film. For this purpose, a small stainless steel thermal circulation loop has been constructed, in which solution flows past the corrosion specimen while it is being irradiated with electrons from a Van de Graaff generator. The electron beam can be controlled to allow energies of 0.1 to 2 Mev and currents from 0 to 100 μa, which gives a maximum power input of 200 watts. The system can withstand pressures of 1000 psi, thus allowing studies to be made at 250°C. Provisions are made for measuring pressure continually and for adding oxygen to the system to prevent precipitation. Temperatures of the specimen and of various positions on the loop will be continually measured and automatically controlled. The specimen, in the form of a rod or thin tube, is easily removable for observation. The specimen will be irradiated over only a fraction of its length, thereby allowing comparison with unirradiated blank on the same sample. Preliminary considerations indicate that, with expected flow rates of the order of 1 ft/sec and with thin tube specimens, local heating by the electron beam will result in temperature gradients between solution and specimen of less than 10°C. The system has been assembled and initial experiments are under way.

ADDITION OF BROMOTRICHLOROMETHANE TO CYCLOHEXENE INITIATED BY ULTRAVIOLET LIGHT AND BY GAMMA RAYS

J. G. Burr, Jr.

A study has been initiated to determine the nature and yields of free radicals produced in organic systems by gamma radiation. Some preliminary experiments have been made in which the yields produced by a known chain reaction[10] (the addition of bromotrichloromethane to cyclohexene) initiated by ultraviolet light are compared with those

[8] Based on a yield for ferrous oxidation of 15.6 ferrous ions oxidized per 100 ev.

[9] F. H. Sweeton, W. C. Yee, and C. H. Secoy, *In-Pile Corrosion by Homogeneous Solutions*, this report.

[10] M. S. Kharasch and H. W. Friedlander, *J. Org. Chem.* 14, 239 (1949); M. S. Kharasch and M. Sage, *J. Org. Chem.* 14, 537 (1949); H. W. Melville, J. C. Robb, and R. C. Tutton, *Discussions Faraday Soc.* 10, 154 (1951); *Op. cit.* 14, 150 (1953).

produced by cobalt gamma radiation. The 1-bromo-2(trichloromethyl)cyclohexane produced was determined by converting it to a conjugated olefin and then measuring the ultraviolet absorption at 2500 Å. An air-saturated mixture of bromotrichloromethane and cyclohexene in the mole ratio 2:1 gave a quantum yield (comparison made with a uranyl sulfate actinometer) of product of 1.8. The same mixture that was irradiated with cobalt gamma rays gave a yield of 280 product molecules per 100 ev absorbed. These results indicate a long chain reaction in the radiolysis but not in the photolysis. Additional study is necessary to determine the effects of radiation intensity, concentrations, presence of dissolved oxygen, etc.

SOME EFFECTS OF HYDROGEN AND OXYGEN ON THE PHOTOLYSIS OF HYDROGEN PEROXIDE SOLUTIONS

C. Hochanadel

The photolysis of hydrogen peroxide solutions containing dissolved hydrogen, oxygen, or both gases is being studied to obtain information concerning the relative rates and pH dependencies of the various intermediate reactions which are presumed to be common to both the photolysis and radiolysis reactions. Reactions are carried out at low peroxide concentrations and high light intensities, in which the decomposition is not a chain reaction. The effect of dissolved hydrogen is to increase the quantum yield, as shown previously,[11] whereas hydrogen and oxygen together cause a decrease in yield. Typical rate curves are shown in Fig. 30, and yield vs. peroxide concentration curves are shown in Fig. 31. In all cases, the concentrations of dissolved gases are maintained constant during an experiment. The results can be explained in terms of the reactions

$$H_2O_2 \xrightarrow{h\nu} 2OH \qquad (1)$$

$$H_2O_2 + OH \longrightarrow H_2O + HO_2 \qquad (2)$$

With dissolved hydrogen, the yield is increased by reactions

$$H_2 + OH \longrightarrow H_2O + H \qquad (3)$$

$$H_2O_2 + H \longrightarrow H_2O + OH \qquad (4)$$

[11] C. Hochanadel, *Chem. Quar. Prog. Rep. Dec. 31, 1952*, ORNL-1482, p. 41.

With both dissolved hydrogen and oxygen, the yield is decreased by the reaction

$$O_2 + H \longrightarrow HO_2 \qquad (5)$$

The quantum yield in the photolysis of air-saturated or evacuated peroxide solutions[12] is independent of pH from 0.2 to 7. In solutions containing

[12] D. E. Lea, *Trans. Faraday Soc.* 45, 81 (1949).

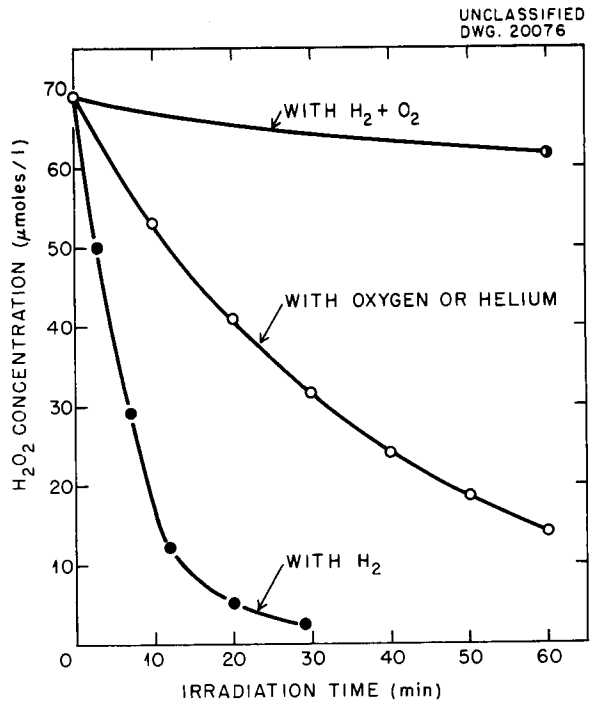

Fig. 30. Effects of Dissolved Oxygen, Hydrogen, or Hydrogen Plus Oxygen on the Photolysis of Hydrogen Peroxide Solutions.

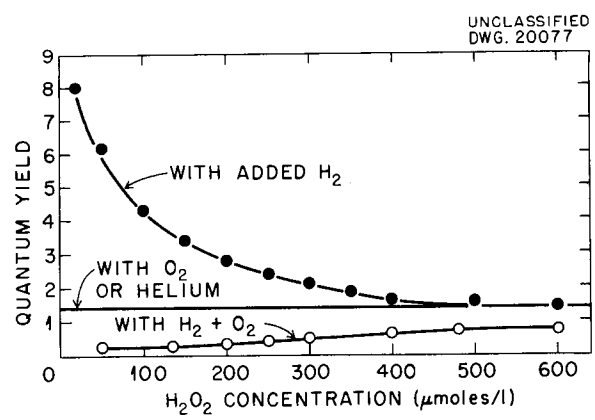

Fig. 31. H_2O_2 Concentration vs. Quantum Yield.

dissolved hydrogen, the quantum yield drops at pH less than 2, as shown in Fig. 32. This is in agreement with results obtained in radiolysis reactions[13] and indicates an effect of pH on reaction 3, although the subsequent reaction 4 may also be pH dependent.

HYDROGEN PEROXIDE FORMATION BY COBALT GAMMA RADIATION

T. J. Sworski

Oxygen Effect

The rate of formation of hydrogen peroxide in water containing oxygen is dependent upon the oxygen concentration as shown in Fig. 33. The rate of formation of hydrogen peroxide at any given hydrogen peroxide concentration is higher in water that is initially saturated with oxygen than in water that is initially saturated with air. This oxygen dependence is interpreted as resulting from two competing reactions involving the hydrogen atom.

$$H + O_2 \longrightarrow HO_2$$

$$H + H_2O_2 \longrightarrow H_2O + OH$$

The steady-state concentration of hydrogen peroxide in pure water is thus dependent upon the oxygen concentration.

pH Effect

The presence of acid has a pronounced effect upon the formation of hydrogen peroxide.[6,14] This effect has been interpreted by Ebert and Boag as resulting from an effect of pH upon the ionization of the HO_2 radical.

$$HO_2 \rightleftharpoons H^+ + O_2^-$$

They conclude that the important back reaction causing the approach to a steady state at pH = 7 is as follows:

$$O_2^- + H_2O_2 \longrightarrow OH + OH^- + O_2$$

In acid solutions, Ebert and Boag concluded that the corresponding reaction does not occur.

$$HO_2 + H_2O_2 \longrightarrow H_2O + OH + O_2$$

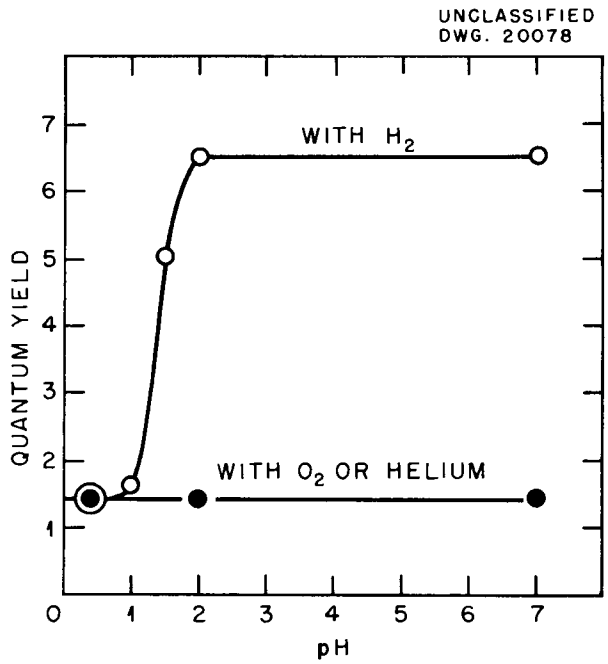

Fig. 32. Effect of pH on the Photolysis of Hydrogen Peroxide Solutions (40 μmoles of H_2O_2 per liter) Containing Either Dissolved Oxygen or Hydrogen.

In the photochemical decomposition of hydrogen peroxide, the HO_2 radical is a postulated intermediate. There is no effect of variation of the acid concentration, however, upon the quantum yield for hydrogen peroxide disappearance in the range pH 1 to 7.[12] It thus seems unlikely that the pH effect in radiation chemistry is associated with the HO_2 radical.

The oxygen effect present at pH = 7 is absent at pH = 2, as is shown in Fig. 33, although the initial yield appears to be the same. The pH effect and the oxygen effect are thus closely related. It is concluded that the pH effect is upon the reaction of hydrogen atom with hydrogen peroxide; the rate of this reaction decreases with increasing acidity.

Reduction Reactions in Acid Solutions

It has been shown that, in acid solutions, the rate of reduction of cerium(IV) is equivalent to the rate of hydrogen peroxide formation.[6] This stoichiometry has been reported for the reduction of chromate solutions by x rays.[15] The reduction of

[13] T. J. Sworski, *Chem. Quar. Prog. Rep. June 30, 1952*, ORNL-1344, p. 30.

[14] M. Ebert and J. W. Boag, *Discussions Faraday Soc.* 12, 189 (1952).

[15] H. Fricke and E. R. Brownscombe, *J. Am. Chem. Soc.* 55, 2358 (1933).

$K_2Cr_2O_7$ in 0.8 *N* sulfuric acid was investigated. A yield of 0.42 molecule reduced per 100 ev that was observed in 0.8 *N* sulfuric acid is stoichiometrically equivalent to the reported yield of 1.26 molecules of hydrogen peroxide per 100 ev.[6] The $K_2Cr_2O_7$ was determined by its absorption at 350 mμ. The molar extinction coefficient for $K_2Cr_2O_7$ in 0.8 *N* sulfuric acid, measured at 350 mμ, was found to be 2740, relative to a standard of 2240 for ferric ion at 305 mμ at 25°C.[16]

Hydrogen enhances the rate of $K_2Cr_2O_7$ reduction in the same manner that it enhances hydrogen peroxide formation. Other systems, such as $KMnO_4$ reduction, will be examined to determine whether it is generally true that hydrogen peroxide is the intermediate in reduction reactions in acidic solutions.

SOME EFFECTS OF COBALT GAMMA RADIATION ON AQUEOUS BENZENE SOLUTIONS

T. J. Sworski

Hydrogen peroxide,[17] in addition to phenol,[18] is a principal product resulting from the chemical effect of ionizing radiation on aqueous benzene solutions. In order to explain this formation of hydrogen peroxide, it has been assumed that phenyl radicals do not react with hydrogen peroxide. This conclusion has also been reached in a study of the oxidation of benzene by Fenton's reagent.[19]

The changes in ultraviolet absorption spectrum of a dilute, aqueous, air-saturated benzene solution were recorded, as a function of irradiation time, by a Cary recording spectrophotometer as illustrated in Fig. 34. Hydrogen peroxide, in the concentrations produced, does not appreciably absorb. Phenol production is evident by the development of an absorption peak at 270 mμ. The development of another absorption peak at about 345 mμ is evidence of an additional unidentified product of irradiation.

The absorption at 345 mμ is tentatively attributed to a peroxide of benzene. This absorption peak increases in intensity of absorption until the

(16) C. J. Hochanadel and J. A. Ghormley, *J. Chem. Phys.* 21, 880 (1953).

(17) T. J. Sworski, *J. Chem. Phys.* 20, 1817 (1952).

(18) G. Stein and J. Weiss, *J. Chem. Soc.*, p. 3245 (1949).

(19) J. H. Baxendale and J. Magee, *Discussions Faraday Soc.* 14, 160 (1953).

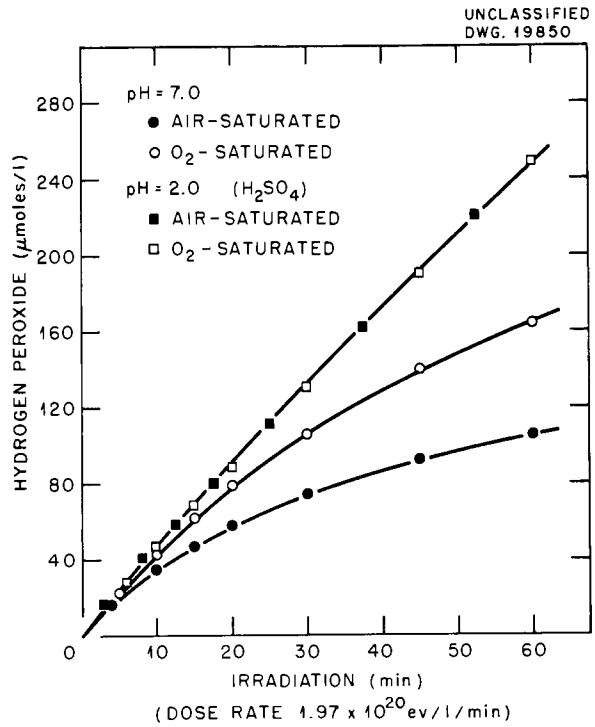

Fig. 33. Effect of pH and Oxygen Concentration on Hydrogen Peroxide Formation in Water by Cobalt Gamma Radiation.

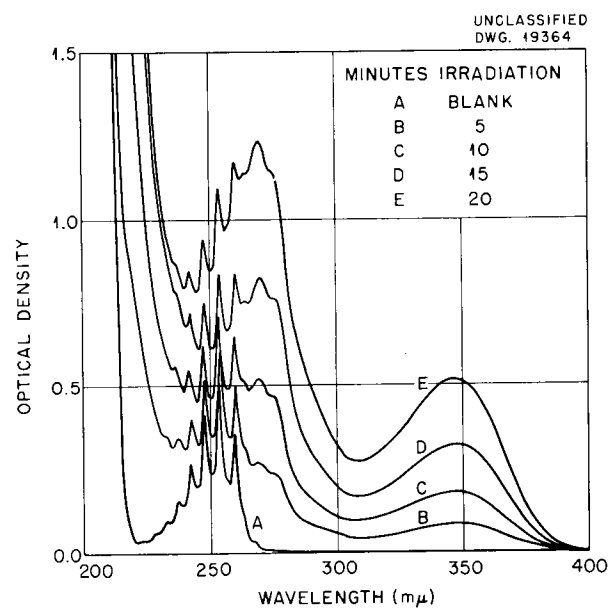

Fig. 34. Ultraviolet Absorption Spectra of Air-saturated Aqueous Benzene Solutions Irradiated with Co^{60} Gamma Rays.

oxygen becomes depleted, when an onset of disappearance occurs that is similar to that reported for hydrogen peroxide.[17] In acid solution, the absorption peak shifts to shorter wave lengths, thereby interfering with the phenol absorption peak. Thus the application of Carr's method[20] for the analysis of phenol in acidic solutions[21] is not valid. This shift in spectrum, which is reversible, may be due to the effect of acid upon the dissociation of the peroxide.

[20] M. E. J. Carr, *Nature* 167, 363 (1951).

[21] T. J. Sworski, *Chem. Quar. Prog. Rep. Dec. 30, 1952*, ORNL-1482, p. 40.

The rate of formation of the assumed peroxide increases with decreasing oxygen concentration, thus indicating the following competition:

$$H + O_2 \longrightarrow HO_2$$

$$H + PhO_2 \longrightarrow PhO_2H$$

In a proposed mechanism,[22] phenol is produced through the intermediate formation of phenylperoxy radicals (by combination of phenyl radicals with oxygen) which are assumed to hydrolyze with reresultant production of phenol and hydroperoxy radicals.

[22] T. J. Sworski, *Abstracts of the First Annual Meeting of the Radiation Research Society, Iowa City, June 22-24, 1953.*

CHEMISTRY OF SOLID STATE

THERMAL EXPANSION IN LAYER LATTICE STRUCTURES

M. A. Bredig

Thermal expansion is strongly anisotropic in substances such as graphite, boron nitride, calcium hydroxide, and magnesium hydroxide, all of which possess typical layer structures. In the hydroxides, coefficients of expansion measured perpendicular to the atomic layers are 5 to 20 times larger than those measured parallel to the layers. In graphite and boron nitride, in the low temperature range, the large, perpendicular expansion may even be accompanied by a contraction within the layers. This behavior has generally been attributed to the comparative weakness of the binding forces in the direction perpendicular to the layers. It appears that this type of anisotropy of thermal expansion is not the only one to be expected theoretically if factors frequently neglected, such as the mutual polarization (deformation) of the ions, are considered. Indeed, recent experimental observations on one of the two crystal modifications of PbO are strongly indicative of the reverse behavior in this case, namely, small expansion in the direction perpendicular to the atomic layers.

The measurements were carried out in the temperature range from 100 to 1100°K by means of x-ray diffractometers to which devices permitting heating and liquid-nitrogen cooling were attached. The experimental conditions did not favor a high accuracy of absolute values of lattice constants but did permit satisfactory determination of the relative changes in the size of the three crystallographic axes as a function of temperature. According to the data presented in Fig. 35, hexagonal cadmium iodide, with a very strong anisotropy of thermal expansion in favor of the *c* axis, behaves very much like the alkaline earth metal hydroxides of similar structure. Tetragonal stannous oxide also shows an increase in the *c/a* ratio with temperature, though a smaller one. The red form of lead oxide, which is isostructural with SnO, as well as lithium hydroxide, which is "anti-isostructural" with SnO, exhibits practically complete isotropy of thermal expansion. Thus, despite the similarity of the three compounds with respect to layer-type structure, SnO is the only one that

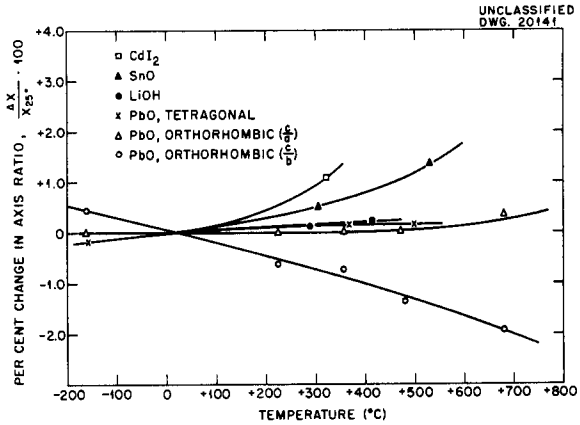

Fig. 35. Change of Crystallographic Axis Ratio with Temperature.

behaves "normally." The "abnormality" of the other two is surpassed by the yellow, orthorhombic modification of plumbous oxide, which also is said to have a layer structure but which is somewhat different from that of the tetragonal form. Figure 35 demonstrates the behavior of this yellow crystal modification; the strongest expansion is, by far, in the *b* direction, with the *c/b* ratio decreasing with increasing temperature and the *c/a* ratio remaining essentially constant. The structure of this phase, according to Byström,[1] is characterized, like that of the red form, by layers of oxygen ions that are perpendicular to the *c* axis and sandwiched between double layers of lead ions. X-ray diffraction permitted the determination of the positions of only the lead ions with sufficient certainty. Besides the very pronounced plate-like crystal habit, however, recent neutron diffraction measurements made by S. W. Peterson which have already fully confirmed the structure of the tetragonal form appear to be also indicative of the essential correctness of the orthorhombic structure as proposed by Byström, though in the absence of single crystal data, this is not yet entirely conclusive.

How, then, can the "abnormal" expansion of the orthorhombic form be explained? An explanation seems possible if the crystal is considered to be built up of the ions (called "quanticules" by

(1) A. Byström, *Arkiv Kemi, Mineral. Geol.* 16B, No. 14, 1 (1943).

Fajans[2,3]) Pb^{++} and O^{--}. O^{--} is one of the smallest, most highly charged, and therefore most highly polarizing, anions. Pb^{++} is one of the largest and, especially because of its two comparatively loosely bound 6*s* electrons, most polarizable cations. A combination of the two is bound to produce a situation in which the effect of polarization by an anion, frequently obscured by other factors, of a cation, should be especially noticeable. In Bystrom's structure of the yellow form of PbO, each lead ion is situated at the apex of a slightly distorted trigonal pyramid, the basis of which is formed by three oxygen ions at a distance of 2.15 to 2.19 Å from the lead ion. This one-sided, unusually close approach of the oxygen ions leads to, or is actually conditioned by, the shifting of the electron cloud, especially of the two 6*s* electrons of the Pb^{++} ions, into the space between Pb-O-Pb "sandwiches." When, with rising temperature under the influence of thermal vibration, general expansion of the crystal lattice takes place, the average lead-to-oxygen distance increases and the average amount of polarization, or deformation, of the lead ion necessarily decreases. In effect, the reversal of the one-sided deformation of the lead ion means a decrease in the size of the lead ion in the direction away from the triangle of oxygen ions, which is essentially the direction of the *c* axis of the crystal. Although this effect is not large enough to produce an actual contraction in the *c* direction, it is assumed here to be responsible for the unusual smallness of the thermal expansion in this direction. In this explanation it is assumed that the principal repulsive and attractive forces holding adjacent sandwiches together are provided by the repulsion of the electron shells of the Pb^{++} quanticules in adjacent layers and the attraction between Pb^{++} quanticules of one sandwich and the O^{--} quanticules of the next one at an internuclear distance of approximately 4 Å, rather than by any unqualified "metallic binding" between lead "atoms" of adjacent layers.[3]

The observation that the tetragonal form of PbO does not seem to exhibit the effect of preferred expansion within the layers is of special interest in connection with the foregoing explanation of an "anomalous" anisotropic thermal expansion. However, tetragonal PbO deviates greatly from the "normal" behavior and exhibits about half the change to the extreme of the orthorhombic form: it lacks preferred expansion in the direction of the tetragonal axis. It is thought that this is due to the considerably lower degree of polarization of the lead ion in the tetragonal form. The lower degree of polarization is associated with the larger Pb-O separation of 2.30 Å, instead of 2.15 to 2.19 Å, for four, rather than three, oxygen-ion neighbors of lead. In stannous oxide, where the Sn-O distance is also smaller than 2.30 Å, namely, 2.21 Å, lower polarization of the considerably smaller Sn^{++} ion may be the principal reason for the essentially "normal" anisotropy of expansion. It should also be noted that the cations of these oxides are arranged in a network of squares within each layer. They are not so numerous and so closely packed as the iodide ions in cadmium iodide; therefore they do not screen the negative field of the oxygen ions as effectively as the iodide ions, which are arranged in triangles and closely packed, screen the positive field of the cadmium ions. Cadmium iodide is a more truly layer-type-structure compound.

The results with lithium hydroxide, which like tetragonal PbO expands rather isotropically, are of interest for an evaluation of the role of the hydroxyl ion, as compared with that of other anions, and in relation to the anisotropy in divalent metal hydroxides such as calcium hydroxide. A deformation (polarization) of the hydroxyl ion in the field of the four nearest lithium-ion neighbors is probably associated with proton-Li^{+} repulsion and results in elongation in the *c* direction. The deformation appears to be diminished, with general expansion, at a rate similar to that of the polarization of the Pb^{++} ion by the O^{--} in tetragonal PbO and more rapid than that of the Sn^{++} in SnO. Although calcium and magnesium hydroxides do exhibit smaller anistropy of expansion than does cadmium iodide, the decrease in anisotropy is much less apparent than in lithium hydroxide. This probably results from the overwhelming importance of the weakness of the forces in the *c* direction in which, as in the dihalides, the anions shield the cation field in numbers that are twice those in lithium hydroxide. However, the effect of the permanent-dipole nature of the OH^{-} ion must not be overlooked, for it may account for at least part of the decrease in anisotropy that is discussed here.

[2] K. Fajans, *Chem. Eng. News* 27, 900 (1949); *Ceram. Age* 54, 288 (1949).

[3] K. Fajans and N. J. Kreidl, *J. Am. Ceram. Soc.* 31, 105 (1948).

It is to be emphasized that the validity of most of the foregoing remarks rests upon the correctness of the interpretation of the crystal structure of the orthorhombic form of lead oxide. In considering the question of why the smallest of the three axes (the *b* axis) rather than the *a* axis is the direction of greatest expansion, the structure proposed receives further support from the observation that the (010) planes, which are perpendicular to the *b* axis and in which, or near which, all the lead and all the oxygen ions are located, are considerably smoother than the (100) planes, which are perpendicular to the *a* axis. In addition, the *b* axis is also distinct from the other two because it represents the direction common to both glide planes characterizing the space group of the crystal. For confirmation of the structure, it is hoped that single-crystal neutron-diffraction measurements of orthorhombic yellow PbO will, in time, be available. J. Schenck of the Physics Division recently attempted to grow large single crystals but was unsuccessful, probably because of the low symmetry of the crystal structure, which may require a much steeper temperature gradient than was available in the apparatus used. Further plans include thermal-expansion measurements and structure determinations by neutron diffraction of cesium and thallium oxides (Cs_2O and Tl_2O) and similar substances containing highly polarizable cations in combination with the highly polarizing O^{--} quanticule. Also, it is planned to study other substances such as thallous fluoride (TlF), the orthorhombic structure of which, though usually classified as a deformed sodium chloride type, has dimensions which show a certain relationship to layer-type structures.

MOLTEN METAL-METAL HALIDE SYSTEMS

M. A. Bredig H. R. Bronstein
J. W. Johnson W. T. Smith[4]

Sodium–Sodium Chloride

Experimental difficulties described in a previous progress report[5] led to a series of new measurements of the solubility of sodium metal in molten sodium chloride, in which the ball check-valve type of capsule[6] was employed instead of the simple tube used previously. In these tests, continuous, automatic, rather than intermittent, manual shaking was usually employed for an equilibration period of 2 hours. A comparison of these latest results (Fig. 36) with the older ones[7] shows that there is fair agreement at temperatures below 900°C but that in the range between 900 and 1000°C, the older data are considerably lower than the new ones. The discrepancy is attributed to the prevention, by use of the check valve, of loss of sodium from the liquid-salt phase on cooling. This loss must have been due to partial vaporization of the metal when the old type of capsule was cooled, particularly from the higher temperatures. In the old capsule, "blowing" of the molten liquid from the bottom to the top of the capsule was indicated by a sudden incandescence of the top during rapid cooling.

If all the more recent data are used, it might be thought that a differential heat of solution at saturation could be estimated from the temperature-dependence of the solubility. However, it seems difficult, if not impossible, to explain as large an

[4] Consultant from the University of Tennessee.

[5] M. A. Bredig, J. W. Johnson, H. R. Bronstein, and W. T. Smith, *Chem. Quar. Prog. Rep. Dec. 31, 1952*, ORNL-1482, p. 30.

[6] M. A. Bredig, J. W. Johnson, H. R. Bronstein, and W. T. Smith, *Chem. Quar. Prog. Rep. Sept. 30, 1952*, ORNL-1432, p. 16.

[7] M. A. Bredig, J. W. Johnson, H. R. Bronstein, and W. T. Smith, *Chem. Quar. Prog. Rep. June 30, 1952*, ORNL-1344, p. 28, Fig. 11.

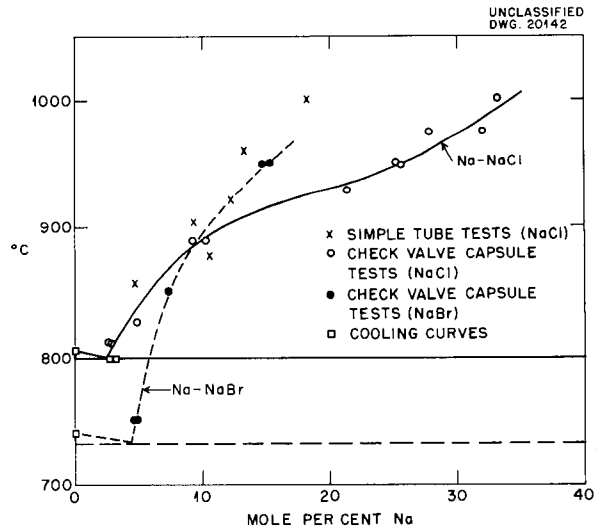

Fig. 36. Na-NaCl and Na-NaBr Equilibrium Diagrams.

entropy change as would seem to follow from a $\Delta H = 42$ kcal/mole of sodium. As Raoult's law is not expected to hold here and as new experience with other salt-metal systems indicates interesting complications arising from mutual solubility of the two components further discussed below, apparently it is not at all permissible to calculate ΔH in this manner. An appropriate thermodynamic treatment is possible only after a determination of activities; therefore a determination will be attempted in the future by partial vapor-pressure measurements of the metal and salt.

Although not specifically designed for such a purpose, the tests were also utilized to approximately determine the density of the solutions. The volume of the lower part of the capsule that was cut off for analysis of the salt phase was determined at room temperature and corrected for thermal expansion of the steel and for the widths of the saw cut. In Fig. 37, the volume thus determined per mole of sodium chloride of the solution is plotted vs. metal concentration for comparison with the sum of the volumes of sodium chloride and sodium metal as separate phases; the sum is corrected for increase in temperature. The curves show rather strikingly the large volume contraction that takes place on forming the solution. This observation appears noteworthy, particularly in connection with the modified version of the Harker-Cubiciotti "hole" theory explained in earlier reports[8] and further discussed below.

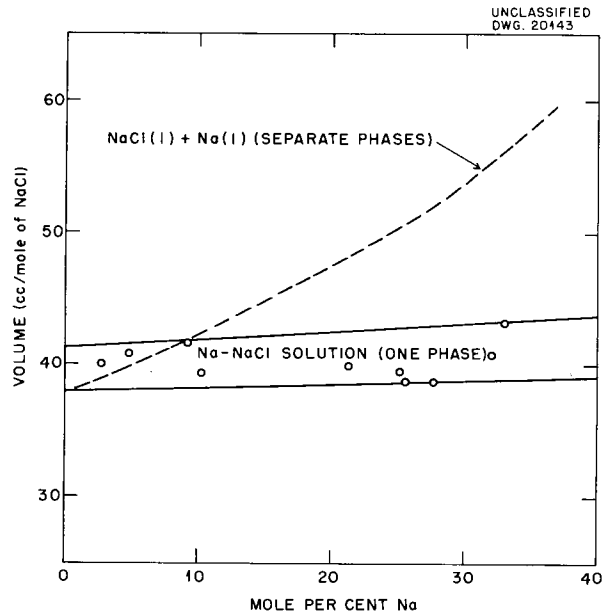

Fig. 37. Volume of Solution of Sodium Metal in Molten Sodium Chloride.

Sodium–Sodium Bromide

Five tests made thus far at 750, 850, and 950°C in the sodium–sodium bromide system indicate a solubility of 4.5 ± 0.1 mole % at a monotectic temperature of 733°C, which compares with 740°C for the melting point of pure sodium bromide, and an apparent differential heat of solution at saturation of 15 kcal. The above critical observations for the sodium–sodium chloride system also apply to this figure of 15 kcal, though perhaps to a minor degree. The thermodynamic formula,

$$N_2 = \frac{L\Delta T}{RT^2},$$

which connects the mole fraction (N_2) and melting-point depression (ΔT) through the heat of fusion of the solvent (L), yields, for the observed $\Delta T = 7$°C, $N_2 = 2$ mole %. The discrepancy between the figures of 2 and 4.5 mole % may be due to a number of reasons, among which are deviation from Raoult's law and solubility of sodium in solid sodium bromide. When compared with the sodium–sodium chloride system, the larger solubility near the melting point of the pure salt, as well as the much smaller temperature dependence, may be considered to be in agreement with the aforementioned theory; that is, the larger bromide ions should favor lower coordinations for sodium ions or, somewhat related, sodium halide molecule formation and should facilitate metal solution by thus providing more numerous and larger holes for occupation by solute atoms or molecules. On the basis of these results, a larger solubility of sodium in sodium iodide, possibly even with a negative temperature coefficient, and a smaller solubility of sodium in sodium fluoride near its melting point is anticipated, but with a large temperature dependence and possibly with a rather low temperature of complete miscibility.

This relationship between the nature of the anion and the absolute magnitude, as well as the temperature dependence of the metal solubility in the salt phase, appears to be the reverse of that found by

[8] M. A. Bredig, J. W. Johnson, and W. T. Smith, *Chem. Quar. Prog. Rep. Dec. 31, 1952*, ORNL-1482, p. 32.

the Berkeley group[9] for the metal–metal dihalide systems of the Group II elements. The difference may be connected with the relatively much greater influence of temperature on the number of "octahedral" vacancies in the case of the alkali metal monohalides, a number that is, in the dihalides, essentially equal to the number of the cations and is constant with temperature.

Potassium–Potassium Fluoride

In connection with the investigation of the solubility of alkali metal in the lithium fluoride–sodium fluoride–potassium fluoride ternary eutectic, a study of the individual salt–metal systems has been started with experiments on the potassium–potassium fluoride system. The results indicate an even steeper rise of solubility with temperature, seemingly corresponding to a ΔH of 55 kcal, than was observed in the case of the sodium–sodium chloride system. However, the results obtained seemed rather erratic, and the difficulties were at first attributed to failure of the two liquid phases to separate, possibly because of the formation of emulsions. Table 33 gives a summary of the data. It may be seen that in tests Nos. 3, 4, and 6, at high temperatures, 975 to 1000°C, the concentration of potassium metal found in the salt-sampling portion of the capsule, as well as in the metal phase, was accurately the same as the total concentration of potassium in the capsule as a whole. In tests Nos. 7, 9, 1, and 2, a solubility of potassium metal in the salt is reflected that rises from approximately 8 mole % at 865°C to 20 mole % at 905°C. Repetitions (Nos. 8 and 10) of the tests at 865°C, with a considerably larger ratio of the amount of potassium metal to that of the salt in the mixture, gave much higher analyses of the material contained in the salt-sampling portion of the capsule. Also, a considerable volume of a metallic phase was found below the check valve

[9] D. D. Cubiciotti, *J. Am. Chem. Soc.* 74, 1198 (1952); G. v. Hevesy and E. Lowenstein, *Z. anorg. u. allgem. Chem.* 187, 266 (1930).

TABLE 33. MUTUAL SOLUBILITY OF POTASSIUM METAL AND POTASSIUM FLUORIDE

EXPERIMENT NO.	TEMPERATURE (°C)	CHARGE			ANALYSIS		REMARKS
		KF (g)	K (g)	K (mole %)	K IN SALT PHASE (mole %)	KF IN METAL PHASE (mole %)	
13	658	16.9	9.4	45.3	*	7.3*	
12	750	18.0	13.2	52.1	*	18*	
11	830	17.6	11.3	48.9	*	38*	
5	865	18.0	9.7	44.5	(13.4)**	49	Average: 47 ± 3
7	865	17.8	8.9	42.7	9.7	42	
8	865	15.4	10.3	49.8	(37.9)**	49.3	
9	865	16.9	8.8	43.7	7.4	45	
10	865	18.7	11.8	48.4	(22.6)**	47	
1	881	25.0	8.0	32.2	15.6	49.3	
2	905	25.0	8.3	33.0	21.7	56	
4	975	25.0	10.4	40.0	40.1		
6	980	10.0	15.0	70.0	70.0	68	
3	1060	25.0	11.0	41.0	41.5	41.8	

*The phase in equilibrium with the solution is *solid* KF.

**Value to be discarded because salt-sampling part of capsule was found to be not completely filled with salt phase but was partly filled with metal phase.

on top of the salt phase. This seems to have been due to a diminution of the amount of the salt phase to a volume smaller than that of the sampling part of the capsule. Analysis of the metal phase found above the check valve in all five of the tests at 865°C yielded an average of 46 ± 3 mole % of KF dispersed in some manner in the potassium metal. The good agreement in these figures favors the assumption of a true solution.

In order to exclude, with greater certainty, the possibility of formation of emulsions, two isopiestic, vapor phase, equilibration tests were run. The stainless steel container used consisted of two vertically mounted capsules which were in vapor-phase communication through a horizontal tube. In the two tests, the temperature of the salt phase contained in one compartment was held 32 and 40°C above that of the metal contained in the other. After 4 hr of continuous automatic stirring for equilibration at 910°C (salt phase), more than half (namely, 2.5 and 3 g) the original amount of the potassium metal was found to have been transferred over to the 1.5 g of salt in the higher-temperature vessel to form a mixture containing 75 mole % of potassium metal. If it is assumed that equilibrium was attained, this mixture must actually have been one liquid phase, that is, a true solution, in potassium metal, of 25 mole % of potassium fluoride. This result effectively rules out the formation of an emulsion. It is strongly indicative of wide ranges of metal solubility, not only on the salt but also on the liquid metal side of the equilibrium diagram, which may extend to complete miscibility at slightly higher temperatures. This rather astounding conclusion is now being checked in another experiment: the observation of the rise of the boiling point of potassium metal under several atmospheres of argon gas pressures with the addition of increasing amounts of potassium fluoride. If the conclusion is confirmed, it may be considered strongly indicative of the existence of large solubilities, including complete miscibility, of salts in other metals (for example, rubidium fluoride in rubidium, or cesium fluoride and possibly chloride in cesium metal), especially in those cases in which the anion of the salt may be small enough to fit into the free spaces between large metal atoms.

In addition to the experiments in the region of two liquid phases, one test was carried out at 830°C, approximately 20°C below the monotectic temperature in the region where solid salt is in equilibrium with the liquid metal phase. As much as 38.4 mole % of potassium fluoride was found to be soluble in liquid metal at this temperature. Additional tests at 750 and 658°C gave 18 and 7.3 mole %. These significant results obtained with solid salt are further evidence against the assumption of incomplete separation of two phases as the cause of the high fluoride content of the metal portion of the charge and for true solubility of salt in metal. This fact will readily remove the difficulty connected with the false, high, positive value of ΔH and suggests a search for considerable salt solubility in the metal in others of these systems, particularly in those exhibiting strong positive temperature dependence of solubility, such as in the sodium–sodium chloride system. Figure 38 gives a summary of the data on the KF-K system.

A few determinations of the density of solutions of potassium in molten potassium fluoride (Fig. 39) show that in contrast to the sodium–sodium chloride system, potassium, beginning at the low concentrations, retains some of its own volume. In other words, potassium widens the "structure" of the fluoride melt. This effect must be largely due to the much larger ratio in the potassium–potassium fluoride system of the size of the metal atoms to that of the anions of the salt ($R_{K^+}:R_{F^-} = 2.31:1.33 = 1.74$, as against $R_{Na^+}:R_{Cl^-} = 1.86:1.80 = 1.03$).

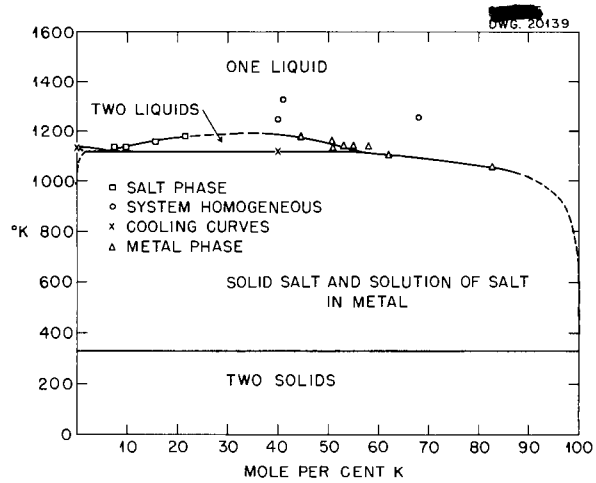

Fig. 38. KF-K Phase Equilibrium Diagram.

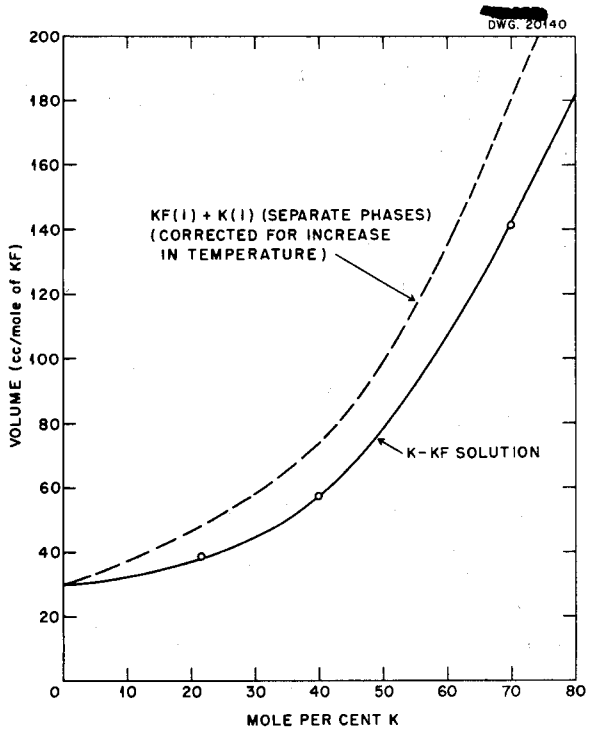

Fig. 39. Volume of Solution of Potassium Metal in Molten Potassium Fluoride.

Calcium–Calcium Chloride

In a previous report,[10] a few experiments were discussed which essentially confirmed the result of the Berkeley work. However, the supplementary observation may be added here that the equilibrium diagram of this system[11] seems to require a modification as far as the surprisingly high temperature dependence of the solubility of solid calcium in molten calcium chloride is concerned. It appears also that the large change, at the melting temperature of calcium metal, in the slope of the solubility curve cannot be reconciled with the comparatively small entropy of fusion in calcium metal. Indeed, the experimental data do not seem to rule out the possibility of extending the solubility curve down to the eutectic horizontal at a concentration nearer 15 than 0 mole % and thus allow a much smaller change in the slope in question. For the same reason, this appears to be true to a lesser extent for the strontium–strontium iodide system, in which solubilities of less than 30 rather than 36 mole % at the transition temperature of solid strontium metal and of 22 rather than 17 mole % at the eutectic temperature below 500°C are indicated.

---

[10] M. A. Bredig, J. W. Johnson, H. R. Bronstein, and W. T. Smith, Jr., *Chem. Quar. Prog. Rep. March 31, 1952*, ORNL-1285, p. 72.

[11] D. D. Cubiciotti and C. D. Thurmond, *J. Am. Chem. Soc.* 71, 2149 (1949).

INSTRUMENTATION

MULTICHANNEL PULSE ANALYZERS

C. J. Borkowski J. Eddlemon
F. Porter J. K. East
H. Hurst

A multichannel pulse analyzer has been described,[1] in which a cathode-ray beam is deflected vertically across a metal target plate which is essentially a grid having open and closed spaces that are equal. Each time the beam passes an opening in the grid a pulse is obtained from the signal plate which is directly behind the grid.

A satisfactory method was finally devised for making the grids. Flat nichrome ribbon, 0.0325 by 0.010 in., which is commercially available, was spot-welded across two ¾-in.-wide stainless steel strips. The spacing between the pieces of ribbon was controlled by a jig which held two grid ribbons at a time. By using this method, 61 channel grids were made with an error of less than 1% between the width of the spaces and the width of the ribbon.

One grid having 127 channels in a 4-in. length was made and inserted into an experimental 5CP1 cathode-ray tube. Although a marked defocussing of the beam was observed at the extremities of the 4-in. deflection, sufficiently well-resolved pulses were obtained to make it feasible to construct a 120-channel-analyzer cathode-ray tube.

The Allen B. DuMont Laboratories has completed a 61-channel pulse-analyzer tube which was made to the authors' specifications and is similar to the one previously described.[1] The tube is 3 in. in diameter and 14 in. long. Figure 40 is a photograph of the output of the signal plate of this tube and shows the pulse shape obtained with the beam sweeping across the target grid. With a beam current of 10 μa, a spot size of about 0.008 in. is obtained. By using an anode accelerating voltage of 2000 volts, a deflecting voltage of 4 volts per channel is required. Since this tube was received only recently, no performance data on the channel width stability have been obtained.

Oscillograph Galvanometer Pulse Height Analyzer

A ten-channel galvanometer type of pulse-height analyzer has been described,[2] in which the amplitude of a voltage pulse from an amplifier is determined by converting the voltage pulse into a number of pulses proportional to its amplitude. This conversion is accomplished by applying the pulse to a Hathaway oscillograph galvanometer, which in turn deflects a light beam across the photocathode of a photomultiplier tube that is partially masked by a grid structure having equal open and closed spaces. In this manner, pulses of light are generated at the photocathode. The light pulses are counted with a scaler to determine the original pulse amplitude, and a pulse is stored in the channel corresponding to the number of secondary pulses.

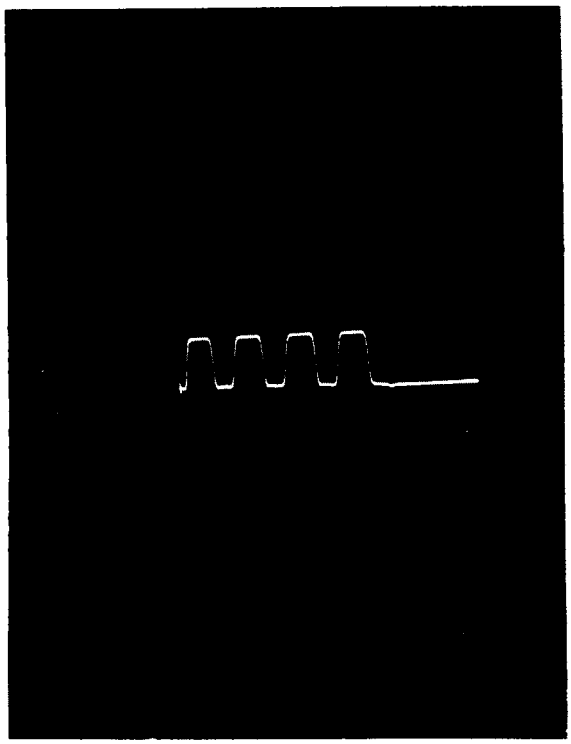

Fig. 40. Pulses Obtained from Collector Plate of Pulse Analyzer Cathode-Ray Tube.

The ten-channel analyzer described above has been successfully extended to 20 channels by using a ring type of scaler as the pulse counter and 20 binary scalers with Veeder Root recorders for the storage elements of the separate channels.

A second galvanometer type of pulse-height analyzer has been constructed and is undergoing calibration and testing at the present time. This

[1] C. J. Borkowski, F. Porter, and J. K. East, *Chem. Quar. Prog. Rep. Dec. 31, 1952*, ORNL-1482, p. 43.

[2] *Ibid.*, p. 45.

analyzer has 32 channels, with provisions for extending the number of channels to 64. The design has been modified to incorporate a gate which prevents pulses larger than a prescribed value from entering the analyzer. The operation of the upper-limit gate is as follows: A time delay which is inserted between the linear amplifier and the pulse analyzer permits an interval of time in which the voltage pulse to be measured may be presented to a pulse-height selector circuit. If the pulse exceeds the selected upper limit, the pulse-height selector circuit triggers and furnishes a 5-μsec signal to the analyzer gate circuit. This signal blocks the entry of the delayed primary pulse. The upper-limit gate circuit prevents unnecessary overloading of the analyzer circuits and saves considerable analyzer time, since only 5 μsec is required to reject a large pulse, while 150 μsec is required to measure its amplitude. The benefits are most evident when observing low-energy events in the presence of more intense high-energy radiations.

The pulse-sorting and final-storage elements of this second analyzer have been changed with the objective of performing these functions in a 64-channel analyzer with fewer tubes and lower power consumption. For the 64 channels, including storage circuits, 106 vacuum tubes are required which consume 150 watts of filament power and 100 watts of plate supply power.

The binary scale of 64 which is used to count the secondary pulses and which drives the decoding matrix has a few unusual features. It is capable of resolving pulses spaced less than 0.1 μsec apart and furnishes a minimum of 100 volts of plate swing to the external load. The later stages are required to supply up to 8 ma of current to the load. The success of the circuit shown in Fig. 41 is due, in large measure, to the desirable characteristics of the 6AF4 triodes used. These tubes have a very low plate resistance, a moderately high transconductance, and a low amplification factor.

Channel-Selector Matrix

Once the scaler has recorded a number of counts proportional to the amplitude of the energy pulse, an element is required which will decode the recorded counts from the scaler and will actuate the appropriate storage channel. For this purpose a channel-selector matrix is utilized. Driven by

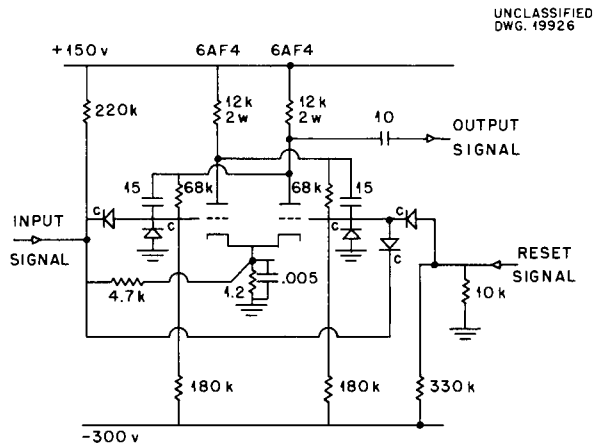

Fig. 41. Binary Scaler with a 0.1-μsec Resolving Time.

the scaler, this matrix provides a signal path for an interrogating pulse which actuates a rate-meter storage circuit corresponding to the selected channel.

The basic component of the matrix is a neon bulb which serves as a gate. Each neon bulb is connected through a 100-k resistor to the plate of a tube in one of the scaling stages and through another 100-k resistor to the B supply voltage. The neon bulb fires and remains conducting during the time the scaler tube conducts. The 220-mmf blocking capacitors provide continuity for the signal path and isolate the d-c voltages present in the circuit.

As an example of the performance of the channel-selecting matrix, the path of an interrogating pulse may be followed through the matrix shown in Fig. 42 for the case of one pulse recorded in the binary scaler. It is evident that there exists only one path through the matrix for the interrogating pulse and that this path ends at the channel-1 output.

A channel-selecting matrix of the type described has been extended to furnish a transfer circuit for information from a binary scale of 64 to 64 separate storage channels. With such a matrix, it is necessary to use an 800-volt, 3-μsec-wide, interrogating pulse in order to obtain an output pulse of approximately 25 volts. The ratio of desired to undesired output pulses is approximately 3. Because of the relatively long time constant in the coupling network between neon bulbs, the interrogating pulse must not be applied to the matrix for

approximately 35 μsec after pulses have ceased to enter the scaler.

The interrogating pulse, after passing through the channel-selector matrix, drives a very simple and stable counting-rate meter, as shown in Fig. 43. Three ranges of counting rates are covered – 2, 20, and 200 counts/sec full scale. In the meter circuit, time constants of 20, 100, and 400 sec are provided. One position of the time-constant switch allows the damping capacitor to be discharged through a 10-ohm resistor.

A gas tetrode, RCA type 5696, is used in the rate-meter circuit. Ten tubes of this type have been operating continuously at a fixed counting rate for 3000 hr with no failures and with a maximum change in output current of only 2%.

The damping capacitor is a 25-volt, 4000-mf, electrolytic type (Mallory HC2540). The leakage resistance and voltaic action of these capacitors were found to have a negligible effect upon the accuracy of the indicated counting rate.

The outputs of the 32 rate meters are connected to a multipoint Brown recorder which plots the energy spectrum directly.

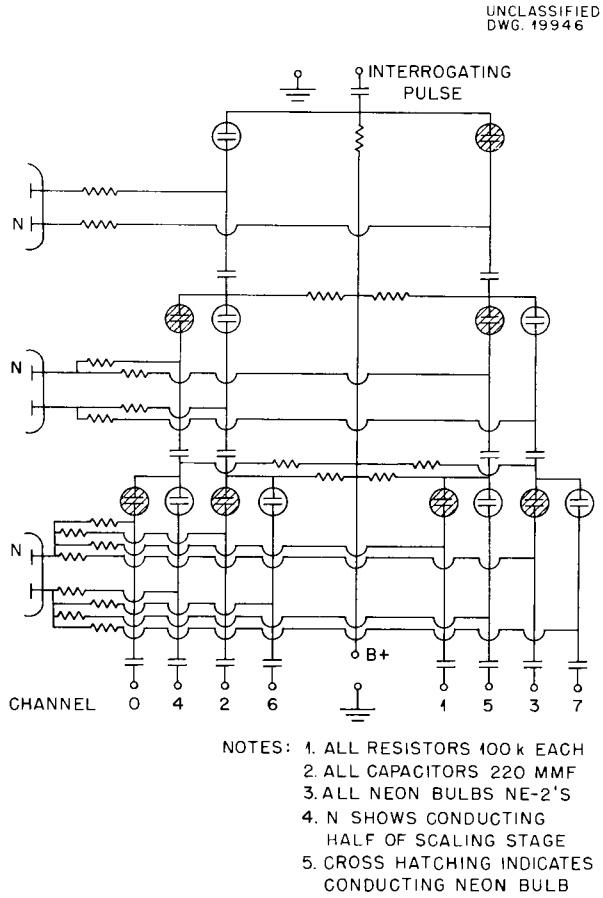

Fig. 42. Neon Bulb Channel-Selectro-Matrix.

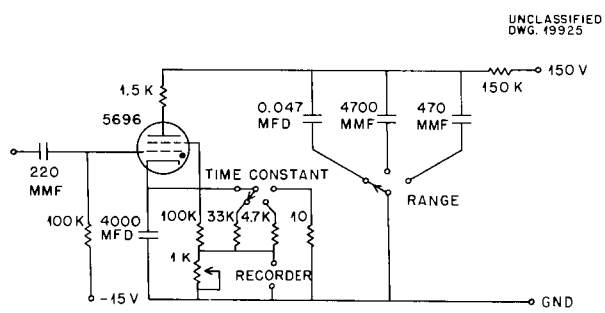

Fig. 43. Thyratron Rate-Meter Circuit.

REACTOR CHEMISTRY

BEHAVIOR OF THE SILVER, SILVER SULFATE AND THE MERCURY, MERCUROUS SULFATE ELECTRODES AT HIGH TEMPERATURES

M. H. Lietzke R. W. Stoughton

No suitable reference electrode has been reported for use in solutions at temperatures above 100°C, hence it seemed of interest to study the high-temperature behavior of two electrodes which have been used as reference electrodes at room temperature to determine whether their useful range could be extended above 100°C. The two electrodes chosen for this study were the silver, silver sulfate and the mercury, mercurous sulfate electrodes. The potential of the electrode pair was measured as a function of temperature from 25 to 250°C in 0.05, 0.2, and 0.5 *M* sulfuric acid. The measured potentials were then compared with potentials predicted on the basis of thermodynamic calculations.

When the Ag, Ag_2SO_4 electrode is used in conjunction with the Hg, Hg_2SO_4 electrode, the cell reaction is $2Hg + Ag_2SO_4 \longrightarrow Hg_2SO_4 + 2Ag$. If saturated electrodes are used, the potential for the cell combination, calculated from the ΔF for the reaction, should be +42.3 mv at 25°C. This means that the silver sulfate electrode is 42.3 mv more noble than the mercurous sulfate electrode at 25°C. The ΔS for the cell reaction at 25°C is −16.4 e.u., hence dE/dT (the temperature coefficient of the potential) is −0.36 mv/deg at 25°C.

In order to evaluate the potential of the cell combination at higher temperatures, it is necessary to calculate ΔF for the reaction at several temperatures in the range of interest. This can be done by integration of the expression

$$\left(\frac{\partial \frac{\Delta F}{T}}{\partial T}\right)_p = -\frac{\Delta H}{T^2}$$

where

$$\Delta H = \Delta H^0 + \int \Delta C_p \, dT$$

The equations giving C_p for each substance as a function of temperature are:

$$C_p(Ag) = 5.09 + 2.04 \times 10^{-3}\, T + 0.36 \times 10^5\, (T^{-2})^{(1)}$$

$$C_p(Hg_2SO_4) = 13.13 + 64.0 \times 10^{-3}\, T^{(2)}$$

$$C_p(Hg) = 7.010 - 1.092 \times 10^{-3}\, T^{(3)}$$

$$C_p(Ag_2SO_4) = 23.1 + 27.9 \times 10^{-3}\, T^{(1)}$$

When ΔC_p is expressed with these equations and the integration is performed, the following equation is obtained for the free energy of the reaction as a function of temperature:

$$\Delta F = -4358 + 31.9T \log T - 21.2 \times 10^{-3}\, T^2 - \frac{0.36 \times 10^5}{T} - 64.3T$$

Then E may be evaluated at any desired higher temperature, since $E = -\Delta F/nF$.

The silver, silver sulfate and mercury, mercurous sulfate electrodes were contained in small, fused-silica compartments 1½ to 2 in. long. The electrode compartments were sealed in a steel bomb which was fitted with electrically insulated leads. The quartz electrode compartments were sealed at one end and were fitted at the other end with Teflon plugs through which platinum wires passed. The wires leading to the electrodes were coated with Teflon paint to insulate them from the solution in the bomb proper. The solution in the electrode compartment communicated with the solution in the bomb by means of a quartz capillary sealed to the side of the quartz compartment. The bomb itself was fitted with a silica liner to prevent attack on the steel by the sulfuric acid. The

(1) K. K. Kelley, *Contributions to the Data on Theoretical Metallurgy. X. High-Temperature Heat-Content, Heat-Capacity, and Entropy Data for Inorganic Compounds*, Bulletin 476, U.S. Department of the Interior, Bureau of Mines, Washington, 1949.

(2) Derived from data in *Handbook of Chemistry and Physics*, 33rd ed., Chemical Rubber Publishing Co., Cleveland, 1951.

(3) Derived from data in T. B. Douglas, A. F. Ball, and D. C. Ginnings, *J. Research Nat. Bur. Standards* 46, 334 (1951).

potential measurements were made with a vibrating-reed electrometer and were recorded on a Brown recording potentiometer.

The bomb containing the electrodes was surrounded by a heating jacket controlled to ±2°C at the higher temperatures. This amounted to about ±0.6 mv in the potential reading, which was sufficiently precise for the present work.

In a typical experiment, the electrodes were prepared and sealed in the bomb. Potential measurements were continued until equilibrium was reached at room temperature. Then the temperature was raised to an appropriate value, and measurements again were made until a steady value was obtained. The time necessary for the electrodes to come to equilibrium depended upon the acid concentration. In the 0.5 *M* H_2SO_4, equilibrium was established almost immediately, while in the 0.2 *M* H_2SO_4, equilibrium was established overnight. It was necessary to wait several days for the electrodes to come to equilibrium in 0.05 *M* H_2SO_4.

The silver sulfate was prepared by precipitation from a solution of silver nitrate and was washed by decantation. The mercurous sulfate was Baker and Adamson reagent grade.

Figure 44 shows the potentials obtained with the silver sulfate and the mercurous sulfate electrodes as a function of acid concentration and temperature. The potentials, as measured in 0.5 *M* H_2SO_4, corresponded almost exactly with the theoretical line for the cell reaction

$$2Hg + Ag_2SO_4 \longrightarrow 2Ag + Hg_2SO_4$$

As the acid concentration was decreased, the potentials became more negative than was expected.

The fact that Hg_2SO_4 hydrolyzes to form a greenish basic sulfate, $Hg_2O{\cdot}Hg_2SO_4{\cdot}H_2O$, has been reported. According to Mellor,[4] approximately 0.0008 *M* H_2SO_4 is sufficient to prevent formation of the basic salt at room temperature. Hence, a mercurous sulfate electrode in 0.05 *M* H_2SO_4 should attain the theoretical potential against a silver sulfate electrode, and this was observed in the present work. To check on the behavior of mercurous sulfate solutions at higher temperatures, an aliquot of saturated mercurous sulfate solution in 0.05 *M* H_2SO_4 was sealed in a small pyrex tube and heated to 250°C. Small, yellow crystals of what appeared to be HgO formed on the side of the tube. They were probably formed by the reaction

$$Hg_2SO_4 + H_2O \longrightarrow Hg + HgO + H_2SO_4$$

In the case of Ag_2SO_4, no basic hydrolytic product has been reported. To check on this, a quantity of Ag_2SO_4 and water was sealed in a silica tube and heated to 250°C. Visual observation revealed no change in the appearance of the Ag_2SO_4 crystals up to 250°C, and the crystals contained the 2:1 ratio between Ag^+ and SO_4^{--} after cooling. Hence, Ag_2SO_4 does not hydrolyze appreciably under the conditions of the experiment.

If the mercurous sulfate disproportionates and hydrolyzes at higher temperatures, the cell reaction becomes, in the limit,

$$Hg + Ag_2SO_4 + H_2O \longrightarrow 2Ag + HgO + H_2SO_4$$

The ΔF for this reaction is about +12,560 cal, which gives a value for E of −272 mv. The ΔS for the reaction is −41.0 e.u., hence dE/dT = −0.89 mv/deg. Examination of the equation indicates that higher sulfuric acid concentrations will tend to repress this reaction and hence favor the simple reaction $2Hg + Hg_2SO_4 \longrightarrow 2Ag + Hg_2SO_4$.

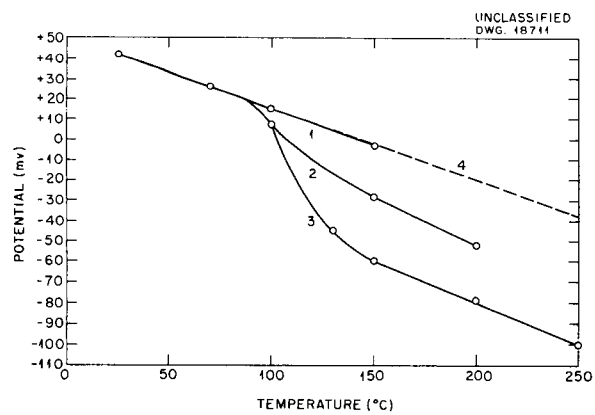

Fig. 44. Potentials Obtained with the Silver, Silver Sulfate and the Mercury, Mercurous Sulfate Electrodes as a Function of Temperature. 1. Electrodes in 0.5 *M* H_2SO_4; 2. Electrodes in 0.2 *M* H_2SO_4; 3. Electrodes in 0.05 *M* H_2SO_4; 4. Theoretical plot for the electrodes with no hydrolysis.

[4] J. W. Mellor, *A Comprehensive Treatise on Inorganic and Theoretical Chemistry*, Vol. IV, p. 966, Longmans, Green and Co., London, 1923.

This is what was observed experimentally. In 0.5 M H_2SO_4, the experimental plot coincided with the calculated plot over the temperature range studied, while in the lower acid concentrations, the potential of the Ag_2SO_4 electrode was more negative than that predicted.

It was not possible to extend the runs in 0.5 and 0.2 M H_2SO_4 to higher temperatures because the H_2SO_4 attacked the silver above 150 and 200°C, respectively, and destroyed the electrodes. The run in 0.05 M H_2SO_4 was not extended above 250°C because the Teflon used as a plug and as an insulating coating on the wires is known to soften just above 250°C.

It is proposed that at 25°C and up to about 100°C the potential of the electrode pair corresponds to the reaction

$$2Hg + Ag_2SO_4 \longrightarrow 2Ag + Hg_2SO_4$$

Above 100°C, this is also the cell reaction in sufficiently high H_2SO_4 concentrations. In lower acid concentrations, it is proposed that the potential corresponds to a combination of this reaction and the reaction

$$Hg + Ag_2SO_4 + H_2O \longrightarrow 2Ag + HgO + H_2SO_4$$

It is probable that as the temperature is raised this reaction is approached as a limit after perhaps several stages of basic salt formation.

CATHODIC PROTECTION OF TYPE 347 STAINLESS STEEL EXPOSED TO URANYL SULFATE SOLUTIONS

M. H. Lietzke

The corrosion of stainless steel in the presence of uranyl sulfate solutions constitutes one of the major problems in the long-term operation of a homogeneous reactor. The corrosion becomes especially severe at higher uranium concentrations and elevated temperatures. Hence, it seemed of interest to determine whether cathodic protection might not decrease the corrosion rate of type 347 stainless steel exposed to uranyl sulfate solutions. Experiments were performed at 100 and 250°C with uranyl sulfate solutions containing both 30 and 300 g of uranium per liter.

The experiments at 100°C were performed in refluxing uranyl sulfate solutions. In each series of experiments, three runs were made simultaneously: (1) the stainless steel specimen (2 cm square) was immersed in refluxing uranyl sulfate solution; (2) the stainless steel specimen was immersed in refluxing uranyl sulfate solution while oxygen gas was bubbled through the solution; and (3) the stainless steel specimen was maintained cathodic at 12 ma/ft^2 in refluxing uranyl sulfate solution while oxygen gas was bubbled through the solution. The oxygen gas was bubbled through the solutions to keep the uranium oxidized to the hexavalent state during the electrolysis. Current for the cathodic protection was supplied from a d-c rectifier; a piece of platinum foil served as the anode.

The experiments at 250°C were performed in stainless steel bombs. A piece of platinum foil insulated from the bomb by means of a soapstone fitting was used as the anode, while the bomb itself served as the cathode. Fifteen milliliters of 30% hydrogen peroxide was charged into the bombs at the start of each run to keep the uranium oxidized as corrosion or electrolysis proceeded.

After 100 hr in the case of the runs at 100°C and after 70 hr in the case of the runs at 250°C, the experiments were stopped and the uranyl sulfate solutions were analyzed for nickel as a measure of the extent of corrosion. The corrosion rates were calculated on the basis of mils per year during the first 100 or 70 hr (mpy/100 hr or mpy/70 hr). Stopping the experiments after 70 to 100 hr is justified on the basis of observations that the rate of attack of the stainless steel in the uranyl sulfate solutions is not constant, but decreases with time. The greatest rate of corrosion appears in about the first 100 hr, then the rate decreases to a much smaller value.[5]

Results at 100°C

Three series of runs were made at 100°C: (1) with uranyl sulfate solution containing 30 g of uranium per liter; (2) with uranyl sulfate solution containing 300 g of uranium per liter; and (3) with uranyl sulfate solution containing 300 g of uranium per liter and 100 ppm of chloride ion added as potassium chloride. The results are summarized in Table 34.

As is evident from Table 34, cathodic protection did not decrease corrosion of the steel to any greater extent in the uranyl sulfate solutions than did the mere presence of oxygen. The increased corrosion rate observed when the current was

[5] J. C. Griess, Jr., private communication.

TABLE 34. SUMMARY OF CATHODIC PROTECTION DATA OBTAINED DURING 100 hr AT 100°C

TEST SPECIMEN	RATE OF CORROSION (mpy)
30 g of Uranium per Liter as UO_2SO_4	
UO_2SO_4 solution + stainless steel	0.35
UO_2SO_4 solution + stainless steel + O_2	0.14
UO_2SO_4 solution + stainless steel + O_2 + cathodic protection	0.14
300 g of Uranium per Liter as UO_2SO_4	
UO_2SO_4 solution + stainless steel	0.28
UO_2SO_4 solution + stainless steel + O_2	0.21
UO_2SO_4 solution + stainless steel + O_2 + cathodic protection	0.21
300 g of Uranium per Liter as UO_2SO_4, 100 ppm Chloride Ion	
UO_2SO_4 solution + stainless steel	0.92
UO_2SO_4 solution + stainless steel + O_2	0.84
UO_2SO_4 solution + stainless steel + O_2 + cathodic protection	1.01

passed into the solution containing chloride may have been caused in some way by chlorine liberated at the anode. One possibility is that the platinum anode suffered attack by the chlorine, thereby releasing platinum into the solution. This platinum could then be deposited on the cathode and, by local action, increase the corrosion rate of the steel.

Results at 250°C

Runs were made at three different current densities at 250°C. (The corrosion data are summarized in Table 35.) In all cases, the uranyl sulfate solutions contained 300 g of uranium per liter.

There is no significant trend in the corrosion rates at the various current densities. The average value is 16 mpy/70 hr. The average value of the corrosion rate without cathodic protection is 36 mpy/70 hr. Thus, cathodic protection of the stainless steel bomb at 250°C decreased the corrosion rate in the uranyl sulfate solution by a factor of 2.3 over that of the unprotected steel. In all cases, the bomb wall was covered with a black-brown coating of corrosion products. The uranyl sulfate solution itself was clear and unreduced, although in a few cases it contained a small amount of suspended iron oxide.

Conclusions

Cathodic protection does not significantly decrease the corrosion rate of type 347 stainless steel in uranyl sulfate solutions at 100°C. In the presence of chloride ion, the rate of corrosion may actually be increased owing to reactions which follow the liberation of chlorine at the platinum anode. At 250°C, cathodic protection decreases by a factor of about 2.3 the corrosion rate of type 347 stainless steel in uranyl sulfate solutions containing 300 g of uranium per liter. Increasing the current density above 15 ma/ft^2 seems to have no further effect upon reducing the rate of corrosion.

THERMAL-PHASE STABILITY STUDIES OF THE ThO_2-H_3PO_4-H_2O SYSTEM

P. A. Agron W. L. Marshall

The low neutron cross section and the availability of phosphorus favor the consideration of some of its complex anions in reactor-breeder systems. Controlled operation of present-day

TABLE 35. SUMMARY OF CATHODIC PROTECTION DATA OBTAINED DURING 70 hr AT 250°C

RUN NUMBER	CORROSION RATE (mpy)
No Cathodic Protection	
1	40
2	33
3	38
4	31
5	36
Cathode Current Density 15 ma/ft^2	
1	19
2	13
Cathode Current Density 36 ma/ft^2	
1	11
Cathode Current Density 80 ma/ft^2	
1	15
2	19

homogeneous reactors for economical power and breeding purposes requires a fluid that is stable, thermally and radiation-wise, above 200°C. Previous attempts[6,7,8] to obtain thermally stable fluophosphate complexes of thorium were unsuccessful. The marked solubility of thorium orthophosphate in concentrated phosphoric acid was observed, and the adverse corrosion picture in concentrated phosphoric acid deterred further work. At present, the resurvey of all possible breeder systems has led to a renewed interest in the thorium-phosphorus systems.

[6] P. A. Agron and E. G. Bohlmann, *Chem. Quar. Prog. Rep. Sept. 30, 1950*, ORNL-870, p. 73.

[7] P. A. Agron and E. G. Bohlmann, *Chem. Quar. Prog. Rep. Dec. 31, 1950*, ORNL-1036, p. 55.

[8] P. A. Agron, *Chem. Quar. Prog. Rep. March 31*, ORNL-1053, p. 78.

The solubility of thorium in concentrated phosphoric acid at temperatures above 100°C has been explored. The thermal stability of this system in closed pyrex and silica tubes was observed and the results are listed in Tables 37 and 38.

The thorium orthophosphate was obtained from the A. D. Mackay Chemical Company, and the chemical analysis is given in Table 36. The weight loss at 110°C for this salt indicates six waters of hydration. The ThO_2 was prepared by igniting thorium nitrate hydrate at 900°C.

TABLE 36. ANALYSIS OF A. D. MACKAY CHEMICAL COMPANY THORIUM ORTHOPHOSPHATE

	THORIUM (wt %)	PHOSPHORUS (wt %)
Experimental	46.2*	12.5*
Calculated for $Th_3(PO_4)_4 \cdot 6H_2O$	58.6	10.5

*Data by J. F. Emery and J. H. Edgerton, Analytical Chemistry Division.

Thorium phosphate salt was dissolved in concentrated phosphoric acid (85%) at 150 to 225°C to give solutions with phosphate-to-thorium mole ratios of 5:1 and 7:1 at the elevated temperature. On cooling below 100°C, these systems became gel-like in nature. The original solution, containing a mole ratio of 10:1, was prepared by dissolving ThO_2 in concentrated H_3PO_4 at 200°C. (It is significant that refractory ThO_2 dissolves easily in phosphoric acid. This technique might be useful in reprocessing thorium breeder systems.) Small amounts of water were added to the original solutions to produce the dilutions given in Tables 37 and 38. Hydrolytic precipitation occurs at the interface of the water-gel layer when the water is added, but the precipitate dissolves readily on complete mixing. The densities of some of the final solutions are given in Table 37.

An unsuccessful attempt was made to prepare a solution with a 3:1 mole ratio of H_3PO_4 to ThO_2 by dissolving the oxide in concentrated H_3PO_4 at 250°C. Therefore it is probable that homogeneous solutions with ratios of H_3PO_4 to ThO_2 much lower than 5:1 cannot be obtained.

TABLE 37. PHASE-STABILITY STUDIES OF THE ThO_2–H_3PO_4–H_2O SYSTEM AT ELEVATED TEMPERATURE

SOLUTION NUMBER	MOLE RATIO OF PHOSPHATE TO THORIUM	THORIUM (g/liter)	THORIUM (wt %)	DENSITY AT ROOM TEMPERATURE	OBSERVATIONS UPON RAISING TEMPERATURE
1	10	269	14.01	1.783	Extensive precipitation at 210 to 240°C
2	10	298	15.94	1.870	Extensive precipitation at 250°C
3	10	363	17.55	2.069	1 hr at 320°C, ½ hr at 300°C, 2½ days at 300°C; no precipitation
4	10	407	18.71	2.176	A few translucent platelets at 385°C
5	10	422	19.38	2.180	Not run
6	5	600	30.9		Precipitation at 170°C
7	5	748	34.1	2.193	Precipitation at 230°C
8	5	870	36.5		Precipitation at 350°C
9	5	1000	38.4		No precipitation at 350°C, at least for 3 hr

TABLE 38. THERMAL STABILITY OF CONCENTRATED $Th_3(PO_4)_4$–H_3PO_4 SOLUTIONS IN PYREX AND SILICA TUBES

SOLUTION NUMBER	CONTAINER MATERIAL	MOLE RATIO OF PHOSPHATE TO THORIUM	THORIUM (g/liter)	OBSERVATIONS
A-1	Pyrex	5	1000	No precipitation at 350 to 400°C for ½ hr; precipitation occurs over week-end at 300°C
A-2	Pyrex	5	1000	No precipitation at 355°C for ½ hr; precipitate forms in 22 hr at 300°C
A-3	Pyrex	5	870	No precipitation on heating to 350°C; however, on holding at 300°C, precipitate forms
A-3′	Silica	5	870	No precipitation at 325°C for ½ hr and 300°C for 2 days; several crystals form after additional 2 days at 300°C; no change occurs after 3 more days at 200°C
B-1	Pyrex	7	500*	No precipitation at 350 to 400°C for ½ hr; precipitation occurs over week-end at 300°C
B-2	Pyrex	7	450*	No precipitation at 300°C for 2 hr; corroded through tube overnight at 300°C
B-2′	Silica	7	450*	No precipitation at 300°C for over 24 hr

*Estimated concentration on basis of 50% thorium in salt.

Short-term experiments in both silica and pyrex capillary tubes were run in the phase-study apparatus described previously.[9] When the temperature was slowly raised, the point at which a white solid appeared was recorded. The reversibility of these systems has not been established in the observed time periods. The experimental data are given in Table 37 and are shown in Fig. 45. The data indicate the approximate stability limits and the concentrations of H_3PO_4 necessary to stabilize these amounts of thorium.

Thermal stability tests of several of the solutions over longer periods than the short-term experiments are listed in Table 38. The variation in results as a function of time and container material would suggest that there is less corrosion in the silica tubes than in the pyrex tubes.

Corrosion

Efforts were made to explore the corrosion effect of the ThO_2-H_3PO_4-H_2O solutions on titanium and zirconium metal. Two tubes were prepared that contained the respective metal samples immersed in the solution No. 3 given in Table 37. Each tube was inserted into the phase-study apparatus at about 120°C. Reaction started immediately on the surface of the titanium to produce a gas, and after 5 to 10 min, the solution had become a deep blue, thus indicating the presence of Ti^{+++} ion. The temperature of the tube was raised to 400°C, and gas evolution increased with temperature. The reaction with zirconium to form a gas was somewhat slower than that with titanium but was much too fast, at least under these conditions, for consideration of the use of zirconium as a container material. The corrosion-stability study of these systems in a special phosphate glass is in progress. Long-term stability studies of several of these solutions will be carried out in platinum-lined bombs.

[9] H. W. Wright, W. L. Marshall, and C. H. Secoy, *Chem. Quar. Prog. Rep. Sept. 30, 1952*, ORNL-1432, p. 53.

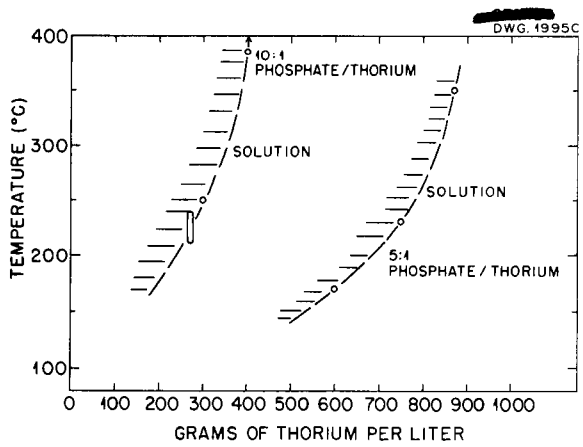

Fig. 45. Thermal Phase Stability of the ThO_2–H_3PO_4–H_2O System.

Light Scattering

Concentrated solutions Nos. 1, 4, and 5, listed in Table 37, were placed in 5-cm^3 Corex cells and exposed to a collimated carbon-arc light. A Tyndall beam of scattered light was observed in these solutions but not in the case of a control experiment of concentrated H_3PO_4. When the solutions were left undisturbed for several weeks, the intensity of the scattered light did not appear to vary. This indication of a colloidal solution is not surprising since it is also observed in the alkali-phosphate systems.[10]

The survey indicates that the neutron-economy requirements of a breeder system may be reached in concentrated phosphoric acid and that a non-conventional container material will be required to solve the problem of corrosion in this medium. This difficulty is partly compensated for by the relatively low vapor pressures existing in the region of 200 to 250°C at the high thorium concentrations. The pressures developed under radiation conditions (at room temperature and at elevated temperatures) remain to be determined.

Radiation-stability studies of concentrated H_3PO_4 and of some of the above solutions are contemplated. The addition of U^{4+} and UO_2^{++} to the phosphate system is also being considered for the one-core reactor-breeder.

[10] U. P. Strauss, *Molecular Dimensions of the Glassy Sodium Phosphates*, NYOO-3892 (March 1953).

IN-PILE CORROSION BY HOMOGENEOUS SOLUTIONS

F. H. Sweeton W. C. Yee
C. H. Secoy

More tests have been made, by using the method described in the previous report,[11] on the corrosion of type 347 stainless steel by homogeneous reactor solutions under neutron radiation. During these new irradiations, the partial pressure of oxygen was in the range of 100 to 500 psi instead of 500 to 1100 psi, as in the previously reported tests. All the solutions in the new tests consisted of UO_2SO_4, $CuSO_4$, and water. The $CuSO_4$ concentration was 0.01 *M* in each case and the UO_2SO_4 concentration was changed from test to test. All the tests were made at a neutron flux of approximately 3.5×10^{12} neutrons/cm^2·sec, and the isotope enrichment of U^{235} was varied to give the desired power density.

The data for each of the tests are given in Figs. 46 and 47. The experimental conditions common to all the tests described in each graph are shown in the block, and those conditions which are different are listed near the particular curves.

[11] F. H. Sweeton and W. C. Yee, *Chem. Quar. Prog. Rep. Dec. 31, 1952*, ORNL-1482, p. 56.

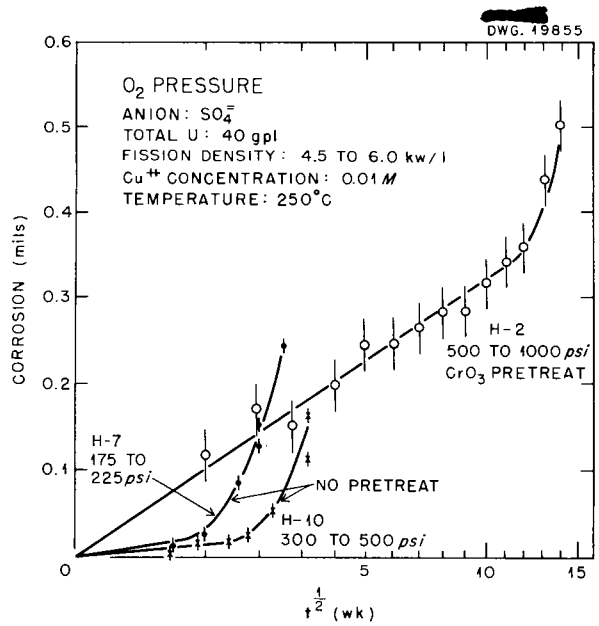

Fig. 46. Effect of Varying Oxygen Pressure.

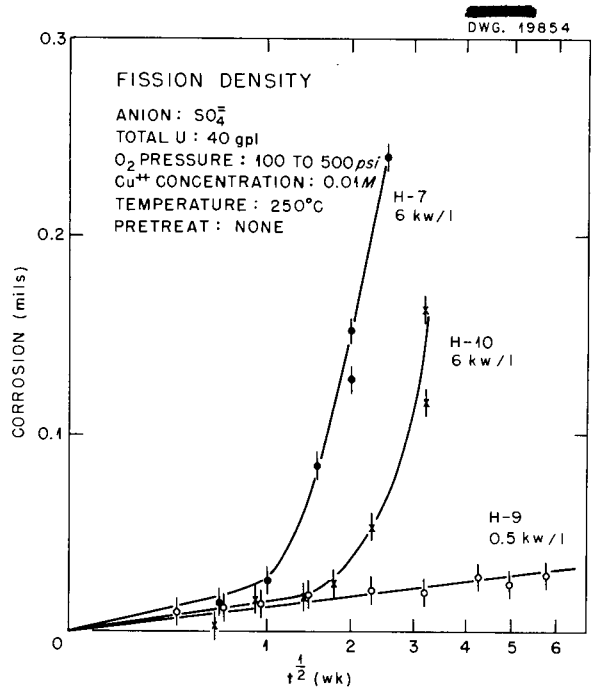

Fig. 47. Effect of Varying Fission Density.

Figure 46 shows the results of an early test, H-2, and of the duplicate tests, H-7 and H-10. Test H-2 differs from the other two in that it starts with a pretreated surface and has a higher partial pressure of oxygen.

Figure 47 compares the results of tests H-7 and H-10 with those of test H-9, in which the power density was much less. At the termination of test H-9, no upward break in corrosion had been shown.

Table 39 gives the results of two previously reported out-of-pile tests that can be compared with the in-pile tests. Unfortunately, because of experimental difficulties, the only determinations of corrosion were made at the ends of the test. Comparison of Table 39 with Figs. 46 and 47 shows that the out-of-pile corrosion is less than the in-pile corrosion, but not by a large factor.

Since only a few tests have been completed, it is impossible to draw any definite conclusions. The only direct check of reproducibility is by comparing tests H-7 and H-10. Both tests give the same type of curve but vary somewhat in the delay period before the corrosion rate increases.

TABLE 39. OUT-OF-PILE CORROSION TESTS OF UO_2SO_4–$CuSO_4$ SOLUTIONS IN STAINLESS STEEL AT 250°C

EXPERIMENT NUMBER	TOTAL URANIUM (g/liter)	CONCENTRATION OF Cu^{++} (moles/liter)	PRETREATMENT	PARTIAL PRESSURE OF O_2 (psi)	DURATION OF TEST (weeks)	CUMULATIVE CORROSION (mils)
H-3	44	0.01	None	560	9	0.02_1
H-4	44	0.01	CrO_3*	450	9	0.009_1

*2% CrO_3 treatment at 280°C for over 4 hours.

The present data do suggest the following generalities, which will be proved or disproved as further tests are made:

1. Some of the data, particularly those of test H-9, indicated that the corrosion starts out as a function of the square root of time. Such a function would be very advantageous for long-term corrosion, as it would mean a constantly decreasing rate.

2. In many of the tests (H-7, H-8, H-9, and H-10), the corrosion during the first week or two is relatively small and may not be significantly different from that in out-of-pile tests.

3. In many cases (H-7, H-8, and H-10), however, a plot of corrosion against the square root of time shows a sharp upward break after the relatively low initial corrosion.

The apparent linearity of the corrosion as a function of the square root of time suggests that the process is controlled by diffusion, perhaps through the surface film. The sudden increase in the corrosion rate could be attributed to cracking or flaking of the film.

Plans are being made to increase the effort in this program, the important immediate objectives being to determine the dependence of corrosion rate on power density, to study the behavior of other metals, particularly titanium and zirconium, and to ascertain the causes for the sudden increase in corrosion rate.

RADIATION STUDIES OF PERTECHNETATE SOLUTIONS

J. W. Boyle C. H. Secoy

The stability of the pertechnetate ion under irradiation is of academic, as well as practical, interest in the study of the pertechnetate ion as a possible corrosion inhibitor in aqueous-metal systems at elevated temperatures in the presence of ionizing radiations.

In degassed, sealed, silica ampoules containing $KTcO_4$ solutions, both with and without UO_2SO_4, it has been found that TcO_4^- is apparently stable under reactor irradiation. The gas analyses for three ampoules containing a solution of 0.02 *f* $KTcO_4$ and two ampoules containing a solution of $\sim 3.7 \times 10^{-3}$ *f* $KTcO_4$ and ~ 30 g of U^{235} per liter as 93%-enriched UO_2SO_4, together with the spectrophotometric analyses for the solutions containing $KTcO_4$ only, indicated either no reduction of TcO_4^- or a steady-state level of reduced technetium compounds below the limits of detection. A maximum of about 2 or 3×10^{21} ev of energy was absorbed for each milliliter of solution present.

Potassium pertechnetate solutions are also stable under Co^{60} alpha-ray radiation when air is present. If hydrogen is bubbled through a solution of $KTcO_4$ while under irradiation with alpha rays, a brown colloidal material (particle size approximately 0.05 to 0.08 μ) is formed, which is presumed to be TcO_2. Hydrogen-sweeping alone at room temperature will not reduce TcO_4^-. The TcO_4^- is reduced probably by hydrogen atoms, as reduction takes place only during irradiation with hydrogen-sweeping.

These facts are consistent with the present concepts for the mechanism of water decomposition by radiation. Both molecular products and radicals are formed by radiation.

$$2H_2O \rightsquigarrow H_2O_2 + H_2 \qquad (1)$$

$$H_2O \rightsquigarrow H + OH \qquad (2)$$

When copious amounts of hydrogen are swept through the water under irradiation, essentially all the oxidizing entities are removed or converted to reducing agents. The H_2O_2 is largely converted to water (or oxygen which is swept out of the water), and the OH radicals are converted to H atoms.

$$OH + H_2 \longrightarrow H_2O + H \qquad (3)$$

The pertechnetate ion is then reduced by the hydrogen atoms. As no oxidizing agents are present to convert the reduction products back to TcO_4^-, the reduced technetium compounds remain.

$$TcO_4^- + 3H + H^+ \longrightarrow TcO_2(\text{colloidal}) + 2H_2O \qquad (4)$$

Equation 4 indicates a pH rise, and such an increase has been measured in unbuffered solutions; the appearance of a brown colloidal material has also been noted. The colloidal material is thought to be TcO_2 even though the color of TcO_2 is black.[12] The equivalents of ceric ion required to oxidize one molecule of the reduced technetium compound back to TcO_4^- are being determined.

$$2H_2O + TcO_2 + 3Ce^{4+} \longrightarrow TcO_4^- + 3Ce^{+++} + 4H^+ \qquad (5)$$

The colloidal material absorbs over a wide range of wavelength, and the absorption increases smoothly and quite markedly in the ultraviolet region. The colloidal material formed during a few minutes of radiation in a 1000-curie Co^{60} source will almost completely obscure the absorption peaks of TcO_4^-. Although TcO_4^- has two absorption peaks in the ultraviolet region, the stronger one having a molecular extinction of approximately 4300, they are useless as an analytical tool when the colloidal material is present.

A method of analysis has been developed that uses ceric sulfate as an oxidant for the reduced technetium compound. It is stated[12] that TcO_2 can be slowly oxidized to TcO_4^- by Ce^{4+}. The oxidation is rapid for the colloidal material, being complete within a few minutes at room temperature. Reaction 5 can be easily followed spectrophotometrically by adding known amounts of Ce^{4+} and by measuring the amount remaining after the reaction is complete.

Ce^{4+}, Ce^{+++}, and TcO_4^- absorb in the ultraviolet region, the main peaks of Ce^{+++} and TcO_4^- falling close together. Ce^{4+} has a strong absorption peak at 3200 Å and the molecular extinction is ~5270. The absorption peak of Ce^{4+} at a wavelength of 3200 Å is a good one to measure because TcO_4^- absorbs very slightly, the molecular extinction is ~300, and Ce^{+++} does not absorb. The small amount of absorption by TcO_4^- at 3200 Å does not interfere in the Ce^{4+} determination, as TcO_4^- absorption is small and of a known value. The absorptions of Ce^{4+} and TcO_4^- simply add, with no interference. At shorter wavelengths, the absorptions of Ce^{+++} and Ce^{4+} do interfere with each other. When measurement is made, it is important to have the solution ≥ 0.8 *N* in H_2SO_4, as Ce^{4+} absorption decreases markedly at lower acid concentrations.

It was found that radiation cells containing sintered glass bottoms for gas bubbling were unsatisfactory because some of the colloidal material collected on the sintered glass, and therefore representative aliquots were not obtained. A suitable cell consists of a 10-ml graduate cone with a tube type of bubbler attached by a ground-glass joint. After irradiation, the bubbler is removed, a measured amount of Ce^{4+} reagent is added, and the absorption is measured at 3200 Å to determine how much Ce^{4+} remains unreacted.

The results obtained thus far with the new cell are meager. A 10-min irradiation of neutral, 2×10^{-4} *f* $KTcO_4$ in the maximum flux position in a 1000-curie Co^{60} source gives, with hydrogen bubbling, approximately 1.7 eq of TcO_4^- reduced per 100 ev absorbed. Doubling the rate of hydrogen bubbling through the solution seems to have no effect on the rate of reduction. Less reduction occurs per unit energy input as the radiation time is increased. Further work is necessary before an understanding of this system can be obtained.

SOLUBILITY OF HYDROGEN AT HIGH TEMPERATURES AND PRESSURES IN SOLUTIONS OF URANYL SULFATE

C. E. Ronneberg C. H. Secoy

The full elucidation of the reactions involved in the recombination of hydrogen and oxygen in solution as catalyzed by dissolved copper sulfate

[12] J. W. Cobble, *The Thermodynamics of Technetium and its Compounds*, p. 16, Doctorate Dissertation, University of Tennessee, June 1952.

under the conditions that prevail in the aqueous, homogeneous reactors of interest (high temperatures and pressures) requires a knowledge of the solubility of hydrogen in aqueous solutions of uranyl sulfate. This knowledge will be significant in connection with the operation of the HRE.

The solubility of hydrogen in pure water has been shown to increase with temperature above a certain minimum temperature (about 200°F).[13] A direct method was used to determine the solubility, that is, the amount of dissolved hydrogen in a known amount of water for a range of temperatures and pressures.

The direct determination of the solubility of hydrogen in solutions of uranyl sulfate is impossible because the uranyl ion is reduced by hydrogen, with the consequent precipitation of lower oxides of uranium.[14] However, the solubility of hydrogen in systems containing sufficient oxygen to prevent the reduction of the uranyl ion can be determined directly, and the work at BMI is proceeding by this method. In fact, insofar as the application of the data to homogeneous reactor systems is concerned, this is not an objection, since such reactor systems will also contain oxygen.

The method described below also determines the solubility of hydrogen in systems containing oxygen and, furthermore, in solutions containing a low concentration (approximately 10^{-3} *M*) of $CuSO_4$. The principal advantages of the method are the experimental simplicity and the supplementary information concerning liquid-phase, hydrogen-oxygen, reaction kinetics that can be obtained.

Kinetic Method for the Determination of the Solubility of Hydrogen

The recombination of hydrogen and oxygen in solution to form water is catalyzed by even very small amounts of dissolved copper sulfate. The rate of the reaction can be conveniently followed by observing the rate of decrease of the pressure of the mixture of gases (principally hydrogen, oxygen, and steam) above a solution of uranyl sulfate, with added copper sulfate, in a suitable bomb that initially contains a known amount of hydrogen and oxygen measured in terms of their partial pressures. Under these conditions, the uranyl sulfate is not reduced. The rate of decrease in the pressure (dP/dt) of the gaseous mixture in equilibrium with the solution depends upon the rate of the recombination reaction and the ratio of the volume of the gaseous mixture, $V_{(g)}$, to the volume of the solution, $V_{(l)}$. The following equation can be shown to apply:[15]

$$\frac{dP}{dt} = -\frac{V_{(l)}\,P k_{(soln)}}{a_{H_2} Q_{H_2}} \qquad (1)$$

where P is the pressure of the hydrogen-oxygen mixture at time t, a is Henry's constant for hydrogen ($a = P_{H_2}/[H_2]$), $k_{(soln)}$ is the molar solution-rate constant for the recombination reaction and has been shown to be a true constant for a fixed solution composition and at a fixed temperature, and Q_{H_2} is defined by[15]

$$Q_{H_2} = \frac{V_{(g)}}{RT} + \frac{V_{(l)}}{a} \qquad (2)$$

where $V_{(g)}$ and $V_{(l)}$ are the volumes of the gas and liquid phases, respectively, and R and T have their usual significance.

The quantity $-dP/dt \cdot 1/P$ can be called a pressure rate constant and is designated by the symbol $k_{(\pi)}$. Equation 1 can be put in the following form by substitution from Eq. 2 and rearrangement,

$$\frac{1}{k_{(\pi)}} = \frac{a}{RT} \cdot \frac{1}{k_{(soln)}} \left(\frac{V_{(g)}}{V_{(l)}}\right) + \frac{1}{k_{(soln)}} \qquad (3)$$

It is obvious from Eq. 3 that for a particular solution and at a fixed temperature the value of $1/k_{(\pi)}$ depends only on the volume ratio $V_{(g)}/V_{(l)}$. When $1/k_{(\pi)}$ is plotted against $V_{(g)}/V_{(l)}$, a straight line is obtained, the slope of which is equal to $a/RT \cdot 1/k_{(soln)}$ and the intercept on the $1/k_{(\pi)}$ axis is equal to $1/k_{(soln)}$. Thus by determining

[13] H. A. Pray, C. E. Schweichert, and B. H. Minnich, *The Solubility of Hydrogen, Oxygen, Nitrogen, and Helium in Water at Elevated Temperatures*, BMI-T-25 (May 15, 1950).

[14] H. F. McDuffie, *et al.*, *HRP Quar. Prog. Rep. Aug. 15, 1951*, ORNL-1121, p. 146.

[15] C. H. Secoy, *et al.*, *Chem. Quar. Prog. Rep. March 31, 1952*, ORNL-1285, p. 99.

the rate of pressure change for a particular solution at a selected temperature for a series of volume ratios, both a and $k_{(soln)}$ can be calculated. Unfortunately, experimental errors are magnified by the reciprocal relationship and by the extrapolation to zero gas volume, and very careful work will be required if either a or $k_{(soln)}$ is to be determined with reasonable accuracy.

A titanium-bomb reaction vessel with a capacity of 67.23 ml has been fabricated. It was designed to have a very comfortable safety factor at pressures as high as 2500 psi. The change in pressure during an experiment is followed with a Baldwin pressure gage and a Brown recorder. The bomb is kept at a temperature of 250°C in a rocking, aluminum-block furnace. A Brown Elect-O-Pulse time-proportioning relay is used to control the heating circuits in three heater coils. The temperature control is such that the temperature variation does not exceed 0.05°C during periods when the thermal equilibrium is dependent upon the control of the regulator. However, certain adventitious events, such as the sticking of a mercury-plunge relay, can occur during the course of an experimental run to cause a temperature variation somewhat greater than 0.05°C. In general, however, temperature control is within a range of 0.10°C.

A series of runs using a solution of 0.005 *M* sulfuric acid and 0.001 *M* copper sulfate has been completed at 250°C. The principal purpose of this series was to check the adequacy of the apparatus and the validity of the theory. The data are shown graphically in Fig. 48, in which the experimental values of $1/k_{(\pi)}$ are plotted against the volume ratio $V_{(g)}/V_{(l)}$. Although there is considerable scatter to the points, the graph indicates that the scatter is due to random experimental errors and not to any fallacy in the theory. Several possible improvements in apparatus and technique have been suggested by these experiments, and much better data should be possible. Furthermore, extension of the measurements to higher values for the volume ratio and a reduction of the copper concentration, thus reducing the value of $k_{(soln)}$ and increasing the value of $1/k_{(soln)}$, should increase the certainty of the results.

The line drawn in Fig. 48 is the result of the application of the method of least squares to the data. This yields an intercept of 0.13 and a slope of 0.827, from which $k_{(soln)} = 7.7\ hr^{-1}$ and

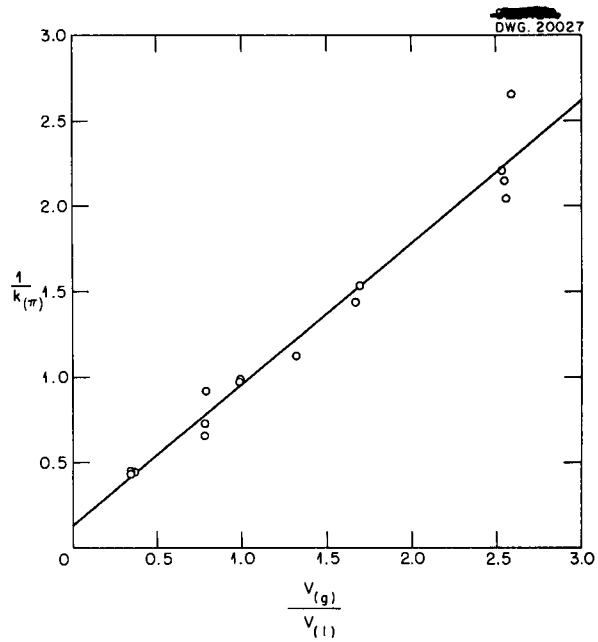

Fig. 48. Preliminary Test Data for the Solubility of Hydrogen at 250°C.

a = 4020 psi/mole·liter are calculated. The uncertainty in the data indicates that a could lie at any point between about 2500 and 6500 psi/mole·liter. The value of a taken from the BMI data is in the range of 7000 to 8500 psi/mole·liter, thus indicating that hydrogen is somewhat more soluble in 0.005 *M* sulfuric acid than in water at 250°C. Much more consistent data must be obtained before reliable values for the solubility are possible.

HOMOGENEOUS CATALYSIS: THE MECHANISM OF THE REACTION BETWEEN DISSOLVED HYDROGEN AND OXYGEN IN AQUEOUS SOLUTIONS OF CUPRIC SALTS

H. F. McDuffie L. F. Woo
C. H. Secoy

During the past six months, laboratory experiments have been carried out to obtain data bearing on the question of what copper-containing species is [are] the active catalyst[s] responsible for the reaction between dissolved hydrogen and oxygen in aqueous solutions at temperatures in the neighborhood of 250°C. The significant developments

from this work, which will be discussed in this report, include:

1. the use of cupric perchlorate-perchloric acid mixtures to show that copper is apparently uncomplexed by perchlorate, to provide an estimate of the rate constant for uncomplexed copper, and to show that hydrogen ion does not participate directly in the activated complex;
2. extension of the previously reported data for copper sulfate-sulfuric acid mixtures to higher concentrations of acid;
3. determination of the effect of uranyl sulfate concentrations up to 1 *M* upon the rate constant for copper, in both the presence and absence of added sulfuric acid;
4. correlation of rate data with direct observation (in the Marshall, semimicro, phase-study apparatus) to determine the region of hydrolytic precipitation of copper and uranium in dilute solutions of sulfuric acid and uranyl sulfate;
5. evidence that, in systems containing low concentrations of sulfate, some species appears to have considerably more catalytic activity than does uncomplexed cupric ion.

All experiments were carried out at 250°C, and solutions which were 0.0010 *M* with respect to copper at room temperature were used. In the present report, all concentrations are expressed as those at room temperature, but all values of k_{Cu}, calculated according to the formulas set forth in previous reports,[16] have been corrected for the expansion in volume and the resulting changes in concentration on going to 250°C. It should be noted that all values of k_{Cu} are based on the solubility of hydrogen in water, as reported in BMI-T-25, and that any changes in these solubility values that occur while changes are being made in the nature of the solutions tested will result in different values for the rate constant.

Catalysis by Cupric Perchlorate–Perchloric Acid Mixtures

Perhaps the simplest hypothesis which could be advanced to explain the recombination of hydrogen and oxygen in the presence of dissolved cupric compounds would involve a reaction of dissolved hydrogen with the cupric ion. Accordingly, it was very desirable to determine the activity of copper under conditions which would tend to minimize any complexing of the cupric ion by anions of the solution. The known usefulness of the perchlorate ion for this purpose and for a variety of systems at room temperatures suggested that cupric perchlorate be tested. At a concentration of 0.0010 *M*, precipitation was found to occur at 250°C, but the presence of 0.005 *M* perchloric acid was found sufficient to maintain phase stability at this temperature. Recombination experiments were run with perchloric acid concentrations of 0.005, 0.010, and 0.050 *M* in the presence of 0.0010 *M* cupric perchlorate with the results shown in Table 40. The constancy of k_{Cu} at 5.0 suggests that this may be the value for the activity of uncomplexed cupric ion. The data further indicate that no complexing by perchlorate takes place and that there is no direct participation of hydrogen ions in the reaction (except for the suppression of the hydrolytic precipitation).

TABLE 40. HOMOGENEOUS RECOMBINATION OF HYDROGEN AND OXYGEN IN CUPRIC PERCHLORATE SOLUTION

EXPERIMENT NUMBER	EXCESS ACID (moles)	$k_{Cu} \times 10^{-3}$ (moles^{-1}·hr^{-1}·liter)
B-49	0.000	3.5*
B-48	0.001	7.1*
B-151	0.005	5.0
B-152	0.010	5.0
B-153	0.050	5.0

*Phase instability.

All experiments with perchlorate have been of short duration to avoid excessive corrosion of the stainless steel apparatus by traces of chloride ion released by the decomposition of perchlorate.

Effect of Sulfuric Acid

Table 41 and Fig. 49 present data showing the effect of adding sulfuric acid to solutions of 0.0010 *M* copper sulfate. The intolerable lack of precision at concentrations of acid below 0.005 *M* was found to be paralleled by the appearance of

[16] H. F. McDuffie, E. L. Compere, and H. H. Stone, *Chem. Quar. Prog. Rep. March 31, 1952*, ORNL-1285, p. 89.

precipitates when these solutions were heated to 250°C in small glass tubes in the Marshall, semi-micro, phase-study apparatus. The precipitation of copper from solution at these temperatures had not been anticipated, since the solubility of copper sulfate in water from 100 to 180°C is reported as 43 to 45 wt % with practically no temperature dependence. The suggestion that the precipitation is hydrolytic in nature is supported by the effectiveness of excess acid in preventing its appearance, which parallels, in this case, the observations on the hydrolytic precipitation of uranium from dilute uranyl solutions. The high precision obtained at concentrations of acid above 0.005 M

TABLE 41. HOMOGENEOUS RECOMBINATION OF HYDROGEN AND OXYGEN IN PRESENCE OF ADDED SULFURIC ACID

H_2SO_4 (moles/liter)	EXPERIMENT NUMBER	$k_{Cu} \times 10^{-3}$ (moles^{-1}·hr^{-1}·liter)	$\sqrt{[H_2SO_4]}$
0.00	B-1	6.7	
	B-18	6.7	
	B-73	7.7	
	B-74	9.8	
	B-77	9.7	
	B-85	6.1	
	B-89	7.3	
	B-99	8.0	
	B-102	6.0	
0.00040	B-47	11.2	0.02
0.0010	B-33	20.6	0.032
	B-136	6.4	
	B-140	12.7	
	B-144	12.3	
0.0020	B-34	19.6	0.045
	B-137	12.7	
	B-141	12.98	
	B-142	11.8	
0.0030	B-35	19.2	0.055
	B-138	14.1	
	B-139	12.2	
	B-143	27.6	
	B-145	11.0	
	B-146	15.9	
0.0050	B-130	14.2	0.071
	B-135	14.2	
	B-147	14.6	
0.010	B-131	12.6	0.10
	B-134	12.7	
0.020	B-109	10.5	0.141
	B-114	10.6	
0.050	B-132	7.2	0.223
	B-133	6.9	

supports the view that the experimental technique is not responsible for the scatter observed at lower concentrations.

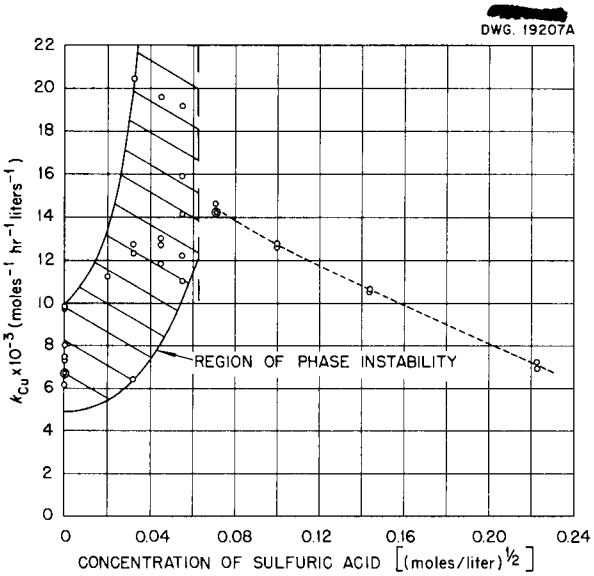

Fig. 49. Effect of Sulfuric Acid Concentration on Hydrogen and Oxygen Recombination in 10^{-3} M Cupric Sulfate Solution at 250°C.

Effect of Uranyl Sulfate

Table 42 and Fig. 50 illustrate the effect of adding uranyl sulfate of varying concentrations to solutions of 0.0010 M copper sulfate. As with the sulfuric acid discussed above, a region of irreproducibility and phase instability was noted up to a uranyl sulfate concentration of around 10 g of uranium per liter, and the activity was lowered at increasing concentrations of uranyl sulfate.

Effect of Uranyl Sulfate Plus Sulfuric Acid

Table 43 and Fig. 51 illustrate the effect of uranyl sulfate concentration upon the activity of 0.0010 M cupric sulfate in the presence of 0.020 M sulfuric acid. It will be noted that these data begin, in a sense, at a place on the curve of Fig. 49 where the activity is already considerably below the maximum and where the addition of more sulfuric acid further depresses the activity. Similarly, the addition of uranyl sulfate depresses the activity. It is also noted that the precision in the concentration region below 10 g of uranium per liter is much better than was observed in the absence of the sulfuric acid. Figure 52 shows the effect of the combination of uranyl sulfate

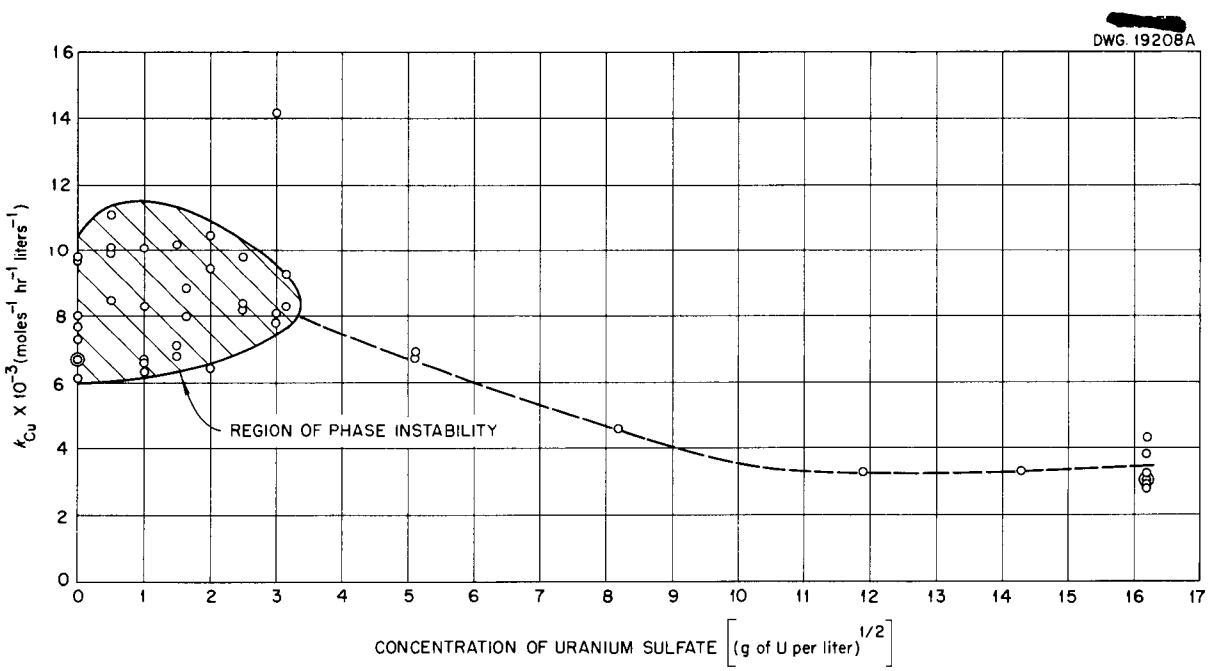

Fig. 50. Effect of Uranium Sulfate Concentration on Hydrogen and Oxygen Recombination in 10^{-3} M Cupric Sulfate Solution at 250°C.

TABLE 42. HOMOGENEOUS RECOMBINATION OF HYDROGEN AND OXYGEN IN PRESENCE OF ADDED URANYL SULFATE

URANYL SULFATE (g of uranium per liter)	EXPERIMENT NUMBER	$k_{Cu} \times 10^{-3}$ (moles^{-1}·hr^{-1}·liter)	$\sqrt{\text{g of uranium per liter}}$
0	B-1	6.7	0
	B-18	6.7	
	B-73	7.7	
	B-74	9.8	
	B-77	9.7	
	B-85	6.1	
	B-89	7.3	
	B-99	8.0	
	B-102	6.0	
0.25	B-78	8.5	0.5
	B-84	10.1	
	B-92	11.1	
	B-100	9.9	
1.0	B-72	6.7	1.0
	B-75	8.3	
	B-79	6.3	
	B-88	10.1	
	B-93	6.6	
2.25	B-80	10.2	1.5
	B-87	6.8	
	B-94	7.1	
2.62	B-62	8.9	1.62
	B-66	8.0	
4.0	B-81	9.45	2.0
	B-86	10.5	
	B-96	6.4	
6.25	B-82	9.8	2.5
	B-90	8.4	
	B-97	8.2	
9.0	B-83	8.1	3.0
	B-91	7.8	
	B-98	14.2	
10.0	B-71	8.3	3.16
	B-76	9.3	
26.2	B-63	6.8	5.1
	B-67	6.9	
83	B-68	4.6	8.2
142.5	B-69	3.3	11.9
205	B-70	3.3	14.3

TABLE 42 (continued)

URANYL SULFATE (g of uranium per liter)	EXPERIMENT NUMBER	$k_{Cu} \times 10^{-3}$ (moles^{-1}·hr^{-1}·liter)	$\sqrt{\text{g of uranium per liter}}$
262	B-64	2.7	16.2
	B-65	3.0	
	B-106	3.2	
	B-107	4.3	
	B-108	2.9	
	B-119	3.8	
	B-120	3.0	

TABLE 43. HOMOGENEOUS RECOMBINATION OF HYDROGEN AND OXYGEN IN PRESENCE OF 0.020 M SULFURIC ACID AND ADDED URANYL SULFATE

URANYL SULFATE			EXPERIMENT NUMBER	$k_{Cu} \times 10^{-3}$ (moles^{-1}·hr^{-1}·liter)	TOTAL SULFATE (moles/liter)	$\sqrt{[\text{SULFATE}]}$
As g of Uranium per Liter	As $\sqrt{\text{g of Uranium per Liter}}$	As Moles per Liter				
0	0	0	B-109	10.5	0.021	0.145
			B-114	10.6		
1.0	1.0	0.0042	B-110	7.0	0.0252	0.158
			B-113	7.2		
2.25	1.5	0.0095	B-124	8.0*	0.0305	0.175
			B-128	6.1		
4.0	2.0	0.0168	B-111	5.5	0.0378	0.194
			B-115	6.2		
			B-116	6.1		
			B-118	8.9-6.6**		
6.25	2.5	0.026	B-125	7.5*	0.047	0.217
			B-129	5.9		
9.0	3.0	0.038	B-112	7.3	0.059	0.242
			B-117	8.1		
12.25	3.5	0.051	B-126	6.8	0.072	0.268
			B-127	7.1		
25.0	5.0	0.105	B-148	7.2	0.126	0.355
100	10.0	0.420	B-149	5.6	0.441	0.665
208	14.4	0.873	B-150	3.1	0.894	0.945

*Evidence of excess activity as a result of contamination of reaction vessel in previous runs.

**Poor experimental data.

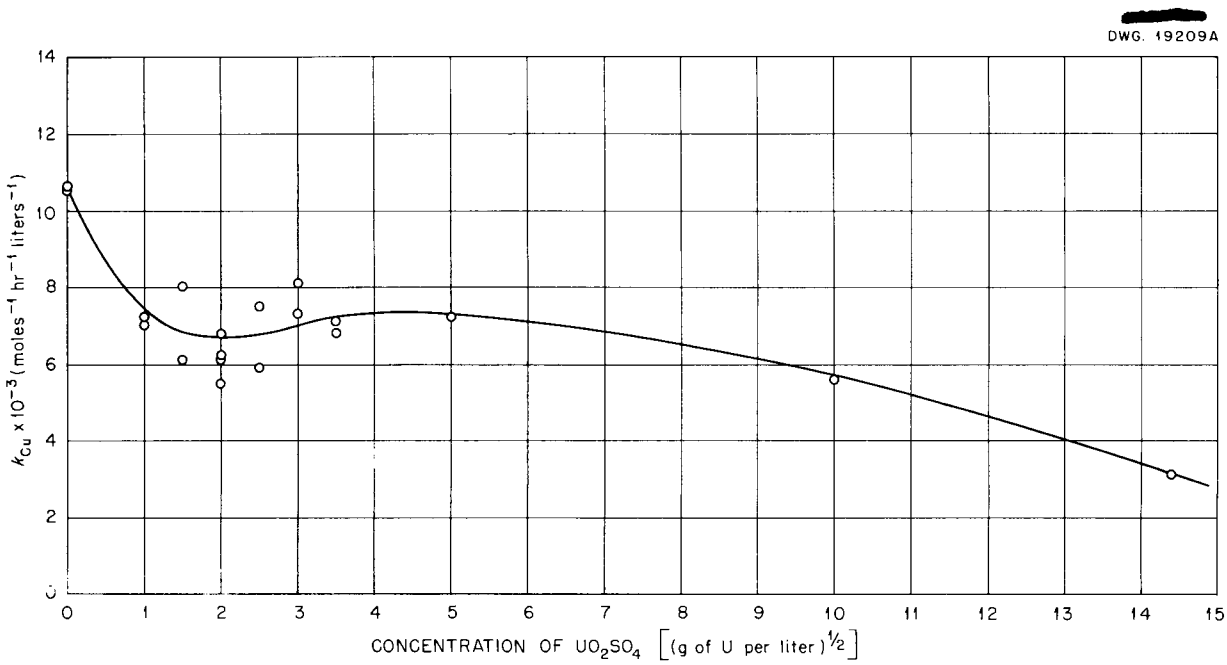

Fig. 51. Effect of Uranyl Sulfate Concentration on Hydrogen and Oxygen Recombination in 10^{-3} M Cupric Sulfate Solution at 250°C.

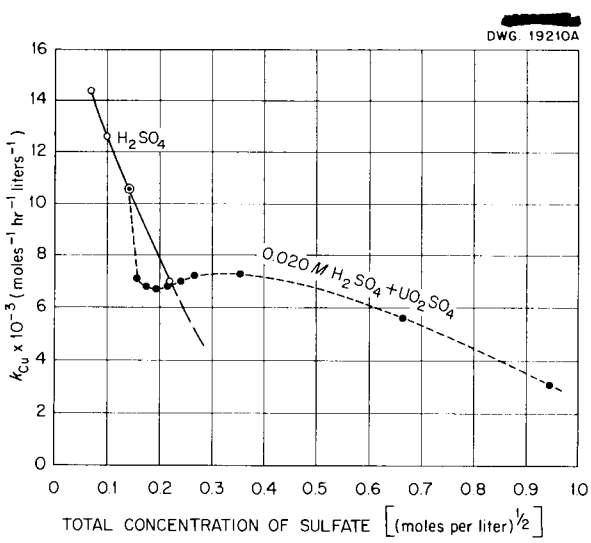

Fig. 52. Effect of Sulfuric Acid and Uranyl Sulfate on Hydrogen and Oxygen Recombination in 10^{-3} M Cupric Sulfate at 250°C.

plus 0.020 M sulfuric acid superimposed on the effect of sulfuric acid alone.

The constant activity obtained with cupric perchlorate in the presence of varying amounts of perchloric acid suggests that this value is characteristic of the cupric ion in the uncomplexed (except possibly by water) state. The higher values obtained in the presence of low concentrations of sulfate and sulfuric acid indicate that one or more species involving a complex with sulfate or bisulfate may be present with much higher activity than that of uncomplexed cupric ion. The presence of the region of hydrolytic precipitation interferes seriously with the determination of the effects of sulfate ion concentration and bisulfate ion concentration below 0.005 M, and this is just the concentration region where it is most desirable to know the effects. However, efforts are being made to separate the effects of sulfate, bisulfate, acidity, etc. by experiments in which perchloric acid and sodium or lithium hydroxide are used as inert balancing agents. Also, the proximity of the region of maximum activity to the region of hydrolytic precipitation raises the possibility of heterogeneous catalysis

by cupric hydroxide or related compounds. Interest at the present time is in homogeneous activity, and it is being assumed that clear solutions at elevated temperatures can show only homogeneous catalysis. Any evidence to the contrary will, of course, be considered.

In attempting to arrive at the active species and the mechanism for the reaction, it must be remembered that this is a *homogeneous* catalytic activation of molecular hydrogen. Almost all known hydrogenation catalysts are solids, but a few instances of homogeneous catalysis have been described in the literature. Calvin[17] has described the reduction of quinone in quinoline solution, catalyzed by cuprous acetate. Weller and Mills[18] have extended the work of Calvin in attempts to arrive at the mechanism of the reaction and they concluded that the active catalyst is a cuprous acetate dimer in a complex with two molecules of quinoline. The apparent activation energy was determined to be around 15 kcal/mole in the temperature range 78 to 100°C. The reduction of quinone and cupric acetate and hydrogen-deuterium exchange were all found to take place at comparable rates, thus indicating that the rate-determining step in each reaction was probably the activation of a hydrogen molecule by the catalyst complex. Weller and Mills state: "It appears by no coincidence that a cuprous dimer, rather than a monomer, is necessary for catalytic action. Breaking a hydrogen-hydrogen bond requires the expenditure of a large amount of energy, and it is probable that in order to achieve the dissociation, two strong copper-hydrogen bonds must be formed; in other words, the dimer is necessary to provide simultaneous acceptors for the two hydrogen donors." In striking analogy to the hydrogen-quinone reaction and to the recombination reaction of hydrogen-oxygen presently under study, Wender, Orchin, and Storch[19] have been studying the "oxo" reaction of hydrogen-carbon monoxide mixtures with various alcohols and carbonyl compounds. They consider the active catalyst to be dissolved dicobaltoctacarbonyl, $(Co(CO)_4)_2$, which, upon reaction with molecular hydrogen, is converted to cobalt hydrocarbonyl, $HCo(CO)_4$. Comparison with the quinone reduction reaction shows the strong similarity; in both cases, molecular hydrogen reacts with a dimeric metal complex to form a compound in which the hydrogen atoms have been separated. Perhaps the closest approach to the conditions which are used for hydrogen-oxygen recombination has been provided by the work of Ipatieff *et al.*[20] Cupric sulfate, nitrate, chloride, acetate, and formate have been reduced to metallic copper by using elevated temperatures (above 90°C) and high pressures (above 100 atm) of hydrogen. Pure, microcrystalline, metallic copper has been obtained in such experiments, none of which were conducted in the presence of oxidizing reagents. No evidence of a dimer complex of copper as the active catalyst for the reduction of copper salts in aqueous solutions (which would extend the analogy with the other reactions of molecular hydrogen and homogeneous catalysts) has been reported.

The activation energy found[21] for hydrogen-oxygen recombination catalyzed by cupric sulfate dissolved in uranyl sulfate solutions (40 g of uranium per liter) over the temperature range 190 to 260°C was in the neighborhood of 23 kcal/mole, whereas that reported for the quinone reduction catalyzed by cuprous acetate dimer in quinoline solution was 15 kcal/mole. It might be expected that the 23-kcal reaction would be so slow at 100°C as to be unmeasurable with usual techniques. Furthermore, in the hydrogen-oxygen recombination, there is always oxygen present to oxidize the cuprous copper to cupric (more rapidly than the cupric is reduced by hydrogen). It would be very interesting to repeat the work of Weller and Mills by using a hydrogen-oxygen mixture instead of a hydrogen-quinone system and by testing the effect of excess acetate ion upon the catalytic power of the cuprous acetate. It would also be interesting to test a hydrogen-quinone system in aqueous solutions of cuprous or cupric salts at temperatures in the range 100 to 250°C. Tests of cupric acetate are planned for recombination studies at 250°C, although it is not certain

(17) M. Calvin, *Trans. Faraday Soc.* 34, 1181 (1938); *J. Am. Chem. Soc.* 61, 2230 (1939).

(18) S. Weller and G. A. Mills, *J. Am. Chem. Soc.* 75, 769 (1953).

(19) I. Wender, M. Orchin, and H. H. Storch, *J. Am. Chem. Soc.* 72, 4842 (1950).

(20) V. N. Ipatieff, B. B. Corson, and I. D. Kurbatov, *J. Phys. Chem.* 43, 589 (1939); Wl. Ipatiew and W. Werchowsky, *Berichte* 42, 2078 (1909); Wl. Ipatiew and Wl. Ipatiew, Jr., *Berichte* 62, 386 (1929); Wl. Ipatiew and Wl. Ipatiew, Jr., *Berichte* 60, 1982 (1927).

(21) C. H. Secoy, *HRP Quar. Prog. Rep. March 15, 1952*, ORNL-1280, p. 170.

that the acetate will be stable under these conditions.

Although there is no direct evidence that the copper catalyst for the recombination reaction at 250°C in aqueous solutions is characterized by pairing of the copper ions (as seems to be the case for the other reactions discussed), it is still of interest to examine those ions which are known to form pairs in aqueous solutions. Mercurous salts certainly do this. Moreover, Ipatieff and Werchowsky reported that mercury and silver salts are reduced by hydrogen, even at room temperature. Accordingly, couples of copper-mercury and copper-silver salts will be tested for possible synergism. (Exploratory experiments with cupric solutions in the presence of liquid mercury, carried out for another purpose, have already shown certain interesting anomalies with respect to the recombination rates.)

On the assumption that no complexing is involved in catalysis by cupric perchlorate, the effects of concentration and temperature will be examined with this material.

DECOMPOSITION OF PEROXIDE IN AQUEOUS URANIUM SYSTEMS

M. D. Silverman C. H. Secoy

Studies of the thermal decomposition of peroxide in uranyl sulfate solutions, both in the absence and presence of various catalysts, have been reported elsewhere.[22] The following paragraph summarizes this work.

The decomposition of peroxide in uranyl sulfate solutions has been found to be first order in peroxide and independent of the uranium concentration. The rate also appears to be independent of the acidity of the solution. First-order specific reaction rate constants have been determined at 53, 78, and 100°C. A conductance method has been developed for following the decomposition at rates which preclude the successful use of the chemical method employed for early work on this problem. The conductance method, which agrees with the chemical method to within 5%, has been used for investigating catalytic effects from possible corrosion and fission-product species in uranyl sulfate solutions. Allowable homogeneous reactor operating levels have been estimated from the data.

Mechanism of Peroxide Decomposition

When hydrogen peroxide is introduced into an aqueous uranium solution, there is an immediate reaction according to the following equation

$$UO_2^{++} + H_2O_2 \rightleftharpoons UO_4(aq) + 2H^+ \quad (1)$$

That the hydrogen peroxide reacts essentially quantitatively in the absence of excess acid can be demonstrated by the consistency of the change in hydrogen ion concentration with the stoichiometry of the equation given above, whether or not the solubility of uranyl peroxide is exceeded. This change in hydrogen ion concentration can easily be detected in dilute uranium solutions, that is, less than 0.2 *M*; in concentrated solutions, the change is masked by the buffering action of the salt.

Grieger *et al.*[23] have reported equilibrium data for systems containing solid uranyl peroxide in uranyl sulfate solution. Evidence that the equilibrium indicated by Eq. 1 exists has been independently confirmed.[24] If an equilibrium exists for the reaction in Eq. 1, even in the absence of solid uranyl peroxide, then the addition of excess hydrogen ion should shift this equilibrium to the left. Furthermore, if the rate of decomposition of peroxide changes markedly because of this addition (of hydrogen ion), it would indicate that two different modes of decomposition of peroxide are possible, or that two different species are being decomposed.

No attempt was made in the previous work[22] to elucidate the mechanism whereby peroxide is decomposed in these uranium systems at 100°C.

---

(22) M. D. Silverman, G. M. Watson, and H. F. McDuffie, *Journal of Reactor Science and Technology* (Sept. 1953, in press).

(23) P. F. Grieger, E. W. Christopherson, and J. W. Gates, Jr., *Tuballoy Peroxide. Part I. The Equilibrium Constant. Precipitation of Tuballoy Peroxide from Ammonium Nitrate Solutions*, CD-4021 (April 28, 1945); P. F. Grieger, E. W. Christopherson, and J. W. Gates, Jr., *Tuballoy Peroxide. Part II. The Influence of Sulfate on the Solubility and Rate of Precipitation of Tuballoy Peroxide*, CD-4016 (April 19, 1945); P. F. Grieger and J. W. Gates, Jr., *Tuballoy Peroxide. Part III. Discussion of the Solubility of Tuballoy Peroxide in Sulfate Solutions Based on the Tubanyl Sulfate Association Hypothesis*, CD-4023 (May 28, 1945).

(24) Private communication from H. H. Willard; also verified by the authors.

However, two alternative modes of decomposition were suggested:

$$\text{A.}\quad UO_4 + 2H^+ \longrightarrow UO_2^{++} + H_2O_2 \quad (2)$$

$$H_2O_2 \longrightarrow H_2O + \tfrac{1}{2}O_2 \quad (3)$$

$$\text{B.}\quad UO_4 \longrightarrow UO_3 + \tfrac{1}{2}O_2 \quad (4)$$

$$UO_3 + 2H^+ \longrightarrow UO_2^{++} + H_2O \quad (5)$$

Previous work[22] indicated that the rate-determining step in each of the modes presented above does not involve hydrogen ion.

Data presented below indicate that, in the solutions previously employed,[22] the decomposition proceeds through mode B and not through A. However, in the presence of a large excess of hydrogen ion, the rate of decomposition is markedly decreased and the mode of decomposition is that given in A.

When solid uranyl peroxide is present, the concentration of only the other three species have to be determined in order to obtain an equilibrium constant for the reaction given in Eq. 1. Grieger *et al.*[23] neglected the concentration of uranium and peroxide present as dissolved uranyl peroxide and analyzed only for total uranium and total peroxide in the presence of a large excess of uranium and hydrogen peroxide. However, in the absence of any solid uranyl peroxide, the concentration of both the hydrogen peroxide and the uranyl peroxide would have to be known to obtain an equilibrium constant for the reaction. This appears to be extremely difficult analytically. From a study of the rate constants over a wide range of hydrogen ion concentration, a possible method of determining the concentration of these two species was devised. The rate of decomposition of peroxide in the absence of any uranyl peroxide (pure hydrogen peroxide in acid) is very slow, and the rate in the presence of uranyl peroxide with no added acid is quite fast. Intermediate rates of decomposition are obtained by adjusting the hydrogen ion concentration. By using the rate constant, k_3 (from these intermediate runs) and by knowing the rate constants k_1 and k_2 for the decomposition of the species UO_4 and H_2O_2 at either end of the "range," it is possible to calculate the concentration of both the uranyl peroxide and hydrogen peroxide present from the equation,

$$k_3 a = k_1 x + k_2(a - x)$$

where a is the known amount of hydrogen peroxide added, x is the concentration of uranyl peroxide, and $(a - x)$ is the concentration of unreacted hydrogen peroxide. It is assumed that the rate of decomposition in the absence of excess hydrogen ion is due practically entirely to the uranyl peroxide species. By this method, values have been obtained for the concentration of uranyl peroxide and hydrogen peroxide in these solutions, and preliminary equilibrium constants have been calculated.

Since the rate of decomposition of peroxide in these solutions appears to be directly proportional to the concentration of dissolved uranyl peroxide and since the latter is directly proportional to the uranyl ion concentration, it is conceivable that this method for determining the rates of decomposition could be pushed a step further to obtain a measure of the complexing of uranyl ion by different anionic species. Early work indicates that the method holds definite promise in this regard.

The experimental apparatus, techniques, and procedure are largely the same as those reported previously[22] for the chemical method. Again, the ceric sulfate–ferrous ammonium sulfate titration was employed in which orthophenanthroline was used as the indicator.

The uranyl perchlorate solution was prepared by adding a weighed amount of a previously analyzed UO_3 preparation to concentrated perchloric acid and by diluting to a convenient concentration. The final solution was analyzed to confirm the stoichiometric ratio of uranium to perchlorate.

The data obtained thus far are summarized in Tables 44 and 45. Initially, it appears that in the presence of a large excess of hydrogen ion, the decomposition of peroxide proceeds through mode A shown above and that when no excess hydrogen ion is present, the decomposition proceeds through mode B.

Preliminary values for the equilibrium constant K in both sulfate and perchlorate systems are given in the last column of Tables 44 and 45, respectively. The average values are $K_{SO_4} = 4.7$ and $K_{ClO_4} = 1.1$ at fairly constant ionic strength, μ. These values may be refined with additional data. The difference in the K values gives a measure of the complexing action of sulfate ion on uranyl ion, although the data at present are not adequate for a quantitative treatment.

TABLE 44. DECOMPOSITION OF PEROXIDE IN URANYL SULFATE SOLUTIONS AT 100°C

TOTAL URANIUM CONCENTRATION (M)	TOTAL H^+ CONCENTRATION (M)*	IONIC STRENGTH, μ**	OBSERVED RATE CONSTANT, $k_3 \times 10^3$ (min^{-1})	CALCULATED CONCENTRATION ($M \times 10^4$)		EQUILIBRIUM CONSTANT, K
				UO_4	H_2O_2	
0	2.3	2.3	0.240 (k_1)			
0.034	0.004	2.0	86.6 (k_1)			
0.030	0.32	2.2	55.0	12.64	7.36	5.9
0.023	1.01	2.2	8.94	1.89	18.11	4.7
0.034	2.0	2.6	5.1	1.00	19.0	6.2
0.030	2.3	2.4	2.18	0.50	29.5	4.1
0.63	0.015	1.9	129 (k_1)			
0.56	1.16	2.9	79.3	15.35	9.65	3.8
0.63	2.32	4.2	38.5	7.43	17.57	3.6

*Excess acidity added as $HClO_4$.
**Adjusted by adding $NaClO_4$.

TABLE 45. DECOMPOSITION OF PEROXIDE IN URANYL PERCHLORATE SOLUTIONS AT 100°C

TOTAL URANIUM CONCENTRATION (M)	TOTAL H^+ CONCENTRATION (M)*	IONIC STRENGTH, μ**	OBSERVED RATE CONSTANT, $k_3 \times 10^3$ (min^{-1})	CALCULATED CONCENTRATION ($M \times 10^4$)		EQUILIBRIUM CONSTANT, K
				UO_4	H_2O_2	
0	2.0	2.0	0.815			
0.034	0.022	2.0	206			
0.092	0.15	2.3	136	13.2	6.80	0.5
0.089	0.50	2.2	26.3	2.48	17.5	0.4
0.081	1.00	2.2	11.6	1.05	18.9	0.7
0.062	2.00	2.3	4.75	0.384	19.6	1.2
0.60	0.054	4.4	169			
0.59	0.50	4.1	123	14.6	5.42	1.1
0.565	0.99	3.9	57.3	6.71	13.3	0.9
0.60	2.0	3.8	30.1	3.48	16.5	1.4

*Excess acidity added as $HClO_4$.
**Adjusted by adding $NaClO_4$.

APPARATUS FOR PHASE-STABILITY STUDIES AND CORROSION TESTS ON 2-ml SOLUTION VOLUMES

W. L. Marshall C. H. Secoy

In August and September of 1952, exploratory investigations were made on aqueous uranyl fluoride solutions containing dissolved fluorides and hydroxides of alkali and alkaline earth metals.[25] Similar explorations were made on sulfate systems. Some of the solutions which contained 300 g of uranium per liter and which had pH values of 5.00 to 6.00 showed phase stability up to and above 300°C. However, it was not possible to make accurate observations in silica tubes on the high-pH solutions because of the reaction of silica with the solutions to form insoluble silicates. As the temperature was raised, the formation of precipitates occurred at about 220°C in all solutions having a pH between 5.00 and 6.00. It was necessary to study the phase stability and corrosiveness of these solutions in stainless steel, titanium, or platinum-lined bombs. It was deemed desirable to have a small apparatus in which many solutions could be tested with relative ease, since the large-scale apparatus currently available made this exploratory multitesting procedure impractical. If the apparatus were small and simple in design, many such units could be operated at a minimum of cost. Such an apparatus has been designed.

Description of Apparatus

A schematic drawing of the apparatus is shown in Fig. 53. The thermostat system consists of a 4-liter stainless steel beaker containing a liquid salt mixture of KNO_3, $NaNO_3$, and $LiNO_3$[26] which melts at about 120°C and is held at the required temperature by suitable heating elements and a stirrer. The container tube for holding the small bombs is fabricated from stainless steel and is heliarc welded at the bottom. The inside dimensions are $^{11}/_{16}$ in. in diameter and 8 in. in length. After the unit is loaded with a maximum of three bombs, it is attached to a conventional laboratory motor and rotated in the thermostat at 1800 rpm.

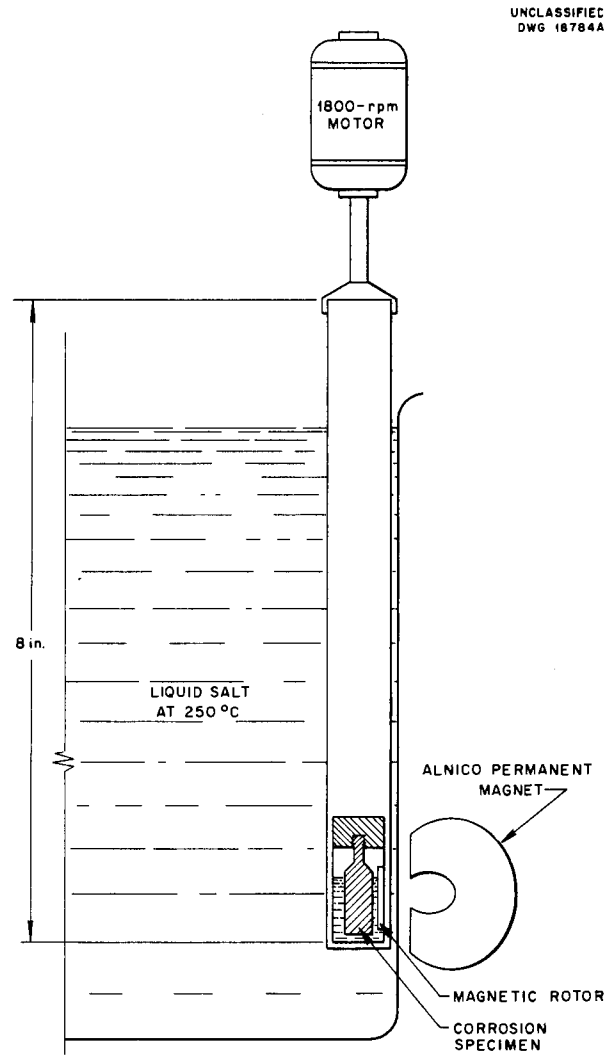

Fig. 53. Experimental Apparatus for Phase Study and Corrosion Experiments.

The outside dimensions of the stainless steel or titanium bombs are $1^3/_4$ in. in length and slightly over $^5/_8$ in. in diameter. The contained volume is 3.2 ml. Teflon is used successfully as a gasketing agent. The Teflon ring gasket fits into a groove in the bomb cap, which prevents the ring from extruding from the gasketing surface. Because of the expansion characteristics of Teflon, the bomb cap can be tightened with hand-pressure alone. The expansion of the Teflon when the temperature is raised will seal the bomb. Similarly, upon cooling, only hand-pressure is needed to open the bomb. In actual operation, however, a small wrench is used to tighten the bombs.

---

(25) H. O. Day *et al.*, *Chem. Quar. Prog. Rep. Sept. 30, 1952*, ORNL-1432, p. 64.

(26) J. A. Beattie, *Rev. Sci. Instr.* 2, 458 (1931).

Teflon appears to be a satisfactory seal for aqueous solutions at temperatures up to 325°C, at least for this type of gasket.

The magnetic rotor is prepared by sealing a permanently magnetized metal in either type 347 stainless steel or a titanium capsule. The ends of the capsule are heliarc welded. No leakage occurs between the magnetized metal and the external system.

Teflon caps placed on the ends of the rotor have been used in some instances to eliminate erosion caused by metallic contact between the rotor and the bomb surface.

Corrosion specimens are fabricated from the metal to be tested. A specimen is screwed into the bomb cap and it rotates with the bomb, which, in turn, rotates with the container tube.

Under operating conditions, a container tube is loaded with three bombs, each containing a solution, a corrosion specimen, and a magnetic rotor. The unit is lowered into the thermostat and rotated at 1800 rpm. Three sets of two alnico permanent magnets are adjusted to fit closely to the sides of the thermostat adjacent to the respective bombs. These magnets cause the rotors within the bombs to revolve around the inside diameter and provide mixing. Three container tubes containing three bombs each can be operated in one 4-liter thermostat bath.

Proposed Use of Apparatus

It is proposed to use this apparatus both for phase-stability studies, in which case, the corrosion specimen will be omitted, and for corrosion studies. With respect to phase-stability investigations, the solution being studied will be run at the requisite temperature, the bomb will be cooled and opened, and the solution will be examined. Since cooling and opening of the bomb are completed in 60 sec, there should not be too much reversal of equilibria for liquid-solid systems.

With regard to corrosion runs, the corrosion test specimen will be included in the bomb, and photomicrographs will be made of the specimen before and after a run. The specimen also can be weighed and the solution can be analyzed for corrosion products.

The erosion on the sides of the bomb caused by the revolving rotor is one of the disadvantages of this apparatus. It is anticipated that the use of Teflon caps on the ends of the rotors might eliminate this erosion difficulty.

If oxygen pressure within the bomb is desired, a calculated amount of 30% hydrogen peroxide can be added to each bomb before it is sealed. The peroxide decomposes at temperatures above 100°C and yields oxygen.

COMMENT ON THE SYSTEM URANYL DICHROMATE–WATER

W. L. Marshall C. H. Secoy

In 1950, J. S. Gill, C. H. Secoy, and W. L. Marshall observed the apparent solubility of uranyl dichromate in the supercritical fluid that exists above the critical temperature for mixtures of UO_3-CrO_3-H_2O which are soluble at room temperature. There was some doubt at that time as to whether uranium actually was dissolved in the fluid. With the advent of the semimicro phase-study apparatus,[27] tube explosions were eliminated, and thus an easy method of investigation of this system was afforded.

In the present work, solutions of chromium trioxide in water, from 1.0 to 4.0 *M*, were observed in silica tubes in the semimicro apparatus. Decomposition of dichromic acid to refractory Cr_2O_3 occurred between 325 and 370°C. No orange-red color was observed in the supercritical fluid; however, vision was obstructed somewhat by the deposit of Cr_2O_3 on the tube surfaces. It appears that the orange-red color previously observed by Gill, Secoy, and Marshall in the supercritical fluid was not due to a compound containing chromium.

Further investigations were made on stoichiometric $UO_2Cr_2O_7$ from 0.50 to 0.050 *M* and on solutions containing 20% excess and 20% deficient UO_2^{++} in the same concentration range. In all experiments, the supercritical fluid had an orange-red color. There were always deep-red crystals present above the critical temperature of the system.

This investigation is of interest because Thamer, Bidwell, and Hammond recently showed that uranium oxide dissolves in the supercritical fluid of the system UO_3–H_3PO_4 at certain compositions of UO_3 and H_3PO_4.[28]

---

[27] H. W. Wright, W. L. Marshall, and C. H. Secoy, *Chem. Quar. Prog. Rep. Sept. 30, 1952*, ORNL-1432, p. 53.

[28] B. J. Thamer, R. M. Bidwell, and R. P. Hammond, Los Alamos Scientific Laboratory, private communication (1953).

EXPLORATORY PHASE INVESTIGATIONS OF SYSTEMS INVOLVING $CuSO_4$, UO_2SO_4, H_2SO_4, AND H_2O AT URANIUM CONCENTRATIONS BELOW 30 g PER LITER

W. L. Marshall C. H. Secoy

An exploration has been made on the following systems with regard to the temperature at which either hydrolytic or true solubility precipitation occurs:

$CuSO_4$–H_2O,

UO_2SO_4–H_2O,

UO_2SO_4–$CuSO_4$–H_2O,

UO_2SO_4–$CuSO_4$–H_2SO_4–H_2O.

The interest in these systems originates from the use of copper for the catalytic combination of hydrogen and oxygen in aqueous homogeneous reactor fuels as investigated by H. F. McDuffie *et al.* of the Chemistry Division.

The micro phase-study apparatus previously described was utilized for this investigation.[27] About 50 tubes containing the solutions were prepared and tested during the course of the work.

The purpose of the work was to map boundaries – not to obtain exact solubility or hydrolytic precipitation temperatures. Accordingly, the temperature was raised slowly, but not slowly enough to determine the precise precipitation temperature. This exact investigation would have delayed attainment of data to a considerable degree. Also, not much emphasis was placed on data obtained below 200°C, the prime interest being in the behavior between 200 and 300°C. The actual phase-stability temperatures at equilibrium may be as much as 10 to 20°C below the values reported. In some systems, namely, UO_2SO_4–$CuSO_4$–H_2O and UO_2SO_4–$CuSO_4$–H_2SO_4–H_2O, the solid phase appeared to dissolve rapidly at room temperature after precipituting at the upper temperature, but it did not dissolve rapidly at temperatures just below the solid-phase appearance temperature. For the other two systems, the precipitations appeared to be irreversible, at least under the experimental conditions.

There is a remote possibility that reaction occurred with the pyrex and silica tubes used in this work. However, some tests were made at 250°C on solutions which had shown precipitation at temperatures between 200 and 240°C. Upon inserting tubes containing these solutions into the furnace at 250°C, precipitation occurred in as little as 5 seconds. It does not seem likely that the solution reacts this fast with the pyrex or silica.

The System $CuSO_4$–H_2O. Hydrolysis data for the system $CuSO_4$–H_2O from 1.0 to 1.0×10^{-3} *M*, as evidenced by precipitation of a bright blue-green solid phase, are given in Table 46. The solid phase must be a hydrolysis product because it appears in the same temperature range over such a wide change of concentration. Further evidence of hydrolysis is given in the rather complete investigation by Posnjak and Tunell.[29,30] Table 47 shows their data, converted into mole ratios, for the composition of solutions in contact with a solid product of hydrolysis.

TABLE 46. HYDROLYTIC PRECIPITATION OF $CuSO_4$

$CuSO_4$ (*M*)	TEMPERATURE AT WHICH PRECIPITATION WAS FIRST OBSERVED (°C)
0.00116	115
0.00402	100
0.0161	115
0.0532	111
0.103	126
0.204	125
1.01	142

The System UO_2SO_4–H_2O. Temperatures at which hydrolytic precipitation of a yellow solid occurs in the UO_2SO_4–H_2O system are given in Table 48. The data indicate that the minimum concentration of a UO_2SO_4–H_2O solution must be 0.017 *M* to achieve phase stability at 250°C.

[29] E. Posnjak and G. Tunell, *Am. J. Sci.* 218, 1 (1929).

[30] G. Tunell and E. Posnjak, *J. Phys. Chem.* 35, 929 (1931).

TABLE 47. THE SYSTEM $CuO-SO_3-H_2O$

Calculated from data by Posnjak and Tunell[29,30]

TEMPERATURE (°C)	CONCENTRATION (moles/1000 g of solution)		MOLE RATIO, SO_3/CuO
	CuO	SO_3	
50	0.0063	0.0062	0.98
	0.016	0.016	1.00
	0.21	0.21	1.00
	0.44	0.45	1.02
100	0.00013	0.00025	1.92
	0.0010	0.0011	1.10
	0.0025	0.0025	1.00
	0.048	0.050	1.04
	0.15	0.15	1.00
	0.46	0.48	1.04
200	0.0025	0.0062	2.48
	0.021	0.037	1.76
	0.30	0.37	1.23
	0.57	0.80	1.40

TABLE 48. HYDROLYTIC PRECIPITATION OF UO_2SO_4

UO_2SO_4 (M)	TEMPERATURE AT WHICH PRECIPITATION WAS FIRST OBSERVED (°C)
0.00624	225
0.0125	215
0.0150	210
0.0166	255
0.0208	325 to 355
0.0312	No solid phase, two-liquid layer ot about 330°C
0.0625	No solid phase, two-liquid layer at about 315°C
0.125	No solid phase, two-liquid layer at about 306°C

The System $UO_2SO_4-CuSO_4-H_2O$. In the work with the $UO_2SO_4-CuSO_4-H_2O$ system the UO_2SO_4 is held constant at 0.021 *M* and the $CuSO_4$ concentration is varied. It appears from the data given in Table 49 that a phase-stable system of $CuSO_4-UO_2SO_4-H_2O$ with 0.021 *M* UO_2SO_4 and more than 0.0021 *M* $CuSO_4$ could not be maintained at 250°C.

The System $UO_2SO_4-CuSO_4-H_2SO_4-H_2O$. There are four conditions of the $UO_2SO_4-CuSO_4-H_2SO_4-H_2O$ system which have been considered. These are the effect of H_2SO_4 on 0.021 *M* UO_2SO_4 containing 0.02 or 0.10 *M* $CuSO_4$ and the effect of H_2SO_4 on 0.126 *M* UO_2SO_4 containing 0.02 or 0.10 *M* $CuSO_4$. The data are given in Table 50.

TABLE 49. HYDROLYTIC PRECIPITATION IN THE SYSTEM UO_2SO_4–$CuSO_4$–H_2O

(0.021 M UO_2SO_4)

$CuSO_4$ (M)	TEMPERATURE AT WHICH PRECIPITATION WAS FIRST OBSERVED (°C)	APPROXIMATE COLOR OF CRYSTALS
0.00210	250	Yellow
0.00368	255	Dull blue-green and yellow
0.00525	250	Dull blue-green
0.0101	190 to 215	Dull blue-green

TABLE 50. HYDROLYTIC PRECIPITATION IN THE SYSTEM UO_2SO_4–$CuSO_4$–H_2SO_4–H_2O

UO_2SO_4 (M)	$CuSO_4$ (M)	H_2SO_4 (M)	TEMPERATURE AT WHICH PRECIPITATION WAS FIRST OBSERVED (°C)	COLOR OF PRECIPITATE
0.0210	0.020	0.00514	240	Questionable yellow
0.0210	0.020	0.0103	236	Questionable yellow
0.0210	0.020	0.0154	260	Questionable yellow
0.0210	0.020	0.0206	285	Questionable yellow
0.0210	0.100	0.0206	196	Bright blue-green
0.0210	0.100	0.0308	244	Bright blue-green
0.0210	0.100	0.0412	280	Bright blue-green
0.0210	0.100	0.0514	No crystals observed, two-liquid layer at about 342°C	Bright blue-green
0.126	0.100	None	240	Bright blue-green
0.126	0.100	0.0103	288 Two-liquid layer at 298°C	Bright blue-green
0.126	0.100	0.0206	None, two-liquid layer at 306°C, raised to 350°C with no solid appearing	

Since 0.126 M UO_2SO_4 stabilizes 0.100 M $CuSO_4$ at 250°C, the same concentration of UO_2SO_4 should stabilize 0.021 M $CuSO_4$. No work was done on this latter system.

The general conclusions that can be drawn from this work are:

1. Copper sulfate hydrolyzes and subsequently precipitates in the temperature range 90 to 140°C, at least at concentrations from 1.0 to 1.0×10^{-3} M.

2. At 250°C, the minimum concentration of UO_2SO_4 possible without hydrolytic precipitation is approximately 0.017 M. Constituents such as $NiSO_4$, other corrosion products, $CuSO_4$, and fission products will alter this value because of the solubility or hydrolysis effects of additional components on phase equilibriums.

3. At 0.021 M UO_2SO_4, solutions containing more than 2×10^{-3} M $CuSO_4$ will not be phase stable at 250°C.

4. Approximately 0.015 M H_2SO_4 will be required to maintain phase stability for the solution which is 0.021 M UO_2SO_4 and 0.020 M $CuSO_4$. A solution 0.035 M in H_2SO_4 will be required to maintain phase stability for 0.021 M UO_2SO_4 and 0.10 M $CuSO_4$. For 0.126 M UO_2SO_4 that is 0.02 M in $CuSO_4$, no H_2SO_4 will be needed at 250°C, but approximately 0.005 M H_2SO_4 will be required for 0.126 M UO_2SO_4 that is 0.10 M $CuSO_4$.

FURTHER INVESTIGATION ON THE USE OF A CATION-EXCHANGE RESIN FOR THE ANION ANALYSIS OF URANYL SALTS IN WATER

W. L. Marshall C. H. Secoy

The use of a cation-exchange resin for the removal of uranyl ion from uranyl sulfate solution and subsequent titration of the acid eluent for sulfate has been described previously.[31] This method is extended to include other anions of uranyl salts, namely, the nitrate, chloride, perchlorate, and dichromate, and offers much promise because of the speed and precision of analysis.

The description of the ion-exchange column and the preparation of Dowex-50 have been given previously; therefore, this report will be concerned only with the experiments involving the additional anions.

A sample was prepared by dissolving approximately 1 g, weighed to 0.1 mg, of specially prepared Mallinckrodt UO_3 (HNO_3 <0.3 mole %) in a measured volume of standard acid and diluting to 35 cc. A sample solution was run through the column at 8 cc/min, the column was washed free of acid to produce a final eluent volume of 100 cc, and the eluent was titrated for anion by means of a pH meter in which standard NaOH was used as the titrating agent. Dichromic acid was titrated to the end point for chromate ion.

At the above-mentioned flow rate through the column, the resin capacity of Dowex-50 (200 to 400 mesh, 12% cross linkage) was about 3 to 4 milliequivalents per cubic centimeter of wet resin. A sample could be run in approximately 20 min, including titration time. The resin was regenerated easily by washing it with 3 M H_2SO_4, followed by a wash with distilled water.

Runs were made with nitrate, chloride, perchlorate, and dichromate anions; the samples contained 0.8, 1.0, and 1.2 anion equivalents per equivalent of UO_2^{++}. The average deviation of the results from the actual amount of anion present was about ±0.15%. Investigations by other groups[32,33] have indicated equal success with uranyl fluoride solutions. The greater part of this investigation was carried out with the above-mentioned resin; however, later work has shown that elution times can be shortened by using a lower-mesh resin.

THE SYSTEM UO_3–SO_3–H_2O

E. V. Jones J. S. Gill
C. H. Secoy

Even though the solubility of UO_3 in uranyl sulfate solutions has been studied for over a year and a large amount of data has been reported[34] for isotherms at 25, 100, 175, and 250°C, a complete isotherm with identification of the solid phases has not been achieved. Recent efforts have been concentrated on the 25-deg isotherm, and results to date indicate that this portion of the system is far more complicated than was first suspected. At least two previously unknown crystalline solid phases have been found, both of which are probably basic salts. One of these has the approximate composition $8UO_3 \cdot 3SO_3 \cdot 14\text{-}20H_2O$. The other is richer in UO_3 and may even be some form of anhydrous UO_3 for which x-ray diffraction data have not been reported previously. Both materials are unstable in water and yield a UO_3-rich solution and a residue of $UO_3 \cdot H_2O$.

The experimental techniques have largely consisted of modifications of the Schreinemakers' wet-residue method and x-ray diffraction studies of the solid phases.[35] Elucidation of the data for

(31) W. L. Marshall *et al.*, *HRP Quar. Prog. Rep. Nov. 15, 1951*, ORNL-1221, p. 107.

(32) J. H. Edgerton *et al.*, ORNL, private communication.

(33) L. A. Stephens *et al.*, Y-12 Plant, private communication.

(34) E. V. Jones, *HRP Quar. Prog. Rep. July 1, 1952*, ORNL-1318, p. 147; E. V. Jones, J. S. Gill, and W. L. Marshall, *HRP Quar. Prog. Rep. Oct. 1, 1952*, ORNL-1424, p. 105; E. V. Jones, W. L. Marshall, J. S. Gill, and C. H. Secoy, *Chem. Quar. Prog. Rep. Sept. 30, 1952*, ORNL-1432, p. 51.

(35) Preparation and interpretation of the x-ray diffraction patterns have been the work of R. D. Ellison of the Chemistry Division, whose help is gratefully acknowledged.

this system has proved to be rather difficult because of several factors. Discontinuities in the liquidus curve at transition points are nearly indiscernible, the temperature coefficient of solubility is very low, and the rates of equilibration are slow.

OXIDATION OF SULFUR DIOXIDE IN URANYL SULFATE SOLUTION

D. W. Sherwood C. H. Secoy

Present plans for the intermittent addition of acid to the in-pile loop involve the addition of a mixture of a measured amount of sulfur dioxide and oxygen to react in the presence of the ions of the solution to form sulfuric acid. A series of laboratory experiments has been made to test the feasibility of this procedure with reference to the speed of the oxidation and the possible reducing action of the sulfur dioxide with regard to the uranyl ion in solution. The data obtained indicate that there has been no damage to the solution and that the desired oxidation occurs in less than 1 hr at 200°C.

The solution contains 40 g of uranium per liter (as uranyl sulfate) and was made approximately 3.3×10^{-3} *M* in nickelous ion and 1.5×10^{-2} *M* in cupric ion to simulate the probable composition of the operating solution after exposure to loop metal. The nickel and copper were added as sulfates.

In each determination, approximately 0.9 cc of the above solution was used, and the operations were carried out in quartz tubing. The solution was first degassed, and the desired quantity of sulfur dioxide was subsequently added by allowing a pressure of approximately 6.5 mm of the gas to flow into an evacuated chamber about nine times the volume of the refrozen solution which was also in the container. The solution was then brought to room temperature for absorption of the gas, which was calculated to be 71 cc (STP) per liter of solution – the desired amount for loop operation.

After very slow refreezing of the solution containing the sulfur dioxide, nearly an atmosphere of oxygen (650 to 700 mm) was added and the quartz tube was sealed off. This left some ten times the calculated quantity of oxygen necessary to react with the sulfur dioxide, though less than the pressure of 70 psi indicated for the loop. (No appreciable hydrogen pressure is indicated for loop operation.) In one run, five times the above amount of sulfur dioxide was used and in another case, ten times this amount was used. Such additions were made by repeating the addition, by absorption, of the calculated amount the appropriate number of times.

When ten times the calculated amount of sulfur dioxide was added, the last four additions resulted in the formation of a yellow precipitate – probably of uranyl sulfite or a uranyl double salt. This precipitate disappeared promptly when it was heated.

The sealed tubes were heated in a small furnace (resistance-wire-wound aluminum block) for 1 hr at 200°C, were cooled, and then were opened for analysis. The results are given in Table 51. The small amounts of sample made analyses somewhat difficult; however, the following points may be noted:

1. In most cases, a small increase in uranyl ion concentration was found. This may be due to incomplete condensation of water vapor before subjecting the sample to evacuation. Each sample was pumped several times after it was frozen, and a water loss may have occurred. In each case, the sulfate ion increase in concentration was greater than the uranyl ion increase except for samples 7-2 and 8-1 which were not heated, and these two samples failed to show the greater gain for sulfate ion. Thus, the analyses for sulfate indicate an increase without exception. Inaccuracies of gas measurement and analytical difficulties apparently preclude quantitative correlation with the extremely small amount of sulfur dioxide added. However, sample 10-1, which received some ten times the usual sulfur dioxide charge, shows a correspondingly large sulfate increase.
2. Analysis for sulfite shows about the calculated amount for samples not heated (Nos. 7-2 and 8-1), while samples which were heated showed no detectable sulfite even though large amounts of sulfur dioxide were added.
3. The pH of each solution showed a decrease from that of the original solution, and the change was less for those solutions not heated to oxidize the sulfur dioxide.

Hence, it is concluded from these experiments that the proposed method for oxidation of sulfur

[redacted]

TABLE 51. ANALYSES OF SULFUR DIOXIDE OXIDATION SAMPLES

SAMPLE NUMBER	IONIC CONCENTRATIONS (M)						ΔpH	REMARKS
	SO_3^{--}	UO_2^{++}	SO_4^{--}	ΔUO_2^{++}	ΔSO_4^{--}	$\Delta SO_4^{--} - \Delta UO_2^{++}$		
3-24-1		0.189	0.190					Original solution
3-24-2		0.227	0.239	0.038	0.049	0.011	−0.41	
6-1		0.249	0.254	0.060	0.064	0.004	−0.29	
7-1		0.194	0.204	0.005	0.014	0.009	−0.42	
7-2	0.00225	0.202	0.200	0.013	0.010	−0.003	−0.16	Not heated
8-1	0.00263	0.194	0.192	0.005	0.002	−0.003	−0.26	Not heated
10-1	<0.00038	0.192	0.244	0.003	0.054	0.051	−1.12	Given ten times the calculated amount of SO_2
11-1	<0.00038	0.183	0.201	−0.003	0.011	0.014	−0.77	Given five times the calculated amount of SO_2

dioxide in uranyl solution to offset acidity decrease caused by corrosion is a satisfactory one with respect to the chemistry involved.

VAPOR PRESSURES OF AQUEOUS URANYL SULFATE SOLUTIONS

H. O. Day, Jr. C. H. Secoy

Some vapor pressures of uranyl sulfate solutions at various concentrations and temperatures were reported previously.[36]

After moving to new quarters in Building 4500, a new, differential pressure apparatus was constructed; the details of the apparatus are given in an HRP report.[37]

Vapor-pressure data for several more concentrations of UO_2SO_4 solutions have been obtained with the new apparatus. These data cover the concentration range of about 0.6 to 4.2 *m* and a temperature range of 25 to 90°C. Work at a low concentration of about 0.1 *m* is in progress. At present, the relative partial molal free energies of water in the UO_2SO_4 solutions are being calculated from the experimental data. By use of the procedure followed by Harned and Nims,[38] the data are being smoothed by plotting the first-order differences between the relative partial molal free energies of water in a constant composition UO_2SO_4 solution vs. temperature. From this plot, an equation expressing the relative partial molal free energy of water in constant composition UO_2SO_4 solution as a function of temperature will be derived.

From the smoothed data, the activity coefficients of UO_2SO_4 will be derived by use of the Gibbs-Duhem equation. In addition, estimates of the relative partial molal heat contents and relative partial molal heat capacities of the components, and the relative molal heat content and relative molal heat capacities of the solution will be made by usual thermodynamic procedures.

[36] H. O. Day, Jr., *HRP Quar. Prog. Rep. July 1, 1952*, ORNL-1318, p. 138; H. O. Day, Jr. and W. L. Marshall, *HRP Quar. Prog. Rep. Oct. 1, 1952*, ORNL-1424, p. 104.

[37] H. O. Day, Jr., *HRP Quar. Prog. Rep. March 31, 1953*, ORNL-1554, p. 109.

[38] H. S. Harned and L. F. Nims, *J. Am. Chem. Soc.* 54, 423 (1932).

[redacted]